

PERKIN-ELMER

ELECTRO-OPTICAL DIVISION

NORWALK, CONNECTICUT


ENGINEERING REPORT NO. 8287TWO-GAS ATMOSPHERE SENSOR SYSTEM
CONCEPTUAL DESIGN STUDY
PHASE I FINAL REPORTDATE: MARCH 16, 1966

Distribution of this report is provided in the interest of
information exchange. Responsibility for the contents
resides in the author or organization that prepared it.

PREPARED FOR: NATIONAL AERONAUTICS AND SPACE ADMINISTRATIONLANGLEY RESEARCH CENTERLANGLEY STATION, HAMPTON, VIRGINIA

NASA CONTRACT NAS1-5678

CONTROL NO. L-5908


PROJECT MANAGER
GROUP MANAGER
DEPARTMENT MANAGER

N66 35950

(ACCESSION NUMBER)

261
(PAGES)CR-66175
(NASA CR OR TMX OR AD NUMBER)

(THRU)

1
(CODE)14
(CATEGORY)

TABLE OF CONTENTS

<u>Paragraph</u>	<u>Title</u>	<u>Page</u>
	ABSTRACT	vii
1.0	INTRODUCTION AND SUMMARY	1
2.0	RECOMMENDED DESIGN CONCEPT	6
2.1	Ultraviolet Subsystem (H ₂ O and O ₂ Channel)	23
2.1.1	Optics - Ultraviolet Subsystem	27
2.1.2	Detector - Ultraviolet Subsystem	34
2.1.3	Chopper - Ultraviolet Subsystem	37
2.1.4	Source - Ultraviolet Subsystem	38
2.1.5	Electronics - Ultraviolet Subsystem	43
2.2	Infrared Subsystem (CO ₂ Channel)	48
2.2.1	Optics - Infrared Subsystem	50
2.2.2	Detector - Infrared Subsystem	59
2.2.3	Chopper - Infrared Subsystem	61
2.2.4	Source - Infrared Subsystem	61
2.2.5	Electronics	62
2.3	Total Pressure (P _T) Subsystem	65
2.4	Electronics Packaging Concept	65
2.4.1	Electronic Module	68
2.4.2	Wiring Subassembly	75
2.4.3	Microcircuits	78
2.4.4	Environmental Considerations	83
2.4.5	Specifications	90
2.5	Design Studies	93
2.5.1	Linear Integrated Circuit Study	93
2.5.2	Use of Dip Brazing for Fabrication of the Two-Gas Atmosphere Sensor Housing	103
2.5.3	Chopper Methods for Two-Gas Atmosphere Sensor	105
2.5.4	Sapphire as an Ultraviolet Optical Element	116
3.0	SPACECRAFT INTERFACE CONSIDERATIONS	119
3.1	Gas Control Techniques System Study	119
3.1.1	General	119
3.1.2	System Description and Qualitative Performance	119
3.1.3	Detailed System Analysis	123
3.2	Visual Readout Compatibility	131
3.3	Operational Supplies	132
3.4	Maintainability	132
3.5	Redundancy	132

TABLE OF CONTENTS (Continued)

<u>Paragraph</u>	<u>Title</u>	<u>Page</u>
4.0	ASSESSMENT OF SENSOR TECHNOLOGY	134
4.1	Zero Gravity Operation	134
4.2	Exposure to Hard Vacuum	134
4.3	Effect of Error in CO ₂ and H ₂ O Measurement on N ₂ Measurement	136
4.4	Ability of Two-Gas Atmosphere Sensor to Meet Reliability and Flight Qualification	138
4.5	State of Development	140
4.6	Operational Life	141
4.7	Shelf Life	141
4.8	Complexity	142
4.9	Energy, Material, and Atmospheric Sample Requirements	143
4.10	Weight of Special Equipment	144
 <u>Appendix</u>		
A	Signal Processing	145
B	Computer Ray Trace	165
C	Transmission and Absorption Measurements	177
D	Test Reports, Limited-Rotation Motor	186
E	Typical Flight Qualification Test Plan	197
 <u>Bibliography</u>		221

LIST OF ILLUSTRATIONS

<u>Figure</u>	<u>Title</u>	<u>Page</u>
1(a)	Two-Gas Atmosphere Sensor Conceptual Design	2
1(b)	Two-Gas Atmosphere Sensor Conceptual Design (Optical Cover Removed)	3
2	CO ₂ Sensor, NASA Flight Model	4
3	Gas Sensor Timing Generator	13
4	Torquer Timing Sequence	14
5	Electronic System Conceptual Block Diagram	15
6	O ₂ , H ₂ O, N ₂ , and Pt Subsystems Schematic	16
7	CO ₂ Subsystem Schematic	17
8	Two-Gas Atmosphere Sensor Optical Schematic	20
9	Torquer Angular Position and Optical Channel Outputs	21
10	High Resolution, Far-Ultraviolet, Spectrum of Oxygen (Model 350)	24
11	Relative Absorption of Gas Constituents	26
12	Diffraction Grating	30
13	Folding Mirrors	31
14	Ultraviolet Sample Cell	32
15	Prototype Xenon Lamp	41
16	Spectral Output of Xenon Lamp	42
17	DC Restorer Output Signal	44
18	Processing Block Diagram	44
19	CO ₂ Measurement System Optical Schematic	49
20	CO ₂ Transmission Characteristics	50
21	Absorption Spectra of Typical Closed Environment	51
22	Dual Wavelength Filter	52
23	Spectrometric Run - First Half, Dual-Wavelength Filter	54
24	Spectrometric Run - Second Half, Dual-Wavelength Filter	54
25	Spectrometric Run - Detector Filter	55
26	Gas Compartment Window	56
27	Spectral Transmission of Coated Silicon	57
28	Lens Element (IR System)	58
29	IR System Spectral Characteristics	59
30	Apollo CO ₂ Detector	60
31	CO ₂ Subsystem Block Diagram	62
32	Overall Packaging Concept	66
33	Typical Cordwood Module	68
34	Module No. 5	71
35	Module Form Factors	72
36	Wiring Subassembly (Encapsulant Partially Removed)	75
37	Wire-Wrap Roll Pin	77
38	Module Form Factors (Using Microcircuits)	79
39	Alternate Microcircuits/Cordwood Module Packaging	82
40	Typical Thermal Paths	84

LIST OF ILLUSTRATIONS (Continued)

<u>Figure</u>	<u>Title</u>	<u>Page</u>
41	Tuning Fork Optical Chopper Improved Design	107
42	Torsional Chopper	108
43	Life Curves For Type 600 ($\pm 15^\circ$) Flexure Pivots (Bendix Corp.)	110
44	Scanner, Thermopile Detector, Far IR Detector Window and Knife Edge Field Switching Mirrors	111
45	Scan Angle Plot	112
46	UV Transmission of Single Crystal UV Grade Sapphire	117
47	Cabin Gas Control Diagram - Total Volume Control Mode	120
48	Cabin Gas Control Diagram - Input Mixture Control Mode	121
49	Suit Gas Control Diagram	122
50	Simplified Servo Diagram for Oxygen Replenishment Control	124
51	Simulated Time Response of Oxygen Concentration in a Sys- tem With a 1.0 Minute Transport Lag Time	130
52	Oxygen Output Characteristics	131

ABSTRACT

The use of a combined $N_2 - O_2$ atmosphere in long-duration manned spaceflight missions requires the development of sensor instrumentation that will accurately measure partial pressures of the principal constituents in the mixed-gas cabin atmosphere. This instrumentation, designated as a Two-Gas Atmosphere Sensing System, provides the partial pressure information as an electrical signal for integration into a functional atmosphere control system.

The design concept developed during this study program utilizes two sensor channels and a total pressure transducer to provide five different measurements (partial pressures of O_2 , CO_2 , H_2O , N_2 , and total pressure) and electrical signals proportional to these measurements for interface with the cabin atmospheric-control system.

The technique preferred and recommended for the sensor system is that of optical absorption. The radiant energy source for the O_2 and H_2O sensor operates in the ultraviolet spectrum at 1470\AA and the CO_2 sensor utilizes the 4.27μ band of the infrared region. The system will directly measure the partial pressure of O_2 , CO_2 , and H_2O using the optical absorption technique with accuracies of 2%, 2%, and 5% respectively. The system will also measure P_T with an accuracy of 1% and will compute the partial pressure of N_2 from these measurements to an accuracy of 5%. The optical absorption metrology used in this system has the following advantages:

1. Small size, weight and low-power consumption - All of the Two-Gas Atmosphere Sensing System instrumentation is contained in one unit having an estimated volume of 100 in^3 , an estimated weight of 6.5 pounds, and a power requirement of less than 5 watts.
2. Long operating and shelf life - The system has no wearout or consumable components.
3. Insensitive to magnetic fields, ambient temperature, or gravity.
4. Operates at ambient pressure - The system requires no auxiliary gas pumping or vacuum system and is not affected by vacuum exposure.

5. No lubrication is required.
6. No specific operation use attitude is necessary.
7. Fast response time - System will have a response time constant of 1.0 seconds.
8. Flight qualification design compatibility.
9. No gas consumption - No reference gas is required, nor does the system consume any of the sample gas.
10. Automatic gain stabilization - Long term stability.
11. Low sample flow rates with minimum pressure drops - Continuous monitoring and readout.

The electronics are common to the two sensor channels and the pressure transducer, which permits minimum size and weight, and greater reliability. The system is designed to utilize linear integrated circuits, which will further reduce bulk and enhance reliability.

1.0 INTRODUCTION AND SUMMARY

This report describes the results of the Phase I conceptual design study for a Two-Gas Atmosphere Sensor System which is considered for anticipated extensions of the Apollo mission duration capability. The Phase I study effort was performed by the Perkin-Elmer Corporation, Norwalk, Connecticut, for the National Aeronautics and Space Administration, Langley Research Center, Langley Station, Hampton, Virginia, under Contract No. NAS1-5678. The study was in progress from 15 November 1965 to 15 March 1966 and was accomplished in accordance with the provisions of the contract.

Photographs of a full size mock-up and an artist's representation of the recommended design concept are shown in Figure 1 and the design is discussed in detail in Paragraph 2.0. State-of-the-art electronics packaging, which will provide a system of minimum size as evidenced in the full size mock-up accompanying this report, is described in Paragraph 2.4 and reliability aspects of the proposed system are discussed in Paragraph 2.5. The information on electronic packaging was provided by Francis Associates, Inc., Marion, Massachusetts. The report includes a review of spacecraft interface considerations (Paragraph 3.0) an assessment of sensor technology, (Paragraph 4.0), and significant results established during the study effort.

The application of the Two-Gas Atmosphere Sensor System to the spacecraft model has been reviewed for the recommended operational criteria. This report includes a detailed discussion of the difficulty in control of this spacecraft model along with recommended locations for the sensor. It is shown in the study, for example, that sampling from the exhaust lines or within the space capsule will lead to formidable controls system problems. Recommendations are therefore made for sensor installation on the inlet lines of a pre-mix gas supply.

Recommendations have been made for cabin atmosphere replenishment techniques based primarily on the addition of a predetermined mixture of nitrogen and oxygen. Investigation of the visual readout compatibility of the system indicates that the output readily lends itself to the display of the portions of the partial pressure ranges that are considered most significant. For example, there is no appreciable difficulty encountered in displaying the analog voltage for the oxygen partial pressure having a range of 0 to 5 volts for a variation in oxygen partial pressure of some arbitrary limits, such as 100 to 200 millimeters Hg of partial pressure. Likewise, the zero point on the total pressure indication can be set at some selected point and could operate over a range of 200 to 400 or more millimeters Hg of total pressure. There are a minimum of operational supplies required for the duration of the missions indicated. Either the 45 day or 120 day anticipated mission can be accomplished without the use of calibration gases or external supplies beyond the normal 28 volt system.

The continuous closed-loop operation of the system, which automatically compensates the changes in its reference, permits continuous performance throughout the mission without use of laboratory type controls or



NASA

MORL TWO-AS
SEI SOK



Figure 1(a). Two-Gas Atmosphere
Sensor Conceptual Design

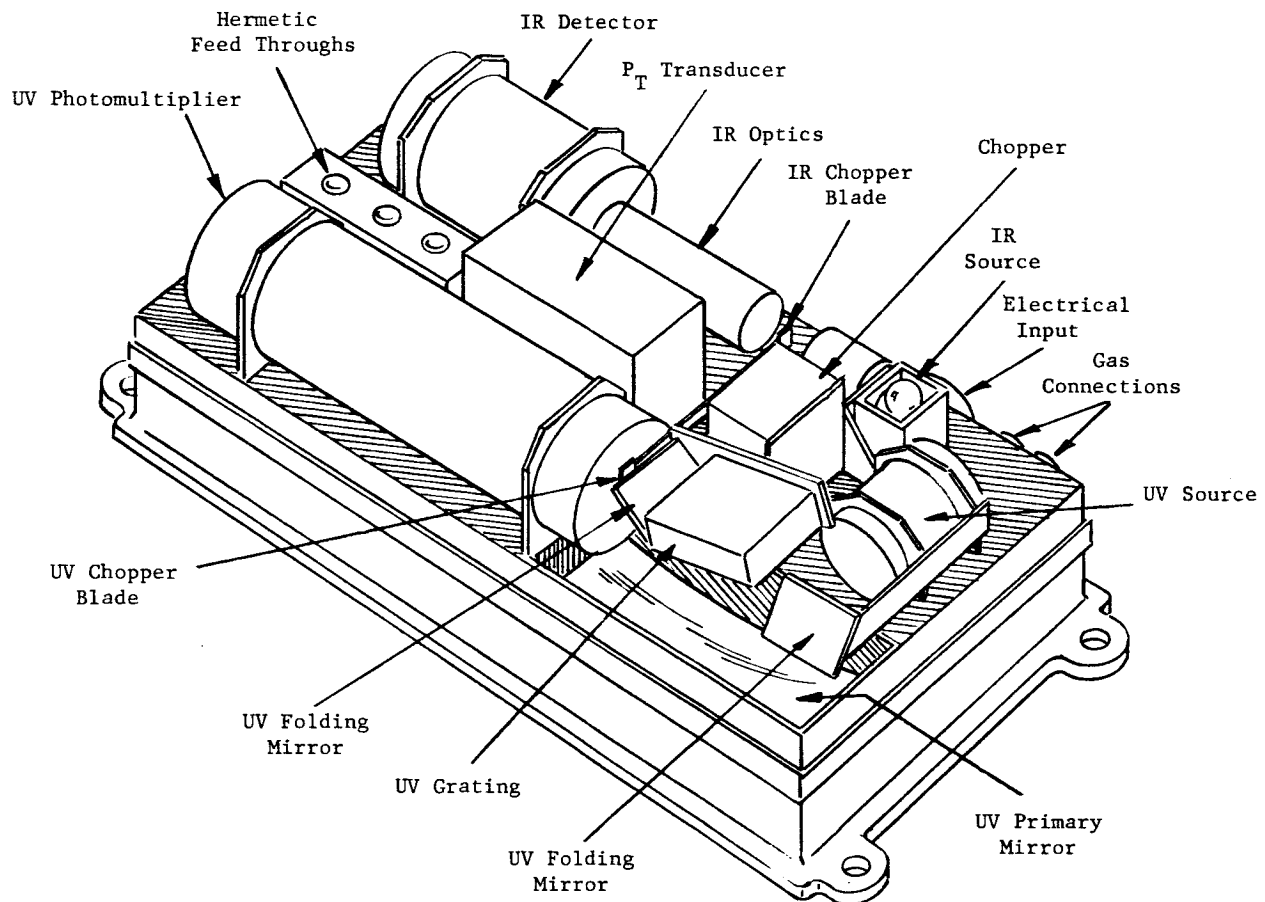
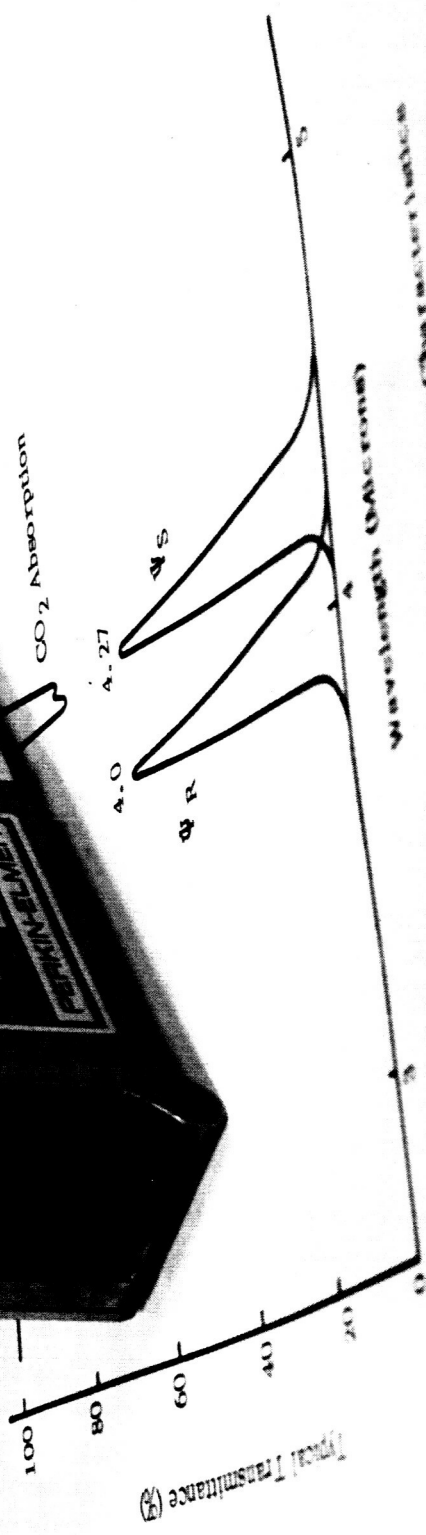
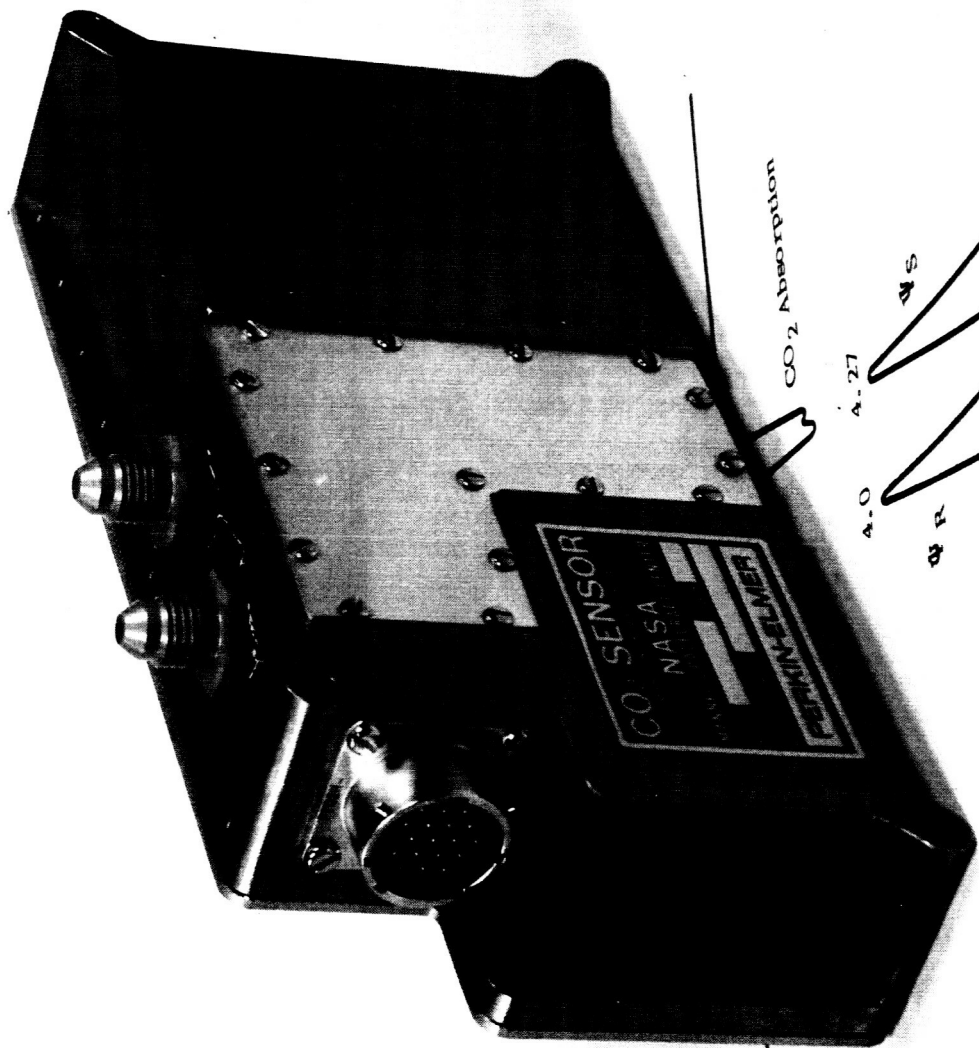


Figure 1(b). Two-Gas Atmosphere Sensor
Conceptual Design
(Optical Cover Removed)

adjustments in either zero or span. It is this aspect of the design that facilitates the utilization of the proposed system in an extended duration spacecraft mission. The philosophy on the maintainability of the system at present is to use high reliability components which would preclude the necessity of either maintenance in the field or during the mission. It would be recommended that complete redundancy be used, that is, extra systems installed rather than depend on the maintenance of a given system with plug-in discrete components. However, the system would be designed so that it could be maintained in the laboratory or could be readily repaired at the factory. The excessive cost in size, weight, and resultant lower operating reliability from the use of extensive plug-in units which could be easily maintained in the field is felt to be an unnecessary burden on the design of the system. The extensive use of plug-in units would make the total system prohibitively large and complex in order to maintain the same level of total reliability.



Typical Wavelength Filter Quartz Window

Assessments have been made of the applicable sensor technology with respect to the specified basic requirements. With respect to zero gravity operation, it is felt that no degradation of the system's performance would occur under zero-G conditions. As discussed further in the report, the performance of the system would not be impaired by the exposure to hard vacuum. The accuracy and response time necessary for control have been synthesized on the basis of the spacecraft model suggested in the statement of work and from some of our own assumptions. There is no difficulty encountered in the response time requirement and the accuracy is within the performance capability of the proposed instrument. The ability to meet the reliability and flight qualifications of any proposed Phase IIb type of hardware is perhaps best demonstrated by the similarity of the system to the Apollo Carbon Dioxide Sensor shown in Figure 2 which is presently undergoing environmental

Figure 2. CO₂ Sensor, NASA Flight Model

qualification tests. To demonstrate its reliability and performance during a simulated flight mission, tests in excess of 1000 hours have been performed under varying stringent environmental conditions. The information gained from these tests will be utilized directly in the design of the Two-Gas Atmosphere Sensor System.

In consideration of some of the additional requirements of the contract guidelines, the state of development of optical absorption sensor techniques was reviewed. As a result, the proposed sensor is considered to be a logical step in the advancement of optical absorption sensor development. Solutions to the problems that have been encountered in the Apollo Carbon Dioxide Sensor, and in the oxygen sensor which Perkin-Elmer has built and has been testing, will be incorporated in the design of a new sensor. Potential for improvement of this type of sensor would be in the component areas rather than in the basic design, since it is felt that in relation to the overall requirements, there are no inherent limitations on the accuracy or the stability of the system with the present method. Details such as the chopping method, the actual detector geometry used, and the reliability of some of the electronic components, will be considered and are the most logical areas for potential improvements.

The operational life of the system is not known, but it is anticipated to extend well beyond any other known method. There are no wearout components or systems within the Two-Gas Atmosphere Sensor and operation in terms of years can be anticipated with occasional adjustment in the analog circuitry due to aging. Shelf life of the system is also undetermined, but investigation with our vendors and our own studies have shown no degradation of performance after a 3 to 5 year shelf life. The critical item in the determination of the shelf life would be electronic components, such as the sintered-anode low leakage tantalum capacitors or other similar components.

The energy, material, and atmospheric sample requirements of the system are minimal. It is only necessary to apply a 28 volt supply to energize the sensor and to mount it on a suitable dimensionally stable surface and provide a few inches of water pressure head at a representable sample point. No other special considerations need be given to the installation in a spacecraft or in the laboratory. The system is independent of orientation and practically independent of normal environments. Shock and acceleration stresses, temperature stresses, acoustical noise, sand and dust, salt spray, rain or oxidizing atmospheres will not impair or change the performance of the system. Selected vibrational stresses at particular frequencies and amplitudes may of course cause a resonance of the system and impair its operation at those particular points. However, operation before and after these frequencies can be achieved and the system can be anticipated to be independent of any frequency below 3 to 5 g's over the frequency range from 5 to 2000 cps.

2.0 RECOMMENDED DESIGN CONCEPT

Functional Description

The recommended system will use optical absorption techniques to measure the partial pressures of carbon dioxide (CO_2), water vapor (H_2O), and oxygen (O_2) and will combine this information with a total pressure measurement to obtain the partial pressure of nitrogen (N_2). This system will use an infrared channel for the measurement of carbon dioxide and an ultraviolet channel for the measurement of oxygen and water vapor.

The infrared CO_2 channel will use an incandescent lamp as a source of energy and a silicon lens system to gather this energy and focus it in space to be chopped by a torsional optical chopper. The modulated energy will then be detected by a PEM infrared detector which will supply information to an electronic system.

The ultraviolet O_2 and H_2O channel will use a specially designed ultraviolet lamp, a grating monochromator, and the torsional chopper, which is common to both channels for maximum utilization of components. A photomultiplier detector will be used to measure the modulated ultraviolet energy and supply a signal to the electronic system.

The electronic system will provide electrical signals which are proportional to the partial pressures of the gas constituents. High-quality discrete electronic components and integrated circuits mounted in miniature welded modules will be used for the electronic systems of both the infrared and ultraviolet channels.

The total pressure will be measured by a flight qualified total pressure transducer consisting of a variable reluctance mechanism mounted on a specially designed bellows. The mechanism will be connected electrically as a bridge circuit which will provide an unbalanced signal proportional to the total pressure to an operational amplifier and output driving circuit. This system does not contain any optical members. The electronic system directly associated with the total pressure transducer will be of a construction similar to that used with the infrared and ultraviolet channels.

This particular system has been selected for several reasons. The study has shown that the most reliable system would be one using a torsional chopper and maximum utilization of integrated circuits. In addition, this method provides the maximum signal-to-noise information to the detectors and is least susceptible to environmental stresses which may be imposed on the system. One important reason for the final selection of this system is that it is a natural development and improvement on the present Apollo CO_2 Sensor. Also, it has taken advantage of the solutions to many difficult problems which have been experienced on existing systems and it encompasses the maximum utilization of design information obtained during the study.

Performance Characteristics

The performance of the preferred system may be described in summary as follows:

Oxygen Partial Pressure (PO_2):

Range - Zero to 250 millimeters Hg with expanded scales for a 0-5 volt output corresponding to 125 mm to 250 mm Hg partial pressure of oxygen.

Accuracy - $\pm 2\%$ of full scale

Reproducibility - $\pm 2\%$ of full scale

Water Vapor Pressure (PH_2O):

Range - Zero to 30 mm Hg for a 0-5 volt DC output

Accuracy - $\pm 5\%$ of full scale accuracy and reproducibility

Carbon Dioxide Partial Pressure (PCO_2):

Range - Zero to 20 mm Hg partial pressure of carbon dioxide corresponding to a 0-5 volt DC output.

Accuracy - $\pm 2\%$ of full scale

Reproducibility - $\pm 2\%$ of full scale

Total Pressure (P_T) Characteristics:

Range - 100 to 400 mm Hg total pressure corresponding to 0-5 volts full scale output

Accuracy - $\pm 1\%$ of full scale

Reproducibility - $\pm 2\%$ of full scale

Nitrogen Partial Pressure (PN₂) Characteristics:

Range - 100 to 300 mm Hg corresponding to 0-5 volts
DC output

Accuracy - $\pm 5\%$ of full scale

Reproducibility - $\pm 5\%$ of full scale

The following performance characteristics are common to the entire two-gas atmosphere sensor system.

Operating Temperatures	- 40°F to 90°F
Storage Temperature	- -65°F to 200°F
Vibration, Acceleration, and Shock	- Unspecified
Attitude	- There is no preferred use attitude
Altitude	- No limitation on operating or storage altitude
Operating Life	- One to three years (estimated)
Storage Life	- Estimated in excess of three years
Required Operational Supply	- 28 volt DC supply ± 4 volts. Transients and reverse polarity protection will be provided by an EMI filter on the input power line. A provision will also be made on the output to limit the output voltage swing from -1 to +7 volts in the event of equip- ment failure.
Handling and Storage	- To be accomplished by the use of a special designed carrying case which will isolate the sensor from extreme environmental condi- tions and be a useful storage provision and general protective device for the sensor system.

- | | |
|----------------------|---|
| Response Time | - Less than 10 seconds to reach 90% of the step value of input partial pressure change with a pressure drop of less than 3 inches of water (primarily pneumatic). |
| Flight Qualification | - System to meet typical flight qualifications as defined by the recommended program for flight qualification in the Phase I report. |

Electrical, General

The general signal processing design objective is to select a system that is linear, has a high signal-to-noise (S/N) ratio, is inherently accurate, and has no cross-coupling between signals. To facilitate an understanding of the general problem, the signal processing of the present CO₂ sensor was analyzed, as shown in Appendix A. This analysis shows that, with the optimum cross-coupling between the signal and reference AGC channel, the output signal will take the form of either:

$$a) \quad e_2 = \frac{K_1 A (I_R - I_S)}{K_2 I_R} \quad \text{for an idealized signal, or}$$

$$b) \quad e_2 = \frac{3}{4\pi} \frac{K_1 A (I_R - I_S)}{K_2 (I_R + I_S)} \quad \text{for a typical signal.}$$

From this it was seen that in the typical case the signal processing (exclusive of optical considerations) is nonlinear. The first system objective, therefore, was to make the signal in this new system take on the form of the idealized waveform where each signal level is clearly defined and can be processed to achieve a linear output. Next, the method of demodulation of this signal was considered to determine if either a synchronous square wave, or a narrow pulse sampling system (also synchronous) showed any cleancut advantage or disadvantage for a single gas (Infrared CO₂) channel. This analysis showed that for the synchronous system the S/N power ratio is: (Refer to Paragraph 2.2.3, Appendix A.)

$$S/N \text{ synchronous} = \frac{0.114 (I_R - I_S)^2 \omega_\alpha}{\sigma_n^2 \omega_\gamma}$$

where

$$\begin{aligned} I_R &= \text{Reference level signal} \\ I_S &= \text{Gas level signal} \\ \omega_\alpha &= \text{Noise bandwidth} \\ \omega_\gamma &= \text{Output filter bandwidth} \\ \sigma_n^2 &= \text{Total noise power} \end{aligned}$$

For the sampling system, the S/N power ratio is dependent upon the sample interval, and decreases as the sample interval decreases. When an achievable value of (k_s = Sample time/Total cycle time) for a multigas (ultraviolet H₂O-O₂) channel is considered (k_s = 0.156), the S/N power ratio is: (Refer to Paragraph 2.4.2, Appendix A.)

$$\text{S/N sampling} = \frac{0.099 (I_R - I_S)^2 \omega_\alpha}{\sigma_n^2 \omega_\gamma}$$

which, is only slightly less than for the synchronous system. Thus, a sampling system can be used for a multigas (H₂O-O₂) channel with only a slight signal-to-noise power ratio disadvantage over the synchronous system; however, the synchronous system cannot be used in a multigas channel without signal cross-coupling. From this it is evident that if hardware is developed to process the multigas channel signal, it may be used without appreciable penalty on the single gas (CO₂) channel. This approach affords the greatest utilization of common signal processing and timing hardware and facilitates the use of only one mechanical chopping system for the two detector channels.

The choice of the mechanical chopping system had a direct influence on the complexity of electronics. If a tuning fork is employed, circuitry must be included to drive it at a uniform amplitude, and to independently sample the various signal channels. The sampling circuitry must be phase locked to the fork frequency to ensure timing stability, and must operate at a high multiple of the fork frequency in order to generate at least six sampling pulses per cycle, centered within the signal data area. For the ultraviolet channel where four electrical levels are sensed (zero, reference, H₂O-O₂, O₂), the fork also imposes severe mechanical positioning problems. These problems can be reduced by making the timing nonlinear around the points of maximum fork tine excursion, but this increases the complexity of the timing circuitry by requiring a higher sampling frequency. The higher frequency is, in itself, not prohibitive, but it does reduce the possible sampling interval k_s , which

in turn has a severe effect on the signal-to-noise power ratio. The effect of a higher frequency on the single gas (CO₂) channel could be decreased by providing a separate timing generator; however, this further increases the complexity of the timing unit.

In summary, the tuning fork system introduces the problems of:

- a) Amplitude stabilization as incorporated in the present CO₂ sensor.
- b) Nonlinear timing for specified mechanical motion (the total motion is only about 0.060 inch).
- c) Extremely small aperture sizes in order to achieve a steady detector signal for a given gas sample. It must be borne in mind that the tuning fork is in constant motion, hence the aperture must be a fractional part of the gas sample interval for the signal amplitude to be independent of motion.
- d) Very short electrical signal sampling intervals (relative to the cycle period) to prevent signal cross-coupling and errors due to mechanical motion. Such small intervals ($k_s \leq 0.0625$) lead to poor signal-to-noise power ratios and thus decrease the system accuracy.
- e) Higher processing gains because of small aperture sizes, which decrease the total signal into the detector.
- f) Complex, and perhaps different, sample pulse timing generators for each signal processing channel. The signal processing hardware for each gas channel would also be different.
- g) Use of two different tuning forks, one for the infrared CO₂ channel and one for the ultraviolet O₂-H₂O channel.

In order to overcome these effects, the recommended chopper employs a torquer motor that may be driven to one of a number of discrete positions and held at that position for an indefinite time. Since the device is operated below its resonant frequency, the positioning is independent of the past time history of motion (not true for a tuning fork). Hence, to sample the ultraviolet channel where four signal levels are required, only four mechanical positions and four sampling intervals per cycle are required (six are required for the tuning fork), with a resultant simplification of hardware.

When the actual torquer characteristics are considered, a system can be configured that has the following characteristics:

- a) Simple Torquer Drive and Timing Electronics. Since it is only necessary to step to four positions and to generate four timing pulses, a simple two-stage counter may be used. This counter can be driven from an unsymmetrical multivibrator, which has a 7.5 millisecond ON time and a 12.5 millisecond OFF time. The counter will therefore change state every 20 milliseconds. The binary value of the counter is summed by an operational amplifier that provides an analog voltage output proportional to the binary value of the counter data. This voltage is amplified and used to drive the torquer, which moves proportionally to the input current. With such a system, the mechanical positioning can be repeated within 2.0%. By using the leading edge of the 7.5 milliseconds ON period to trigger the counter, and the subsequent 12.5 milliseconds OFF period to generate the timing pulses, the timing pulses can be made to lag the mechanical motion by 7.5 milliseconds, which is adequate to allow for mechanical positioning. The binary count of the counter is gated with this timing pulse to actually generate four separate timing pulses. A block diagram of the timing unit is shown in Figure 3, and the timing sequence in Figure 4.
- b) Uniform Sample Timing. Since the sequence is simply: 1) position torquer -- 7.5 ms, 2) electrically sample -- 12.5 ms, 3) position torquer -- 7.5 ms, etc., the motion per step can be approximately 4° , which provides a 0.070 inch motion per step when a 1 inch radius arm is used.
- c) Large Aperture Sizes. Since the aperture is not in motion during electrical sampling, the aperture may be large relative to the filter or slit size.
- d) Larger Sampling Intervals due to the signal stability within a step, and fewer steps ($k_s = 0.156$ achievable). This provides a better signal-to-noise power ratio and hence increases the inherent system accuracy.
- e) Decreased Requirements for Amplifier Gain due to larger aperture size, which increases the total signal into the detector and increases system accuracy.
- f) Uniform Sample Pulse Timing for each signal processing channel. This maximizes the amount of common hardware.

An overall block diagram of the recommended system is shown in Figure 5. The operation of the individual sections of this system is depicted in Figures 6 and 7 and will be described in subsequent sections of this report (Paragraphs 2.1.5 and 2.2.5). It will be noted that the DC voltages for all signal processing are obtained from one DC to DC converter. This converter will provide voltages in the order of ± 12 volts throughout the system. This

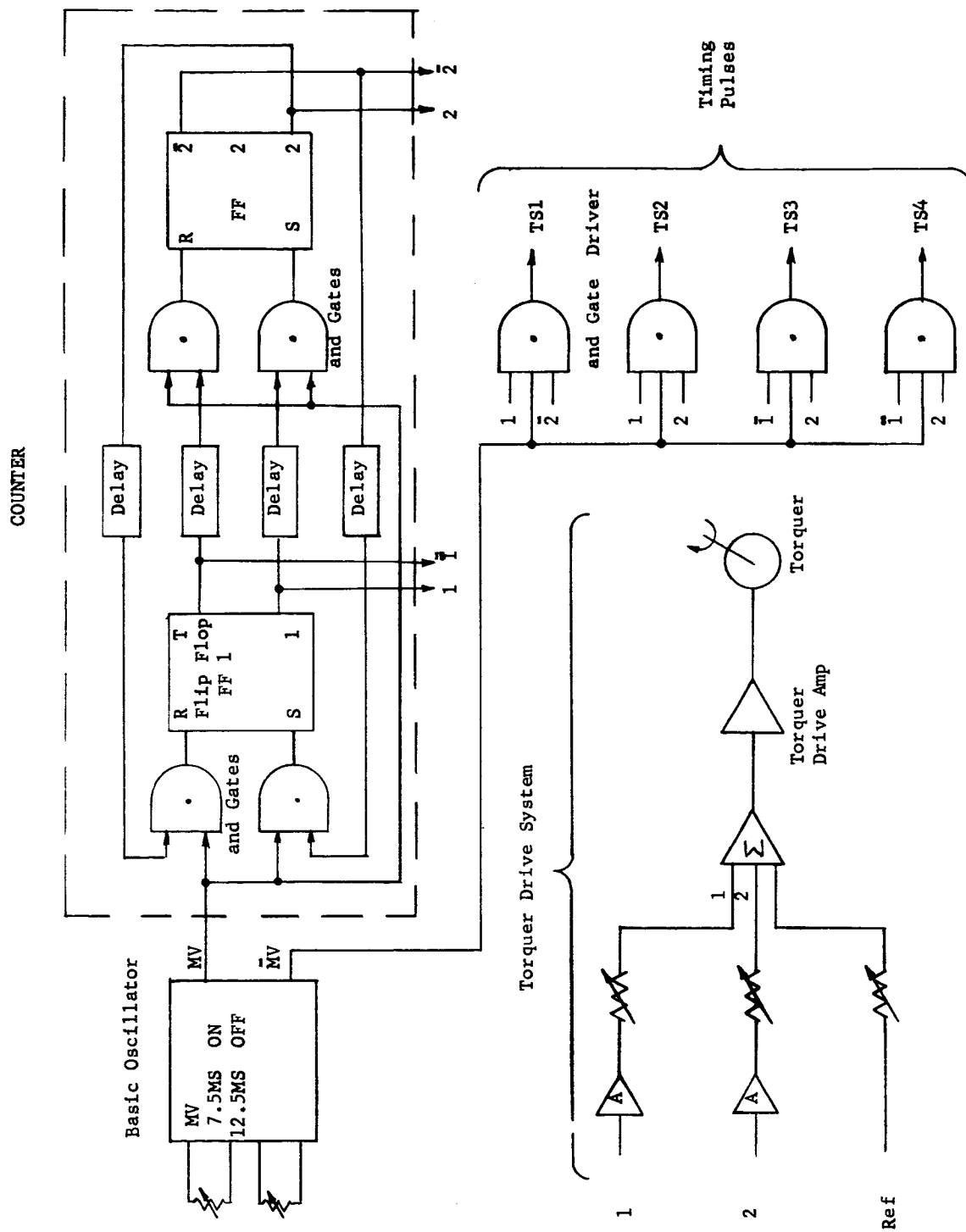


Figure 3. Gas Sensor Timing Generator

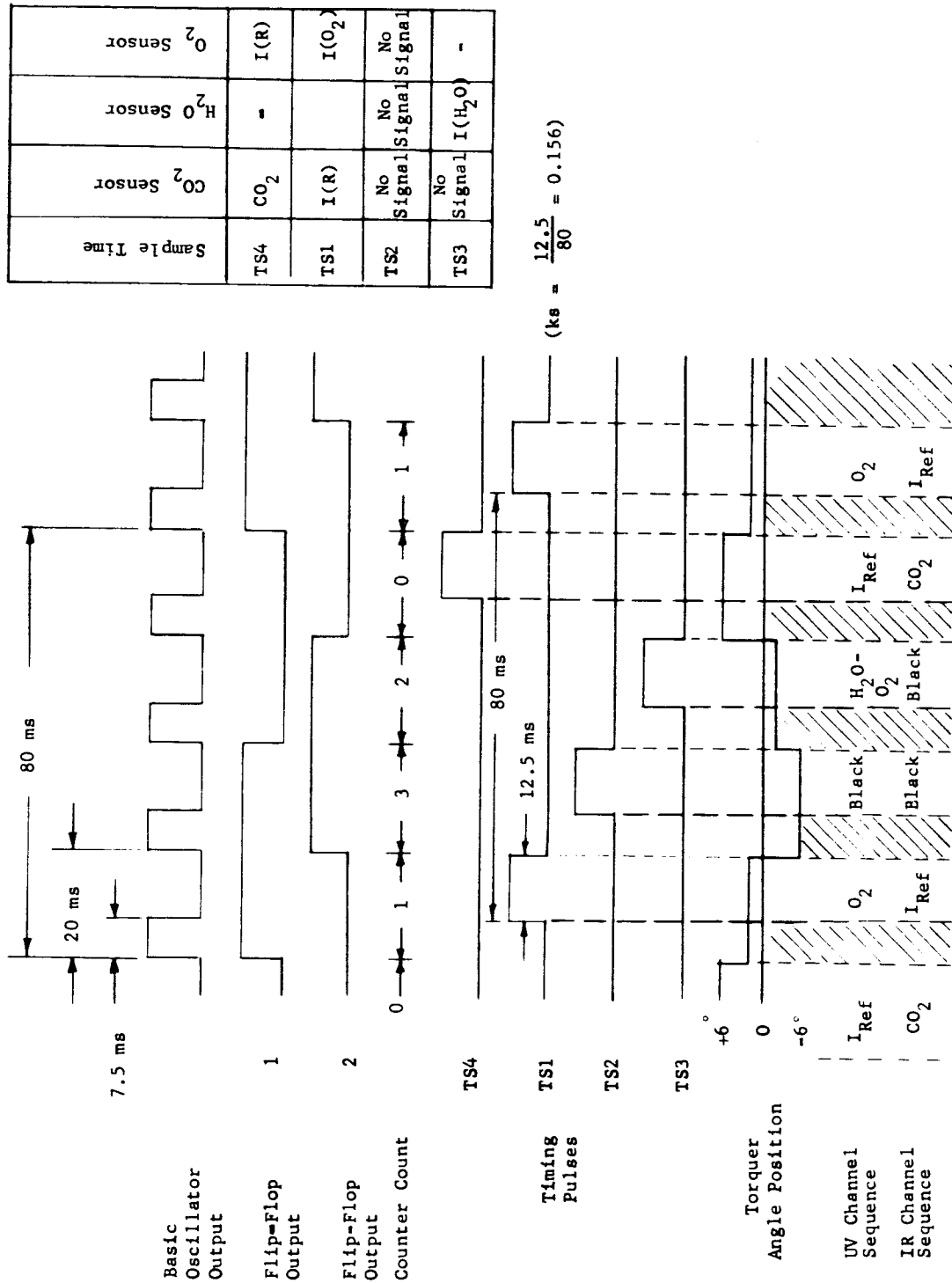


Figure 4. Torquer Timing Sequence

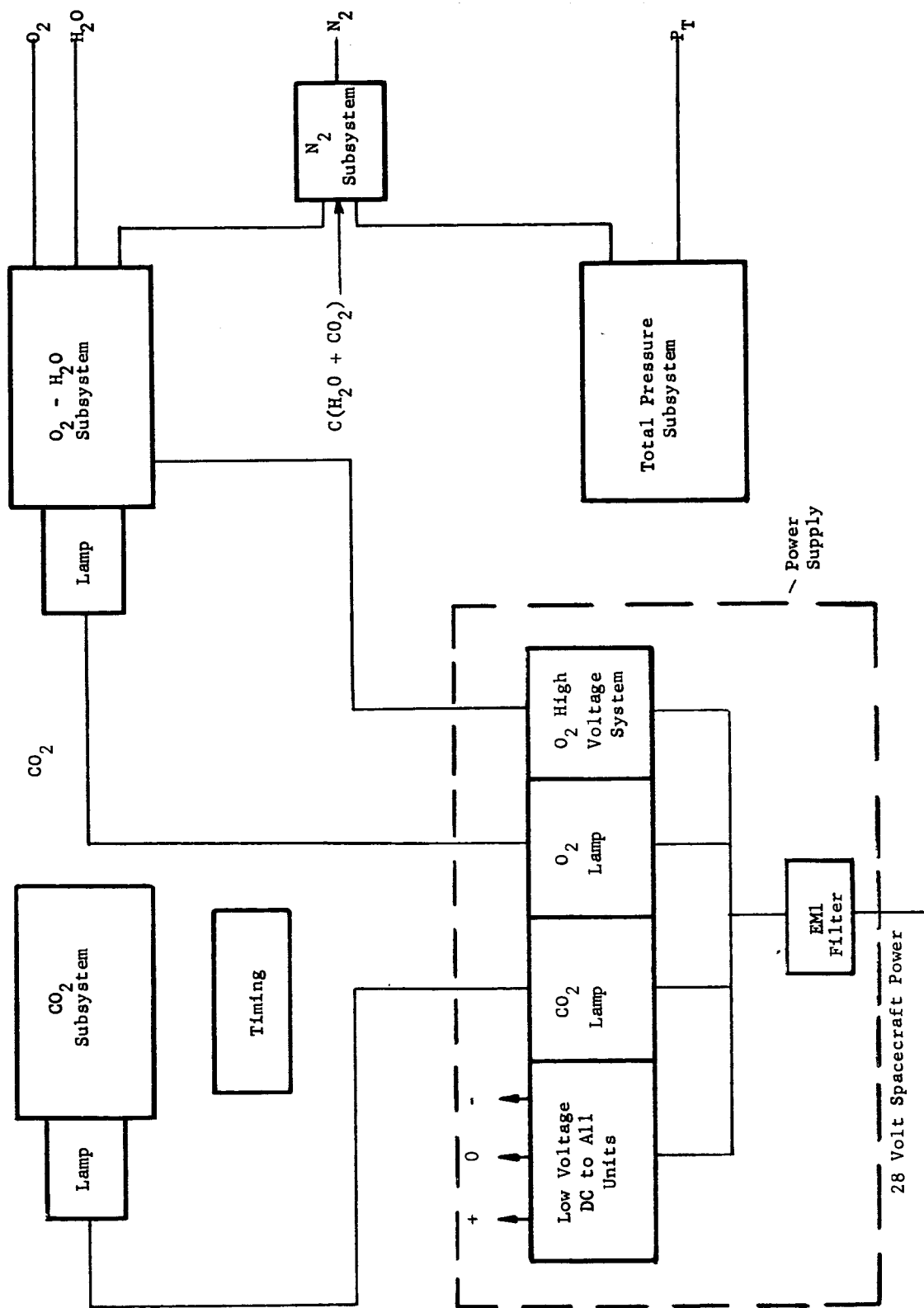


Figure 5. Electronic System Conceptual Block Diagram

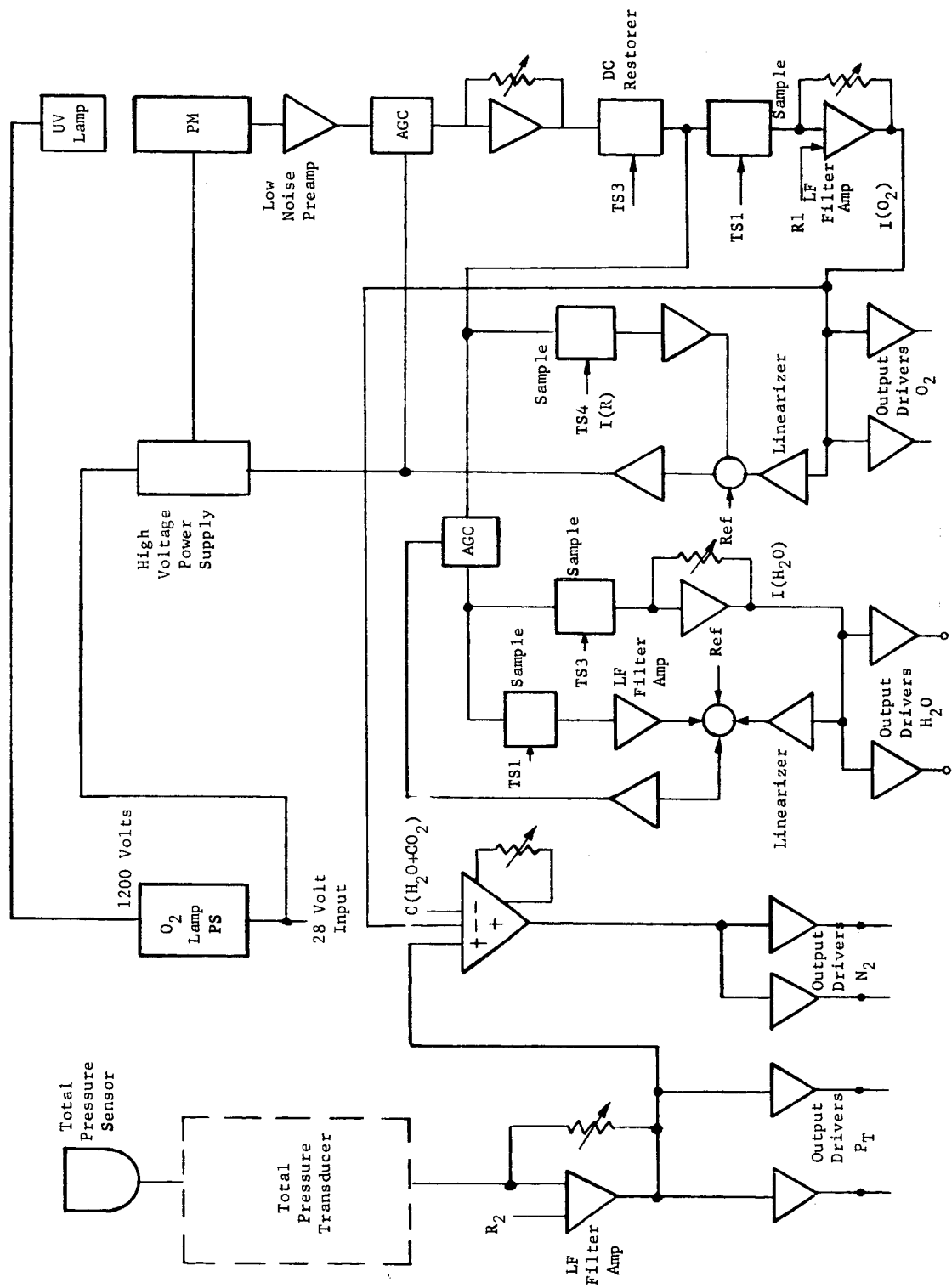


Figure 6. O_2 , H_2O , N_2 , and P_T Subsystems Schematic

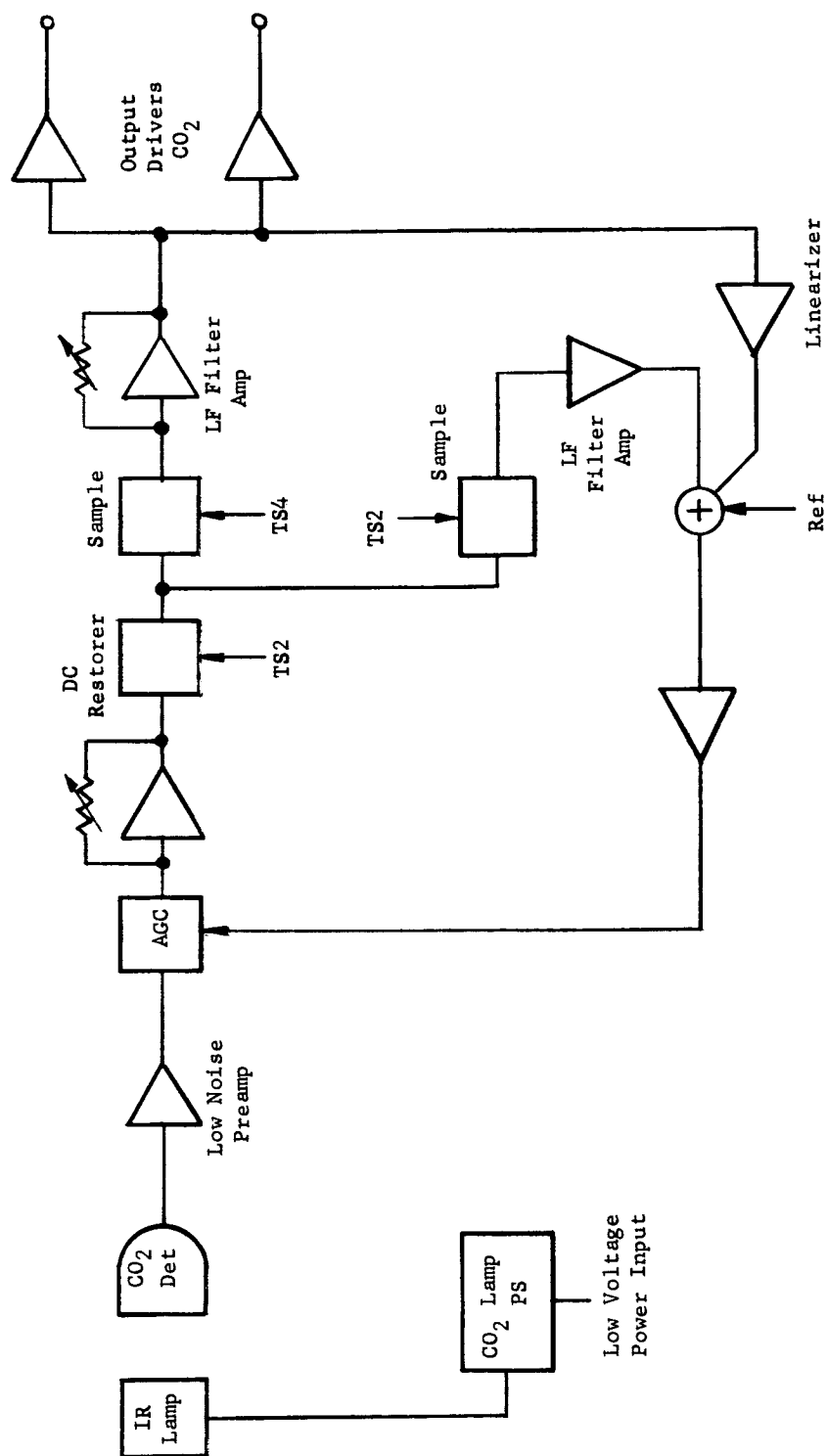


Figure 7. CO₂ Subsystem Schematic

converter and all other supplies will be DC isolated from the 28 VDC input voltage to meet Apollo grounding requirements, and will be driven from a common EMI filter to prevent any undesired RF radiation and to reduce susceptibility to RF conduction.

The system may be constructed with either conventional discrete components or a mixture of discrete components and microcircuits. Although no appreciable power savings is foreseen using microcircuits, a 20-30% savings in volume and weight can probably be realized. For this reason, and in the belief that the reliability of the units will be adequate for the intended missions, the use of microcircuits should be given serious consideration.

Mechanical, General

The recommended mechanical design concept, shown in Figure 1, is a natural development of present designs and has the advantage of the operating experience obtained from the Apollo CO₂ Sensor qualification tests and exhaustive design verification and production tests of that sensor and similar units.

The outstanding advantage of the proposed design is the complete accessibility to adjustments, particularly in the optical component sections. Provision is made to allow rotation, tilting, or lateral motion of the sources and detectors. Alignment of the ultraviolet system is achieved by the rotation of the grating about a line at its ruled surface. The folding mirrors and primary mirror are less critical and are mounted in predetermined positions. All of the optical elements are mounted on an optical bed of high dimensional stability, obtained by the utilization of multiple stiffening members in a dip-brazed housing as discussed in Paragraph 2.5.2.

The mounting of the detectors is not a difficult mechanical problem, however, a thermal analysis has shown that a major portion of optical misalignment with temperature occurs at the detectors because of their relatively larger size. Compensation for temperature-induced changes of the mechanical and optical alignment must be considered at the initial design phase. This is of primary importance in the recommended system due to the minute chopping geometry and miniature sized elements.

Interconnections between the sample cells and the total pressure transducer will be carefully made with primary emphasis being given to the integrity of the seals between the subsystems. A prewelded manifold with solder fittings is considered appropriate for this use. Fittings such as 1/16 O.D. internal swaging types may be used if space permits.

Electrical feed-throughs between the optical side and the electronics side of the sensor will be hermetic types permanently soldered in place for maximum sealing reliability. The entire optics side will be successively evacuated and back-filled with inert gas several times prior to final sealing. The cover seal will either be a molded in-place elastomeric

seal or a solder strip seal. In either method, the unit will meet the hermetic sealing specification of Grade A, MIL-S-8484, that is, a leakage rate of one cc/year per inch of seal, at one atmosphere differential pressure.

The gas connections to the sample point are standard 1/4 inch flare-tube fittings.

Optical, General

The optical design concept is based on system designs already implemented on similar sensors. These designs and their execution are demonstrations of Perkin-Elmer's optical capability and diversity of fabrication techniques. The system, shown in Figure 8, employs such widely diverse components as silicon meniscus lenses, Fabry-Perot type thin film filters, sapphire windows, special mirrors with ultraviolet coatings and a state-of-the-art plane grating. All of the optical elements are of special Perkin-Elmer design and are fabricated at Perkin-Elmer under close engineering supervision.

The principal design guide used in accomplishing the optical design was to make the system as small as possible within the bounds of the photometric requirements. The exhaustive design effort required to accomplish this task is indicated in Appendix B where the ray trace and image evaluation work is outlined.

The selection of the ultraviolet and infrared systems has been based on the best use of a particular technique in these applications, and not solely on a proficiency with one given method. In the infrared system, wavelength selective filters are moved past a fixed image, while in the ultraviolet system, a clear aperture or window is moved past monochromatic images which have been separated by a grating monochromator.

In the infrared system, the image of the source is brought to a sharp focus at the chopping plane to allow precise modulation of the optical energy obtained at the detector. The energy is then passed through a sample cell where the signal wavelength can be used to sense the concentration of the CO₂ in the gas mixture. This energy in turn is focused on the detectors and amplified by the electronics to suitable levels.

The ultraviolet system focuses the image of the entrance slit, which is illuminated by a discharge lamp, on the exit slit and detector. The grating receives collimated rays from the spherical mirror and reflects a spectrally separated pattern of the entrance slit at the chopping plane.

An understanding of the detailed function of the chopper, described in later sections, can be achieved by a brief description of the timing sequence used with a torsional chopper. As shown in Figure 9, when the angular position of the chopper reaches 6 degrees (an arbitrary angle) the slit coincides with an I_{ref} signal for the ultraviolet channel and places the infrared image on the 4.27 μ filter for the infrared channel. In reaching this

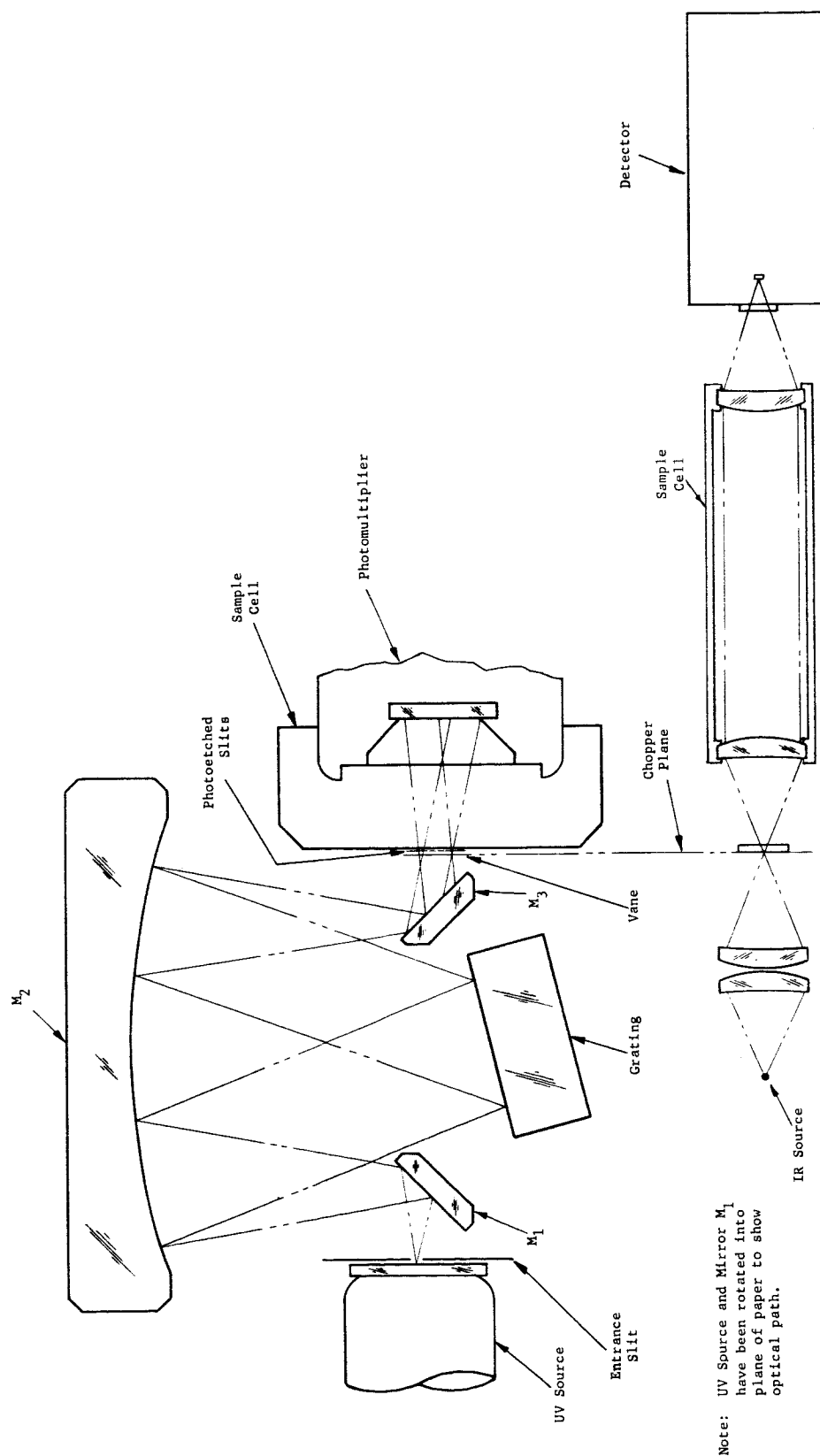


Figure 8. Two-Gas Atmosphere Sensor Optical Schematic

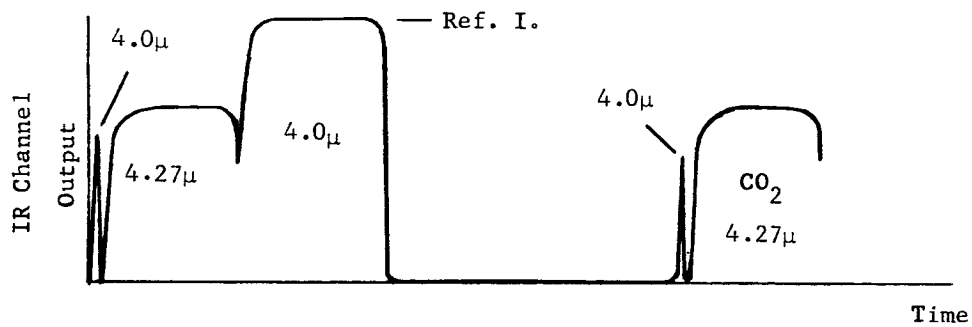
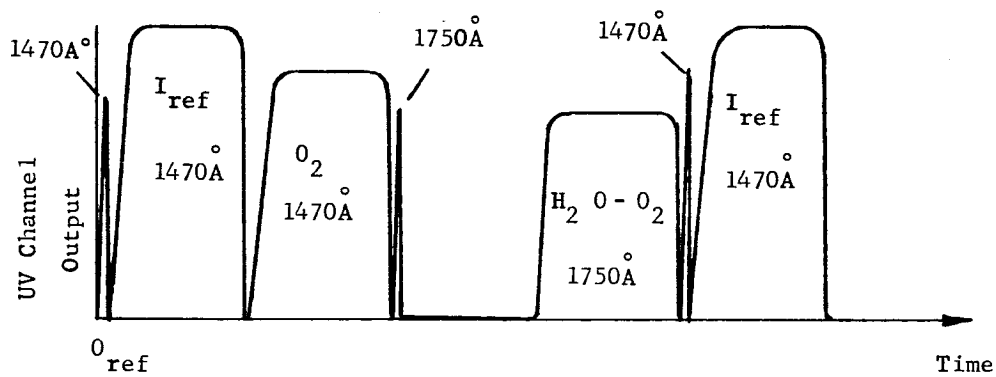
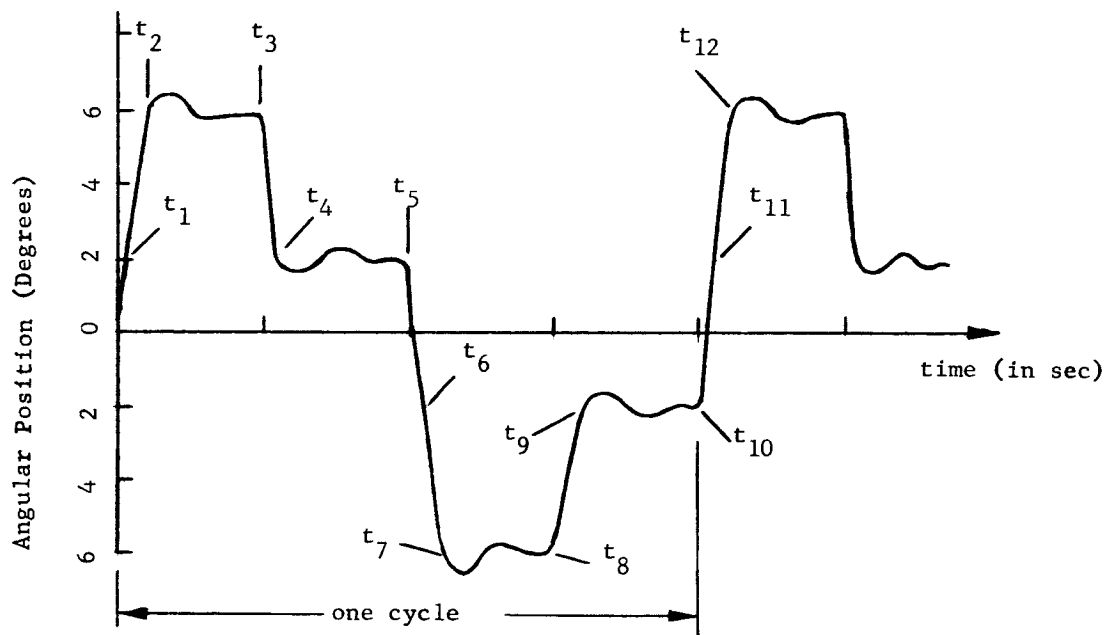


Figure 9. Torquer Angular Position and Optical Channel Outputs

point the chopper quickly passed by the 2 degree position which caused momentary signal spikes in both channels. It will be shown later that these signals will be blanked-out by the signal sampling mechanism. Switching at time t_3 to the 2 degree position results in the O₂ signal for the ultraviolet channel and places the 4.0 μ reference filter at the image of the infrared system. This sampling continues as detailed in Table I for the remaining portion of the cycle. It can be noted from Figure 4 that two zero reference modes are required by the infrared channel since it has one less signal path than the ultraviolet channel and shares the same chopper blade.

TABLE I
TIMING SEQUENCE

Time	Vane Position	Direction of Motor (observer facing detector)
t_0 (Initial Time)	Torquer commanded to +6° position	CW
t_1	1470Å and 4.0 μ transients (spikes) occur as vane passes through +2°	CW
t_2	Vane at +6° position. 1470-1560Å shutter vane passes radiation through 1560Å slit. 4.27 μ filter coincident with fixed CO ₂ mask permitting detector to monitor CO ₂ channel.	CW
t_3	Torquer commanded to +2° position	CCW
t_4	1470-1560Å shutter vane passes radiation through 1470Å slit. 4.0 μ filter coincident with fixed CO ₂ mask permitting detector to monitor reference channel	CCW
t_5	Torquer commanded to -6° position	CCW
t_6	1750Å transient (spike) occurs as vane passes through -2° position	CCW
t_7	Vane at -6° position. Vane totally blocks UV and IR radiation	CCW

TABLE I (Continued)		
<u>TIMING SEQUENCE</u>		
Time	Vane Position	Direction of Motor (observer facing detector)
t_8	Torquer commanded to -2° position	CW
t_9	1750Å shutter vane passes radiation through 1750Å slit	CW
t_{10}	Torquer commanded to $+6^\circ$ position	CW
t_{11}	1470Å and 4.0μ transients (spikes) occur as vane passes through $+2^\circ$	CW
t_{12}	Same as t_2	CW

NOTE

Shutters will be about 10% wider than the fixed slits so that electrical ringing will not be observed.

2.1 ULTRAVIOLET SUBSYSTEM (H₂O AND O₂ CHANNEL)

In the Two-Gas Atmosphere Sensor System the concentration of oxygen and water vapor is to be measured by observing the transmission of UV radiation through a fixed path length of sample gas. Spectral selectivity is obtained by a monochromator. An arc discharge source provides radiant power which is directed through the sample as monochromatic energy and into a wide band photoemissive detector, where its transmission is measured. The O₂ and H₂O subsystem is essentially an ultraviolet system developed for NASA for use on a metabolic rate sensor.

The transmission is logarithmically related to the absorption of the signal energy and, in a fixed length system, is also a function of the concentration of the sample gas at selected wavelengths. Appendix C discusses this relationship and the basic theory of transmission and absorption measurements.

The transmission characteristics of oxygen are quite transparent and uneventful from the far IR through the visible and into the near UV region. A few diffuse weak absorption bands appear between 5300Å and 7700Å as atmospheric

absorption bands, and at wavelengths as long as 1.04μ for the liquid state, but the strong bands for gaseous O_2 lie below 1900\AA . The absorption becomes very pronounced at this point and characterizes the entire region known as the vacuum ultraviolet. The detailed spectra of the O_2 absorption begins with the Schumann-Runge System, with its strong multiple bands and fine line structure. Figure 10 shows a high resolution spectral run of this region.

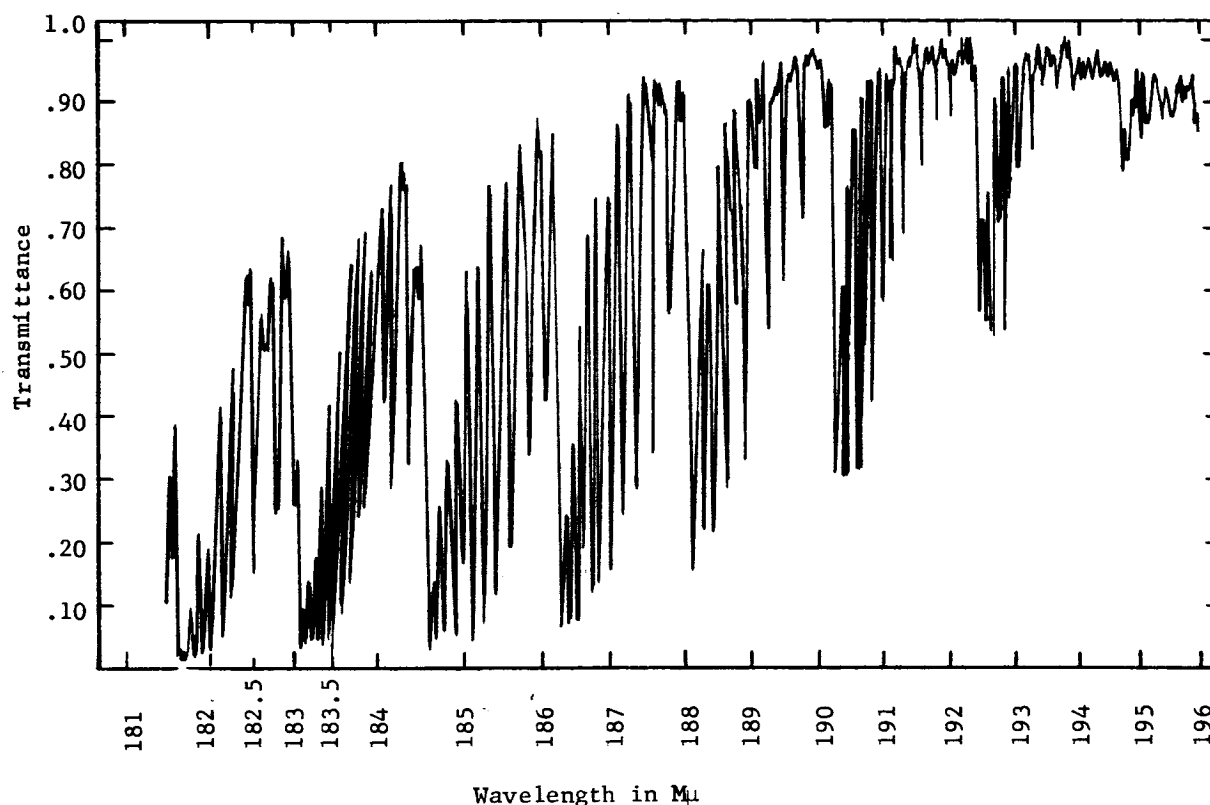


Figure 10. High Resolution, Far-Ultraviolet, Spectrum of Oxygen (Model 350)

The convergence limit for this system is at 1750.4\AA with the beginning of the system reported as high as 2221.0\AA . The regions beyond 1300\AA , toward the X-ray region, are extremely complex without any clear analytic region unique to oxygen alone. It may be of interest to note that several windows appear in the oxygen absorption spectra from 1000\AA to 1300\AA , but the characteristics of materials and components in this region make it presently less suitable than the region from 1300\AA to 1750\AA .

The continuum in the 1300\AA to 1750\AA region is characterized by a broad continuous absorption with a peak value at 1422\AA of an absorption coefficient to a natural log base of $402\text{ cm}^{-1} \pm 20\text{ cm}^{-1}$. The extreme absorption

represented by the coefficient of 400 cm^{-1} is equivalent to obtaining a 40% transmittance from a thickness of atmospheric air of only 0.0045 inch. This extreme sensitivity allows the miniature size used for the sample path lengths for the oxygen measurement.

The relationship between the water vapor absorption and the oxygen absorption in the 1300\AA to 1750\AA region is shown in Figure 11. The O_2 absorption is so much higher than the water vapor absorption at 1470\AA , that it is essentially independent of the water vapor. The significance of the 1470\AA wavelength is that it is the resonance line obtained from the xenon discharge lamp used for the UV source. A wavelength such as that at 1750\AA shows the maximum water to oxygen absorption index, or coefficient. By accurately establishing the oxygen concentration at 1470\AA wavelength, it is possible to stabilize the water vapor measurement with this oxygen signal. In this way, the effect of oxygen at the 1750\AA channel can be eliminated. This is a common technique used in spectroscopy, usually being accomplished by placing a pure solvent in the reference beam of a dual-beam system.

Radiation with wavelength equal to or shorter than 2423.65\AA will produce ozone from air or pure oxygen and the efficiency of the reaction increases with shorter wavelengths. Ozone is also decomposed by UV radiation so that an equilibrium concentration is difficult to determine analytically.

A number of methods exist for the determination of ozone. One of the oldest methods is the absorption of ozone in a buffered potassium iodine solution and the titration of the liberated iodine with a standard solution of sodium thiosulfate. The method is used as an ASTM standard procedure (D 1149-62T) and is well defined.⁸ An electrical adaptation of this method, called a Microcoulomb Ozone Sensor, with which the liberated iodine is measured using a polarized electrode, has been developed by the Mast Development Company of Davenport, Iowa.

UV absorption techniques can of course be used to determine ozone concentrations. Precautions must be taken since photodissociation of ozone in regions below 1600\AA produces oxygen which may interfere. Recent techniques minimize photodissociation during absorption measurements by placing the absorption cell between exit slit and the detector. (This is the method used in the Two-Gas Atmosphere Sensor.) In this manner, only the monochromatic energy is introduced into the sample cell. The total lamp output is therefore not available for the dissociation process.

Measurements have been made in an attempt to determine the concentration of CO caused by the 1650\AA dissociation. No measurable quantities have been observed.

Maximum system accuracy is to be obtained for the oxygen measurement by referencing the same wavelength as that used for the transmission measurement, rather than selecting another wavelength obtained from the xenon source. This will make the measurement independent of the shape of the spectral output from the source and will automatically compensate for any small changes of the resonance line obtained from the source.

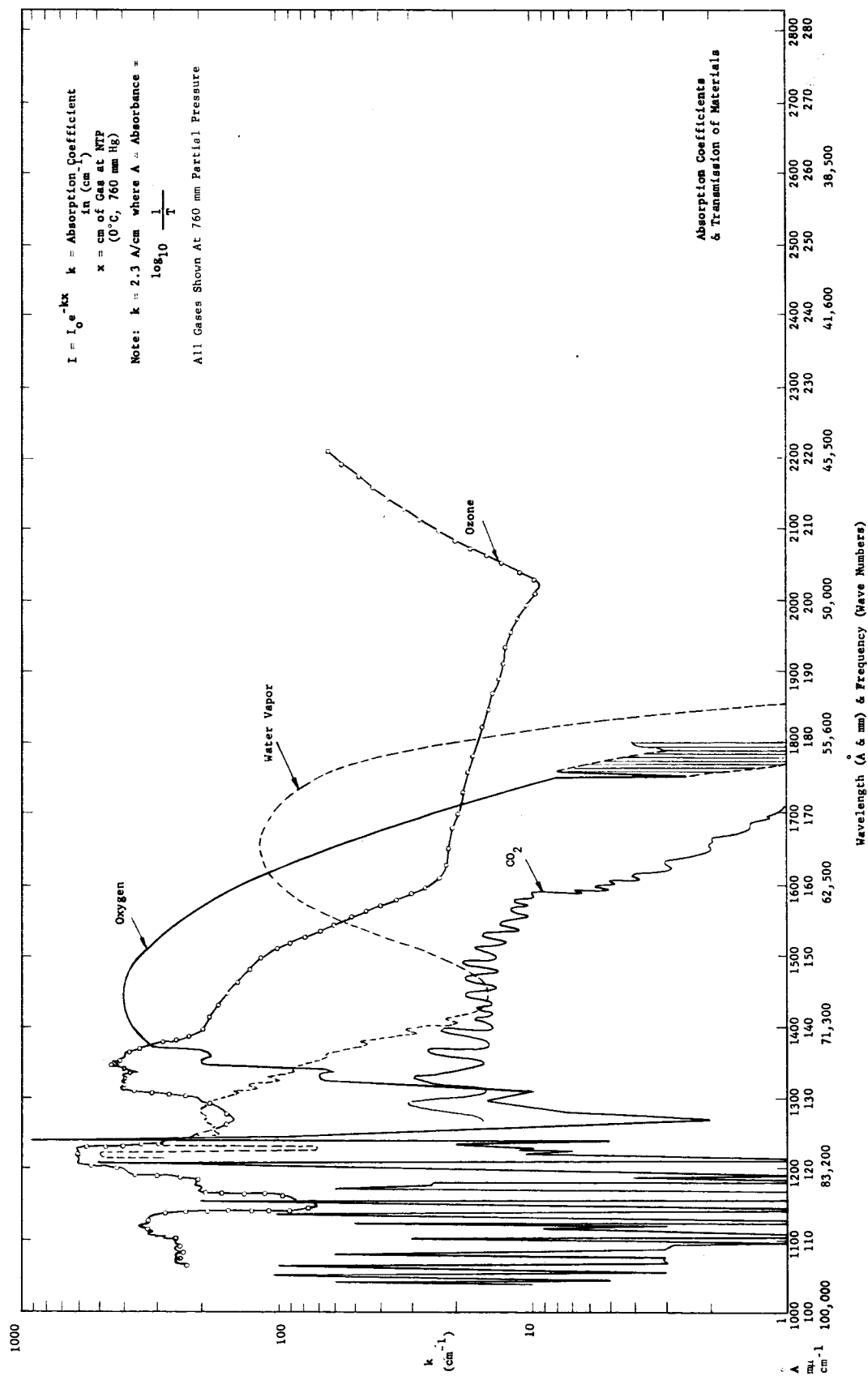


Figure 11. Relative Absorption of Gas Constituents

The absorption coefficients of molecular nitrogen have been measured with photoelectric scanning techniques using intense helium continuum light sources as background. These measurements show that nitrogen absorbs strongly in the vacuum ultraviolet at wavelengths shorter than about 1000Å. The absorption spectrum is complex with many strong bands which in some places are superimposed with ionization continua. For this reason, nitrogen may be used as a back fill gas in the UV monochromator operating at 1470Å-1750Å.

2.1.1 OPTICS - ULTRAVIOLET SUBSYSTEM

To meet, at the same time, the requirements for a fast system, small size, lightweight, maximum freedom from stray light and maximum throughput, a grating instrument of the Fastie-Ebert type was chosen.

A prism-type spectrometer is attractive from the point of compactness but optical losses and stray light are problems. A grating type spectrometer appeared to be required, but there are many ways of using diffraction gratings. Four designs were considered: Paschen, Eagle, Wadsworth, and Fastie-Ebert. These mountings are quite compact, with the exception of the Paschen mount, and offer concomitant saving in weight; however, the Eagle mounting turns out to be somewhat awkward geometrically. Both the Wadsworth and Fastie-Ebert mountings work out well geometrically to provide a good mechanical arrangement of all of the component parts. The chief advantage of the Wadsworth mounting is that it is about half as large as the same grating on a Rowland circle, which is used by both the Paschen and Eagle mounts. Resolving power is unchanged. While the Wadsworth has the added advantage of being stigmatic, the Fastie-Ebert has the advantage of being achromatic. In addition since the Fastie-Ebert mount employs a plane grating it is easier to control a uniform blaze angle during the ruling operation of the master.

An analysis of the astigmatism of the systems showed the astigmatic loss for the Paschen mounting to be about 95% and for the Fastie-Ebert, about 1%. Astigmatic losses in Eagle and Wadsworth mountings are typically very low. The efficiency of each mounting varies as the reflectivity of the system. When the system's reflectivity reaches 80%, the Fastie-Ebert plane mounting is far superior to the grazing incidence mounting and is comparable in efficiency to the other mounts considered.

The optical system consists of a Fastie-Ebert grating monochromator followed by a sample cell and detector. It was necessary to use a dispersive system, rather than a smaller filter system, since there are no filters suitable for this spectral region. Wherever possible, reflecting rather than transmitting elements have been used to permit better transmission of ultraviolet energy through the system.

It was apparent from this study that the Fastie-Ebert system offers considerable experimental advantages. For example, this monochromator is in focus for all wavelengths with fixed entrance and exit slits, fixed illumination angle, and fixed exit beam angle. Its scanning system requires only a simple rotation of the grating about a vertical axis through the grating face. This type of mount can be used effectively down to 1200Å because of the increased reflectivity obtained with aluminum and magnesium fluoride film combinations. An additional sophistication of our system is in the use of folding mirrors to eliminate stray light problems. By the use of these folding mirrors, appropriately placed at the entrance and exit slits, we have achieved a minimum volume design and have eliminated the problem of stray light bypassing the grating and energizing the detector. The particular arrangement worked out for the O₂ - H₂O channels is shown in Figure 8.

The detail functional description of the ultraviolet system may be more clearly understood by reference to Figure 8. The ultraviolet lamp, which is the source of the energy to be measured in the oxygen and water system, is supplied by a current regulated, DC high voltage supply. This supply is the result of many months of design effort on this and other programs. It has the capability of supplying constant current to the source lamp over a wide range of input voltages. This is important since both the peak intensity and the spectral distribution of the output power from the lamp is seriously affected by the input current drive to the lamp. By stabilizing the current we have reduced the excursions of the radiated energy and hence have reduced the requirements for the automatic gain control or ratio computation and stabilization.

The energy from the lamp passes through a high performance grating monochromator, which disperses the output energy and places the selected wavelengths at the proper slits to allow chopping by the torsional chopper.

The ultraviolet lamp (Part No. 607-1049) is a special xenon-filled arc lamp developed by Perkin-Elmer. The xenon (Xe) pressure is chosen to give an output to wavelengths as long as 2000Å, and a sharp peak at 1470Å (sample wavelength). By aligning the optics so that this sharp peak is centered on the sample slit, it can be determined that the selected wavelengths are emerging from both slits, since the separation of the slits and the dispersion of the monochromator are known.

The monochromator provides the means of obtaining energy from the source lamp at wavelengths centered at 1470Å and at 1750Å. Figure 11 shows the spectral absorption characteristic of oxygen and water vapor in the vacuum ultraviolet portion of the spectrum. It can be seen from this illustration that the maximum absorption of oxygen is near 1470Å. The maximum ratio of water vapor to oxygen is near 1750Å. With the concentrations encountered in the Two-Gas Atmosphere Sensor the 1470Å signal is almost entirely a result of the O₂ absorption. In the 1750Å region, the signal is made up of almost equal absorbences of oxygen and water vapor. By dividing the 1750Å signal, made up of the combined O₂ and H₂O, by that of 1470Å which is only the O₂, stabilized H₂O signal can be obtained.

The concave mirror, M_2 , renders the Xe source energy from the entrance slit parallel while relaying the energy to the plane grating, which is a standard Perkin-Elmer grating as shown in Figure 12. The reflective grating disperses the energy which is then brought to focus by the concave mirror. The grating efficiency is about 50% when properly flash-coated with aluminum and a protective coating of magnesium fluoride. The exit slits are placed at the image focal plane. In this configuration, the entrance and exit slits are at symmetric conjugate focal planes. Since the spectral range covered is small, relative astigmatism is minimized, resulting in a highly aberration free system. Mirrors M_1 and M_3 (Figure 13) are used to fold the system in order to conveniently package the source and detector.

Two exit slits will be positioned for radiation at $\lambda = 1470\text{\AA}$, and $\lambda = 1750\text{\AA}$. The exit slit heights and optical material attenuations in the sampling cells will be selected in order to equalize the spectral intensity incident upon the detector. The 1470\AA slit height will be divided into two approximately equal regions: one region for sample gas and the other for reference intensity measurements. This feature will provide more accurate oxygen measurements on a long term basis rather than relying on a continuum wavelength intensity emitted from the Xe source. To monitor the spectral channels sequentially with respect to time, a multiple opening shutter will be mounted to the chopper assembly and placed ahead of the exit slits. The details of the chopper are given in Section 2.1.3.

2.1.1.1 SAMPLE CELL

The chopped monochromatic energy passes through the spectral ultraviolet sample cell as shown in Figure 14. This sample cell uses sapphire windows of selected ultraviolet purity to contain the sample gas. The special design of the sample cell slits and the chopping blade of the torsional chopper allows the detector to observe, first a 1470\AA signal that passes through the gas in the sample cell and then a 1470\AA signal that passes through an empty sample cell. Thus, two signals of 1470\AA wavelengths are alternately received by the detector. The signal passing through the empty cell, which would be unattenuated by the gas, is used as the reference wavelength for the automatic gain control system. The 1470\AA and the 1750\AA signals, which pass through the gas in the sample cell, are the oxygen and the combined oxygen and water vapor signals respectively. By utilizing the same wavelength, that is, 1470\AA for both the gas signal and the reference signal, a system is obtained with maximum stabilization of the oxygen signal. Variations in spectral emission from the discharge lamp will then not affect the stabilization of the most important signal, that is, the oxygen signal. Of course, if there is a degradation or severe change in the spectral distribution of energy from the lamp, the water vapor signal will be affected. However, the system accuracy requirement for the water vapor signal is much less stringent than that for the oxygen signal.

Since, as previously indicated, the strong O_2 absorption dictates a very short path, the design of the sample cell becomes critical. The entire optical path, except for the 0.004 and 0.271-inch sample paths, is evacuated

Figure 12. Diffraction Grating

[illegible]

Figure 13. Folding Mirrors

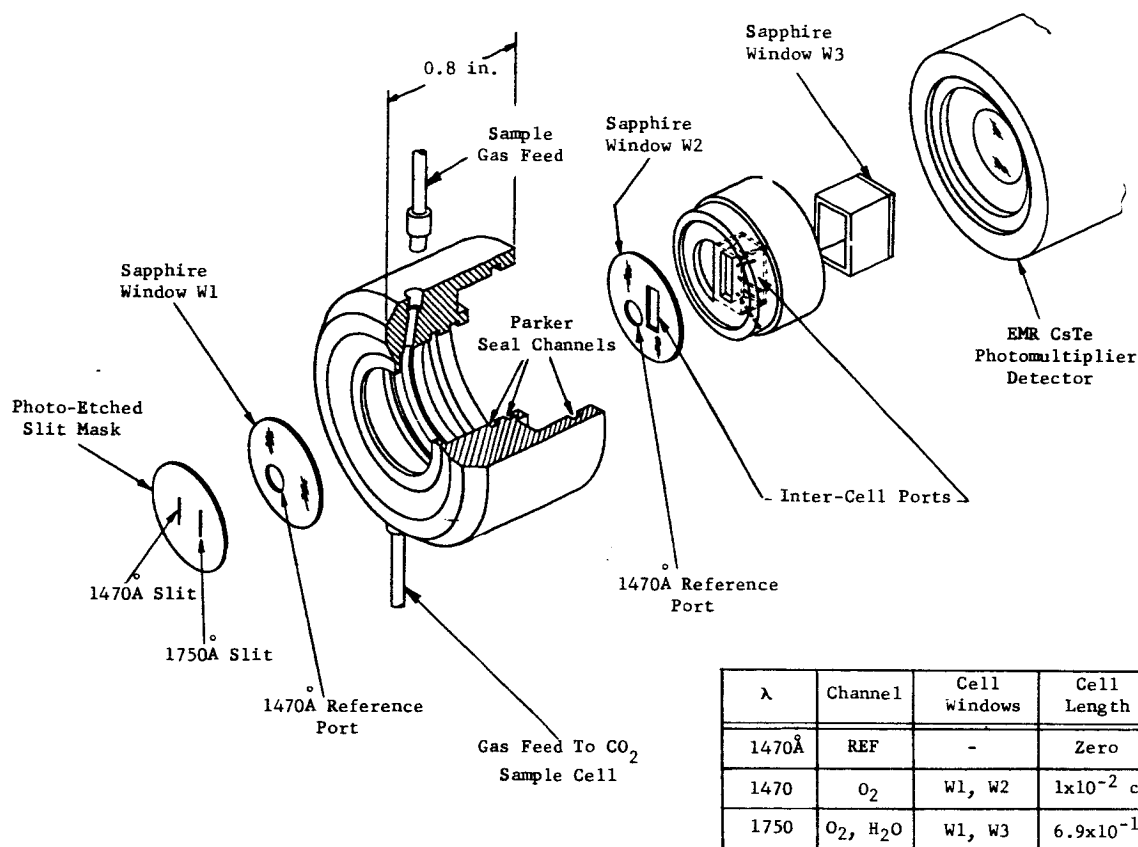


Figure 14. Ultraviolet Sample Cell

or filled with a non-absorbing gas such as N₂. The sample gas must pass through a cell in the optical path, but is sealed off from the rest of the optics. Finally, both the sample cells and optical chamber must be sealed off from the external environment.

The present design consists of 3 UV grade sapphire windows mounted as shown in Figure 14. The 0.004-inch (1×10^{-2} cm) cell has a fixed thickness set by a shim spacer epoxied in place. The 0.271-inch (6.9×10^{-1} cm) cell is adjustable so that oxygen absorption at 1750Å may be set to equal that at 1470Å. The first and second windows have ports to permit 1470Å reference radiation to reach the detector unattenuated by the sapphire. These ports also permit the volume immediately in front of the detector to be evacuated or filled with N₂. The two cells are pneumatically coupled together by a rectangular port in the second window and three holes located in the mechanical structure that holds the second window in place.

Calculations indicate that a path length of 0.004 inch (0.0102 cm) gives 41% transmittance at 1470Å, with an O₂ partial pressure of 181 mm Hg (3.5 psia), and that a path length of 0.271 inch (6.9×10^{-1} cm) gives the same transmittance at 1750Å if no water present or 22% transmittance with an O₂ partial pressure of 181 mm Hg (3.5 psia) and an H₂O partial pressure of 10 mm Hg.

2.1.1.2 OPTICAL MATERIALS

One of the essential efforts of the study was to review and define the characteristics of the useful components and materials for UV applications of the O₂ and H₂O sensor. The major types of components considered were optical materials, sources, and detectors and their utilization in a suitable monochromator for the specific application of the oxygen concentration determinations. There is little agreement evidenced in various UV characteristics of materials. Major emphasis, however, must be placed on the purity and surface condition of the materials. Quartz and sapphire, for instance, have a very wide range of grades of which only a few types are suitable for UV use. Calcium fluoride, which is generally preferred over lithium fluoride, except for extreme UV measurements, often has rare earth impurities with associated absorption bands in the near UV. Because of their high reflectance and good adherence to glass, evaporated aluminum films are the most frequently used coatings for first surface mirrors in the UV. The aluminum film has a higher reflectance than any other single film in most of the UV regions down to 1250Å. The techniques used for the evaporation of the films markedly influence the behavior of the mirrors. The pressures during deposition should be less than 2×10^{-5} mm of Hg and the evaporation should be extremely fast. Super pure aluminum is preferred. Heated substrates are generally not used since they increase surface roughness. The unprotected surface will show a decrease in reflectance as a thin film of aluminum oxide forms with age. This is overcome by either storage in a desiccator or evaporation of a protective film such as magnesium fluoride. This is the usual technique used at Perkin-Elmer. It can be anticipated that with proper techniques, reflectances in the order of 80% can be obtained to 1300Å. These considerations also apply to replicated gratings. The aluminum surface obtained from the replica process is not a good reflector for extreme UV applications and must have a flash coating of fresh aluminum with an immediate magnesium fluoride application. Using this method, efficiencies of the first order of 50% have been obtained at 1400Å. Unprepared surfaces, by comparison, could not be expected to offer more than a 3% efficiency at this wavelength.

For the system, aluminum surfaces overcoated with magnesium fluoride will be used for reflection, while calcium or lithium fluoride and UV purity aluminum oxide (sapphire) will be used for transmission elements. The sapphire will be employed in the sampling cells because of the water vapor present.

2.1.1.3 ALIGNMENT

In order to have the system optically aligned, it is necessary to have all elements approximately on axis and to have the system adjusted so the proper wavelengths pass through the slits.

Since placement of none of the optical elements, except the grating, has proven critical (the energy hitting the photomultiplier window is defocused), the entire system is aligned by designing the parts so that the

optical elements are in the proper places. Adjustments for rotating and tilting the mirrors have proven to be unnecessary. The only necessary adjustments were rotating the grating, so that 1470Å energy goes through the sample slit, and aligning the lamp in front of the entrance slit by moving it back and forth. Since the dispersion of the monochromator and the separation of the exit slits are known, one knows the wavelength emerging from the reference slit.

After the optics are aligned, it is necessary to equalize energies coming through the two slits. Since there is more energy at 1470Å than at 1750Å, the height of the 1470Å slit is trimmed. This gives roughly equal outputs.

An obvious simplification for future units will be to fabricate the exit slit assembly with a fixed distance between slits and a fixed slit width. This type of slit assembly will be photoetched. A height adjustment for the 1470Å slits will be included.

2.1.2 DETECTOR - ULTRAVIOLET SUBSYSTEM

Three detectors were considered for the Two-Gas Atmosphere Sensor. The first was an E.M.R. #54IF-08-18, which is an 18-stage solar-blind multiplier phototube with a CsTe photocathode and LiF window. This was the detector incorporated into the prototype oxygen sensor and gave a satisfactory signal-to-noise ratio, at a gain of 10^4 at 1400V. Its capability was greater than required. The second detector was an I.T.T. vacuum photodiode with a solar-blind CsTe photocathode, Model FW-156. This is essentially the same as the E.M.R. photomultiplier without any gain. No signal was discernible above the noise. The third detector was a miniature (large transistor size) photodiode, Electro-Optical Systems #UV100. This was not a solar-blind type and gave enough signal from the overhead fluorescent lights to easily saturate the preamplifier. When tested in the system, however, no signal could be seen above the noise. It is concluded that a photomultiplier is necessary, but it need only have a gain of 10^4 . The E.M.R. type used in the prototype O₂ sensor could probably be reduced in size by a factor of two and still retain the "ruggedized" configuration. A somewhat larger window and photocathode would be desirable to insure no vignetting of the window and probably simplify sample cell design.

Photoemissive detectors, such as photomultipliers, obtained their spectral characteristics from a cathode photoemissive surface and a particular window material. Complex and composite surfaces are available but in general the useful cathodes are characterized solar-blind detectors made of rubidium or cesium telluride, which cut off at about 3000Å. Window materials of UV grade sapphire or cleaved lithium fluoride are used to allow response down to beyond 1400Å.

Increased interest in the past few years in spectroscopy in the middle and far ultraviolet has supplied the impetus for the development of

photomultipliers specifically designed for these spectral regions. The spectral responses of these detectors have long wavelength cutoffs from the cathode characteristics. This serves as an efficient means of rejecting the scattered radiation in dispersive systems. Difficulty was encountered with lithium fluoride due to the large difference in thermal expansion between the lithium fluoride and the glass used for sealing the body of the photomultiplier.

The design considered for the Two-Gas Atmosphere Sensor would be the well-known venetian blind multiplier design, consisting of successive fused kovar and 7052 glass rings. Each Lallemand-type venetian blind dynode with associated field shaping grid is affixed directly to a kovar ring, which serves as an electrical feed-through. This design is extremely rugged and gives rise to minimal dark currents. Present investigations have been made with 18 dynode stage construction, however, it is anticipated that much smaller units would be used for the Two-Gas Atmosphere Sensor.

Because of the low vapor pressure and stability of the high work function photocathodes, the secondary electron emission characteristics of the dynodes are comparable and independent of the particular photocathode material. The gain of the configuration is extremely stable and the current amplification is reproducible within a few percent over periods of months. The anode dark current of this type configuration is extremely low, being equivalent to 10^{-16} watts input.

2.1.2.1 RELIABILITY ASPECTS

The UV photomultiplier selected for our application is of an extremely rugged construction, most suitable for the shock and vibration of space vehicles. No dynode mount bears its entire weight on lengthened stem leads. The resistors of a voltage divider network are welded between kovar rings, and the entire envelope is vacuum potted in an epoxy fiber glass sleeve. The potting compound is a silastic modified by EMR to make it suitable for use at 150°C.

A high confidence level has been established for EMR photomultiplier tubes both through tests conducted here and by customers. Periodically, vibration tests are made on representative tubes from 70 to 2000 cps at 35 g's to assure that high standards are being maintained.

A group of photomultiplier tubes of the 541 Series were subjected to shocks up to 465 g's for 1.1 millisecond duration by the Associated Testing Laboratories in Winter Park, Florida. Each tube was subjected to 5 successive shocks with electrical performance measured before and after each test. There was no detectable change in performance.

One Model 541F-08 tube was subjected to vibration tests along the transverse and vertical axes of the tube from 1000 to 3000 cps plus a random shake from 20 to 2000 cps at 11.5 g's. No changes in signal-to-noise versus voltage characteristics could be noted. The tube was also subjected to

repeated series of vibration runs in two transverse directions at two times this load factor and subsequently vibrated to destruction at 630 cps and 45 g's.

This particular test was made by the Solar Physics Branch at Goddard Space Flight Center of NASA. It was their observation that the welded joints of the voltage divider network resistors were sufficiently strong and that the glass structure could not be damaged under this type of vibration testing.

Successive life tests have been made in Princeton, New Jersey, on tubes of the 541 Series for two successive periods of 60 hours each to evaluate tube stability. Total measured fluctuation in performance was found to be less than 5%. However, this variation includes changes that may have occurred in test light sources which could not be separately monitored.

Kollsman Instrument Corporation has life tested the Model 541B for a total of 4000 hours with no significant change in performance.

From field information made available by Schlumberger Well Surveying Corporation in Houston, Texas, a test group of 25 photomultipliers was evaluated for a period of over 10,000 total hours without any failures.

The Lincoln Laboratories of Massachusetts Institute of Technology evaluated a Model 541A in a centrifuge under dynamic conditions. The acceleration load on the vertical axis of the tube was in excess of 175 g's with no noticeable change in the output signal during the test period.

Ball Brothers in Boulder, Colorado, has recently evaluated a Model 543A to determine if changes in gain are caused by vibrations up to 3000 cycles. Their tests indicated that the change in gain was certainly less than 2% and probably did not change at all.

These tests demonstrate the high degree of ruggedness and reliability that is achieved through a unique structural design and an elaborately controlled processing. As a consequence, ASCOP photomultipliers have been selected for use in Aerobee sounding rocket experiments, the Trailblazer program for atmospheric re-entry studies, Discoverer and Injun satellites, and balloon experiments by the University of Minnesota and Argonne National Laboratories. Both Sylvania Electric and Kollsman Instrument are using EMR ASCOP photomultipliers in their guidance control systems for space vehicles. All Orbiting Astronomical Observatories will have EMR tubes aboard as will POGO and the OSO.

The following are programs of national interest sponsored by NASA or DOD using EMR Photomultiplier Tubes:

Discoverer - A series of experiments designed to measure electromagnetic activity at or near the poles of the earth by the Air Force and Lawrence Radiation Laboratories.

Trailblazer - Programs for the study of atmospheric re-entry phenomena with work contributed by NASA/Langley and M.I.T. Lincoln Laboratories.

Injun - A study of the behavior of the magnetic belts surrounding the earth in an attempt to find out why the atmosphere behaves as it does. Satellite experiments sponsored by NASA with the State University of Iowa as the principal investigator.

Orbiting Astronomical Observatory - A current program to orbit three separate satellites to map the radiant intensity of stars and nebulosities in the ultraviolet over a 12-month period. The experiments, being designed by Smithsonian Institute, NASA/Goddard, University of Wisconsin, and Princeton University will carry modern astronomy a giant step ahead in understanding the universe.

Orbiting Solar Observatory - A study of the electromagnetic radiation from the sun in the ultraviolet, x-ray, and gamma ray regions. The program satellites are being built by Ball Brothers in Boulder, Colorado, with ultraviolet spectrometers being provided by NASA/Goddard and zodiacal light telescopes by the University of Minnesota.

Polar Orbiting Geophysical Observatories - A group of experiments integrated by S.T.L. with contributions from NASA/Goddard and J.P.L. in the design of spectrometers and photometers to measure auroral spectra and intensities.

Mariner C - A fly-by space vehicle designed and being built by J.P.L. with UV photometers to measure the vacuum ultraviolet radiation in space from the planet Mars.

Operation Tabstone - A series of projects funded by ARPA for surveillance systems of various types.

EMR Photomultipliers, because of their ruggedness, sensitivity, and stability are also being used on large numbers of space probes being boosted by Aerobee rockets to study airglow in the upper atmosphere. The major experimenters have been J.P.L. and Johns-Hopkins University. Also, photoelectric scanners using EMR tubes are being used by Astronomers to study the death of stars. EMR tubes have played a major role in these instruments because of their high sensitivity and low dark currents.

2.1.3 CHOPPER - ULTRAVIOLET SUBSYSTEM

As shown in Figure 9, which is the torquer angular position and optical channel outputs, the UV channel output (the signal obtained by the UV

detector) consists of four different levels of information. The first is the reference signal obtained from the 1470Å signal passing through an empty sample cell. The second is the 1470Å signal passing through the gaseous sample cell. The third is a zero reference signal obtained by blanking the optical signal. Finally, the fourth is the 1750Å signal that passes through the gaseous sample cell. This sequence of signals is repeated each cycle. The four levels of signals are obtained at four discrete steps in the position of the chopper blade, which is driven by a torquer motor.

The torquer motor is a low power, wide band device with flexure bearings. Perkin-Elmer has had good results in using torque motors of this type in previous equipment. The TIROS radiometer application is an example. The chopper blade will move through the described sequential operations at a rate of between 10 and 25 cycles per second. The torsional chopper is electronically controlled in a closed loop system to provide the proper damping and frequency control. Our experience has shown that this device requires a much less sophisticated system than that now used with a tuning fork chopper.

A discussion of the relative merits of the two chopping systems, that is, a tuning fork chopper versus a torsional chopper, is discussed in detail in paragraph 2.5.3.4. The torsional chopper with flexure bearings has the advantage that it can be made to dwell at a particular location in space, allowing the maximum amount of information to be transmitted to the detector. Additionally, being a wide band device very similar to a DC meter movement, it can respond to square wave inputs and can be programmed to stop at particular images in space. It is felt, because of this characteristic, that the torsional chopper is more appropriate for this application where several slits or images are required to be combined on one detector. It is also our belief that the torsional chopper will provide the best signal information and will permit maximum utilization of space for a two channel system. It should be noted that the torsional chopper does not require lubrication and that during operation, its flexure bearings would be stressed at angular rotations much below rating to ensure long life.

Because of the dwell time provided by the torsional chopper, a sampling method of detection of the signal information can be used. This is a decided advantage since minor variations in the chopping geometry of the signal can be effectively blanked out in the signal processing channel. This is an improvement over present methods, which use the extraction of a Fourier component from complex wave forms to provide the information for the signal and reference channels.

2.1.4 SOURCE - ULTRAVIOLET SUBSYSTEM

In order to instrument the UV absorption method of determining gaseous oxygen concentrations, it has been necessary to design a special source of radiant power for use in a particular spectral region. That is,

in a region determined by the natural absorption characteristics of the gas. Many additional restrictions have been imposed on this design by the proposed end-item suitability for use with space flight instrumentation. The more significant of these are: low input power, small size, low temperature operation, inherent ruggedness, and long life. These requirements have essentially been met by lamps already designed for other NASA programs.

The spectral radiance requirement of providing power beyond 2000Å at low temperatures has eliminated any consideration of incandescent sources. Only enclosed, low pressure gas discharge sources were considered in this design. Suitable sources which were considered may be arbitrarily grouped into four categories: 1) hollow cathode glow lamps; 2) cold cathode mercury lamps; 3) hot cathode mercury lamps; and 4) rare gas arcs.

The hollow cathode glow lamp offers the richest yield of lines in the oxygen UV region. With suitable design, careful test and operating life evaluations it would be feasible to meet all of the requirements. The lamp's drawback is in its low absolute emission and lack of a continuum. No suitable commercial lamps are available.

Cold cathode mercury lamps operating in an arc discharge provide two intense, well defined resonance lines in the UV at 1849Å, and 2537Å. They require several hundred volts to start but may be started and operated well within the power requirements. They offer cool operation and have less sputtering problems than the hollow cathode lamps, hence they may be made much smaller.

An effort was made to design a lamp with a filament for lower voltage operation at higher currents. The filament provided the heat necessary to vaporize the mercury for starting. Initial results were encouraging in that a special lamp was fabricated which met our specifications.

Sealing to quartz and providing a reliable and useful window appeared to be the major problems.

The emphasis was moved from mercury lamp to lamps using rare gas discharges, when the spectral requirement for extreme UV operation was recognized. Rare gases, when properly operated in an arc discharge, exhibit very similar spectral emission characteristics. They each start emitting at their respective resonance lines and provide continua that decline in intensity toward the longer wavelengths. The continuum of xenon is the most intense of all the rare gases. It is obtained with reasonable intensity at the lowest pressure, except for helium. The spectral characteristics of the rare gas discharge lamps are summarized below:

Gas	Resonance Line	Long Wavelength Limit of Continuum
Xe	1470Å	2200Å
Kr	1236Å	1800Å

Gas	Resonance Line	Long Wavelength Limit of Continuum
A	1067Å	1650Å
Ne	744Å	1050Å
He	600Å	1050Å (Hopefield Continua)

One design for a xenon lamp is shown in Figure 15. The major problem in its design is the poisoning of the xenon by the window sealant and its subsequent early failure. This problem can be overcome by the application of fabrication techniques already developed by our laser group.

Several early prototype designs were built during 1965 to evaluate the performance of this type of design. Studies were made to determine the gap length required, the xenon pressure in the lamp, the materials to be used for the electrodes, and the processes and procedures necessary to insure the proper performance of this lamp. Of prime importance was obtaining the xenon continuum at a relatively low power, preferably less than one watt. These efforts were quite successful in providing prototype designs of xenon lamps operating from one-half to one-watt total input power, in both AC and DC modes of operation, with a controlled spectral output exactly as characterized by the higher pressure lamps found in the literature. That is, a strong resonance line followed by a broadening toward the infrared portion of the spectra. From the resultant spectrum, shown in Figure 16, it can be seen that energy is available from 1470Å to well beyond 1750Å. Extensive design effort has gone into developing of a suitable drive circuit for this lamp. Early efforts were made at an arc discharge rate of 5-10,000 cycles/second. However, actual measurements made on a vacuum monochromator have shown that suitable performance can also be obtained with direct voltage drive on the lamp. Power is sufficiently low to preclude the possibility of early failures or degradation of performance due to the most common arc lamp failure mode, that is, sputtering of the cathode.

An additional consideration in the design of these source lamps is the sealing required for the windows. Of course the window material must be transparent to the UV radiant power. This limits the use of the most common window materials and allows only the use of either high purity UV grade sapphire or crystal material such as calcium fluoride or cleaved lithium fluoride. Our present designs use calcium fluoride, although this is not considered to be the most satisfactory material, because of the sealing problems that may be encountered. Because the xenon is easily poisoned by the cement used to hold the window to the body of the lamp and because the cement epoxy, or other materials, used to hold the window to the body of the lamp, cannot withstand high bake-out temperatures, it is difficult to clean out the lamps sufficiently to prevent contamination, which will change the spectral output and have an unknown effect on the reliability and long life of the lamps. Barium getters have been used successfully in

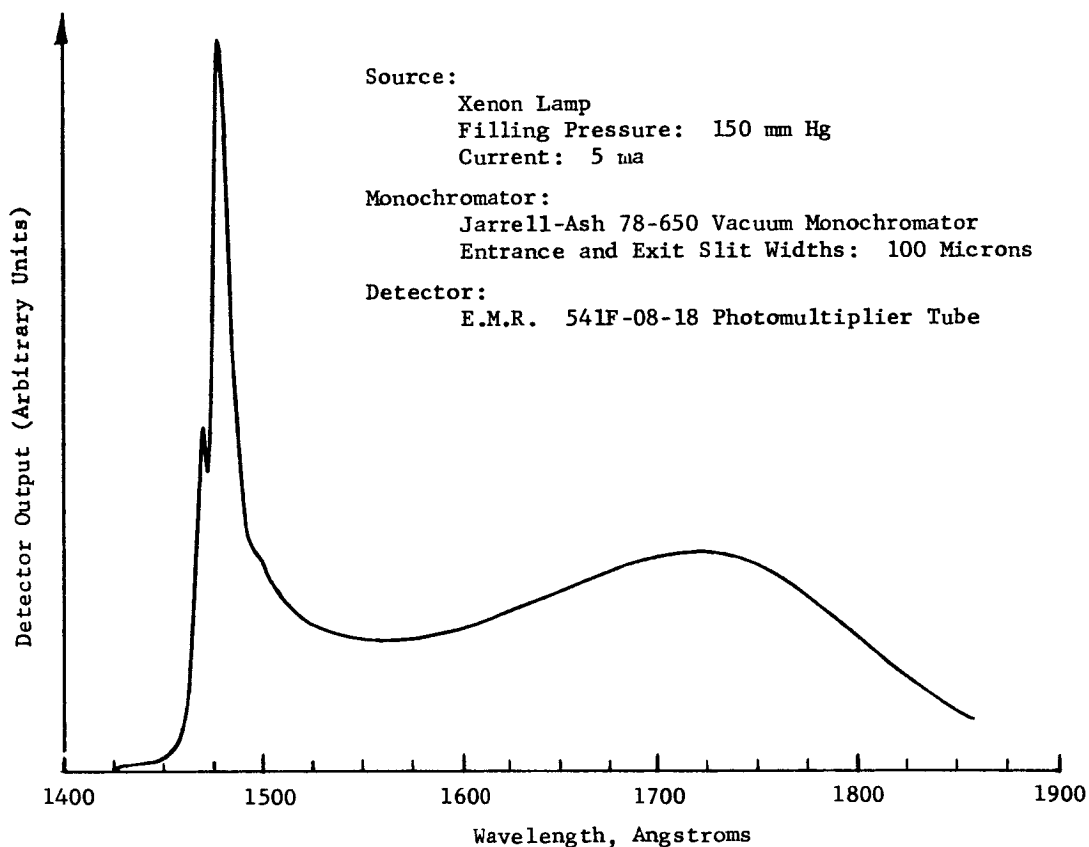


Figure 16. Spectral Output of Xenon Lamp

the lamps and have allowed operation of some lamps for periods of months. No failures of any lamps have occurred due to leakages over time or changes in characteristics, which could not be contributed to either breakage of the lamp or gross leaks resulting from mechanical stresses of mounts or other malfunctions. No sputtering has been evident in any of the lamps tested by us. It would be of great interest to design a lamp using a high purity sapphire window that could be fused to the glass to obtain a seal that would be compatible with high bake-out temperatures. Efforts would be made in the design phase to perfect such a design and obtain working prototype models for tests and possibly final production units. Some problems have occurred with the present lamp in determining the exact position of the arc in space. Stabilization of the position of this arc has been difficult. One possible solution to this problem would be the design of capillary lamps in which the arc would be limited to the bore of a capillary tube connecting two volumes. This is a typical configuration seen by small laser tubes. Several bodies of this type have been made up, but have been unsuccessful in our experiments to date. In conclusion, various improvements in the design are anticipated, but in any case present designs are adequate for laboratory analysis and may be suitable for the actual installation of production units. Testing and the area of improved source design will be efforts of the Phase II portion of the program.

2.1.5 ELECTRONICS-ULTRAVIOLET SUBSYSTEM

The electronic system consists essentially of two AGC loops, each of which provides an analog ratio computation; in the first loop, the circuit automatically and continuously divides the combined oxygen and reference signal to provide a stabilized oxygen signal. The second AGC loop works in a similar manner. In that case the water vapor, oxygen, and reference signal is divided by the oxygen and reference signal to yield a stabilized water vapor signal. The switching system that provides this sequence of operation is shown in the torquer timing sequence diagram of Figure 4. As can be seen from this illustration, the timing pulses are shorter in duration than the position of the torquer angular position. Therefore, the leading edge of the signal pulse, which may contain a transient, is blanked out from the signal processing information.

The stabilized electrical output from the oxygen channel is combined in an analog summing circuit with the signal from the total pressure transducer. In addition, a constant, representing a contribution of the H_2O and CO_2 concentrations is added as a third signal in this circuit. The output of the circuit is then related to the partial pressure of nitrogen. Each of the four outputs provided by the UV channel and total pressure transducer is provided with redundant outputs, which are electrically independent of each other.

The signal processing electronics for the Oxygen (O_2), Water Vapor (H_2O), and Nitrogen (N_2) subsystems, are described in detail in the following paragraphs.

2.1.5.1 OXYGEN (O_2) SUBSYSTEM

The subsystem is based on the use of a photomultiplier detector-amplifier. This requires about 1000 to 1500 volts for operation, and will be encapsulated to eliminate any corona or arcing tendencies. The supply for this is under control of the subsystem automatic gain control loop (AGC), thus, the voltage automatically increases or decreases to compensate for long term light or gain changes. The output of the photomultiplier is wideband amplified and passed through a second AGC stage. The second stage works in conjunction with the variable high voltage power supply to compensate for long term signal shifts (a detail design may show that only one of the two AGC controls is actually required). The signal is then amplified and passed on to the sampling system. The signal at the output of the dc restorer appears as shown in Figure 17.

Either this signal, or its reverse polarity, may be processed by sampling. In the former case, TS_2 is used for dc restoration, establishing the voltage during that interval as the system zero, then, TS_1 is used to sample for the oxygen intensity and TS_4 the reference intensity. Thus, the processing block diagram becomes as shown in Figure 18.

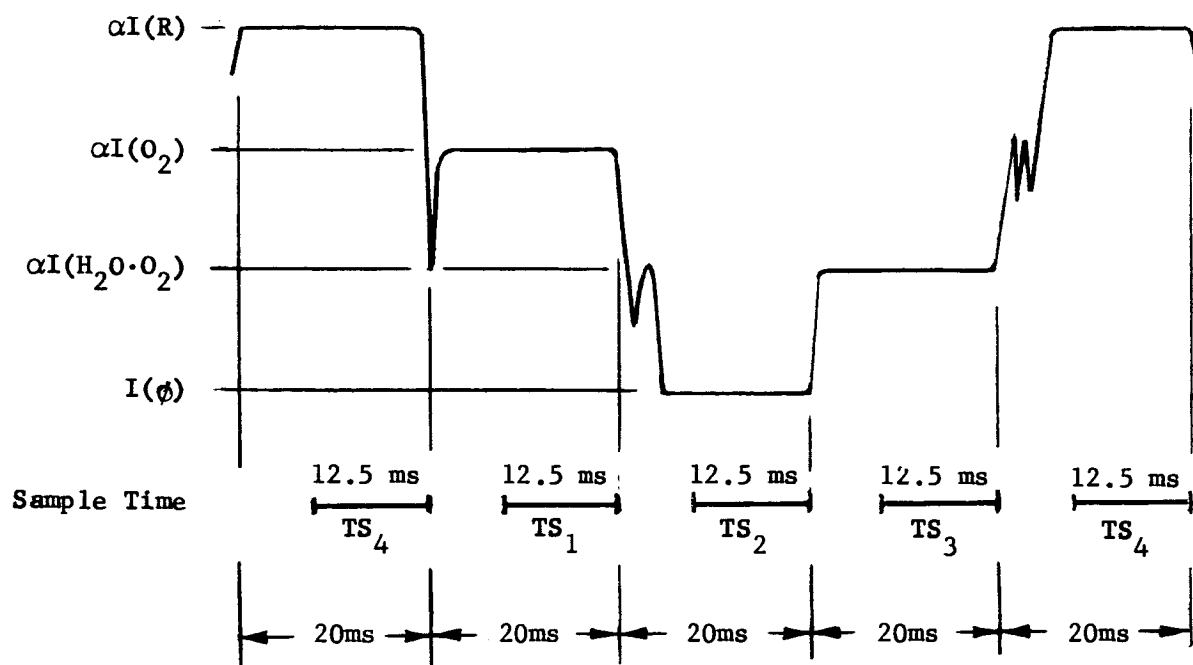


Figure 17. DC Restorer Output Signal

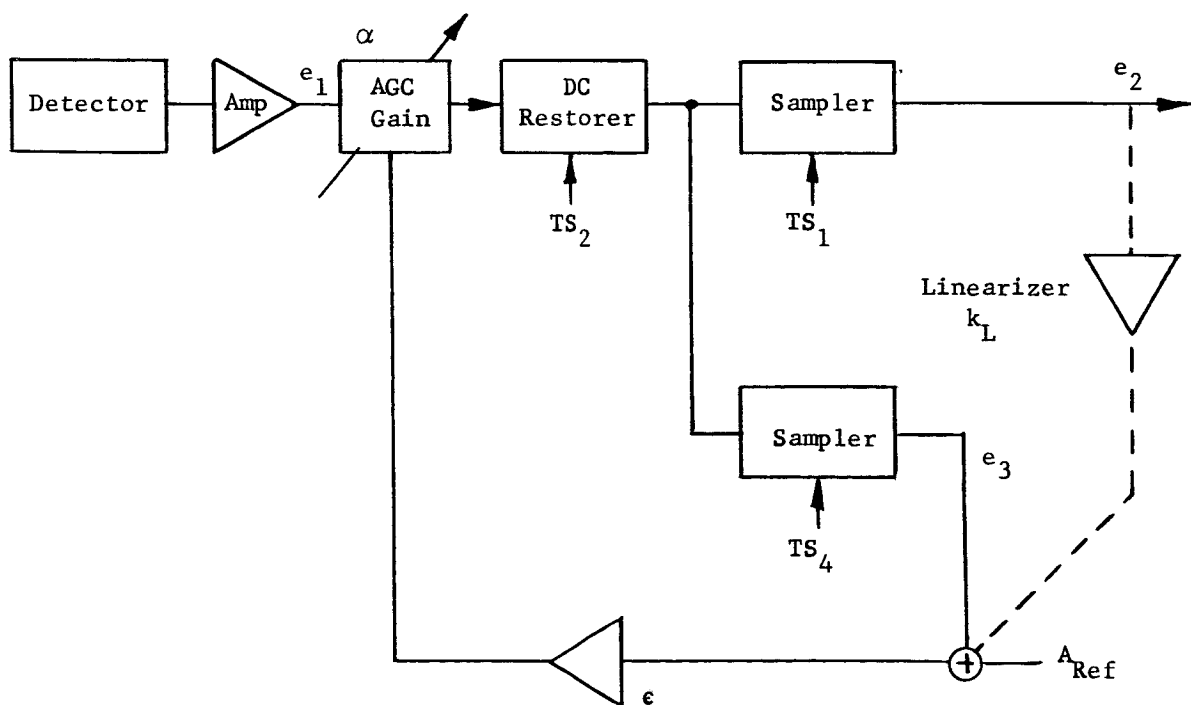


Figure 18. Processing Block Diagram

An analysis of the signal processing shows that:

$$e_2 = \alpha k_1 I(O_2)$$

$$e_3 = \alpha k_2 I(R)$$

where

$$k_1 = \text{gain constant, signal channel}$$

$$k_2 = \text{gain constant, AGC channel}$$

but,

$$\epsilon = e_3 - A \xrightarrow{\text{as a limit}} 0$$

or,

$$\alpha k_2 I(R) - A = 0$$

hence,

$$\alpha = \frac{A}{k_2 I(R)}$$

thus,

$$e_2 = \frac{A k_1 I(O_2)}{k_2 I(R)}, \text{ which is a direct measure of the oxygen/reference ratio.}$$

If the signal polarity is reversed, and the timing of the dc restorer and AGC channels are interchanged, the processing becomes:

$$e_2 = \alpha k_1 [I(R) - I(O_2)]$$

$$e_3 = \alpha k_2 I(R)$$

and,

$$\epsilon = e_3 - A = \alpha k_2 I(R) - A \xrightarrow{\text{as a limit}} 0$$

hence,

$$\alpha = \frac{A}{k_2 I(R)}$$

thus,

$$e_2 = \frac{Ak_1 [I(R) - I(0_2)]}{k_2 I(R)} = \frac{Ak_1}{k_2} \left[1 - \frac{I(0_2)}{I(R)} \right],$$

which also is a direct measure of the oxygen/reference ratio.

Note that in either form, the signal processing is directly linear, and that cross-coupling between the data channel and the AGC is not required to achieve linearity (as is the case for the present CO₂ detector).

Since it is an objective to make the overall system linear, and since the gas absorption is exponential, it is desirable to introduce a non-linearity into the system. This is achieved by a "linearizer" stage shown in dotted lines on Figure 18. This takes a fraction of the output signal and employs it to modify the system gain. In this case:

$$\epsilon = \alpha k_2 I(R) - A - \alpha k_1 k_L I(0_2) \xrightarrow{\text{as a limit}} 0$$

hence,

$$\alpha = \frac{A}{k_2 I(R) - k_1 k_L I(0_2)}$$

thus,

$$e_2 = \frac{Ak_1 I(0_2)}{k_2 I(R) - k_1 k_L I(0_2)}$$

or, if the signal polarity is reversed

$$e_2 = \frac{Ak_1 [I(R) - I(0_2)]}{k_2 I(R) - k_1 k_L [I(R) - I(0_2)]}$$

thus, the linearity of the entire signal system can be modified as desired by the selection of the value of k_L .

The sampling demodulation system is analyzed in detail in Appendix A, Paragraph 2.3, and summarized in Paragraph 2.4.3.B. From this analysis it is evident that the sampling duty cycle, k_s , establishes both the signal and noise output power; both decreasing with a decreasing k_s . In order to maintain a reasonable S/N power ratio, it has been pointed out that k_s should be held as high as practical, and in this case is in the order of 0.156. Although it might appear that slight variations in k_s would upset the calibration,

this can be prevented by employing an integrating sample and hold circuit. Such a circuit is relatively insensitive to variations in k_s , and is instrumented simply as a part of the active low pass filter-amplifier stage that follows the sampler. This filter has a low frequency cutoff, f_y , in the order of 1 cycle per second, in order to keep the system signal-to-noise power as low as possible. The system upper bandpass limit (prior to the filter) is $f\alpha$, and is selected to pass significant signal harmonics. In this case $f\alpha$ is in the order of $5/\Delta T$ to $10/\Delta T$, where $\Delta T = 20$ ms. Hence, $f\alpha$ is in the range of 250 to 500 cps; it is of course desirable to make this as low as possible to minimize noise, which is proportional to $f\alpha$.

The output of the integrating sample and hold circuit is amplified and drives two (redundant) output drivers. These drivers have a signal voltage range of 0 to 5 volts. It should be noted that the input to the signal amplifier includes a constant R_1 . (See Figure 6.) By adjustment of this constant the zero point of the output voltage may be shifted and by adjustment of the gain control the calibration can be set. Therefore, through the use of the two controls it is possible to achieve scale expansion of any desired range of the detector.

2.1.5.2 WATER (H₂O) SUBSYSTEM

The operation of this subsystem is identical in theory to that of the oxygen. The only variants are:

- a) the AGC loop is sampled at time TS_1
- b) the signal output is sampled at time TS_3

The output therefore will be in the form of either

$$e_2 = \frac{A_1 k_1 I(H_2O)}{k_2 I(O_2) - k_1 k_L I(H_2O)}$$

or,

$$e_2 = \frac{A k_1 [I(O_2) - I(H_2O)]}{k_2 I(O_2) - k_1 k_L [I(O_2) - I(H_2O)]}$$

depending upon the polarity convention selected. Note that the water is measured relative to the oxygen. This is done to achieve the greatest system accuracy, since the anticipated water content is small. If subsequent investigation shows that sufficient accuracy can be achieved, this extra AGC loop may be eliminated, and the water measured directly relative to the reference.

The signal output range is 0 to 5 volts, and is available from redundant drivers.

2.1.5.3 NITROGEN (N₂) SUBSYSTEM

The nitrogen content is computed from the total pressure. Although it would be possible to subtract the actual values of the CO₂, O₂, and H₂O from the total pressure to find the nitrogen pressure, it is reasonable to assume that the value of the sum of CO₂ and H₂O will fall within defined ranges, and that a constant may be substituted. Thus, the value of N₂ is actually found by subtracting the sum of a constant (C) and O₂ from the total pressure as shown in Figure 6. This is done in a differential input amplifier. The output signal range is 0 to 5 volts, and is available from redundant output drivers.

2.2 INFRARED SUBSYSTEM (CO₂ CHANNEL)

The CO₂ monitoring subsystem is basically a very simple infrared lens-filter system as shown in Figure 8. The design is based upon models developed under NASA Contract No. NAS 9-1191 and NAS 9-2255 by the Perkin-Elmer Corporation and is similar to the CO₂ measurement system optical schematic in Figure 19.

Basically, the system is a single beam, dual wavelength, filter radiometer with ratio readout. The dual filter, which has the characteristics shown in Figure 20, is mounted opposite the shutter openings of the O₂-H₂O monitor subsystem. The filters are located at a point in the optical system where a small image of the source is formed in space. As the chopper moves the dual filter back and forth across the light beam and a light baffling mask, energy is interrupted at the sample and reference wavelengths.

As a result of the chopper positions and the spectral characteristics of CO₂, the detector signal has the appearance shown in Figure 4. I_R is a measure of the energy received by the detector at the reference wavelength (4.0 microns) where CO₂ does not absorb, the I_S is a measure of the energy received at the sample wavelength (4.27 microns) where CO₂ does absorb. With no CO₂ in the sample, I_S will decrease in amplitude relative to I_R. Thus, the essential information for selectively and quantitatively measuring the amount of CO₂ in the sample is present in the detector signal. An electronic system "decodes" the detector signal, computes the ratio of I_S to I_R, and reads out a continuous DC voltage as a function of the partial pressure CO₂ in the sample gas.

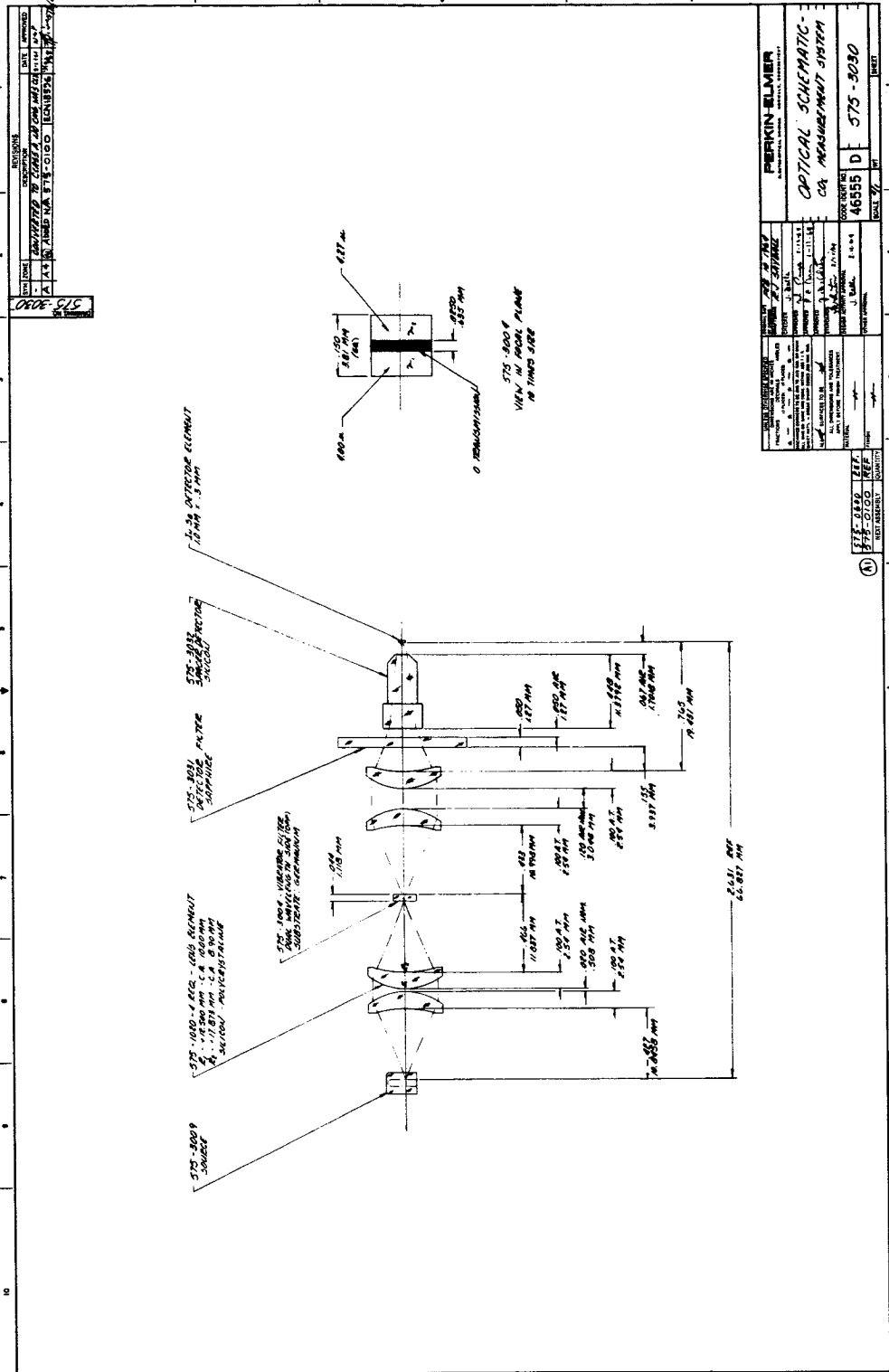


Figure 19. CO₂ Measurement System Optical Schematic

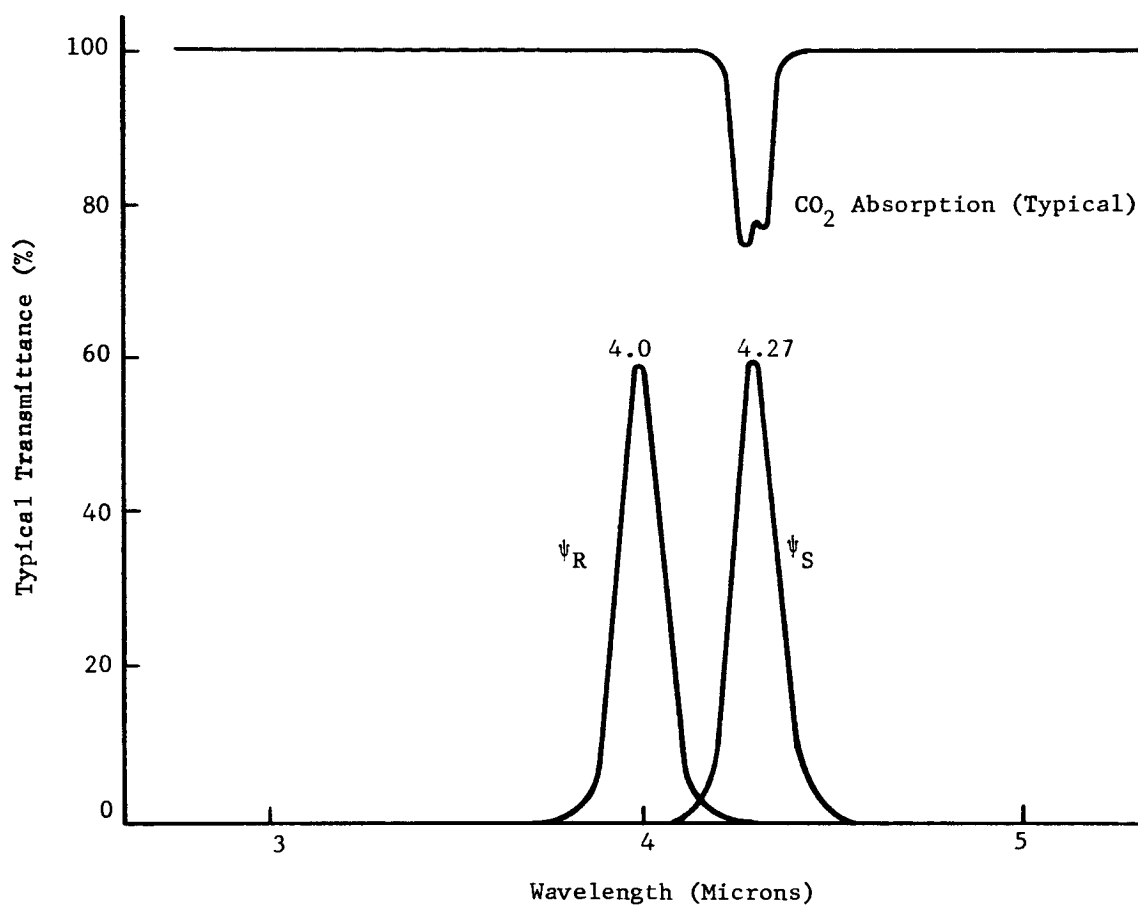


Figure 20. CO₂ Transmission Characteristics

2.2.1 OPTICS - INFRARED SUBSYSTEM

The infrared absorption spectra of gases which might be found in a typical closed environment are shown in the graph of Figure 21. The concentration of the gases was chosen to show the absorption on a 0-100% scale. These concentrations are vastly different than the amounts actually found in a closed environment, but for the purposes of this discussion, tend to indicate a "worst case" condition. From this graph, the wavelength of 4.27 microns was selected for the CO₂ measurement wavelength and a reference wavelength of 4.0 microns was also selected. All other gases will have essentially equal effects at 4.0 and 4.27 microns except CO₂.

The desired spectral characteristics of the system are shown in Figure 20. As shown in the illustration, the system would allow a spectral passband at 4.27 microns coinciding with the CO₂ absorption band and a reference spectral band at 4.0 microns. The reference band basically provides a means of monitoring the infrared source output, dust and dirt on the optics, and detector sensitivity. In order to develop a system with the above described characteristics, specialized optical components are required.

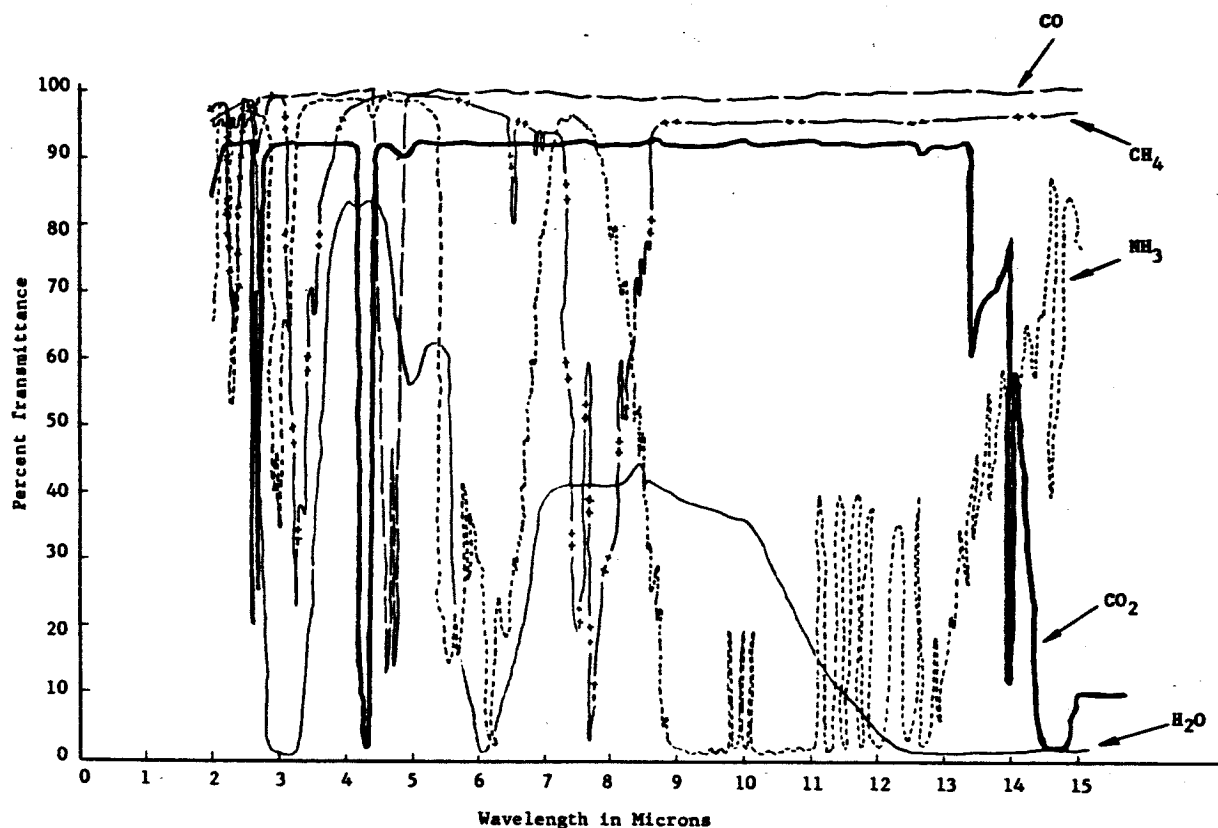


Figure 21. Absorption Spectra of Typical Closed Environment

Optics

The optical system consists of a source (a small, military specification, tungsten lamp), collimating lens, another lens that re-images the source on the dual filter, and finally another lens pair, which re-images the chopped and filtered source image onto the detector target.

The sample cell, approximately 4.5 cm in length, will be located between the third and fourth lens elements and will be pneumatically coupled to the O₂-H₂O subsystem absorption cells.

Dual Wavelength Filter (See Figure 22)

The design and fabrication of a small dual wavelength filter is a unique requirement of the CO₂ Sensor. The most important consideration in designing this component is the input power specification for the unit. Particularly, this specification imposes the following limits on the filter design:

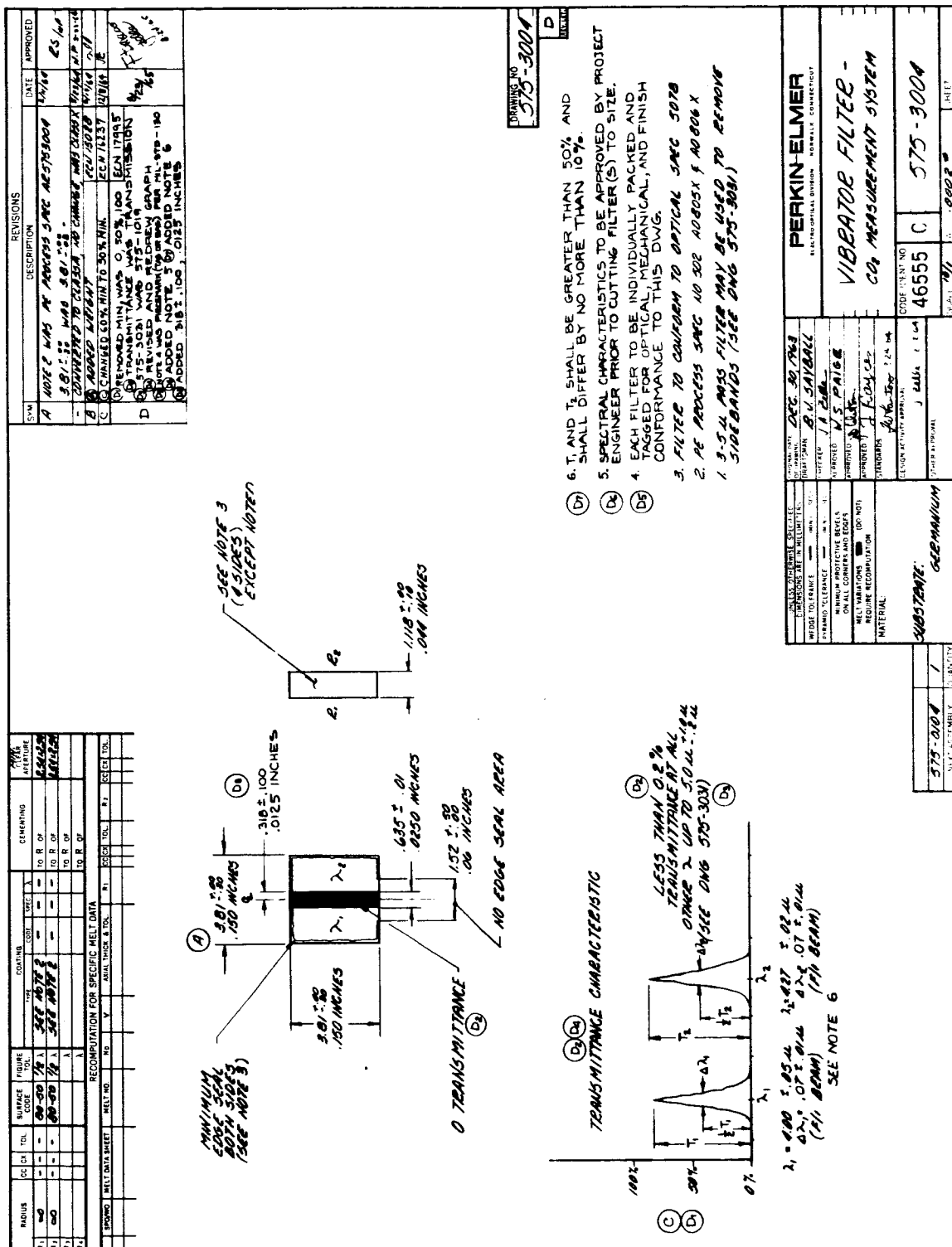


Figure 22. Dual Wavelength Filter

- a) The input power limit forces the use of a very small infrared source. This source has a small image in a 1/1 optical system. Thus, a small image is formed at the chopping point.
- b) A very low-power chopper is also required as a result of the input power specification. For the Apollo CO₂ Sensor this chopper is a tuning fork. In order to keep the power low, it is necessary to keep the fork excursion low which means that the chopping element must be accurate. Also, since the chopping element is directly attached to the fork tine, the element weight must be kept low so that the fork is not required to move a large mass.

The dual wavelength filter serves as the chopping element in the CO₂ Sensor. The above limitations mean that the filter must be small, of low mass, and accurate. In addition, to obtain the proper chopping action, it is necessary for the filter to have a "black" or zero transmission region between the two wavelength transmitting regions.

The basic filter is made from a one-inch square of germanium, 0.044 inch thick. The interference filter for λ_1 , is coated onto the blank through a 0.500 x 0.5125-inch mask. Thus, the mask exposes half of the area plus 0.0125 inch down the center. After coating on λ_1 , the mask is placed over the other half of the substrate and the interference filter for λ_2 is coated on. The result is that the overlap region in the center (0.0250 inch) has both λ_1 and λ_2 filters coated on it. This creates a zero transmittance region, on one side of which is the λ_1 filter and on the other side is the λ_2 filter.

The large dual filter blank is then cut on a diamond wheel to produce many small filter elements, which are 0.15 x 0.15 inch square by 0.044 inch thick. This procedure provides a very simple and efficient method of producing small dual-wavelength filters.

The desired filter characteristics are achieved by carefully controlling the coating material, coating thickness, and number of layers. The entire coating procedure is monitored by measuring the optical coating thickness as it is being applied.

A spectrometric run of one half of the dual-wavelength filter is given in Figure 23. It indicates a 63% transmission spike centered at 4.0 microns. Figure 24 is a spectrometric run of the second half of the dual-wavelength filter and indicates a 61% transmission spike centered at 4.25 microns (4.27 μ would be ideal). One of the filters also has a coating over its entire reverse face, which blocks all wavelengths below 3.50 microns.

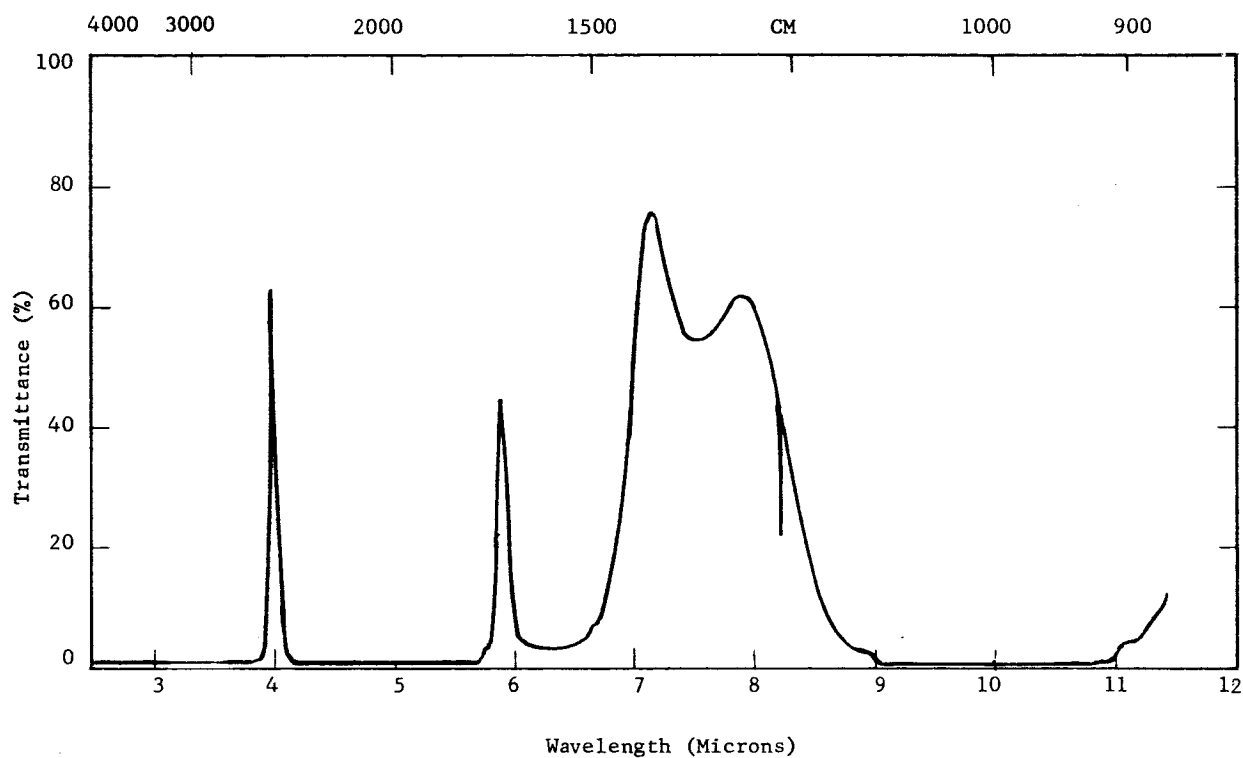


Figure 23. Spectrometric Run - First Half, Dual-Wavelength Filter

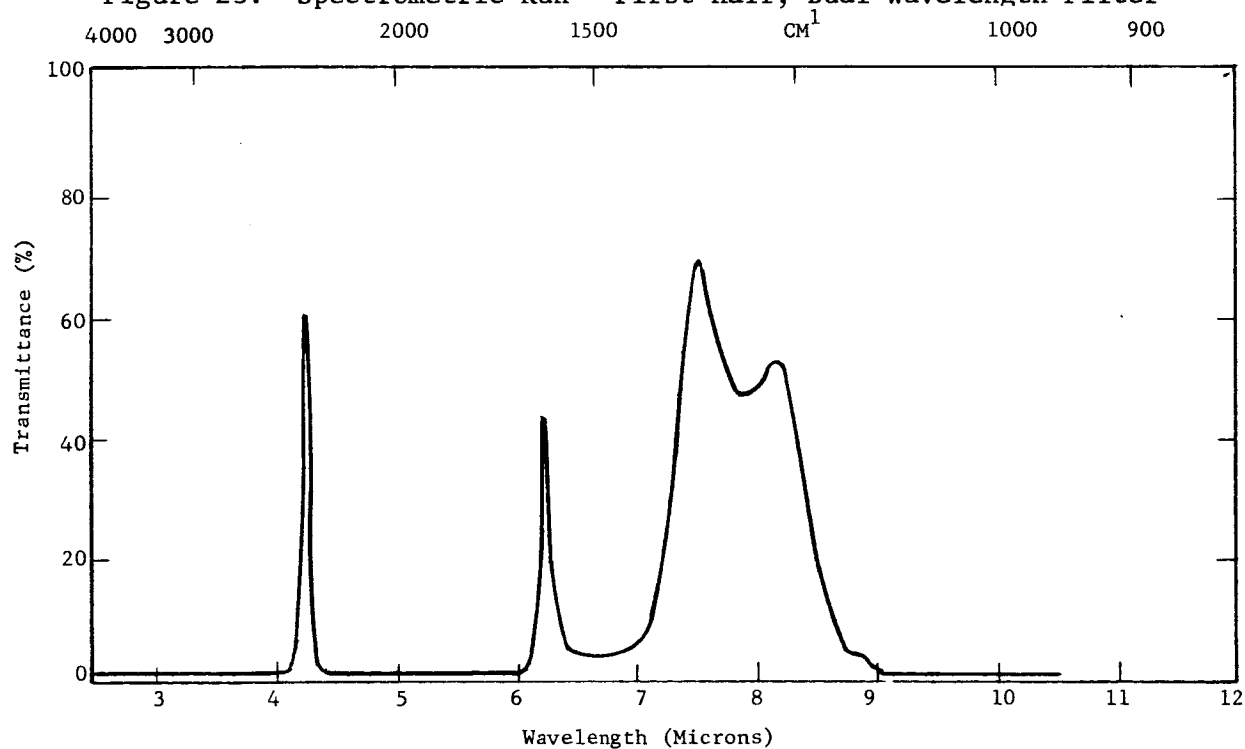


Figure 24. Spectrometric Run - Second Half, Dual-Wavelength Filter

Gas Compartment Window

Figure 25 is a spectrometric record of the window placed between the gas compartment and the detector. It again is a coated filter, but on a

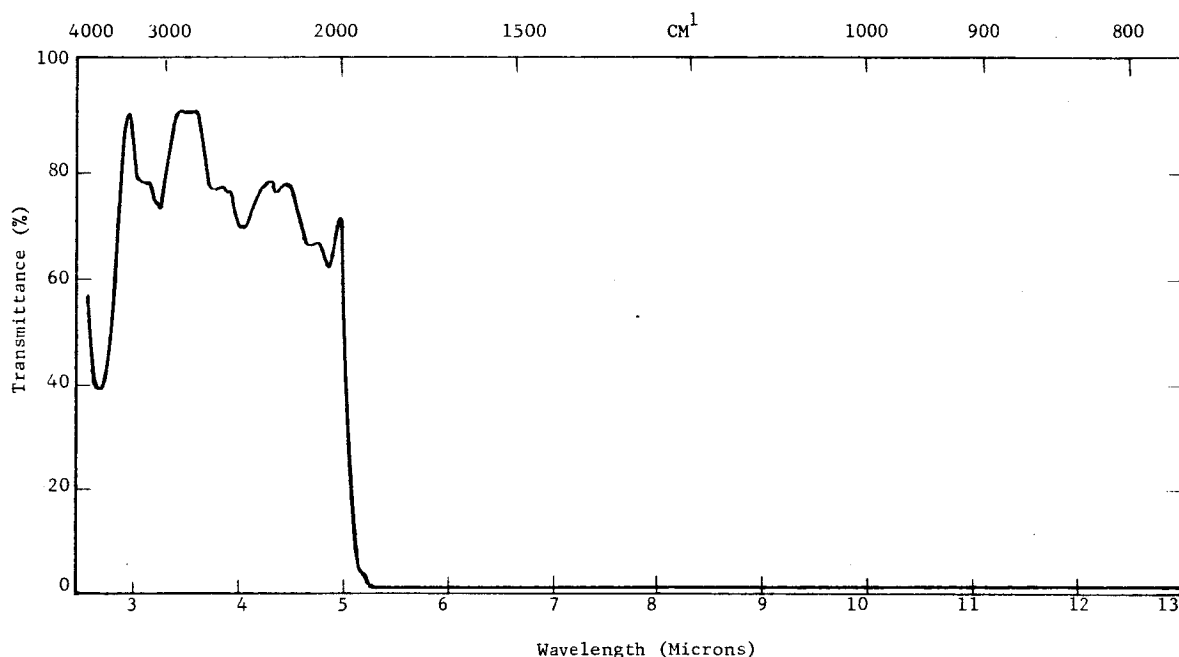


Figure 25. Spectrometric Run - Detector Filter

sapphire substrate as shown in Figure 26. This filter has a cutoff at 5.05 microns and serves to block the wavelength transmission beyond 5.0 microns shown in Figures 24 and 25.

Detector Window

The detector window is a piece of silicon with an anti-reflection coating for peak transmission at 4.0 microns. Figure 27 indicates the transmission of this element. This element is long and comes within 0.067 inch of the detector element which assures a minimum amount of unknown air path outside of the gas compartment.

SYMBOL		REVISIONS		DATE		APPROVED	
SYMBOL		DESCRIPTION		DATE		APPROVED	
A		CONNECTED TO CLASS A AND CLASS BMS CLASS X		10/10/80		[Signature]	
A		ADDED MATERIAL		10/10/80		[Signature]	

UNLESS OTHERWISE SPECIFIED		PERKIN-ELMER	
DIMENSIONS ARE IN MILLIMETERS		ELECTRO-OPTICAL DIVISION NORWALK, CONNECTICUT	
WELD TOLERANCE	± .001	DATE	10/10/80
PRISM TOLERANCE	± .001	DRAWN BY	J. J. BALL
MINIMUM PROTECTIVE BEVELS	1/16" MIN.	CHECKED BY	J. J. BALL
ALL DIMENSIONS TO CENTER UNLESS NOTED		APPROVED BY	J. J. BALL
REQUIRE RECOMPUTATION	(DO NOT)	DATE	10/10/80
MATERIAL		POLYETHYLENE	
SAPPHIRE		(SEE NOTE 1)	
DESIGN ACTIVITY APPROVAL		[Signature]	
OTHER APPROVAL		[Signature]	

19.812 ± .005
.780 INCHES

1.27 ± .05
.050 INCHES

1. SPECIFIC CHARACTERISTICS TO BE SUCH AS TO ELIMINATE ALL SIDE BANDS FROM 575-3000 ABOVE 5 MICRONS BY TRANSMISSION CHARACTERISTIC

2. MINIMUM TRANSMISSION IN 0.80 MICRON REGION = 80% ARE ALSO PROGRESS SAME AS 5753031.

3. FILTER TO CONFORM TO OPTICAL SPEC 5070

4. MATERIAL MAY BE PURCHASED FROM ADOLPH MUELLER, BOX 6001 TRUCKEE, PENNSYLVANIA, P.A.

5. PURCHASE (BAG OR TAG) PER MK-570-180

DESIGN NO. 575-3031

A

SCALE: 1/16" = 1"

CODE IDENT NO. 46555

SCALE: 1/16" = 1"

DATE: 10/10/80

BY: J. J. BALL

APPROVED BY: [Signature]

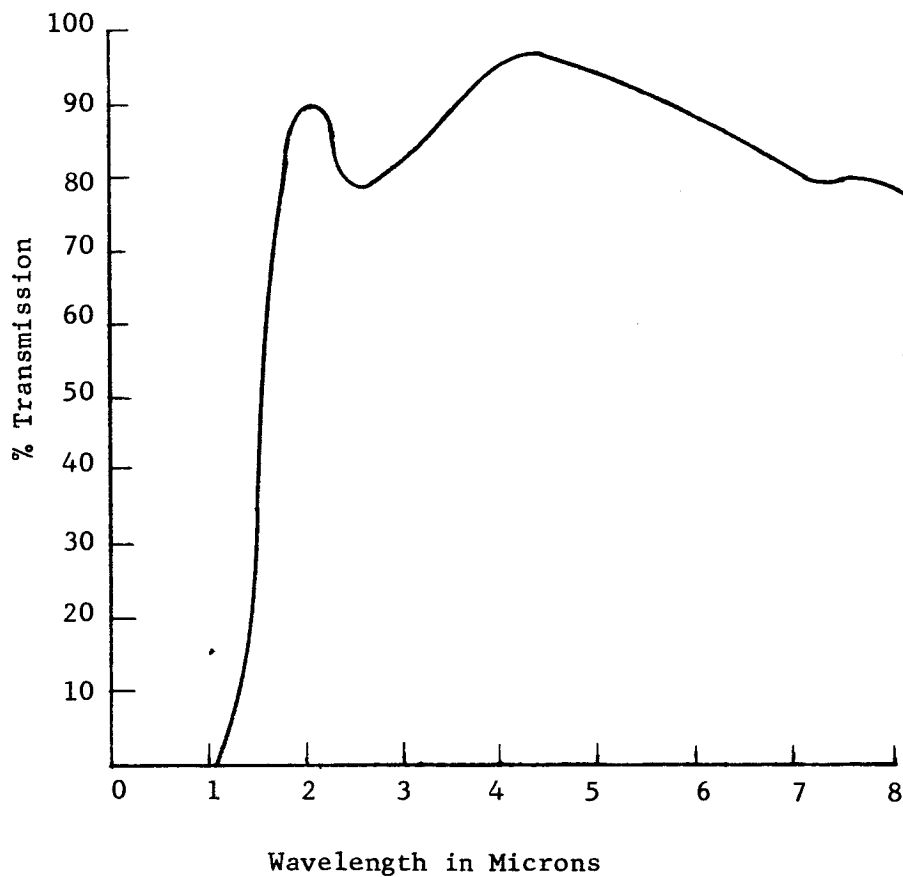


Figure 27. Spectral Transmission of Coated Silicon

Lens Element

A single spherical lens of polycrystalline silicon is used throughout the system and is shown in Figure 28. Silicon was chosen for its high infrared transmission and desired index of refraction. Optical anti-reflection coatings were applied to all lens surfaces to peak the infrared transmission in the 4-micron band to approximately 98 percent.

Optical System

The resultant spectral characteristics of the IR system are shown in Figure 29. This indicates that by careful application of materials and coatings, the overall transmission has been held at 30-35%, although seven optical elements are employed.

Figure 28. Lens Element (IR System)

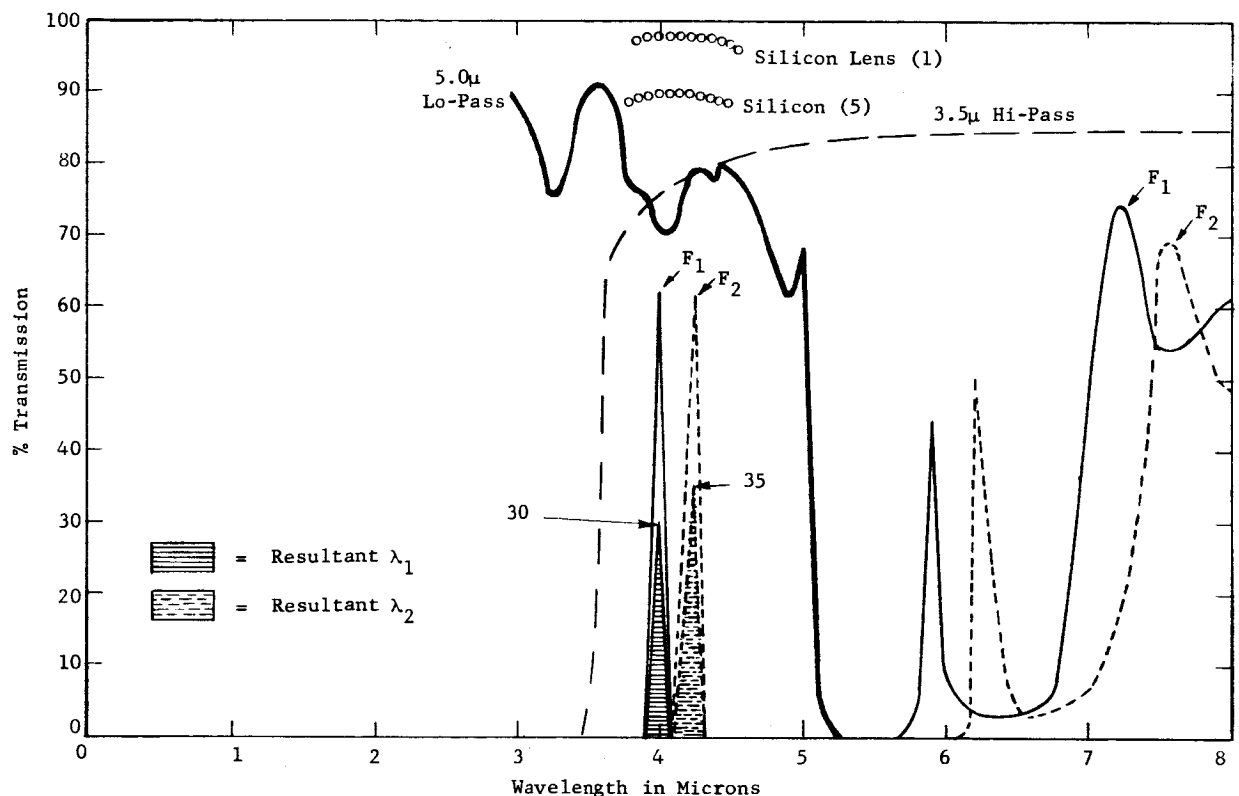


Figure 29. IR System Spectral Characteristics

2.2.2 DETECTOR - INFRARED SUBSYSTEM

The energy from the infrared light source is optically focused on a Photo-Electric Magnetic (PEM) InSb infrared detector. Using the Hall effect, the magnetically biased semi-conductor generates a voltage proportional to the incident infrared energy. The detector is magnetically shielded to protect it from external magnetic fields generated by the chopper and other magnetic devices in the unit. The detector is similar to the unit employed in the present Apollo CO₂ sensor, as shown in Figure 30.

The detector is dc coupled to the low noise amplifier. Although the impedance match is not optimum, insofar as signal noise considerations are concerned, the use of an impedance matching transformer (as used in the present CO₂ sensor) is not recommended. The use of a transformer for such a low frequency of operation (basic rate = 12.5 cps) would be difficult, and in general, would be undesirable from a size, shielding, and environmental shock-vibration susceptibility standpoint. The loss in S/N can be compensated by increasing the signal without a corresponding increase in amplifier noise.

Figure 30. Apollo CO₂ Detector

2.2.3 CHOPPER - INFRARED SUBSYSTEM

The chopper requirements for the CO₂ channel are somewhat less stringent than those for the ultraviolet channel, because only three bits of information are required for the CO₂ system. Whereas the measurement of two gases in the ultraviolet system requires four pieces of information: the signal information for the oxygen and again for the water, the reference information to stabilize the oxygen signal, and zero information as a basic reference. The CO₂ system only requires signal information related to the concentration of CO₂, reference information related to the overall system's transmission, and a zero reference. Three channels of information can be quite successfully obtained by a tuning fork, with relatively small excursions as has been successfully done on the Apollo CO₂ sensor.

The chopper for the carbon dioxide channel can take one of two forms: it can be an independent chopper such as a tuning fork, or it can share a portion of an overall chopper with the ultraviolet channel. Results of our present investigation indicate one of two possible methods, which are compared in Paragraph 2.5.3.4. One method would be to use independent tuning forks for the CO₂ sensor channel and for the O₂-H₂O channels as optical choppers. The simultaneous use of the tuning forks is not generally recommended because of the minimum slit widths, which would be required for a system of this type, and the inefficient utilization of components.

The preferred method is to use a torsional chopper (common to both channels) driven by a torquer motor with flexure bearings. The torsional chopper will allow a simplification of the timing electronics in that it may be driven to any one of a number of discrete positions and held there for an indefinite time.

2.2.4 SOURCE - INFRARED SUBSYSTEM

The infrared source (Part No. 575-3009) is a standard MS type tungsten filament lamp operated at a low voltage to obtain a life-time rating of 10⁶ hours. It was chosen to obtain the maximum 4-micron output with minimum power input. The thin glass wall on this bulb allows infrared transmission out to almost 5.0 microns. The filament active dimension is 0.5 inch by 0.01 inch.

2.2.5 ELECTRONICS

A simplified block diagram of the CO₂ subsystem is shown in Figure 31.

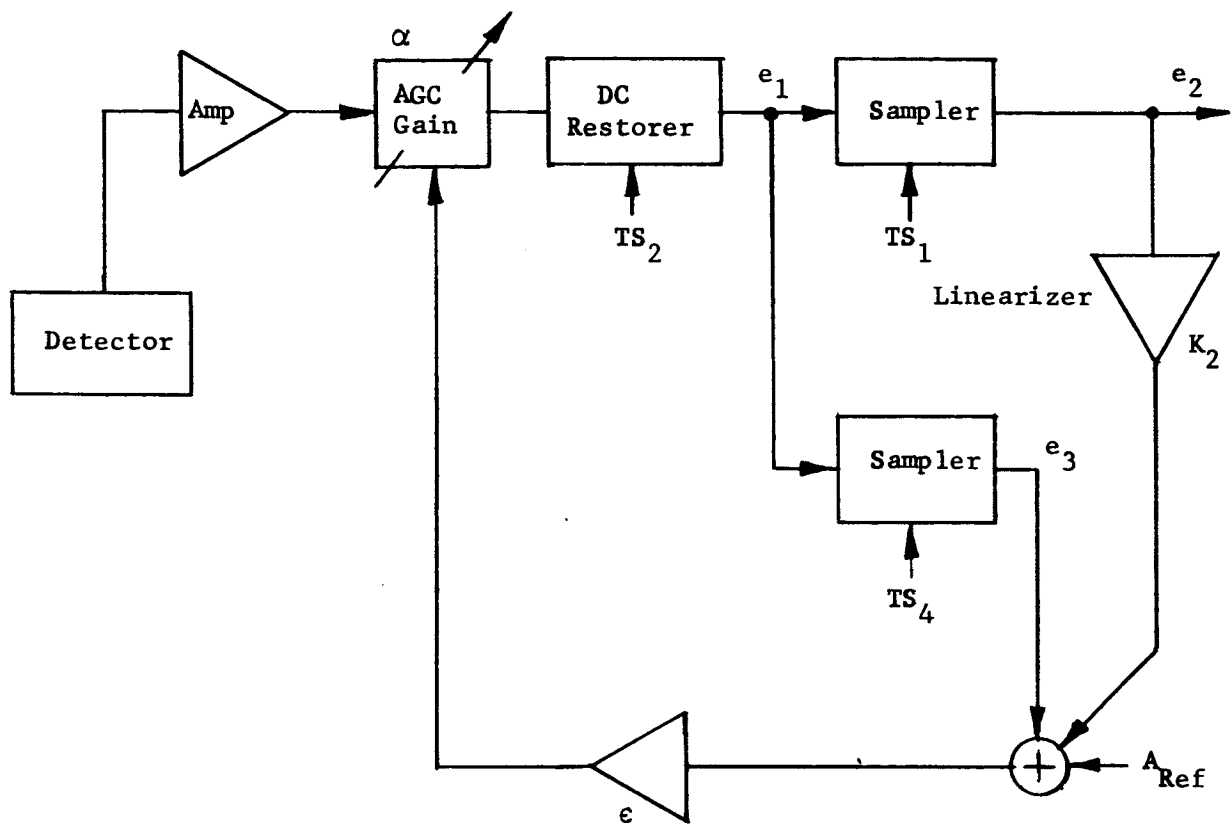
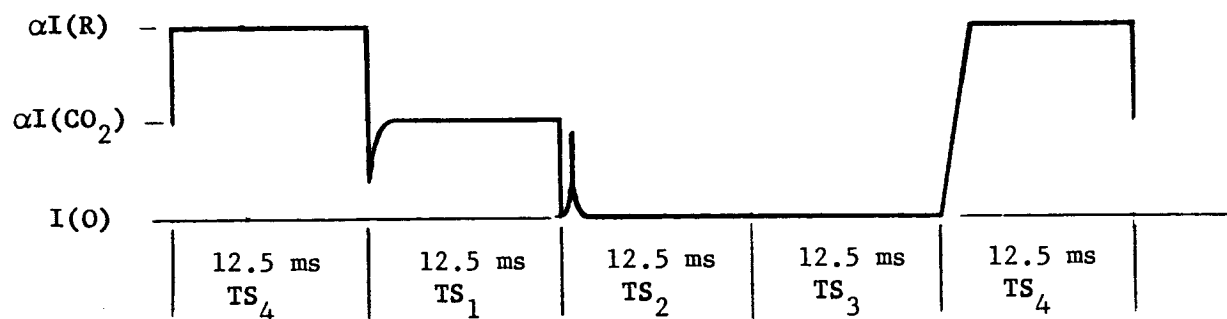


Figure 31. CO₂ Subsystem Block Diagram

The signal waveform at the output of the dc restorer appears as:



Either this signal, or its reverse polarity may be processed by the sampling. In the former case,

$$e_2 = \alpha k_1 I(\text{CO}_2)$$

$$e_3 = \alpha k_2 I(\text{R})$$

and

$$\epsilon = \alpha k_2 I(\text{R}) - A \xrightarrow{\text{as a limit}} 0$$

hence,

$$\alpha = \frac{A}{k_2 I(\text{R})}$$

therefore,

$$e_2 = \frac{A k_1 I(\text{CO}_2)}{k_2 I(\text{R})}$$

In the latter case (i.e., reversed polarity), the timing pulses TS-2 and TS-4 are interchanged, and the output changes to:

$$e_2 = \alpha k_1 [I(\text{R}) - I(\text{CO}_2)]$$

$$e_3 = \alpha k_2 I(\text{R})$$

hence,

$$e_2 = \frac{A k_1 [I(R) - I(CO_2)]}{k_2 I(R)} = \frac{A k_1}{k_2} \left[1 - \frac{I(CO_2)}{I(R)} \right]$$

Either form of e_2 may be used. As in the case of the oxygen subsystem, it is desirable to introduce a non-linearity to make the overall processing, including the gas path, more linear. This is done by feeding a fraction (k_L) of the CO_2 output back into the AGC system, as shown on the block diagram. The output then becomes:

$$e_2 = \frac{A k_1 I(CO_2)}{k_2 I(R) - k_1 k_L I(CO_2)}$$

for polarities as shown, or,

$$e_2 = \frac{A k_1 [I(R) - I(CO_2)]}{k_2 I(R) - k_1 k_L I(CO_2)},$$

if the polarities are reversed and the timing is changed.

The output signal range is from 0 to 5 VDC, and is available from two redundant output drivers.

2.3 TOTAL PRESSURE (P_T) SUBSYSTEM

The total pressure subsystem will consist of a strain gauge transducer of an improved flight qualified design which will be fed from an isolated and regulated electronic converter. The output from the strain gauge bridge will be fed to an operational amplifier which in turn will drive a 0-5 volt full scale signal for the pressure range desired. This output signal will then be operated on in the electronics of the Two-Gas Atmosphere Sensor to subtract the partial pressures of O_2 and a fixed constant to obtain a determination of N_2 total pressure.

The total pressure transducer selected for this application is a flight model similar to that presently manufactured by the Consolidated Controls Corporation of Bethel, Connecticut. This device operates on the variable reluctance principle instead of the usual strain gauge system. A magnetized diaphragm in a sealed capsule is between two electrical sensing coils of an AC bridge. Motion of the diaphragm unbalances the bridge generating a signal proportional to the imposed pressure. This signal is amplified and demodulated for a 0 to 5 VDC output. The sensing device is designated as a 41PD65 High Reliability Absolute Pressure Transducer. To permit scale expansion, a constant R_2 (Figure 6), is fed into the amplifier stage. With this, and the stage feedback gain control, the scale may be expanded and set to provide an output signal range of from 0 to 5 VDC.

This is considered to be the most accurate method for this evaluation. The total pressure transducer is a relatively small portion of the system and will be available as an accurate primary measurement. This total pressure will also be provided as an output for use in evaluating the system.

2.4 ELECTRONICS PACKAGING CONCEPT

The Two-Gas Atmosphere Sensor electronics must be packaged within the specified assembly configuration and volume, and must be as light in weight as possible. Secondary requirements dictate a producible design which will be economical and feasible for the predicted delivery schedule. The assembly must of course be dependable in the anticipated environment, and must be accessible for maintenance and circuit adjustment.

A modular concept is proposed, whereby standard discrete piece parts are assembled in cordwood fashion, interconnected primarily by welding, and then encapsulated in a foam for maximum weight savings. A packaging technique using microcircuits is also considered.

The overall packaging concept for the Two-Gas Atmosphere Sensor electronics is depicted in Figure 32. The 734 electronic parts are packaged into five welded-cordwood, foam-encapsulated electronic modules. Four modules are located in one section of the assembly, while the fifth is located in an adjacent area.

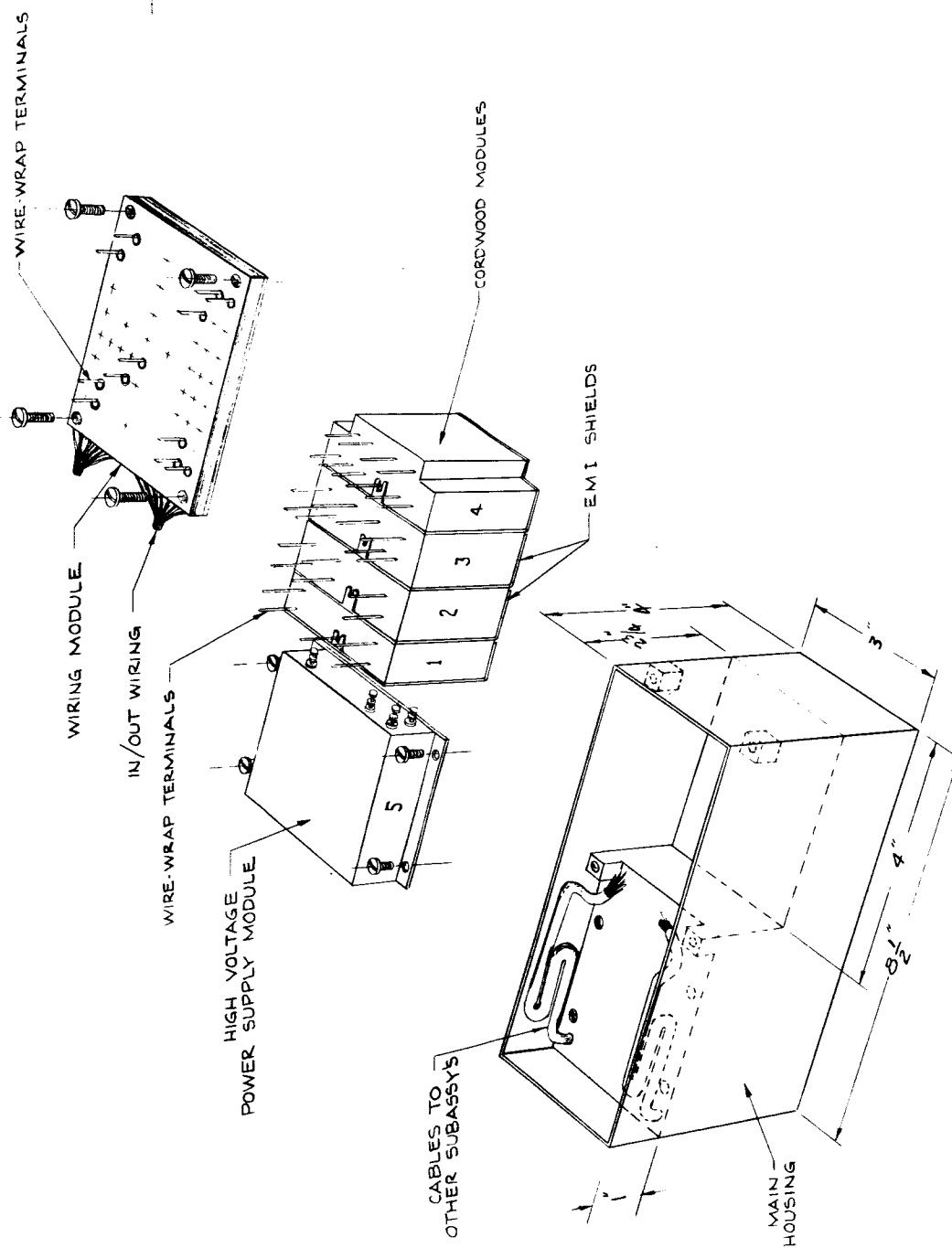


Figure 32. Overall Packaging Concept

The five modules require a volume of 28.38 in³ and weigh 1.40 pounds. The wiring module requires an additional 4.5 cubic inches and 0.12 pound.

The group of four modules is electrically interconnected and also held in place using a wiring module. The wiring module is a point-to-point wired, encapsulated subassembly having split-pin, wire-wrap terminals that mate with the electronic module terminals. The electronic modules are first connected to the wiring module, and then the entire subassembly is placed in the assembly. The wiring module compresses the four modules onto the bulkhead running through the main assembly. It is fastened down by screwing it to tapped bosses located on the assembly sides and the bulkhead. (See Figure 32.)

Since the environment that the electronic modules will have to withstand is not extremely severe, exotic designs and fastening methods are not required.

In order to account for dimensional differences between the heights of the electronic modules, it may be necessary to place a resilient compound at the base of the subassembly.

Wires coming and going to other parts of the assembly pass directly into the wiring module without the need for a friction connector. Thirty-four wires are required. A loop is provided in the cabling to permit partial removal of the electronic subassembly. When modules have to be removed, the four fastening screws are taken out and the entire subassembly is lifted as far from the assembly as the cables allow. Any module can then be removed from the group by unwrapping its interconnecting terminals. In the case of the fifth module, turret-type terminals are provided on one surface to which the in/out wiring is soldered. In the event that this module should require replacement, the wires are unsoldered, the flange screws taken out, and the module completely removed from the subassembly.

The modules are EMI shielded, primarily by the sides of the assembly. Exposed surfaces between the modules are shielded using laminated copper and mylar sheets. The shields are "L" shaped in order to simultaneously provide a thermally conductive path between the modules and the assembly.

Heat generated in the module is conducted through the foam, then to the mylar and copper laminated shield, and on down to the assembly's bulkhead. Some heat is also conducted through the parts and wiring. Total dissipation can vary from 3 to 15 watts. The 2 watt difference exists in the PM power supply and ultraviolet lamp driver module. The group of four modules dissipates one watt of thermal energy.

The PM power supply and ultraviolet lamp driver module is isolated from the remaining modules for several reasons. Since the power dissipation in this module is high (2 to 4 watts), the module is bolted directly to a

metallic surface so that it can efficiently conduct its heat to a large mass. Also, this module contains 700 and 1500 volt output lines which should be located as far away from the remainder of the electronics as possible.

2.4.1 ELECTRONIC MODULE

Five electronic modules are required. Table II depicts the module/part breakdown. A typical electronic module, shown in Figure 33,

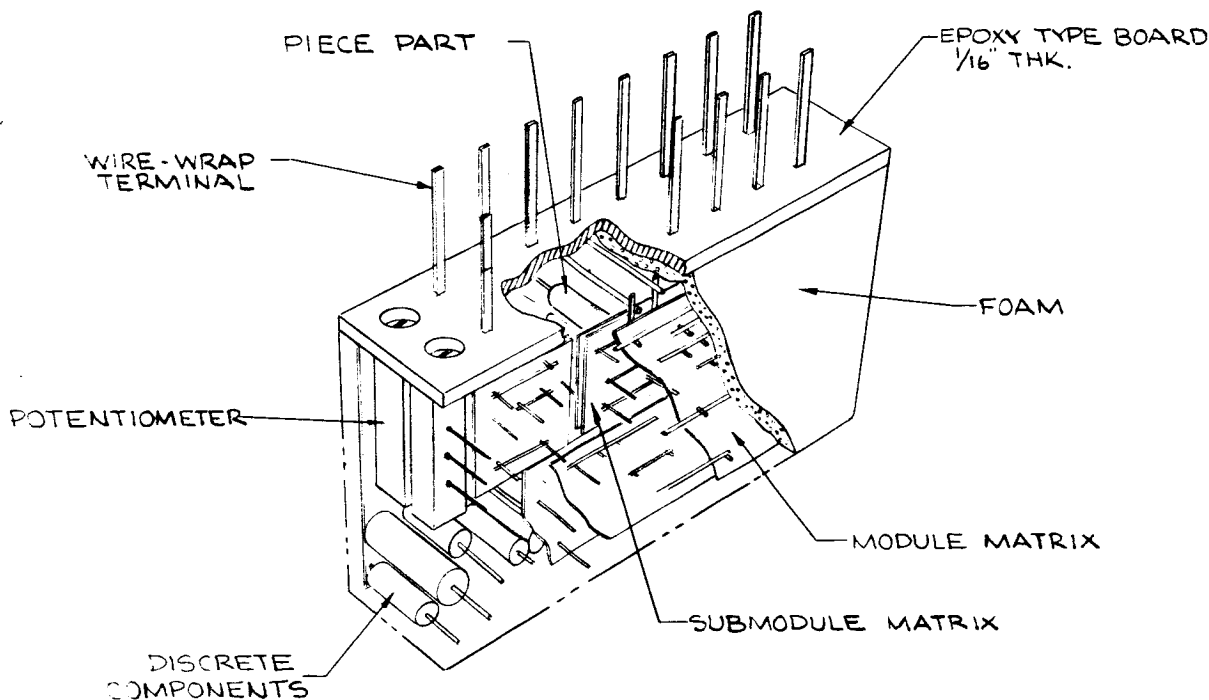


Figure 33. Typical Cordwood Module

consists of several submodules electrically interconnected by two welded matrix layers. The submodules are cordwood, welded units as described in Paragraph 2.4.1.1. After assembly and welding, the entire unit is encapsulated using a 10 lbs./ft³ foam to environmentally protect and house all the parts. The foam encapsulant provides essential thermal, vibration, shock, and acceleration control, while maintaining the foremost packaging criterion—light weight. A laminated copper/mylar sheet is bonded to the modules to provide shielding between adjacent modules. The sheet also provides a conductive path through which some of the module's heat can be carried to the assembly.

Split-pin wire-wrap terminals (0.015 x 0.025 inch) provide electrical connections between the module matrix layers and the wiring module. An epoxy board, 1/16 inch thick, is used as a terminal header in the module. Table III presents the weight calculations for the five modules. The total weight is 1.40 pounds.

TABLE II MODULE/PART BREAKDOWN							
Module #	Submodule #	Circuits	# Parts	Parts/in ³	Vol (in ³)	Power Dissip. (mw)	# Terminals
1	10	Timing Gen. Output Drivers	186	33	5.55	300	37
2	9	CO ₂ , Total Pressure and N ₂ Channels	208	34	6.15	200	19
3	9	O ₂ and H ₂ O Channels	206	34	6.15	200	14
4	4	EMI, DC/DC Conv., CO ₂ Lamp Driver	59	11	5.53	300	9
5	3	O ₂ Lamp Driver P/M P.S.	75	15	5.00	2000 or 4000	10
Totals	35		734		28.38		89

TABLE III
MODULE WEIGHT CALCULATIONS

		(Pounds)
1.	<p>Foam:</p> <p>Assume 60% of module volume is foam Volume of 5 modules is 28.35 in^3 Weight of foam = $(28.38 \times 0.6) 0.0058 \text{ lbs./in}^3 =$</p>	0.099
2.	<p>Parts and Wiring:</p> <p>40% of volume is parts and associated wiring Density is 0.1 lbs/in^3 Weight = $(28.38 \times 0.4) 0.1 =$</p>	1.130
3.	<p>Header Boards:</p> <p>Vol = 0.77 in^3, Density = 0.047 lbs./in^3 Weight = $0.77 \times 0.047 =$</p>	0.036
4.	<p>"T" frame, Module #5:</p> <p>Volume = 0.525 in^3, Density = 0.1 lbs./in^3 Weight = $0.525 \times 0.1 =$</p>	0.053
5.	<p>Shields:</p> <p>Size = $(2.2 + 1.0) (2.8) (0.007)$ inches Copper = 0.003 in., mylar = 0.002 in. thick Weight = $(3.2 \times 2.8) (0.003 \times 0.3 \frac{\text{lbs.}}{\text{in}^3} + 0.004 \times 0.05 \frac{\text{lbs.}}{\text{in}^3}) (4) =$</p>	0.040
6.	Miscellaneous	0.053
Total Weight		1.400

The form factors of the five modules are shown in Figure 35. Modules #1, #2, and #3 are basically the same, but have different thicknesses due to the size of the piece parts. Module #1 contains many small parts, as well as transformers, chokes, and some large bypass or filter type capacitors. Module #4 is also 1.0 inch thick due to the presence of large, bulky parts in the EMI and DC/DC converter circuitry. Moreover, Module #4 is on the end of the module stack where bosses are required in the assembly case sides. (See Figure 32.) Cutouts, 3/8-inch square, are provided in order to permit the electronic subassembly to be installed and removed from the main housing.

Holes are located on the edges of the terminal face of each module (Figure 33) to permit access to each potentiometer while the entire subassembly is fastened in place in the assembly.

Module #5 (Figure 34) contains the ultraviolet lamp driver and PM power supply. Its basic design is different from the other four modules, primarily because of its high heat dissipation (2 to 4 watts), its mounting requirements, the type of electronic parts required, and the high-voltage (700-1500V) output lines. The module consists of three submodules, as well as other large, bulky piece parts. An aluminum, "T" shaped, 1/16 inch thick frame is used to mount the highly dissipative parts and to fasten the module

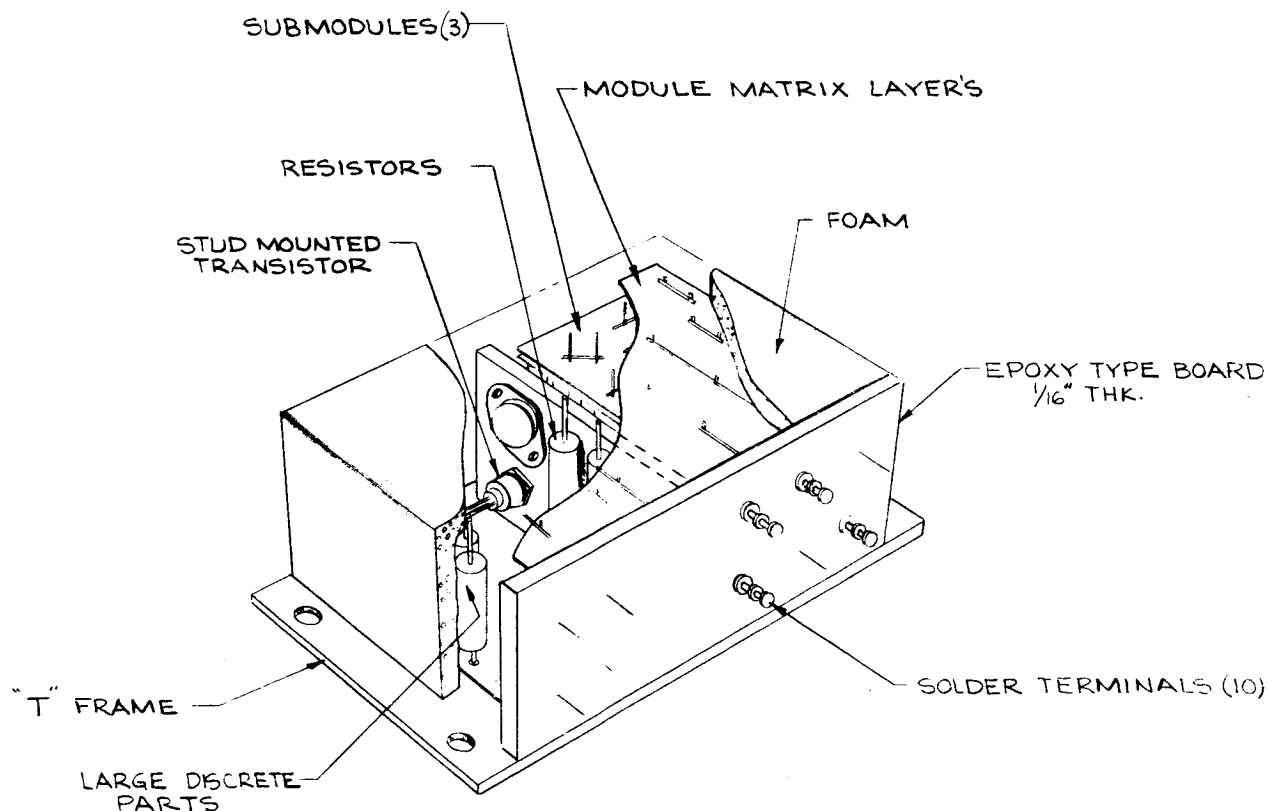


Figure 34. Module No. 5

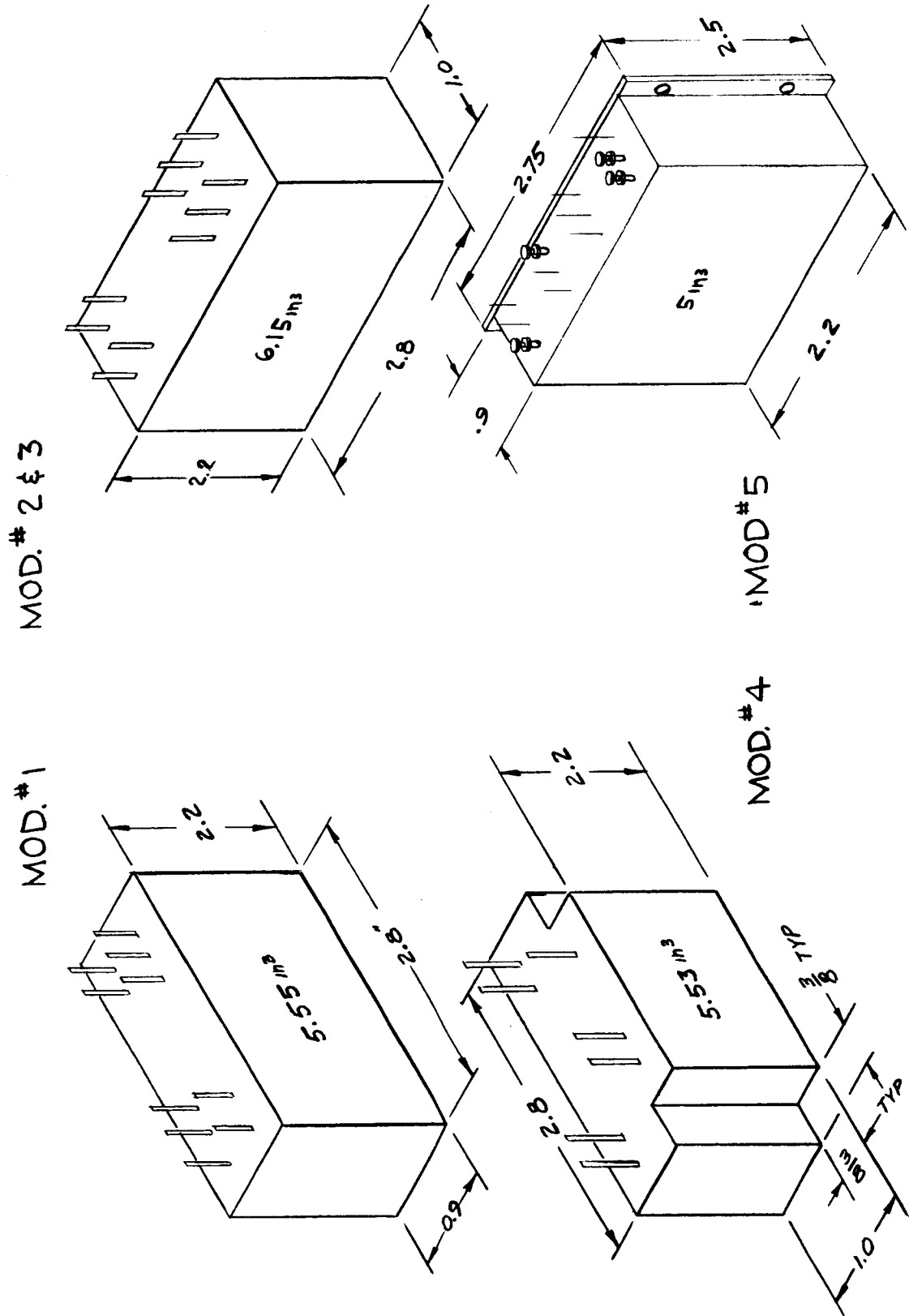


Figure 35. Module Form Factors

to the assembly bulkhead. (Paragraph 2.4.4.1 contains a sample thermal analysis for this module.) The entire module is encapsulated in foam at final assembly.

In/out connections are soldered to turrets on one face of the module. Internal connections to the turrets come from the module's matrix layers or through point-to-point wiring from the larger parts. The high-voltage output lines are located on one end of the terminal area in order to isolate them from the other terminals. High dielectric strength cabling is then soldered to the turrets and fed to the photomultiplier tube and ultraviolet lamp.

2.4.1.1 SUBMODULES

The submodules are functional electronic units fabricated using cordwood techniques. The parts are cordwood stacked for maximum volume efficiency. Each submodule performs a discrete electronic function (i.e., amplifier, demodulator, etc.). There is a total of 35 submodules of approximately 18 types in the complete system. As noted earlier, the 35 submodules are housed in five electronic modules.

The majority of the submodules are considered "throw-away" items in the event of failure. Those requiring discrete part replacement employ procedures similar to those on the present Apollo CO₂ sensor. Here, a fine drilling instrument and template are used to locate the part in question. A skilled operator can penetrate the potting compound and isolate the faulty part. A new part is then loaded and welded in place, and the unit is re-encapsulated.

It should be noted that the submodule approach still permits the removal of a discrete part without removing the entire submodule from the electronic module. Two matrix films must be penetrated in order to do so, however. In some instances, it would be just as simple to remove the discrete part as it would be to remove and replace an entire submodule.

The distinct advantage of submodules is cost and schedule. The modules can be fabricated much faster and cheaper when parallel effort is employed. Also, loss of a part or manufacturing errors have less impact on final assembly than if the parts were assembled as large modules. Design changes which may occur during the early, prototype phase of the program are also more easily controlled using the submodule concept.

There are two means of electrically interconnecting the parts in a submodule, each having distinct advantages. One technique is soldering and printed-circuit boards, the other is matrix and/or point-to-point welding. The printed circuit board approach is the most feasible for automated and simple production techniques.

The matrix or point-to-point welding approach would be, in general, lighter in weight but more expensive to fabricate, since it is not easy

to automate the process. The welding process is more reliable than the flow solder operation, especially if heat sensitive parts are used. The weight of the insulating films and wire is less than the printed circuit board and solder. If high production quantities are contemplated, the printed circuit approach will be investigated. Otherwise, the welded approach is best.

Shielding should not be required between individual submodules within a module. Copper and mylar laminated sheets could be wrapped around each submodule if necessary.

The average submodule, containing 15 to 30 discrete parts, measures approximately 0.6 x 1.0 x 0.75 inch. Each submodule will represent a distinct electronic function and is therefore easily tested. Each submodule will remain unencapsulated until final assembly, when the entire electronic module will be foamed.

2.4.1.2 SHIELDING

The electronic modules are so located that three sides of the modules are already shielded by the assembly case. Shielding between modules is accomplished by bonding a laminated copper and mylar sheet to one of the 2.2 x 2.8 inch sides of each module. A copper tab from each laminated sheet will be bent over and soldered to the ground terminal on each module as shown in Figure 32. The header portion of the modules is not shielded. Based on experience with the Apollo CO₂ sensor, shielding of this surface should not be required.

Since the shield also serves as a heat conductor for the module, it must carry the heat to the base of the subassembly. Therefore, the shield is "L" shaped to cover not only the largest surface area of the module but also to cover the base of the module. Paragraph 2.4.4 shows how the heat is conducted away from the module.

2.4.1.3 MAINTENANCE/REPAIRABILITY

The electronic subassembly is maintainable to the module level. Maintenance at the submodule and piece part levels requires more difficult procedures and, depending on the skill of the operator, may render the units unreliable. The maintenance of the module and/or the submodules should take place in a controlled environment. No maintenance is provided for the field or in flight.

Fault isolation to a module can be easily accomplished without physically removing any module. Since the split-pin, wire-wrap approach permits isolation of the electronic module terminal from the wiring module terminal, without removing the electronic module, the faulty circuit can be quickly isolated. The isolation is done by unwrapping the two wrapped terminals and placing a thin insulating material between them. Once the faulty module is located, the entire subassembly is removed and the faulty module replaced. No electrical connections, other than those of the faulty module, need be broken.

It is then possible to isolate the problem to a faulty submodule by removing the foam covering the wiring matrix. Depending on the particular modules and submodule design, either the submodule or the piece part is removed. This requires a careful drilling and rewelding operation, which can be successfully accomplished. Experience has shown that, when properly executed, the module or submodule can be repaired without any noticeable degradation of reliability. It is also important to note that repair prior to foaming the modules is facilitated by the submodule approach.

2.4.2 WIRING SUBASSEMBLY

Electrical interconnections between modules and to the remainder of the assembly are accomplished using a point-to-point wiring subassembly and stranded hook-up wire as shown in Figure 36. The wiring subassembly

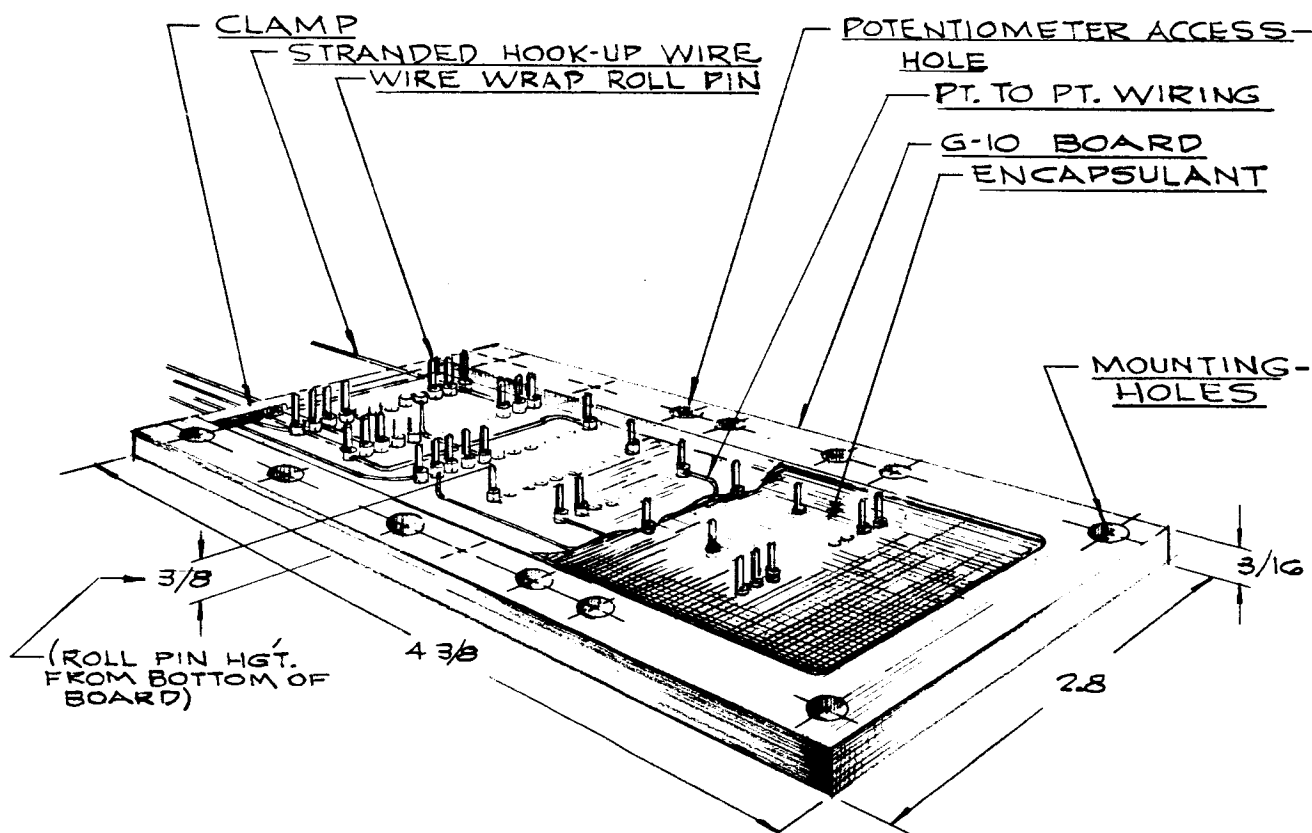


Figure 36. Wiring Subassembly (Encapsulant Partially Removed)

contains split-pin, wire-wrap terminals which are point-to-point interconnected using solid, Formvar-insulated wire. Connections from the wiring subassembly to the other parts of the assembly are performed using stranded wire and percussive-arc welding. The wiring subassembly provides a reliable, simple, lightweight, and easily maintainable means of interconnecting the four electronic modules.

The lightest method known for interconnecting a few electronic modules is to use small, lightweight, point-to-point wiring. However, other requirements such as maintainability, often increase weight and complicate the design. The proposed approach makes maximum use of point-to-point wiring while minimizing the impact of maintainability.

A fiber glass, G-10 type of board with a 3/64 inch thick base is used to support the wire-wrap roll pin. On three sides, the 3/64 inch dimension is increased to 3/16 inch to contain the wiring and encapsulant. The wire-wrap roll pin is tubular in shape in order to allow the electronic module's mating terminal to pass through it without any insertion or withdrawal force. A wire-wrap terminal is provided on one end of the tubular roll pin and mates with the electronic module's terminal. The two terminals are then wrapped together using a separate piece of soft copper wire to form a reliable, gas-tight joint. The resultant connection can be wrapped and rewrapped many times (50 or more) without noticeable degradation to the connection. (A new wrapping wire is used each time the connection is wrapped.)

The clearance in the roll pin ensures that no force is placed on the electronic module's terminal before and after securing the modules. The wire-wrap terminal cross-section will be 0.010 x 0.025 inch and the module's mating terminal will be 0.015 x 0.025 inch. Thus, the effective split-pin wire-wrap cross-section will be 0.025 x 0.025 inch. The wrapping wire will be #30 AWG, solid, dead soft copper.

To interconnect the wire-wrap terminals of the wiring subassembly, solid, insulated wire is routed in a point-to-point fashion. The wire will be Formvar coated. The wire-wrap roll pin has a tab to which the interwiring is welded. This process consists of joining the wire to the tab without removing the insulation. (See Figure 37.) The hot-electrode welding technique will be used. Heat is passed through the welding electrodes to melt away the insulation where the weld is to be made. The joint is then made by the capacitive discharge process. Although the hot-wire technique is relatively new, it is being used on a variety of NASA and military programs, and is being qualified for use on the Apollo/LEM program. Its main features are lightweight, simplicity, repeatability, and reliability. It is often used where a high density of terminals and lightweight are required. A variety of wire types and sizes can be used with this technique, thus matching the electrical requirements with the minimum, lightest wire gauge.

Wires from other portions of the assembly are routed in the wiring subassembly and are also terminated at the wire-wrap roll pin. These wires will be stranded and insulated in order to allow bending during maintenance. They will be percussive-arc welded to the roll pin terminals as shown in Figure 37. This technique allows a reliable and simple joint to be made using stranded wire and a solid terminal. Soldering could also be performed, but the roll pin would have to be redesigned to allow a NASA type joint (i.e., turret or bifurcated) and would be different from the other roll pins. The soldering operation also requires more skill and greater time to perform.

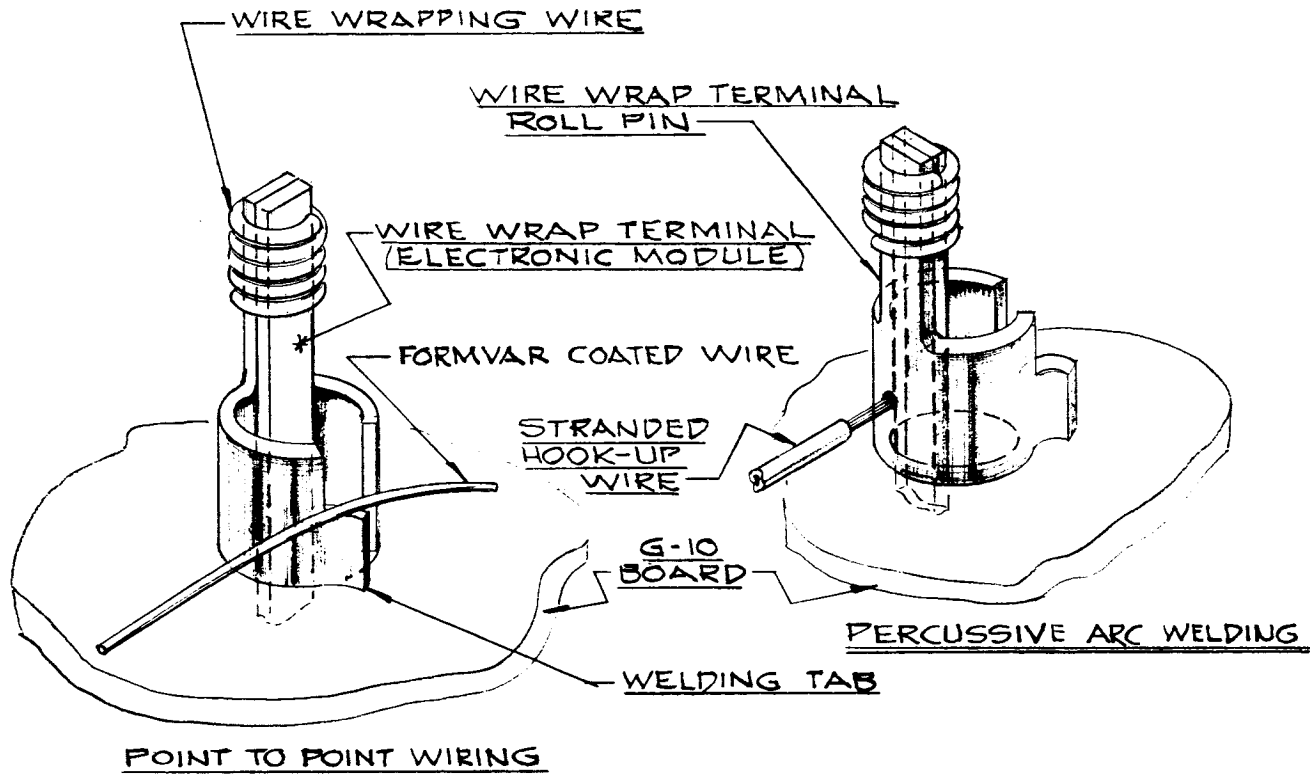


Figure 37. Wire-Wrap Roll Pin

Special considerations are required for some of the wires in the wiring subassembly, and involve the 1000-1500 volt lines from the High Voltage Photomultiplier Tube power supply, the 700 volt Ultraviolet Lamp power supply, and some shielded twisted pairs at the channel inputs. Basically, the high voltage lines and terminals will be laid out so that they are as far away as possible from other lines. They will also require high dielectric strength insulation. The shielded twisted pairs will be terminated at wire-wrap roll pins, with their shields grounded in the immediate vicinity of the roll pins. No friction or special connectors need be used for these applications. Point-to-point wiring, welding, wire-wrap and careful layout will ensure that the electrical requirements are met.

After all of the connections and routing are finished, the cavity containing the wiring will be encapsulated with an epoxy compound. The compound will protect the wiring and provide added rigidity to the wiring subassembly.

When removal of an electronic module is required, the entire electronic subassembly is removed. Then an electronic module is removed by unwrapping it from the wiring subassembly. The in/out cabling will have a stress-relieving hoop in it to allow the wiring subassembly to be partially removed from the assembly. Assuming that the ends of the cables to the other parts of

the assembly are permanently or semipermanently terminated, the wiring subassembly will not be readily removable from the assembly. Unless drastic wiring changes are required or undue damage occurs, it is felt that the wiring subassembly need not be removed from the assembly.

As noted in Figure 36, the size of the wiring subassembly is $3/8 \times 2.8 \times 4-3/8$ inches. The overall weight is 0.123 pound as derived in the following weight table.

Wire	3.08 gms.
Wire-Wrap Roll Pin (0.054 gm/pin x 80 pins)	4.32 gms.
G-10 Epoxy Board ($1.01 \text{ in}^3 \times 30.3 \text{ gm/in}^3$)	30.60 gms.
Encapsulant ($0.8 \text{ in}^3 \times 22.5 \text{ gm/in}^3$)	<u>18.00 gms.</u>
	56.00 gms.

Note: Weight of stranded, in/out hook-up wire has been omitted in the above calculation.

The in/out cables are secured to the wiring subassembly using clamps and conformal coating. The width of the subassembly is slightly less than that of the electronic modules in order to allow them to be placed within the envelope of the electronic packages. Holes are located in the G-10 board, which allow access to the potentiometers located in the electronic modules.

2.4.3 MICROCIRCUITS

To achieve even greater size and weight reductions, a number of electrical functions could be replaced with microcircuits. An analysis of the electronic parts count (Table IV) indicates that 31 of these units could replace 311 standard, discrete parts. The total volume savings is approximately $7-1/2$ cubic inches with a corresponding 0.34 pound weight saving (Table V).

A total of five electronic modules would still be required. One module, the Photomultiplier Tube power supply and Ultraviolet lamp driver, would remain the same as before and also be located in the same place. The remaining four modules would be the same length and width as before, 2.8 and 1.0 in., respectively, but the height would be reduced from 2.2 to 1.5 in. as shown in Figure 38. The manner in which the modules are held in place, fabricated, thermally controlled, and EMI shielded would remain the same.

The functional/modular breakdown is approximately the same as depicted in the table in this section. The relative quantity and distribution of the microcircuits does not require a new packaging design. If there were a large quantity of microcircuits or if they were all concentrated in one section of the design, it would be worthwhile to package them as a separate module. However, in the case of the Sensor's electronics, the microcircuits are widely dispersed with the discrete parts.

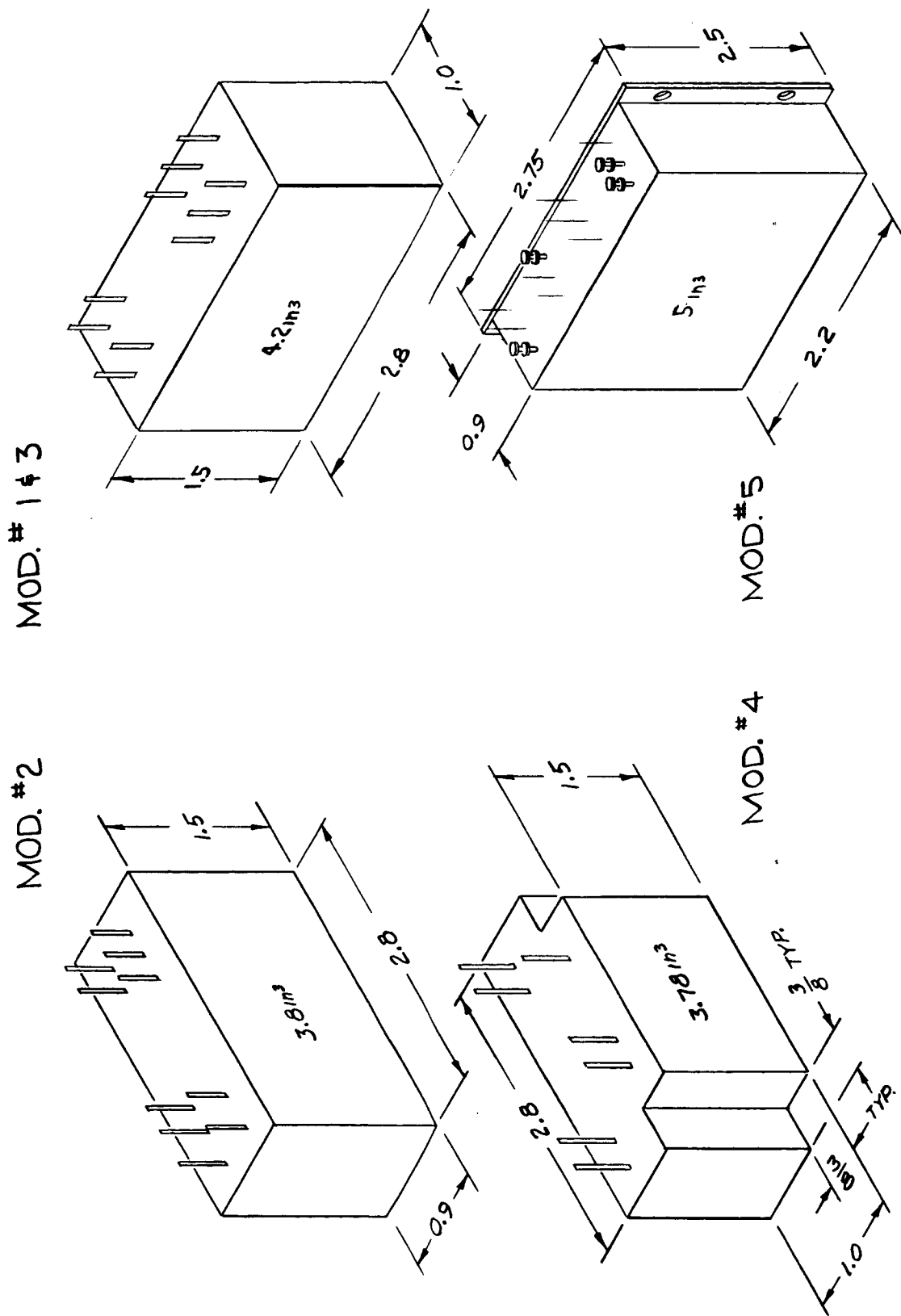


Figure 38. Module Form Factors (Using Microcircuits)

TABLE IV
MODULE/PART BREAKDOWN
(using microcircuits)

Module #	Submodule #	Circuits	# Parts	Parts/in ³	Vol (in ³)	Power Dissip. (mw)	# Terminals
1	6	CO ₂ , N ₂ and Total Channels	101	24	4.20	250	17
2	4	O ₂ Channel CO ₂ Lamp Driver	93	25	3.80	200	14
3	12	H ₂ O Channel Timing Gen.Output Drivers	111	27	4.20	300	31
4	3	DC/DC Conv. EMI	43	11	3.78	250	7
5	3	Ultraviolet Lamp Driver, P/M P.S.	75	15	5.00	2000 or 4000	10
Totals	28		423		20.98	3000 or 5000	79

TABLE V
MODULE WEIGHT CALCULATIONS
(using microcircuits)

		(Pounds)
1.	<p>Foam:</p> <p>Assume 60% of module volume is foam Volume of 5 modules is 20.98 in³ Weight of foam = (20.98 x 0.6) 0.0058 lbs./in³ =</p>	0.073
2.	<p>Parts and Wiring:</p> <p>40% of volume is parts and wiring Density is 0.1 lbs./in³ Weight = (20.98 x 0.4) 0.1 lbs./in³ =</p>	0.838
3.	<p>Header Boards:</p> <p>Volume = 0.77 in³, Density = 0.047 lbs./in³ Weight = 0.525 x 0.1 =</p>	0.053
4.	<p>"T" Frame Module #5:</p> <p>Volume = 0.525 in³, Density = 0.1 lbs./in³ Weight = 0.525 x 0.1 =</p>	0.053
5.	<p>Shields:</p> <p>Size = (1.5 + 1.0) (2.8) (0.007) inches Copper = 0.003 in., Mylar = 0.002 in thick Weight = (2.5 x 2.8) (0.003 x 0.3 $\frac{\text{lbs.}}{\text{in}^3}$ + 0.3 lbs. + 0.004 x 0.05 $\frac{\text{lbs.}}{\text{in}^3}$ (4 foils) =</p>	0.031
6.	Miscellaneous	0.029
Total Weight		1.060

From a cordwood module standpoint, it is possible to house either the "flat-pack" or the "can" type of microcircuit. Figure 39 shows how this

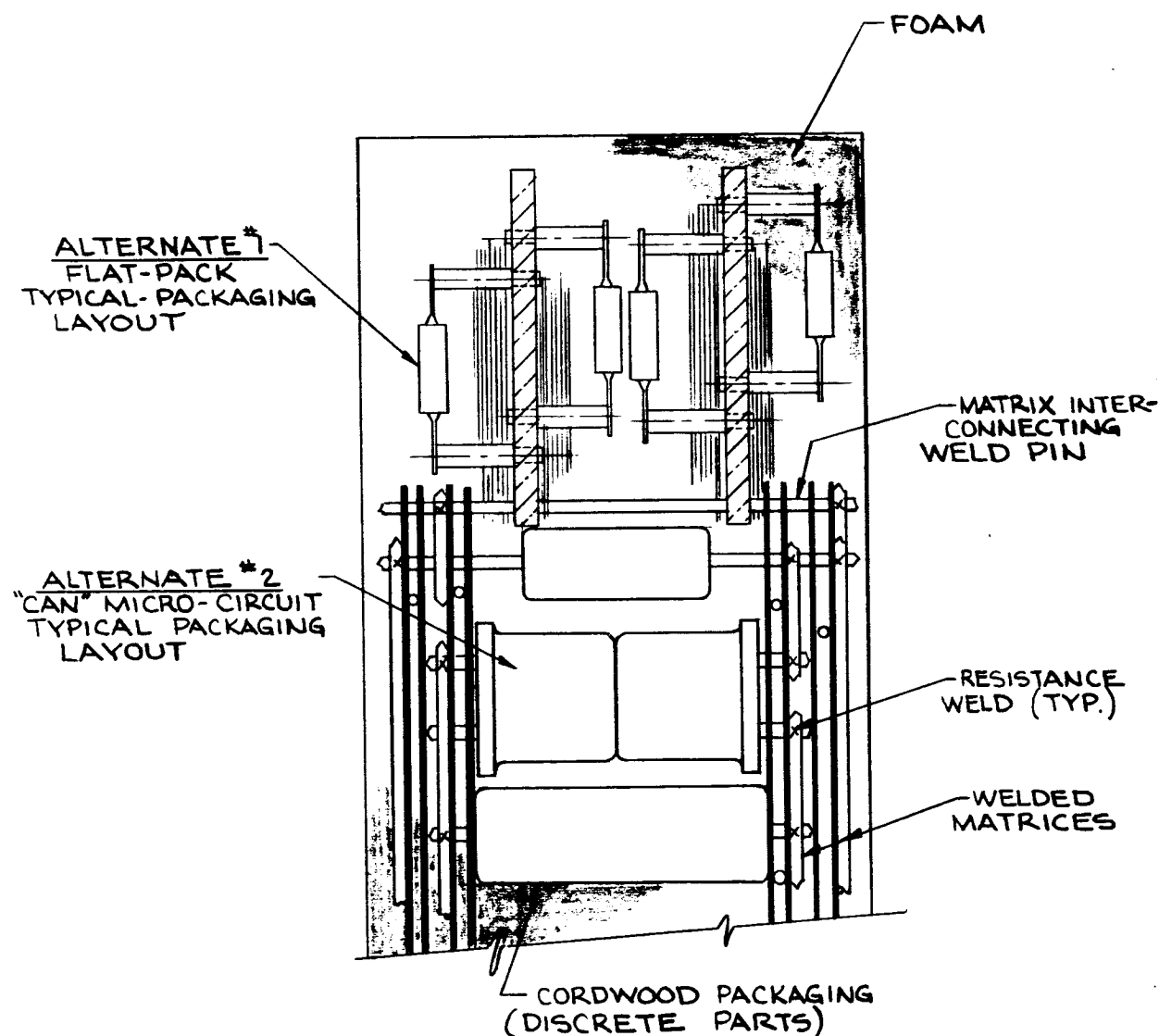


Figure 39. Alternate Microcircuits/Cordwood Module Packaging

is done. If a choice can be made, based on packaging, preference should be given to the "can" type unit. This is because the type of circuitry in which they are used, low-level analog, is such that the discrete electronic parts associated with each microcircuit should be located as close to the microcircuits as possible. A digital circuit, for example, does not normally require that discrete parts be located close to the microcircuit.

The "can" configuration allows "stacking" of parts back-to-back and their direct integration within the cordwood module. The peripheral

resistors and capacitors are located next to each part. The "flat-pack" parts would have to be packaged in a localized area within the module if a high degree of packaging efficiency is to be maintained. Otherwise, scattering them throughout the module requires more wiring and clearance volume.

2.4.4 ENVIRONMENTAL CONSIDERATIONS

Design of the electronics subassembly of the Two-Gas Atmosphere Sensor has been influenced largely by the environments in which it must operate, and to a somewhat lesser degree by the environments in which it must be stored or transported. These environments dictate a lightweight, stiff package with well defined paths for removal of heat.

2.4.4.1 THERMAL DESIGN

Design of the electronics subassembly must provide for proper operation of all circuits when the subassembly is exposed to ambient temperatures or 40° to 90°F. The maximum temperature of any piece part was selected conservatively to be 160°F. Thus, a temperature differential of 70°F exists between the most remote part and the structure to which the electronics subassembly is mounted.

The circuit is so divided into modules that the highly dissipative parts are all in one module, while a rather uniform distribution of low dissipation parts occurs in the others. Thus, two distinct thermal designs may be employed, while adhering to the same general principles.

The basic principles employed in both designs are: (1) conduction as the mode of heat transfer; (2) a thermal path as direct and short as possible; (3) materials selected for adequate thermal conductivity values; (4) a minimum of thermal interfaces; (5) good contact at thermal interfaces.

Module No. 5

The one module containing highly dissipative parts requires particularly careful design, with strict adherence to the principles outlined in the preceding paragraph. Referring to Figure 34, it can be seen that large, dissipative parts are mounted directly to metal structure, which consists of a "T" shaped frame fastened directly to the heat sinking surface. Module parts having low dissipations are placed in submodules, which are bonded to the metal frame. Aluminum is selected because of its high thermal conductivity/weight ratio. Parts which are stud-mounted are insulated electrically from the aluminum by a high thermal conductivity beryllium oxide washer and thermal joint compound. This mounting method can reduce thermal resistance at interfaces to 1°F/watt/in². Parts which are dissipative, but not stud-mounted, such as large resistors, are bonded to the aluminum by a high thermal conductivity adhesive.

A typical thermal calculation for a stud-mounted part is as follows: See Figure 40 for the thermal path:

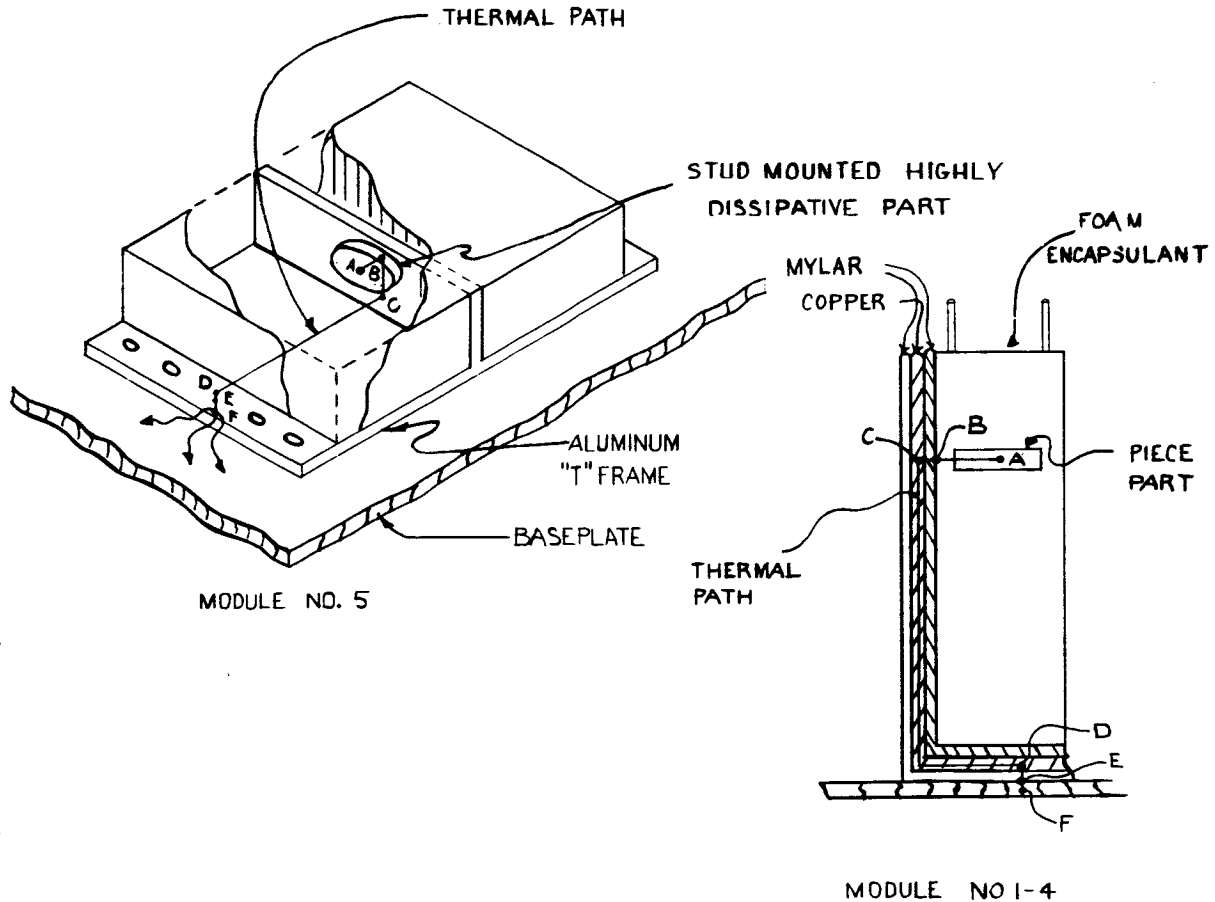


Figure 40. Typical Thermal Paths

- Assume:
1. Part dissipates 1.50 watts, and has thermal contact over a 0.40 in^2 area.
 2. Conductivity of aluminum is $100 \text{ BTU/ft}^2 \text{ hr/}^\circ\text{F/ft}$, and thickness is 0.060 in .
 3. Resistance at thermal interfaces A-B and E-F is 1°F/w/in^2 .
 4. Width of path from B to D is 0.80 in .
 5. Contact area at interfaces E-F is 0.080 in^2 .

$$\Delta t_{A-B} = \frac{(1^\circ\text{F}/\text{w}/\text{in}^2) (1.50\text{w})}{(0.40 \text{ in}^2)} = 3.75^\circ\text{F}$$

$$\Delta t_{B-C} = \frac{\left(\frac{41 \text{ BTU/hr}}{\text{w}} \times \frac{\text{in}}{\text{ft}} \right) (1.50\text{w}) (0.75 \text{ in})}{\left(\frac{100 \text{ BTU/ft}^2\text{hr}}{^\circ\text{F/ft}} \right) (0.80 \text{ in}) (0.060 \text{ in})} = 9.6^\circ\text{F}$$

$$\Delta t_{C-D} = \frac{(41) (1.50/2) (1.25 \text{ in})}{(100) (0.80 \text{ in}) (0.060 \text{ in})} = 8.0^\circ\text{F}$$

$$\Delta t_{D-E} = \frac{(41) (1.50/2) (0.030 \text{ in})}{(100) (0.080 \text{ in}^2)} = 0.1^\circ\text{F}$$

$$\Delta t_{E-F} = \frac{(1^\circ\text{F}/\text{w}/\text{in}^2) (1.50/2)}{(0.08 \text{ in}^2)} = 9.4^\circ\text{F}$$

$$\Sigma \Delta t = \Delta t_{A-F} = 30.9^\circ\text{F}$$

Since the temperature at F is assumed equal to ambient, or 90°F, the temperature at the surface of the part is 90°F + 30.9°F = 120.9°F, which is well within the allowable limit for proper circuit operation. Detailed design calculations will consider reducing the metal thickness (to reduce weight) so that the part temperature more closely approaches the allowable maximum.

Modules No. 1-4

The modules containing low dissipating parts, uniformly distributed throughout, are designed to transfer their heat through the foam and EMI shield to the mounting surfaces as illustrated in Figure 32. These parts do not require individual consideration in thermal design, except that some parts will tend to dissipate somewhat more than others, and these will be located to obtain short thermal paths. Parts which dissipate considerably more power can be foil-wrapped, with the foil carried to the thermal interface to establish a more conductive path than the encapsulant provides.

A typical calculation for uniformly distributed power dissipation is as follows: See Figure 40 for the thermal path and Figure 35 for dimensions:

- Assume: 1. Module #1 dissipates 300 mw, and this wattage is uniformly distributed.

2. Conductivity of foam encapsulant is

$$\frac{0.020 \text{ BTU/ft}^2\text{hr}}{^\circ\text{F/ft}}$$

3. Conductivity of Mylar is $0.086 \text{ BTU/ft}^2\text{hr/}^\circ\text{F/ft}$

4. Conductivity of copper is $225 \text{ BTU/ft}^2\text{hr/}^\circ\text{F/ft}$

5. Thermal interface resistance is 1°F/w/in^2

6. EMI shield is bonded to foam, so that no appreciable thermal interface exists at this point and Mylar is bonded to copper with no appreciable thermal interface.

$$\Delta t_{A-B} = \frac{(41) (0.300\text{w}) (0.45 \text{ in})}{(0.020) (2.0 \text{ in}) (2.8 \text{ in})} = 49.5^\circ\text{F}$$

$$\Delta t_{B-C} = \frac{(41) (0.300\text{w}) (0.002 \text{ in})}{(0.086) (2.0 \text{ in}) (2.8 \text{ in})} = 0.1^\circ\text{F}$$

$$\Delta t_{C-D} = \frac{(41) (0.300\text{w}) (1.45 \text{ in})}{(225) (2.8 \text{ in}) (0.003 \text{ in})} = 9.4^\circ\text{F}$$

$$\Delta t_{D-E} = \frac{(41) (0.300\text{w}) (0.002 \text{ in})}{(0.086) (0.90 \text{ in}) (2.8 \text{ in})} = 0.1^\circ\text{F}$$

$$\Delta t_{E-F} = \frac{(1^\circ\text{F/w/in}^2) (0.300\text{w})}{(0.90 \text{ in}) (2.8 \text{ in})} = 0.1^\circ\text{F}$$

$$\Sigma \Delta t = \Delta t_{A-F} = 59.2^\circ\text{F}$$

The temperature of the structure at F is assumed to equal ambient, or 90°F . Thus the temperature of the piece part is $90^\circ\text{F} + 59.2^\circ\text{F} = 149.2^\circ\text{F}$, which is within the assumed allowable limits for proper circuit operation. This analysis neglects the effects upon gross thermal conductivity of the individual conductivities of the parts and wiring. In a foam-encapsulated module, the parts and their leads play a large role in heat transfer by providing paths of good conductivity in parallel with the foam. It is reasonable to assume, then, that the actual part temperature is considerably less than 149.2°F , although proof of this fact will be made in the detailed design.

2.4.4.2 STRUCTURAL DESIGN

The electronics subassembly will be exposed to shock and acceleration loads which are not considered to be severe, but which must be considered in the design. Figure 32 illustrates the manner in which the modules are mounted to the structure. There are two distinct designs employed which will be discussed individually.

Module No. 5

This module, which contains large, highly dissipative parts, is mounted to the structure independently of the other modules, primarily for thermal reasons. The module itself is "built up" on a "T" shaped aluminum frame to provide a stiff structure, as well as a highly conductive one. It is held to the mounting structure by screws through the ends of the "T" shaped frame. At the time of detailed design, the optimum number and size of screws will be determined, based upon considerations of shock and acceleration loads, weight, and heat transfer requirements.

Modules No. 1-4

These modules are fully encapsulated in lightweight foam and must be held firmly in place by external clamping. The lightest possible clamping device is the wiring board, since the use of this portion of the electronics subassembly eliminates the need for other devices designed solely for clamping. The principle of using material for more than one function is thus upheld, resulting in the lightest possible weight.

The major consideration in clamping modules in this manner is the range of temperatures to which the subassembly is exposed. At low temperatures, materials contract, tending to loosen the modules, allowing them to rattle under vibration. At high temperatures, the materials expand, causing large forces to be imposed upon the materials.

Calculations indicating the adequacy of this design are as follows:

1. Assume a preloading of the bolts at room temperature sufficient to cause 10 lb/in^2 of pressure to remain on the modules at -65°F .
2. Assume the wiring module to be sufficiently stiff so that its deflection may be neglected.
3. Assume no relative movement of the wiring module/bolting boss interface, i.e., no separation of this interface during thermal expansion.
4. Coefficients of thermal expansion are:
 - a. Foam: $22.2 \times 10^{-6} \text{ in/in/}^\circ\text{F} (d_f)$

b. Aluminum: 13.0×10^{-6} in/in/°F (α_{Al})

5. Assume that the lengths of the foam and aluminum are equal. ($l = 2.0$ in).
6. The temperature excursion is -65°F to 200°F or 265°F.
7. Modulus of elasticity of foam (E_f) is 11,000 lb/in².

Deflection of foam Δf = Deflection due to temp. (δ_{tf}) - Deflection due to load (δ_{pf})

Deflection of Aluminum Δ_{Al} = Deflection due to temp. (δ_{tAl}) + Deflection due to load (δ_{pAl})

$$\Delta_f = \Delta_{Al}$$

$$\delta_{pf} = \delta_{pAl}$$

$$\begin{aligned} \therefore \delta_{pf} &= \frac{\delta_{tf} - \delta_{tAl}}{2} = \frac{(\alpha_f - \alpha_{Al}) l \Delta t}{2} \\ &= \frac{(22.2 - 13.0) (10^{-6}) (2.0) (265)}{2} \\ &= 2.5 \times 10^{-3} \text{ in.} \end{aligned}$$

$$\begin{aligned} \delta_{tf} &= \alpha_f l \Delta t \\ &= (22.2) (10^{-6}) (2.0) (265) \\ &= 11.8 \times 10^{-3} \end{aligned}$$

$$\begin{aligned} \Delta_f &= \delta_{tf} - \delta_{pf} \\ &= (11.8 - 2.5) (10^{-3}) \\ &= 9.3 \times 10^{-3} \end{aligned}$$

$$\begin{aligned}
 \text{Stress in foam } (S_f) &= \frac{(\Delta_f) (E)}{l} \\
 &= \frac{(9.3) (10^{-3}) (11,000)}{2.0} \\
 &= 51.3 \text{ lb/in}^2
 \end{aligned}$$

$$\text{Initial pressure} = 10 \text{ lb/in}^2$$

$$\text{Total Stress in foam} = 51.3 + 10.0 = 61.3 \text{ lb/in}^2$$

Foam of 10 lb/ft³ density has a compressive strength of about 300 lb/in². In view of this fact, a greater pre-load may be placed on the bolts. This may become desirable when the overall vibration, shock, and acceleration loads are taken into account.

Wiring Board

The wiring board is used as previously stated, as a clamping bar to apply pressure to the modules. Figure 36 illustrates the construction of this board. It must be designed to withstand the forces imparted to it during thermal expansion.

The following calculations indicate the adequacy of the design in this respect.

1. Consider for simplification, only the raised edges of the board.
2. Treat these edges as two beams fixed at both ends with a uniformly distributed load.

$$\begin{aligned}
 \text{Load on one beam } (W) &= \text{Pressure on modules} \times \text{Module Area}/2 \\
 &= \frac{(61.3 \text{ lb/in}^2) (3 \text{ in}) (4 \text{ in})}{2} \\
 &= 368 \text{ lbs}
 \end{aligned}$$

$$\begin{aligned}
 \text{Maximum moment } (m) &= \frac{Wl}{12} \\
 &= \frac{(368 \text{ lb}) (4 \text{ in})}{12} \\
 &= 123 \text{ in lbs}
 \end{aligned}$$

$$\begin{aligned}
 \text{Moment of inertia} &= \frac{bh^3}{12} \\
 \text{of beam (1)} &= \frac{(0.2 \text{ in}) (0.2 \text{ in})^3}{12} \\
 &= 1.33 \times 10^{-4} \\
 \\
 \text{Stress in beam} &= \frac{Mc}{I} \\
 \text{due to bending} &= \frac{(123 \text{ in lbs}) (0.1 \text{ in})}{(1.33 \times 10^{-4} \text{ in}^4)} \\
 &= 9750 \text{ lb/in}^2
 \end{aligned}$$

The material used, an epoxy-glass, has a flexural strength of 40,000 lb/in². Thus, the design is adequate, since the assumptions made were conservative. The detail design of this part requires a compromise between weight and strength to achieve an optimum configuration.

2.4.5 SPECIFICATIONS

The following specifications and standards are recommended for the electronic packaging portion of this program:

NPC-200-4 Quality Requirements for Hand Soldering of Electrical Connections

This publication should be used as a guide for hand soldering standards, with emphasis on methods and required training.

MSFC-STD-271 Standard for Fabrication of Welded Electronic Modules

This standard should be imposed; however, it does not provide the strict controls required for welding reliability. The contractor should furnish specifications covering the following subjects:

- Welding Equipment
- Production Welding Monitoring
- Welding Process
- Weld Schedule Process
- Weld Schedule Certification

In each case, these documents should be superior to the criteria presented in MSFC-STD-271 and represent proven techniques.

MSFC-SPEC-202 Compound, Potting and Molding,
Elastomeric, Specification for

This specification should be used by the contractor as a guide for preparation of a process procedure and material specification for the material(s) to be used in the program.

MSFC-PROC-412 Procedure for Encapsulating
Electronic Modules

This procedure should be reflected in the contractor furnished process and material procedures. The training requirements, methods, facilities, and equipment requirements should be satisfied.

ND1002002 (Apollo Guidance & Navigation Specification)
Encapsulating With Polyurethane Foam

This process procedure should be used by the contractor as a guide in preparation of process procedures concerning foaming.

NPC-200-3 (NASA Quality Publication) Inspection
System Provisions for Suppliers of Space Materials,
Parts, Components and Services

The contractor should comply with this document in its entirety.

NPC-200-2 (NASA Quality Publication) Quality
Program Provisions

Section 7 - should be adhered to by the contractor for all testing activities.

Section 13 - training of contractor personnel should be mandatory and satisfy NASA requirements for:

- Soldering
- Welding
- Encapsulating.

In addition to the contractor furnished specifications, there are a number of subjects for which no satisfactory NASA-MIL specification can be found. These subjects should be covered by contractor furnished specifications, specifically concerning:

Split-Pin Wire-Wrapping

A specification should be provided covering the design criteria, materials, tool control, process control, inspection, and test requirements for the split-pin wire-wrapping process. Emphasis should be given to control, since this process can be stringently controlled to result in high reliability connections.

Buffer Coating

A process and material specification should be prepared for elastomeric buffer coating of modules and parts. Preparation and handling of the modules during the process should be described in detail.

Workmanship

Workmanship standards reflecting the design criteria should be furnished. All aspects of the design should be covered with one or more standards describing the following:

- Welding
- Wire-Wrapping
- Encapsulating and Foaming
- Any critical Physical Aspects of the Design.

Repair/Rework

The contractor should furnish an allowable Rework/Repair specification. The use of this specification should be the responsibility of Quality Control. The scope of use, discrepant material conditions, limitations, repair methods and repairs, and data recording procedures for discrepant material control should be detailed.

2.5 DESIGN STUDIES

2.5.1 LINEAR INTEGRATED CIRCUIT STUDY

During Phase I of the Two-Gas Atmosphere Sensor Program the feasibility of employing a linear integrated circuits approach to the electronics portion of the proposed system has been under investigation by Perkin-Elmer.

It has been ascertained that several manufacturers produce linear integrated circuits, which are presently available and which appear to fulfill our circuit requirements (Paragraph 2.5.1.1). Since the present "state of the art" of linear integrated circuits is in its infancy, definite precautions must be taken before this technique can be recommended as a design approach. The following factors will have a marked effect on circuit performance and reliability:

Close surveillance of manufacturing processes.

Initial design compensation for drift due to aging.

It is important that these factors be considered thoroughly and used as a criterion in selecting a particular integrated circuit vendor or vendors. It is also essential that any linear integrated circuit, proposed by Perkin-Elmer for incorporation on the Two-Gas Atmosphere Sensor Program be set forth in a detailed purchase specification. Exclusion of any of the aforementioned factors would lead to a recommendation that preference be given to a transistorized circuit design, utilizing MIL- approved transistors.

Circuit performance and reliability are not the only factors affecting the choice of an approach. Other tradeoffs must include such factors as cost, size, weight, and power dissipation in order that the best overall design can be achieved. Specific areas investigated during the linear integrated circuit study are discussed in detail in the following paragraphs.

2.5.1.1 MONOLITHIC LINEAR CIRCUITS

The below-listed circuits were evaluated for possible incorporation into the Two-Gas Atmosphere Sensor System.

- a) Fairchild μ A 709, price \$75.00 for quantity 1-24, delivery 16 to 20 weeks.
- b) Fairchild μ A 702A, price \$50.00 for quantity 1-24, delivery 16 to 20 weeks.
- c) Texas Instruments SN 524A, price \$29.25 for quantity 1-24, delivery 14 to 16 weeks. SN 526A, price \$57.00 for quantity 1-24, delivery 14 to 16 weeks.

- d) Motorola MC 1530, price \$27.00 for quantity 1-24, delivery 14 to 16 weeks, MC 1531, price \$30.00 for quantity 1-24, delivery 14 to 16 weeks.

Of these devices, only the Fairchild μ A 709, and μ A 702A have been tested and approved on any Military or Space Program. Grumman Aircraft is presently using these devices on the LEM vehicle, and their approval for the μ A 702 is based on an IDEP report 515.50.02.0F8-01, a compilation of data from a test performed by RCA. The μ A 709 was approved by Grumman based on its similarity to the μ A 702. Grumman found it necessary to follow this procedure since the μ A 709 is a new device and there is no test data available. Based on above information, and assuming proper use of these devices, the μ A 702 and the μ A 709 can be recommended for use on this program.

2.5.1.2 HYBRID CIRCUIT SOURCES

The following processes for manufacturing hybrid linear integrated circuits were considered during the Phase I effort.

- a) Thick Film Process, National Semiconductor, Danbury, Connecticut.
- b) Thin Film Process, Electra Manufacturing Co., Independence, Kansas; Halex, Inc., El Segundo, California.
- c) Semiconductor Chip Process, General Instruments, Plainview, New York.

A comparison of component ranges and ratings available for each of these processes is presented in Table VI and existing reliability test data is shown in Table VII.

2.5.1.3 FAILURE MODES OF INTEGRATED CIRCUITS

- a) Hybrid Circuits.

The predominant mode of failure, exhibited by thin and thick film hybrid circuits, is breakage of the mechanical interconnections between chips. This mode of failure can be minimized by the following techniques:

- (1) Using gold wire of sufficient thickness to eliminate wire breakage.
- (2) Double bonding of all gold bonds.
- (3) Subjecting all circuits to a vibration screening test.

TABLE VI COMPONENT RANGE AND RATING

TYPE OF COMPONENT	THIN-FILM		THICK-FILM		SEMICONDUCTOR	
	Preferred	Obtainable	Preferred	Obtainable	Preferred	Obtainable
Resistor Values (ohms)	100 to 20,000	25 to 100,000	50 to 300K	10 to 1 Meg	250 to 2500	100 to 20,000
Tolerance (percent)	±5	±1/2	±25%	±2%	±20	±10
Temperature Coefficient (ppm/deg C)	100	10	±200	±25	2500	1000
Power Dissipation (w/sq in)	2.5	5	2.5	5	2.5	5
Capacitor Values (picofarads)	20 to 2000	10 to 20,000	20 to 10,000	10 to 30,000	50 to 150	20 to 500
Tolerance (percent)	±5 to ±10	±1/2	±25%	±10%	±20	±10
Temperature Coefficient (ppm/deg C)	±200	±100	±300	±100	1000	1000
Dissipation Factor (percent)	0.1	0.01	2	0.2	1	0.1
Inductor Values (microhenrys)	1 to 4	10	-	-	None	None
Tolerance (percent)	±5	±1/2	-	-	None	None
Active Devices Diodes Transistors	Any type as add on (Low Power)	Any type as add on (Medium Power)	Any type as add on (Low Power)	Any type as add on (Medium Power)	Any silicon planar type (Low Power)	Any silicon planar type (Medium Power)
Distribution RC	Same as resistors and capacitors	Same as resistors and capacitors	Same as resistors and capacitors	Same as resistors and capacitors	Same as resistors and capacitors	Same as resistors and capacitors
Ckt types available	Wide range of linear & digital circuits	Wide range of linear & digital circuits	Wide range of linear & digital circuits	Wide range of linear & digital circuits	Wide range of digital, limited linear circuits	Wide range of digital, limited linear circuits

TABLE VII
SUMMARY OF FAILURE RATE DATA

Source	No. of Tests	Device Hours	Failures	Failure Rate %/1000 Hours	
				Best Estimate	90% Confidence
MIT	1	2,000,000	2	0.15	0.3
MIT	1	2,000,000	26	1.4	1.8
MIT	1	50,000,000	0	0.0014	0.005
Boeing Operating Life 125°C	9	44,236,000	27	0.06	0.08
Boeing Operating Life Ambient	6	54,320,000	4	0.0088	0.015
ARINC	33	118,331,520	26	0.022	0.028
IDEF Report No. 515.50.02. 00.F8-01 (RCA)	1	200,000	0	.03	0.115

b) Monolithic Circuits.

The predominant failure modes for monolithic circuits are varied and are attributable to poor processing techniques. Variables inherent in the processing of monolithic circuits can generate reliability problems. Some of the most prevalent modes of failure are the following:

- (1) Poor bonding techniques and control.
 - (a) Lead wires touching either substrate edge on the package lid.
 - (b) Formation of aluminum-gold alloy (purple-plague), creating an open circuit between contacts.
 - (c) Lifting of bonds.
- (2) Poor photochemistry.
 - (a) Missing oxide.
 - (b) Random aluminum strips.
- (3) Misalignment of mask caused by high resistance contact.
- (4) Imperfections in bulk material or oxide.
 - (a) Imperfections in silicon crystal resulting in the formation of epitaxial spikes, creating non-uniform junctions during diffusion.
 - (b) Voids or holes in the oxide layer exposing the silicon.
 - (c) Impurities in the oxide creating conductive channels.

2.5.1.4 DRIFT PROBLEMS

Another problem area common to all integrated circuits is electrical parameter drifts with age and temperature. Although the exact magnitude of these drifts is not known at this time, precaution must be taken in the initial design to allow for some drift of electrical parameters.

2.5.1.5 PROCESSES USED TO FABRICATE MONOLITHIC STRUCTURES

There are three basic processes by which a monolithic circuit is presently constructed:

- a) Double-Collector process.
- b) Triple-Diffused process.
- c) Epitaxial-Diffused process.

All of the above result in four-layer monolithic structures. The primary differences are in the steps by which they are processed and the resulting circuit characteristics. The emitter and base impurity distributions for all three processes are essentially alike. Structural and electrical characteristic differences show up in the collector and substrate regions.

Upon examination of the advantages and disadvantages listed below, it is evident that the Epitaxial-Diffused process is the best of the monolithic circuit processes.

Double-Collector Process

The major drawback in the Diffused-Collector structure is the decrease in the number of impurities in the collector as the collector-substrate junction is approached, thus producing a negative impurity gradient. This effect is the exact opposite of that which is desired. Collector-to-base capacitance is determined primarily by the doping level in the collector immediately adjacent to the collector-base junction. Although the collector-base junction will gradually change from P-type (base) to N-type (collector), the collector doping is near a maximum at the collector-base junction, making this capacitance value a maximum. The collector-base breakdown voltage is also reduced by the comparatively high surface concentrations on either side of the junction, as compared to that attained in the other two processes.

Since the base is diffused into the collector region having the greatest conductivity, the series collector resistance cannot be optimized. Since this process grades the collector background, the base region, which must have a carefully controlled gradient, is diffused into a background concentration that varies with distance from the surface of the wafer. This is not a favorable situation and presents problems in controlling the surface concentration of the base region.

Triple-Diffused Process

The Triple-Diffused structure has the advantage of a uniformly doped collector region, thus eliminating a compromise between breakdown voltage and capacitance at the collector-base junction of the diffused-collector structure.

The doping level of the collector can be chosen to minimize the collector-to-base capacitance and maximize the collector-to-base breakdown voltage. The only restriction is that of maintaining low collector sheet resistance in order to obtain low $V_{CE} \text{ (SAT)}$.

However, the Triple-Diffused structure does have two inherent limitations. Since the substrate is diffused, the collector region is the most lightly doped side of the collector-substrate junction. Therefore, the collector-to-substrate capacitance will be determined by the doping level in the collector. Since permissible collector sheet resistance will impose a minimum collector doping level, collector-to-substrate capacitance can never be fully eliminated.

The P-type diffusion, performed for purposes of isolation, must diffuse through half the thickness of the wafer. Therefore, the thickness of the wafer must be limited in order to maintain a reasonable diffusion time cycle. Since the diffusion of these impurities, either N-type or P-type, is isotropic in nature, the diffused layer will diffuse under a masking oxide to approximately the same distance as the depth of diffusion. This under-diffusion will reduce the usable area of each isolation region. The greater the thickness of a wafer, the larger the inactive area of each isolation region.

Epitaxial-Diffused Process

The Epitaxial-Diffused process has all of the advantages of the Triple-Diffused structure and none of its limitations. There are no wafer thickness limitations upon the Epitaxial-Diffused system. The thickness of the N-type collector-epitaxial region is independent of the thickness of the P-type substrate. Since the parent material is the P-type substrate, its doping level may be so chosen that the collector-to-substrate capacitance is independent of the doping level of the collector region. Thus, this parasitic capacitance may be minimized without influencing other device parameters.

2.5.1.6 PARASITIC CAPACITANCE AND COLLECTOR SERIES RESISTANCE PROBLEMS IN MONOLITHIC INTEGRATED CIRCUITS

The means used to interconnect paths between circuit elements in monolithic integrated circuits are thin strips of aluminum deposited on the top of the die. This method requires the collector contact of the transistor to be at the top of the silicon die, rather than at the bottom as with discrete transistors. When the collector is brought to the top of the die, the length of the signal path through the collector increases. The result is an increased collector series resistance. The increased collector series resistance increases the saturation voltage, thereby limiting the maximum operating current level.

Another characteristic unique to monolithic circuits is parasitic capacitance between the collector and the surrounding P-type material substrate. This capacitance and the increased collector resistance increase the collector time constant. The increase in the time constant results in an

increase of noise and a reduction of gain at higher frequencies. This increased time delay at high frequencies also makes it difficult to design stable RC feedback loops.

There is no presently known method for reducing the effect of increased collector resistance generated in monolithic circuits. However, a method has been developed to minimize the parasitic capacitance and to provide isolation. An N^+ layer is grown beneath the N-collector of the transistor. This technique provides the maximum reverse potential for the substrate collector diode and thus increases isolation while reducing the parasitic capacitance.

2.5.1.7 SUMMARY OF ELECTRICAL CHARACTERISTICS OF MONOLITHIC SEMICONDUCTORS

Transistors

Properties of the monolithic transistor are presented in Table VIII, along with typical values for both the non-gold-doped process and the gold-doped process. A comparison of the values for each characteristic reveals how significantly the resistivity of the epitaxial collector influences breakdown voltages, capacitances, series resistance, and frequency response.

The non-gold-doped process with the 0.5-ohm-cm collector is very similar to the 2N918 passivated epitaxial transistor, which is its closest discrete counterpart. The f_T of the 2N918, is about twice as high as that of the monolithic transistor, because the 2N918 has less parasitic capacitance and collector series resistance than the corresponding monolithic transistor.

The maximum frequency (f_{max}) is defined as that frequency at which the matched grounded-emitter power gain is equal to unity. The f_{max} of the 2N918 is considerably higher than that of the monolithic transistor because the discrete transistor has a higher f_T . Since power gain decreases approximately as the square of frequency, the monolithic transistor will have a lower power gain than the discrete transistor.

The gold-doped switching transistor described in Table VIII closely resembles the 2N709, passivated epitaxial discrete transistor. These devices are gold-doped to reduce the amount of stored charge when switched into saturation. The storage time constant is roughly 10 nsec. The f_T for the monolithic transistor is about 500 MC, compared to about 800 MC for the 2N709. $V_{CE(SAT)}$ for the monolithic transistor is greater than for the 2N709 (0.26 volt compared to 0.18 volt). The substrate capacitance is quite detrimental to switching speed of logic circuits since C_{TS} must be charged through the load resistor R_L .

Monolithic transistors find application in analog-circuits such as differential amplifiers. For the differential amplifier circuit, the matching and tracking characteristics of β and V_{BE} are important design considerations. Since both these characteristics are a function of sheet resistance

TABLE VIII		
PROPERTIES OF MONOLITHIC TRANSISTORS		
Transistor Characteristic	Non-Gold-Doped 0.5-ohm-cm Collector	Gold-Doped 0.1-ohm-cm Collector
BV_{CBO}^*	55 volts	25 volts
BV_{EBO}^*	7 volts	5 volts
BV_{CEO}	23 volts	14 volts
BV_{CS}^*	75 volts	25 volts
C_{TE} (forward bias)	6 pf	10 pf
C_{TE} at 0.5 volt	1.5 pf	2.5 pf
C_{TC} at 5 volts	0.7 pf	1.5 pf
C_{TS} at 5 volts	2.9 pf	4.6 pf
β at 10 mA*	50	50
β at 0.1 mA*	30	10
r_{SC}	75 ohms	15 ohms
$V_{CE(SAT)}$ at 5 mA	0.5 volt	0.26 volt
V_{BE} at 10 mA*	0.85 volt	0.85 volt
f_T at 5 volts, 5 mA	440 Mc	520 Mc
f_{max}	1.1 gc	--
τ_S	--	--

*Typical values.

and/or surface effects, excellent matching characteristics are obtained for a pair of transistors fabricated simultaneously within the same monolithic chip of silicon. The V_{BE} ratio can be maintained within $\pm 7.5\%$ for 90% of the units while the β at a high current can be maintained within $\pm 10\%$ for 75% of the units and within 20% for 80% of the units at lower currents. The V_{BE} drift has been found to be $10 \mu\text{V}/\text{deg C}$ over a temperature range from -50 to $+120^\circ\text{C}$.

Diodes

The five types of diodes available in monolithic circuits are summarized in Table IX.

TABLE IX					
SUMMARY OF TYPICAL VALUES FOR VARIOUS DIODE CONNECTIONS					
Characteristic	(a) $V_{CB=0}$	(b) $V_{CE=0}$	(c) $V_{EB=0}$	(d) $I_{C=0}$	(e) $I_{E=0}$
Breakdown voltage, volts	7	7	55	7	55
Storage time, nsec	9	100	53	56	85
Forward voltage, volts	0.85	0.92	0.94	0.96	0.95
p-n-p β	0	3	2	3	3
C_D , pf(5 volts reverse bias)	0.5	1.2	0.7	0.5	0.7
C_p , pf(Substrate at 5 volts negative with respect to collector)	2.9	2.9	2.9	1.2	2.9

Diode (a), in which the collector-base junction is shorted, is the most useful configuration from the standpoint of the requirements for high-speed diodes to be used in digital integrated circuits. This diode exhibits lowest forward voltage drop and no P-N-P action to the substrate. Furthermore, the storage time is quite low, since charge is stored only in the base. The storage time for this diode configuration is reduced considerably when the structure is gold-doped.

The configuration given by diode (d) in which the collector is floating, is also useful for switching circuits. Because of the additional stored charge in the floating collector, this configuration could be used as

a storage diode to be placed in series with the base of the transistor in DTL integrated circuitry. The stored charge feature can be used for obtaining a high-speed turn-off transistor as it comes out of saturation. The fact that this particular structure has the highest forward voltage drop and the smallest parasitic capacitance available, makes it useful from the standpoint of noise immunity in DTL circuits. Diode (b) also exhibits comparable characteristics and can be used in similar applications.

The collector-base configurations of diodes (c) and (e) have the highest reverse voltage ratings. However, both of these devices have relatively high P-N-P betas which limit their use to general purpose diodes.

2.5.1.8 OUTLINE OF TENTATIVE LINEAR INTEGRATED CIRCUIT PROCUREMENT SPECIFICATION

- a) All process steps will be monitored. Inspection and verification of critical processes will be required.
- b) Environmental tests will be performed on completed integrated circuits. The tests will include, but not be limited to, package seal, high temperature bake, temperature cycle, centrifuge, vibration, helium, and gross leak tests.
- c) The integrated circuits will be electrically tested for compliance with Perkin-Elmer's functional electrical requirements.
- d) The devices will be serialized and subjected to radiographic inspection.
- e) Each integrated circuit will be burned-in for 200 hours.
- f) The devices will be retested as in step (c).
- g) Integrated circuits that successfully pass steps (a) through (f) will be shipped to PECO in special containers to prevent damage during transit.

2.5.2 USE OF DIP BRAZING FOR FABRICATION OF THE TWO-GAS ATMOSPHERE SENSOR HOUSING

An investigation of the use of dip brazing for this application was brought about by two major factors. First, a high rejection rate has been encountered with the housing for the CO₂ measurement system which is an investment casting. Secondly, the use of dip brazing has solved some recent difficult fabrication problems for several parts used on military Reconnaissance Cameras by Perkin-Elmer.

2.5.2.1 DISADVANTAGES OF INVESTMENT CASTING

Of all the common casting processes, investment casting has provided the optimum combination of desirable properties for aerospace applications with respect to: strength, thinness of sections, structural integrity, choice of alloy, tooling costs, and lead time.

However, although this process is an effective method for fabricating relatively small quantities of parts, the state-of-the-art is not sufficiently advanced to eliminate problems associated with tooling and mold gating which invariably occur with complex parts.

2.5.2.2 DIP-BRAZING CHARACTERISTICS

The use of dip brazing eliminates all soundness and integrity problems in the bulk of a fabricated part. Such conditions as gas holes, shrinkage porosity, cold shuts, etc., are not possible since wrought material is used. Porosity in the brazing metal is a possible problem as is lack of wetting, however, these are readily controlled by knowledgeable suppliers.

Brazing alloys used in dip brazing may be in the form of paste, preformed wire, or as a cladding on the basic aluminum alloy being used to fabricate the part (if sheet or plate are used). These alloys are generally high silicon alloys (4343 is typical) somewhat similar to commonly used casting alloys (such as 356). The relatively poor mechanical properties of this class of alloys are confined to the joint with dip brazing while with a casting the entire part displays these properties.

High strength alloys such as 6061 and 7005 can be used as the base metal in dip brazing. These alloys show mechanical properties superior in all respects to the best aluminum investment casting alloys. These include higher ultimate, yield, and fatigue strengths as well as better ductility. Wrought high-strength alloys are also inherently more corrosion resistant than high-silicon casting alloys and respond better to anodizing and chromating processes. Distortion problems, common to both casting and dip brazing are more easily corrected with dip brazing, since the alloys used have superior ductility and may be more safely straightened.

Since the salt bath temperature for dip brazing is comparable to the solution annealing temperature, dip-brazed assemblies may be obtained in the T4 condition immediately after brazing by suitable quenching.

The only problem characteristic of the dip-brazing process that essentially does not exist in casting, is that of flux or salt entrapment. Knowledgeable suppliers are equipped to minimize or eliminate this problem. In any case, it is a readily inspectable condition with suitable chemical and radiographic methods available.

In summary it appears that dip brazing for fabricating aluminum alloy assemblies should find increasing application in aerospace components.

By clever use of tabs, interlocks, and other self-fixturing techniques, tooling and fixturing costs for this process are generally minimal, if not zero.

The process should have direct application to the two-gas atmosphere sensor housing with the gas tightness requirement presenting no unusual problems. The result will be a stronger, more fatigue resistant and more corrosion resistant assembly than can be obtained through investment casting.

2.5.3 CHOPPER METHODS FOR TWO-GAS ATMOSPHERE SENSOR

The basic requirement for the optical chopper is to provide mechanical motion to a precision slit or filter mechanism which allows the interruption of an optical image which is fixed in space. This motion is necessary in order to convert the optical image to an electrical signal, which can be operated on by the electronic system. The requirements for this chopping apply to both the ultraviolet and the infrared systems.

The chopper must perform in a manner that maintains the chopping geometry to close physical tolerances, while being operated in a system subject to typical environmental stresses. The miniature nature of the optical systems allows relatively small chopper motions, which eliminates the necessity of having the conventional large geometry chopping motor. The ideal mechanism would be one exhibiting small size, high accuracy, and low power consumption. An exhaustive vendor search has resulted in the selection of two applicable methods: the tuning fork chopper and the torsional chopper.

2.5.3.1 MOTOR DRIVEN CHOPPER

The following design parameters were used as design guides for evaluating the performance of a rotating component (motor) method of driving an optical chopper.

- a) Speed - any discrete value between 3,000 and 10,000 rpm \pm 0.5% at a nominal 28 VDC.
- b) Torque - no value specified. However, must be adequate to spin optical filter assembly.
- c) Life - 3000 hours minimum.
- d) Power consumption - 1.0 watt maximum; design goal 0.27 watt.
- e) Weight - approximately 0.2 pound.

DC Motor - The possibility of utilizing DC motors was investigated using information provided by Globe Industries, Dayton, Ohio. Speed regulation presented one problem in permanent-magnet DC motors since it varies directly with line voltage. Use of a governor, which would alone dissipate approximately

1/2 watt, would provide a speed regulation of only $\pm 1\%$ and after 300 hours the tolerance on speed regulation increases, from wear in the governor. Also, since the brush life would probably not exceed 1000 hours, it was decided that DC motors were not suitable as means of chopping on this program.

AC Synchronous Motor - The use of an AC synchronous motor was next considered. This would require utilization of a solid state inverter. Representative of responses elicited from several motor manufacturers was the following from Gaylord Rives Company of Pasadena, California, who have supplied motors for other space applications:

- a) Motor - 1" x 1", power input 1 watt, price \$300.
- b) Inverter - 2 cubic inches, special design, 0.2 watt power consumption, price \$500.

The most suitable motor found to date is a 400 cps synchronous motor from A.W. Haydon Company, Waterbury, Connecticut. Their type #19101 motor operates at 3000 rpm, 115V rms, 400 cps, 0.63 VA (0.5 watt). The size of this motor, excluding shaft, is 3/8" diameter by 0.313" long. The vendor states that it is feasible to rewind the #19101 motor for 26V rms at 400 cps and thereby simplify the inverter. A. W. Haydon has, however, stated that they do not wish to provide such an inverter.

Disadvantages of the #19101 AC synchronous motor are as follows:

- a) The output shaft is only 0.2047 inch in diameter, which makes it difficult to mount an optical filter on the shaft.
- b) Since the rotor does not run on precision bearings, supplementary gearing to a precision mounted shaft, carrying the optical filter, would be required.
- c) It is questionable whether the motor torque (0.0004 oz.-in. starting and 0.0002 oz.-in. running) is adequate to properly drive the chopper.

As a result of the above-cited studies, it was concluded that for the design parameters given, there is no solution using a motor-driven chopper.

2.5.3.2 TUNING FORK CHOPPER

A tuning fork chopper (Figure 41) appears to be a feasible method of chopping and is presently being considered. Advantages and disadvantages of this method are as follows:

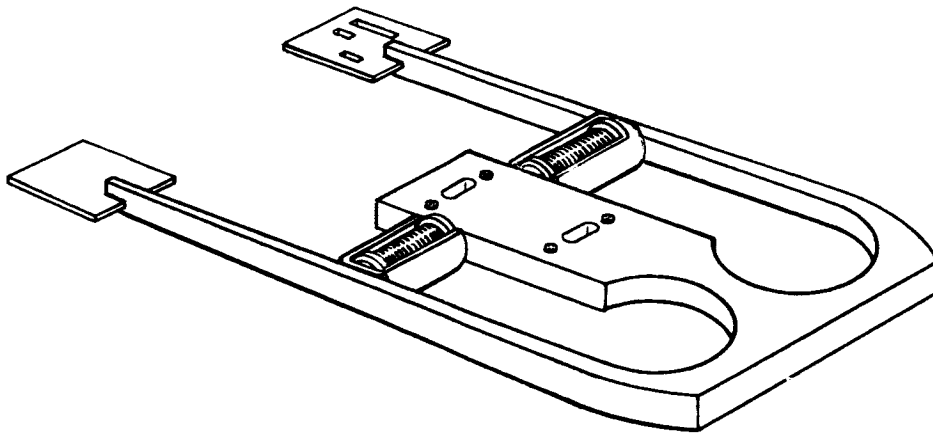


Figure 41. Tuning Fork Optical Chopper Improved Design
(Drawing twice actual size)

Advantages:

- a) Lowest power consumption of any method considered.
- b) Perkin-Elmer has previous experience on this method of chopping on the Apollo Carbon Dioxide Sensor.
- c) Frictional losses are low.
- d) Weight is relatively low.
- e) Frequency stability is high.

Disadvantages:

- a) Requires sophisticated electronics in the drive and pick-off circuits. This leads to an increase in size and failure rate of the entire assembly.
- b) Cannot sample in discrete steps.
- c) Cannot chop below 600 cps without undesirable side effects.
- d) Relatively difficult to mechanically set up and align.

2.5.3.3 TORSIONAL CHOPPER

Another feasible method of chopping is to employ a torsional chopper with flexural pivots (Figure 42). Advantages and disadvantages of this method are as follows:

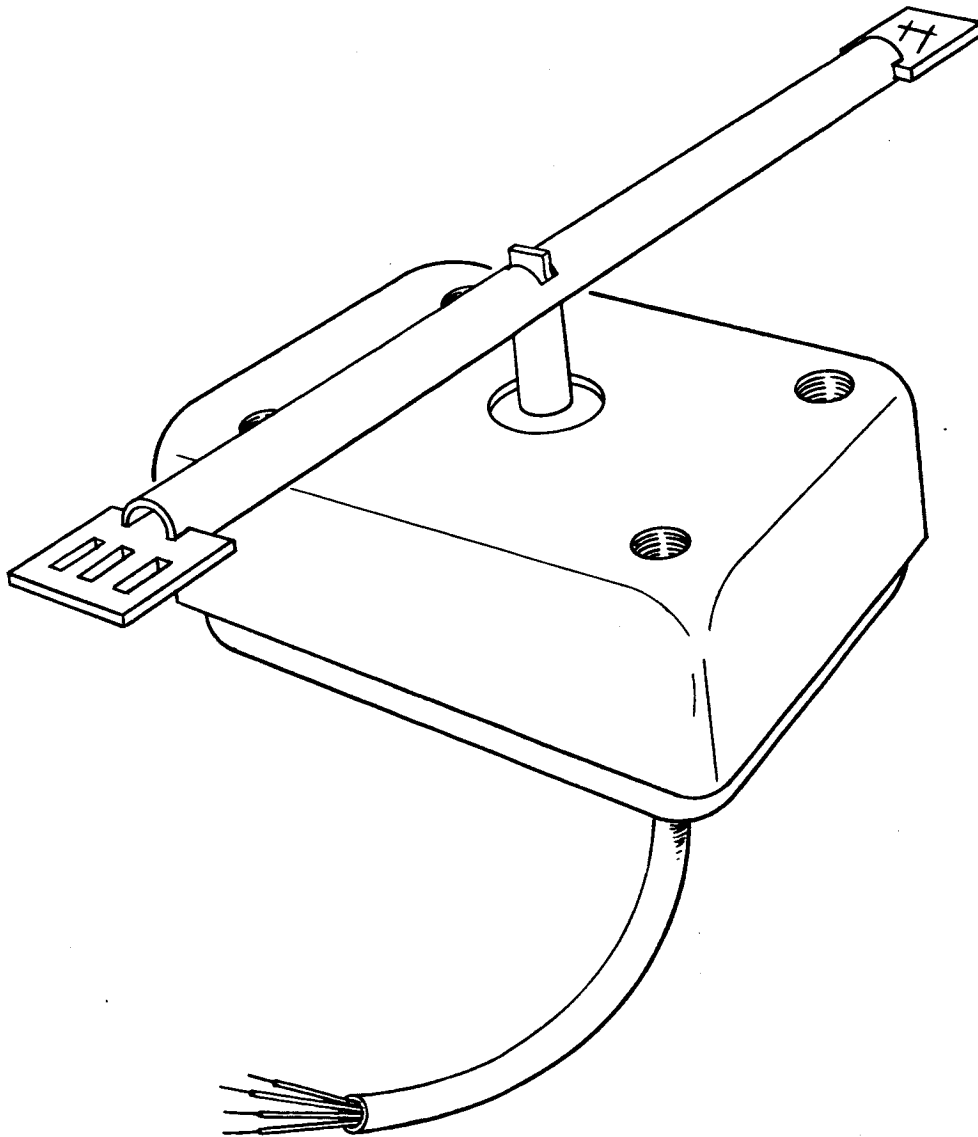


Figure 42. Torsional Chopper

Advantages:

- a) Can sample in discrete steps.
- b) Unlimited life is possible if properly applied.

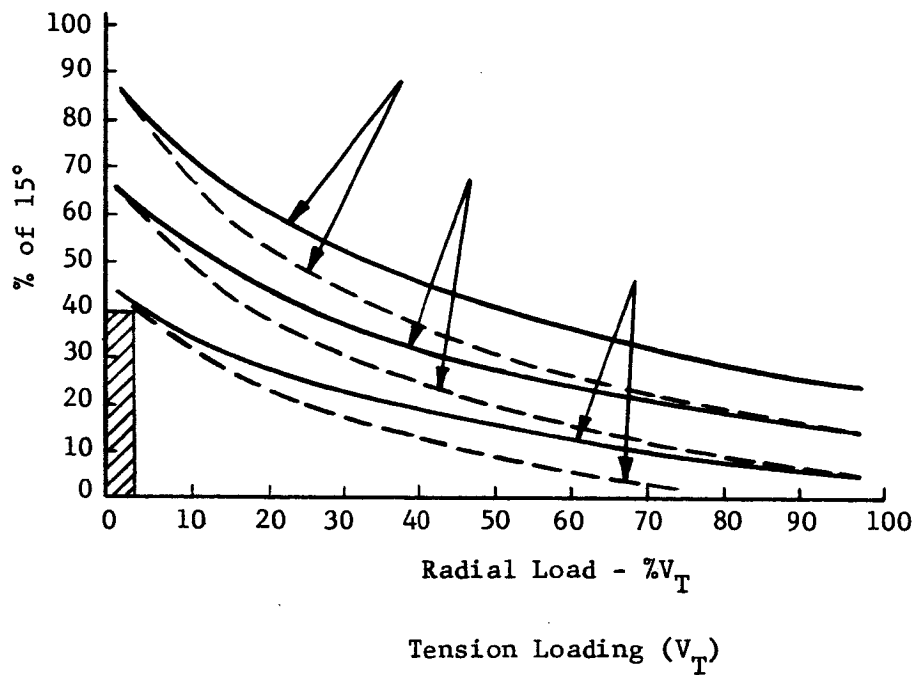
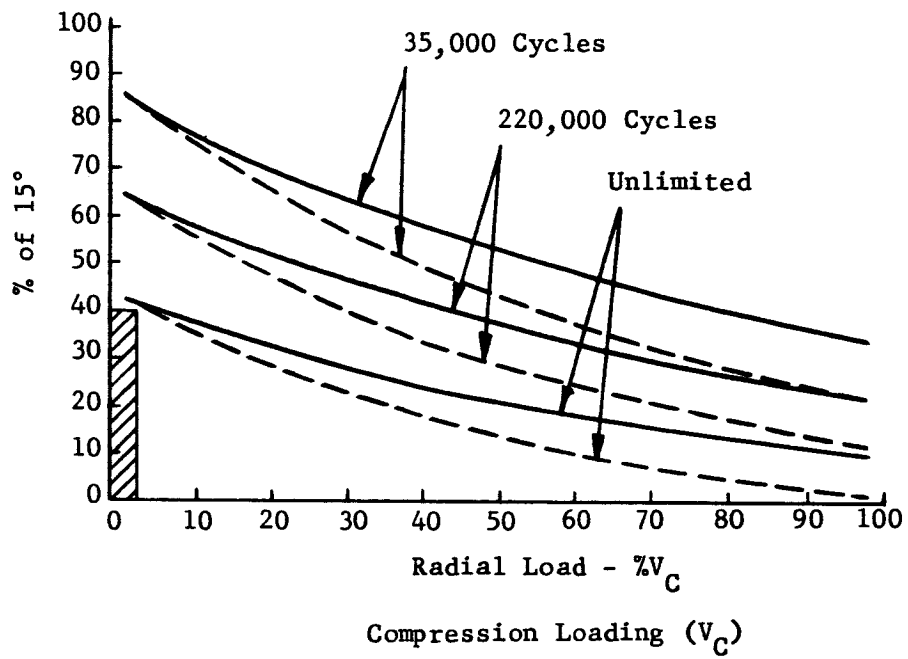


Figure 43. Life Curves For Type 600 ($\pm 15^\circ$) Flexure Pivots (Bendix Corp.)

- c) Low power dissipation.
- d) Less electronics required than the tuning fork method.

Disadvantages: Less familiarity with this method of chopping than with previously mentioned methods.

To get a life rating for a particular flexural pivot assembly, deflection angle and loading must be known. Life curves (Figure 43) from the Bendix Corporation indicate that unlimited life is achievable under the following simultaneous conditions: (See shaded areas on life curves.)

- a) Maximum angle of deflection is 40% or less of the rated flexural pivot deflection angle, ($\pm 6^\circ$ for this application).
- b) Loading is less than approximately 5% of rated loading.

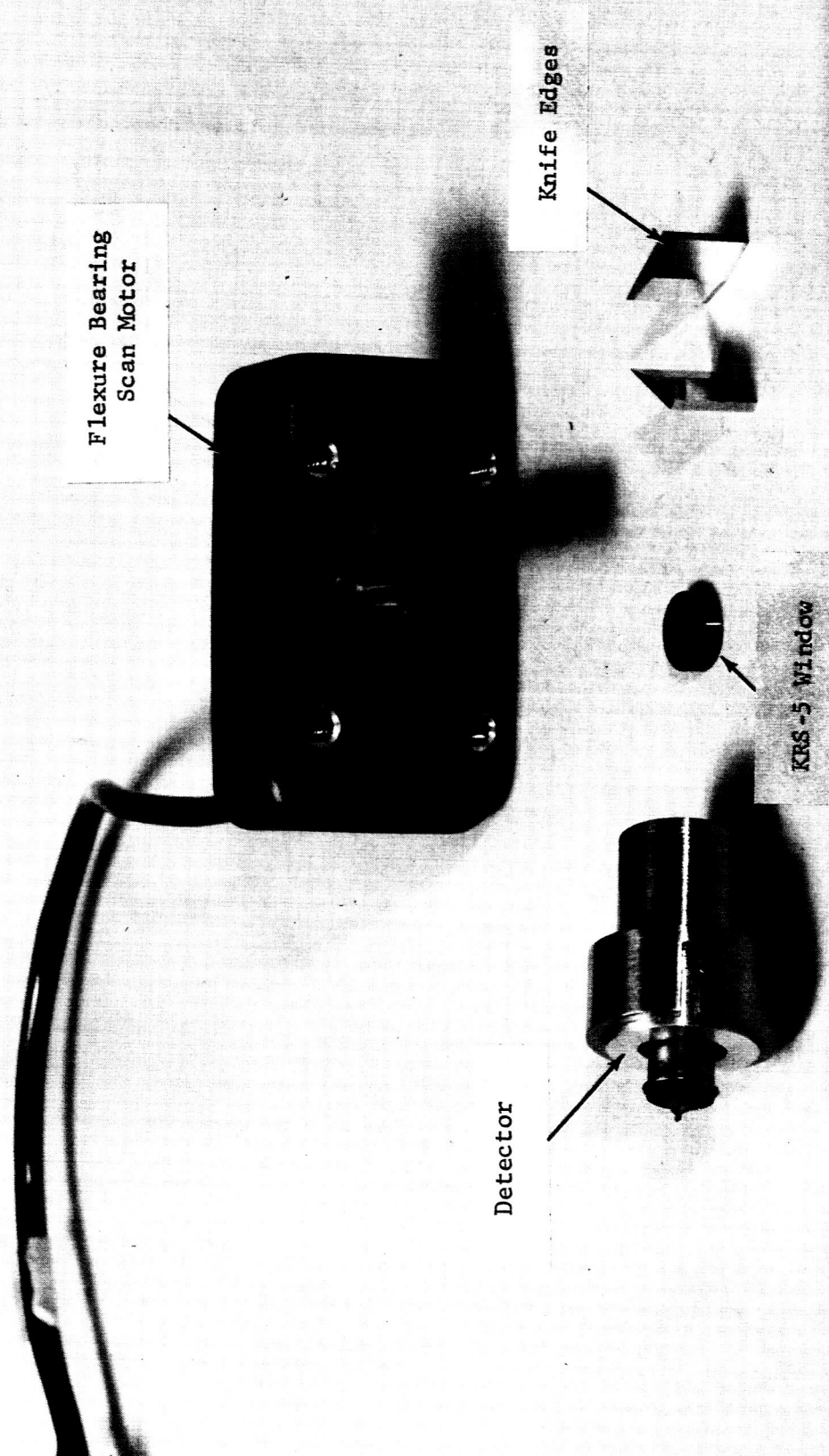
Bendix Corporation has test data on a flexural pivot assembly that has been operating for more than 1,700,000,000 cycles without failure. The Two-Gas Atmosphere Sensor Phase I requirements dictate the use of a device having an operating life of four months. If a torsional chopper were employed, it would very likely be designed to operate at 25 cps, which is approximately 270,000,000 cycles in four months. Hence, a torsional chopper should easily meet the NASA/LRC operating life requirement and is in fact capable of unlimited life.

Tiros Scanner

The scanner utilized in the Tiros Radiometer, NASA contract NAS 5-3894, is a flexure bearing, limited rotational motor as shown in Figure 44. Specifications for the scanner are given in the following table.

SCANNER USED ON TIROS RADIOMETER

- (1) Excitation: 25 cps square wave
- (2) Excursion: 0 to 6.6 degrees, trapezoidal, $\pm 10\%$ overshoot
- (3) Response: D.C. to 125 cps
- (4) Deflection Sensitivity: 3 ma/degree
- (5) Hysteresis: $< .12$ degrees
- (6) Survive Temp - 10 to $+50^\circ\text{C}$: Deflection compensated for constant
(using thermistor) excursion
- (7) Overshoot: Constant
- (8) Vibration: 20 to 2000 cps 10g rms 3-axis
- (9) Weight: 4-5 oz.



Flexure Bearing
Scan Motor

Knife Edges

Detector

KRS-5 Window

Figure 44. Scanner, Thermopile Detector, Far IR Detector
Window and Knife Edge Field Switching Mirrors

This scanner motor utilizes permanent magnet rotor and excited field windings, requires no lubricants, and is ideally suited for deep space vacuum operation. The motor weighs 4 ounces and requires 240 mw of power, including temperature compensation and damping circuitry, for a 3.3° angular deflection. This power requirement can be reduced to less than 100 milliwatts under optimum operating conditions.

The bearing is a 1/8-inch diameter Bendix flexure bearing with a ± 15 degree design limit. Operating at 3.3 degree excursions results in basically infinite lifetime operation since the bearing material is operating significantly below its stress point.

The motor is excited by a 25 cps 24.5 volt square wave input to the drive compensator. On calibration command, the phase of the excitation is reversed and the scan angle changed from 0 to $+3.3$ degrees to 0 to -3.3 degrees. The damping circuit is used to keep overshoot at the angle extremes down to 10% or 0.33 degree. This tolerance requirement is imposed by the spacing of the previously described knife-edge mirrors. The natural resonant frequency of the device is 125 cps. Operation at 25 cps produces a trapezoidal scan angle pattern with approximately 30 degrees phase shift, referred to the excitation waveform leading edge and the 50% amplitude point. Figure 45 shows a plotted angle scan pattern made by a laser beam reflecting from the operating scan mirror and intercepted at incremental positions by a

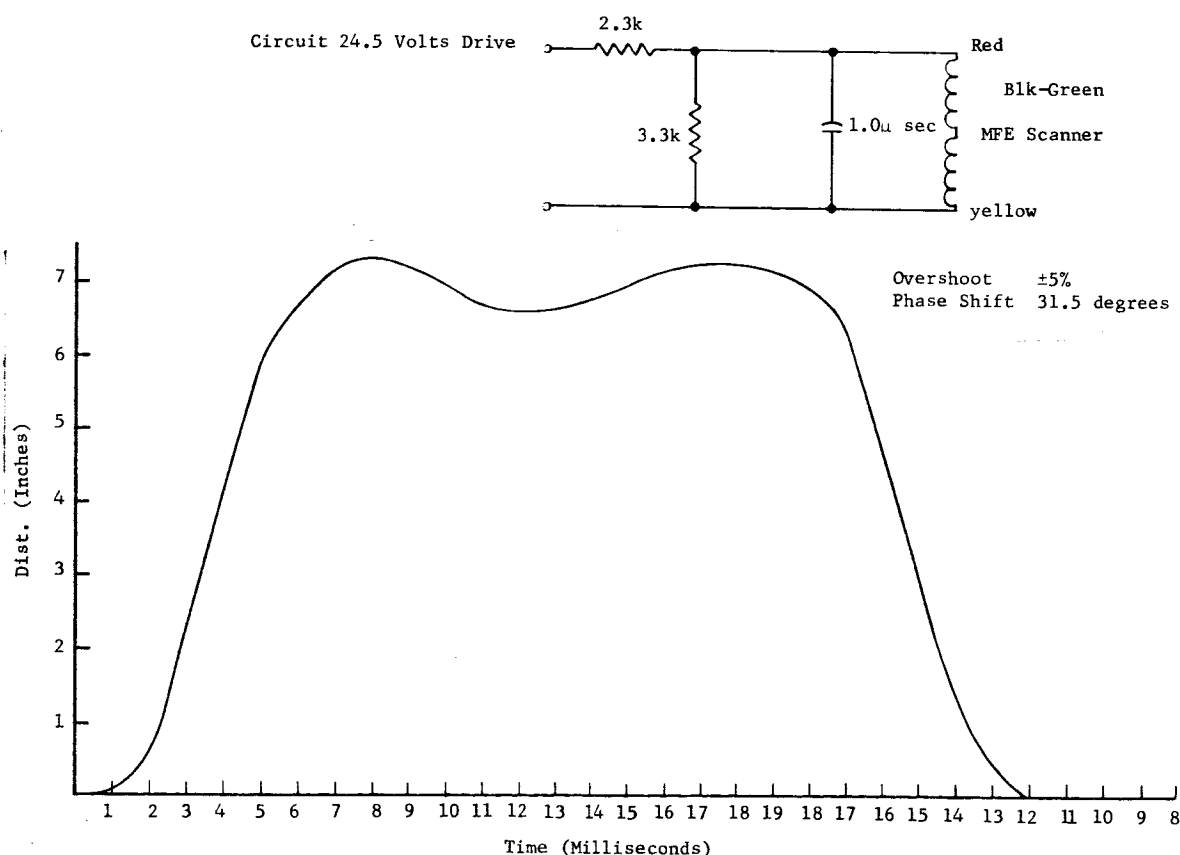


Figure 45. Scan Angle Plot

silicon detector whose output was a pulse displaced in time from the leading edge of the excitation waveform.

The scanner temperature compensation circuit is incorporated to modify the excitation current which changes as a function of the varying DC resistance of the motor windings. Since the scanner is a direct current device, changes in winding resistance produce offsets with excitation. Damping is relatively unaffected by temperature.

Temperature and vibration tests were performed on the compensated scanner which performed well within specifications. See Appendix D.

The total angle excursion varied 2% from 0 to 50°C and the total overshoot varied 2% which is well within the minimum $\pm 10\%$ requirement.

Vibration testing of the scanner included the following:

- (a) 20 to 2000 cps 1 Gp
- (b) 20 to 2000 cps 5 Gp
- (c) 20 to 2000 cps 10 Gp
- (d) 20 to 2000 cps 15 Gp
- (e) 20 to 2000 cps sweep at 40°/minute at 0.25 inch double amplitude and 21.2 Gp.

These tests were performed as an equivalent to white noise tests at 15 G's RMS. Shifts in the position of a laser beam reflected from the scan mirror over a 10 foot path were in the order of 1/4 inch resulting from the above tests. This represents an equivalent angle change of 2 minutes which is well within specification.

Vacuum tests were performed on the scanner resulting in undetectable overshoot changes proving air damping was non-existent.

The scanner was proven to be a very reliable, long-life, rugged, low-power device that could operate in space unpressurized.

2.5.3.4 COMPARISON OF OPTICAL CHOPPING METHODS

The tuning fork employed in the Apollo CO₂ sensor is more complex than tuning forks employed normally for other purposes. This tuning fork is classified as the weighted type because of the mass attached to the end of each tine. The fork is driven by an electro-dynamic transducer system, which consists of a drive coil and pick-up coil magnetically coupled to the fork and driven and controlled by a fork drive amplifier. This system, while sophisticated in nature, has demonstrated its reliability in actual operation. Since the tuning fork is a resonance device, very low power is required for its operation. As an example, the Apollo CO₂ sensor requires only 15 milliwatts to drive the fork at its resonance frequency and provide for sufficient motion to shape the optical signal to an appropriate electronic waveform.

An additional advantage of the tuning fork chopper is that it provides almost complete decoupling of the mechanical motion of the mounting plane of the tuning fork. That is, motion of the tines transmit forces only between each tine and not to the base of the mount, when the unit is properly tuned. The coil transducers, which cause the motion of the tuning fork, are very similar in construction to permanent magnetic loud speakers, except that in our mechanism the steel fork moves instead of the coil as in the speaker. Designs using aluminum tuning fork tines have been made in which case a conical shape magnet and related magnet cup would be used with the drive and phasing coils. The drive coils receive current waveforms required to maintain the tuning fork oscillations. In addition, vibration of the tuning fork near the pickup coil induces an alternating voltage in that coil. This voltage is directly proportional to the amplitude of vibration of the tuning fork, thus permitting the electronic circuit to sense this amplitude and to maintain control. The tuning fork frequency is of course fixed within very narrow limits. Specifications for other uses sometimes limit this to part per million changes of frequency. Our requirements are not this stringent and are readily achieved by a tuning fork chopper.

The conversion factor between the AC voltage induced in the transducer system and the mechanical amplitude of the tuning fork is pre-determined by the design of the transducer elements and tuning of the fork tines. The performance of successive lots of tuning forks can be made within very narrow tolerances. It is of interest to note that this mechanism is used as a chronometric motor for technical applications with constant exposure to abnormal environmental conditions.

The basic accuracy of the tuning fork in a fixed amplitude and under fixed conditions of temperature and pressure is not influenced by pivot friction, lubrication, or the like, and its rate under these conditions is constant for most practical purposes. The lack of the necessity for lubrication is a decided advantage for the environmental conditions anticipated and for the long life requirement imposed for high reliability missions. Effects of altitude on the tuning fork are minimal since they would cause only the change in density of the moving air column, which in principle forms a part of a mass of the vibrating tuning fork. Actual tests performed have shown that pressure

changes from vacuum to a normal ambient pressure have presented no problem, although there may be a small reduction in operating current resulting from the elimination of air damping. The frequency of the tuning fork of our design is essentially unaffected by changes in attitude. This is particularly true if the tuning fork remains horizontal. With the tuning fork's axis vertical, however, a very minor change may occur since the rate in the tines down position is faster than when the fork is horizontal, and the rate in the tines up position is slower than the rate in the horizontal position. The reason for the attitude effect is that in the tines down position, for example, the effect of gravity on the weighted tines is added to the elastic return force of the tuning fork to make the frequency higher than if the gravity effect were absent, as for example in the horizontal position of the fork. This effect is overcome by selecting a fork of high enough frequency so that the tines stiffness is much greater than the contribution of gravity to the elastic return force. Tuning forks below 500 cycles per second and which require chopping motions of 0.050 inch or greater are more susceptible to attitude errors. This type of chopper is particularly useful under shock stress since it is a resonant device. Little, if any, effect is shown up to shock levels that would approach those of a destructive test. Twenty G shocks, for instance, do not appreciably effect the output at all.

A tuning fork chopper mechanism must be provided with vibration isolation if reliable operation is required under conditions which include vibration at the resonant frequency of the fork. However, operation after vibration poses no problem as only the very narrow frequency bands near the resonant frequency or its harmonics will affect the performance of the fork. For example, a 600 cycle tuning fork would not be affected except for frequencies in the neighborhood of 550 cycles to 650 cycles, and again in frequencies from 1100 to 1300 cycles. Performance after exposure to these frequencies during a vibration test does not inhibit the performance of the instrument.

The proven acceptance of this type of mechanism is shown by its wide usage in various satellite programs. For example, the application of a tuning fork to long duration, self-contained timing applications to switch-off experiments and radio transmission in satellites such as the Explorer, Telstar, Tiros, and Sincom have been achieved. Basic development work for this mechanism was done by the Bulova Watch Company for use as a wrist timepiece and is commonly known as the Acutron mechanism.

A disadvantage of this type of mechanism is that because of its high Q it cannot be made to dwell at a particular image in space and for multiple sampling applications it can offer only a limited performance, as a result of its small chopping motion. Larger motions which could be used would then become susceptible to environmental conditions. It was this one undesirable characteristic of the tuning fork that has led us to the investigation of other methods. The only other acceptable method has been a counterpart of the tuning fork for wide band applications, namely the torsional chopper. The torsional chopper is very similar to a dc meter movement which has been upgraded somewhat by the use of flexure bearings. This type of mechanism has the advantage that it can be made to dwell at particular locations in space

allowing the maximum amount of information to be transmitted to the detector. A sketch of such a torsional chopper is shown in Figure 42. The torsional chopper is by design, a wide band device while the tuning fork chopper is a narrow band high Q device. As such, it responds only with sinusoidal motion, allowing it to sweep by an image in space. The torsional chopper, on the other hand, can respond to square wave inputs and can be programmed to stop at particular images in space. Thus, perhaps the tuning fork is better suited to simple chopping on and off, while the torsional chopper is more appropriately used where several slits or images are required to be combined on one detector.

The torsional chopper will provide the best signal information, but the tuning fork provides the best environmental operation. The torsional chopper is relatively new, while the tuning fork chopper has demonstrated its performance in qualification tests. The maximum utilization of space is obtained with the torsional chopper but the best utilization of power is obtained with the tuning fork chopper.

For the proposed system, two tuning forks would be required to replace one torsional chopper. The torsional chopper is fairly insensitive to vibration where the tuning fork chopper is insensitive to shock. Neither method requires lubrication, which is a decided advantage over a motor, and the torsional chopper has the feature of flexure bearings operating at angular rotations much below rating to ensure long life.

The electronics required to drive the wide band device are relatively simple, while a relatively complex sophisticated electronic system is required for the tuning fork chopper. However, this system has been designed and checked out. The final determination of the most suitable system to use will not materially affect the total overall package size, the power consumption, or the reliability. However, the electronics signaling philosophy will be markedly affected by whichever method is used. With the torsional chopper, a sampling method of detection would be anticipated. The tuning fork chopper method, however, uses the extraction of the Fourier components of a complex waveform to provide information regarding the absorption of the gas and the total transmission of the system.

2.5.4 SAPPHIRE AS AN ULTRAVIOLET OPTICAL ELEMENT

The choice of optical materials for use in the ultraviolet region at a wavelength of 1470Å (used for O₂ sensing) is quite limited. Although quartz and fused silica are usable to about 2000Å, below this wavelength only sapphire and fluoride single crystals (such as lithium and calcium fluoride) have useful transmission characteristics. Of these two, sapphire has greatly superior mechanical properties and resistance to moisture and environmental conditions. Although lithium fluoride has higher transmission at 1470Å its moisture sensitivity makes it unsatisfactory for this application.

The ultraviolet transmission of single crystal ultraviolet grade sapphire is shown in Figure 46. The "normal" grade sapphire is unusable at

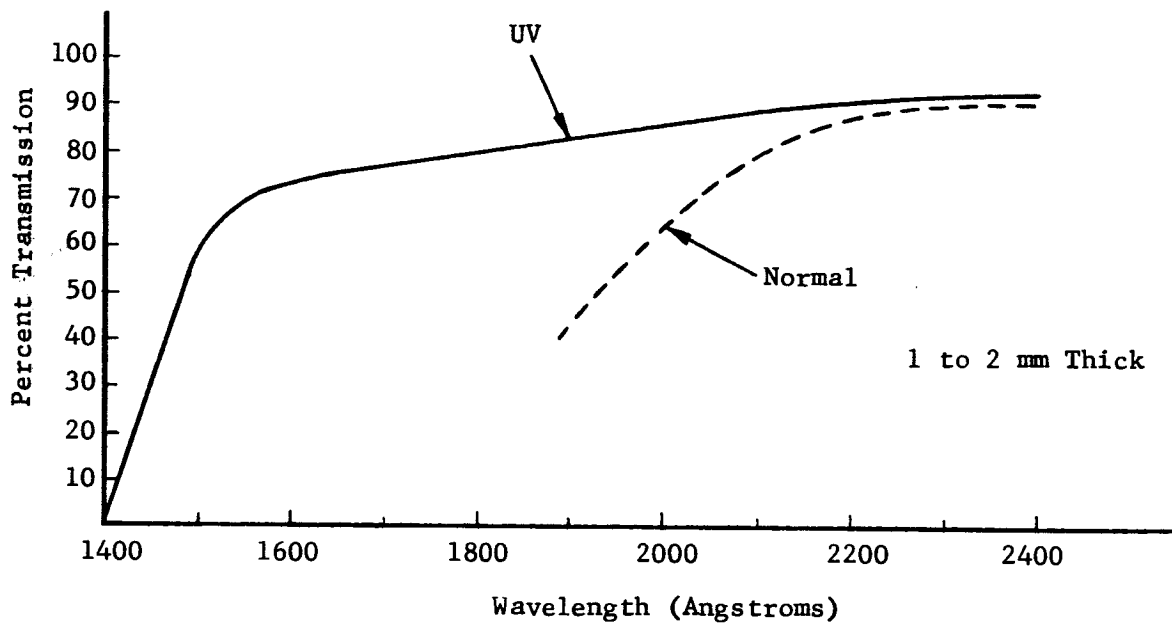


Figure 46. UV Transmission of Single Crystal UV Grade Sapphire

1470Å while the UV grade has 40% transmission. (Information from another source indicates 55% transmission at this wavelength.)

Some of the physical and thermal properties of sapphire single crystals are shown in Table X. The ability of a sapphire window to withstand a 20 psia pressure differential was computed and the thickness required for this was found to be 0.462 mm (0.0182 in.) using a 3 to 1 safety factor. This calculation is shown as follows:

$$P \frac{d^2}{n} = 180,000$$

Empirical relationship from Linde Crystal Products Dept.

Where P = pressure in psia
d = diameter
h = thickness

P = 20 psia using a
3/1 safety factor, let
P = 60 psia

$$\frac{d^2}{n} = \frac{180,000}{60} = 3000$$

$$\frac{d}{n} = 3000 = 54.8$$

For $d = 1.00$ in.

$$h = \frac{d}{54.8} = 0.0182 \text{ in.} = 0.462 \text{ mm}$$

It is apparent that single crystal sapphire is the only window material suitable for this application. Several reliable methods are available for bonding sapphire to metals, glasses, and ceramics.

TABLE X	
PROPERTIES OF SAPPHIRE SINGLE CRYSTALS (Linde Crystal Products Dept.)	
Density (g/cc)	3.98
Hardness (moles)	9
Compressive strength (psi)	300,000
Young's Modulus (psi)	$50-60 \times 10^6$
Tensile Strength (psi)	58,000
Coefficient of thermal expansion (60° orientation; in/in/°C; 20-500°C)	77×10^{-7}
Thermal conductivity (0°C, Cal/cm - °C-Sec)	0.11

3.0 SPACECRAFT INTERFACE CONSIDERATIONS

3.1 GAS CONTROL TECHNIQUES SYSTEM STUDY

3.1.1 GENERAL

Although a variety of gas control techniques may be considered, three particularly suited to optical absorption gas concentration measurement and requiring only simplified controls are described. The two techniques for cabin gas control, shown in block diagram form in Figures 47 and 48, correct for water vapor and carbon dioxide with "open loop" apparatus, i.e., a concentration measurement is not used to control the rate of operation of the contaminant removal apparatus. (It may prove advantageous, however, to save power by controlling the power input to the fans or pumps in this apparatus in accordance with the contaminant concentration.) The partial pressure or concentration of oxygen is controlled by means of a closed loop, i.e., a concentration measurement controls the injection of oxygen into the system. The total volume control mode for cabin oxygen control (Figure 47) has the more simple apparatus, whereas the input mixture control mode (Figure 48) has freedom from loop instabilities which could arise with cabin circulation problems. The latter system also provides a simple refilling arrangement when cabin gas pressure has been reduced below the breathing pressure level.

Figure 49 illustrates a simple suit gas control technique using optical absorption gas concentration measuring apparatus. The principle of operation is similar to that of the input mixture control mode for cabin gas control (Figure 48). In the event that separate sets of measurement and control units are used for cabin gas and suit gas purification, they may be interchanged under emergency conditions to provide additional reliability of the station's life support systems. It would be practical to use this control technique to provide a purified suit atmosphere under circumstances which would permit attaching inlet and exhaust hoses to cabin manifolds. For some operations outside the cabin, it would seem desirable to use a free suit similar to the LEM suit; however, this subject is outside the requirements of our present study.

3.1.2 SYSTEM DESCRIPTION AND QUALITATIVE PERFORMANCE

The cabin gas control system featuring the total volume control mode (Figure 47) is the more simple from the viewpoint of the number of elements required for operation. In practice it would operate as follows: The O_2 , CO_2 , and H_2O partial pressure measuring apparatus maintains the cabin oxygen concentration within limits by means of a proportional control valve, while a total pressure transducer, by means of separate proportional control valves, either vents cabin gas to space or adds nitrogen to the system to maintain the required total pressure. Indicators provide a visual readout of oxygen and contaminant concentration. As will be shown in a subsequent

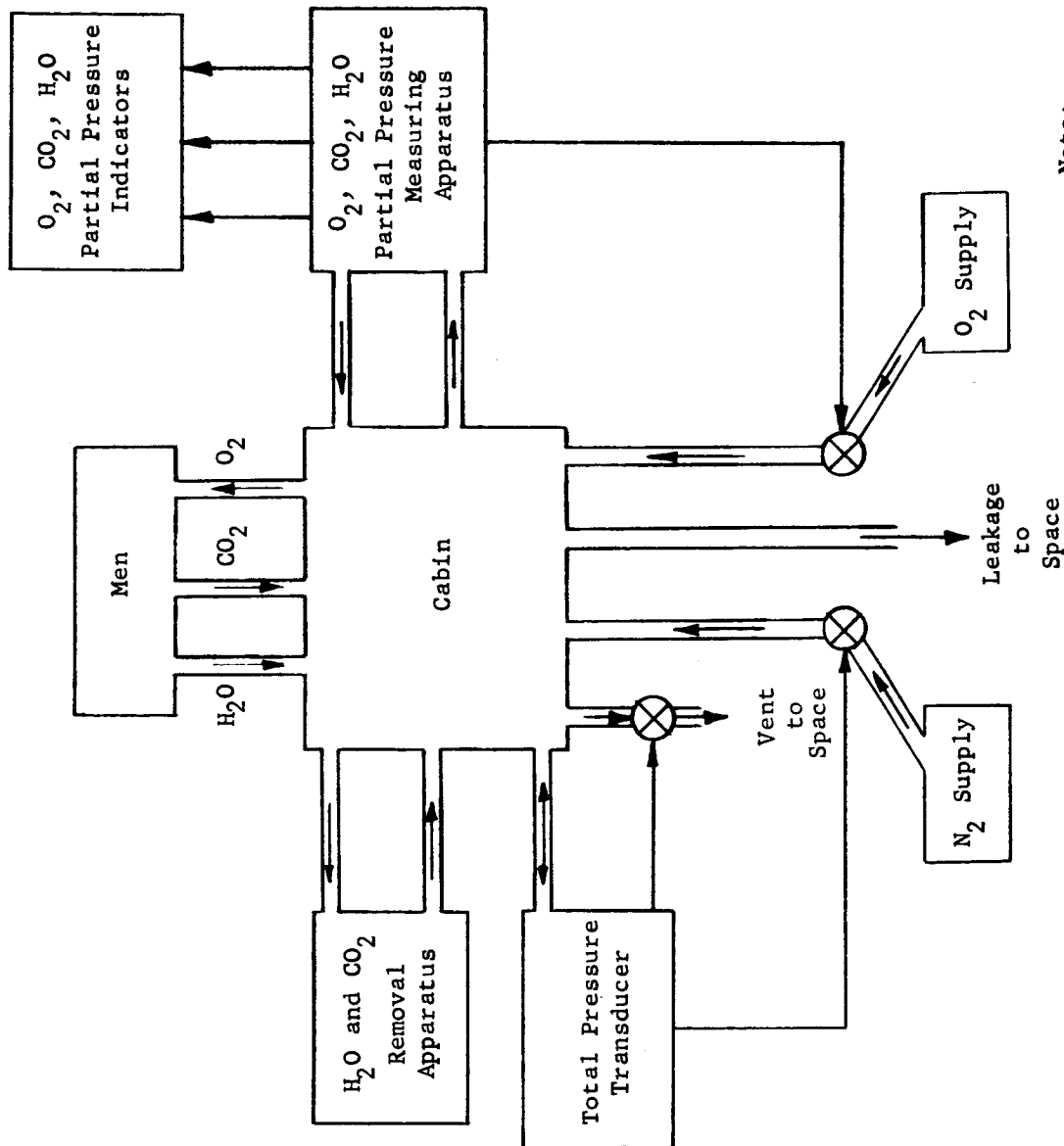


Figure 47. Cabin Gas Control Diagram - Total Volume Control Mode

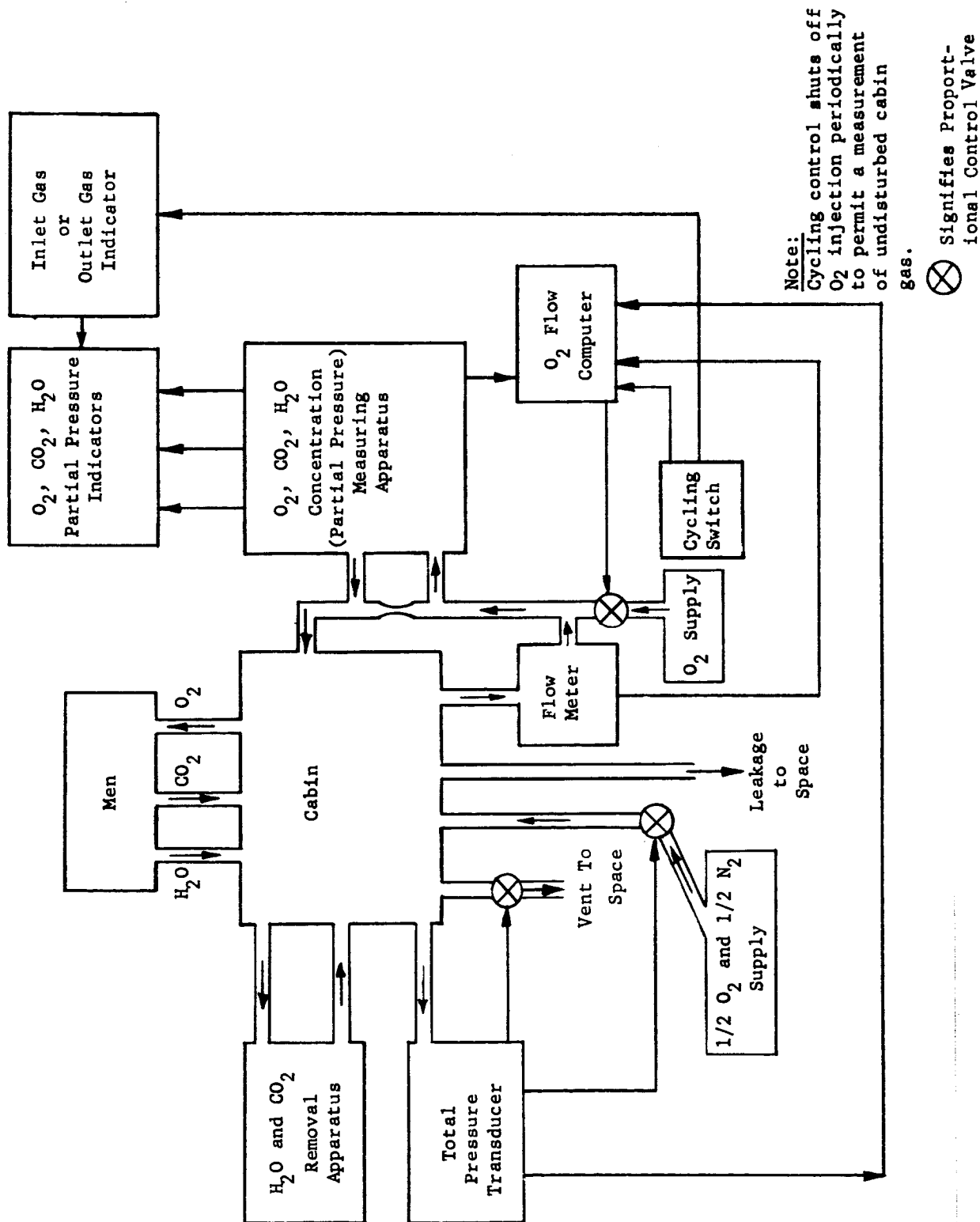


Figure 48. Cabin Gas Control Diagram - Input Mixture Control Mode

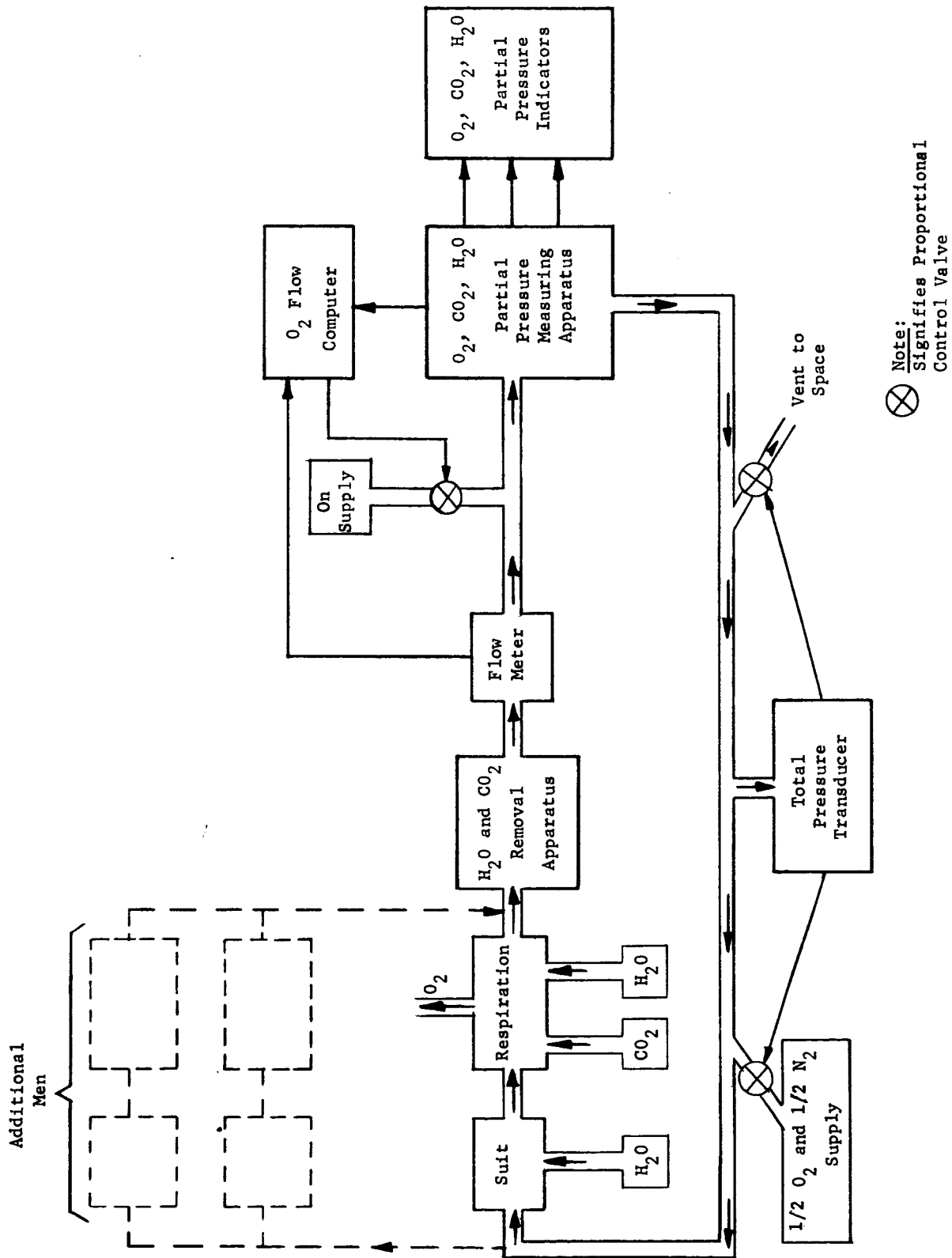


Figure 49. Suit Gas Control Diagram

section of this study, the performance of this type of control system is strongly influenced by the effectiveness of the cabin gas circulation apparatus.

The gas control system shown in Figure 48 features the input mixture control mode which requires the use of a mixed oxygen-nitrogen supply (or a mixing apparatus in the delivery tubes), a flow meter, and some simple electronic computing (generally in the form of potentiometer-type signal multipliers) and time control apparatus. In practice this system would operate similarly to the total volume control mode shown in Figure 47 except that the gas being sampled and replenished is routed through the flow meter and receives the required oxygen injection before passing through the sensor. In this configuration, oxygen is fed directly to the sensor stream in such an amount that the resulting oxygen concentration equals the set value. The cycling switch will periodically interrupt oxygen injection to permit measurement of undisturbed cabin gas. With this system the characteristics of the purified inlet gas are completely predictable and no control instability can occur as a result of the motion of the men or apparatus in the cabin. These motions could cause, at most, a spatial variation of the various gas constituents in the cabin in regions with limited gas circulation.

The proposed suit gas control system, shown in block form in Figure 49, operates in a manner which is qualitatively the same as the input mixture control mode of the cabin gas control system. If an individual wearing one of the suits desires to work with his helmet visor open, he should close the inlet and outlet valves on his suit so the other suits will not be affected and the suit pressure control will not be upset.

3.1.3 DETAILED SYSTEM ANALYSIS

To determine in detail the time and accuracy aspects of the described systems' performance requires first that the constants and input functions be specified. The performance may then be predicted by mathematical analysis.

For purposes of carrying out an illustrative performance calculation, it will be assumed that the air replenishment and control systems can be represented by the elements of the block diagram of Figure 50. Man respiration rates have been drawn from Reference 1, p. 1-6, and cabin volumes and partial pressure requirements have been drawn from the specifications of the development contract, NAS1-5678. For simplicity, the cabins specified have been treated as separate systems but combinations of these should be straightforward. The purification stream rates are reasonable minimums in view of the values mentioned in References 1 and 2. The space-time variation of the cabin gas concentrations is known only very roughly, even assuming an ideal input gas stream. If the cabins are assumed to be ideal cylinders and the resulting Reynolds numbers are calculated, it can be concluded that the flow regime is one of partially-developed turbulence. In view of the cabin obstructions, the flow regime is expected to be that of moderately developed turbulence. This will be superposed on the main gas stream, which itself will

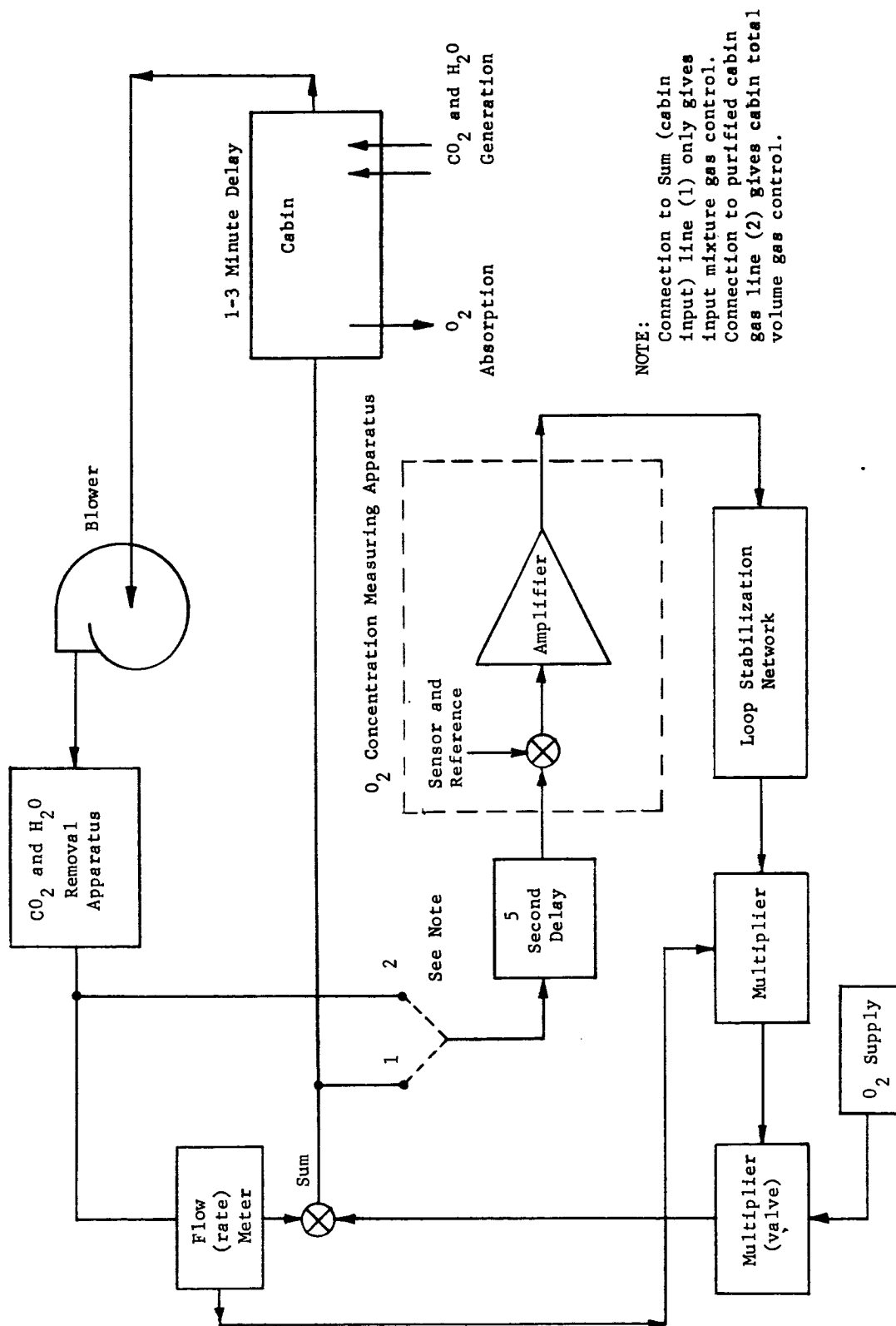


Figure 50. Simplified Servo Diagram for Oxygen Replenishment Control

not be uniform, but will vary from a maximum in the cabin center to zero at the cabin wall. (The main gas stream is assumed to be from end to end, of a cylindrical cabin, for reasons of minimizing the fan power requirements.)

A reasonable, simplified gas input to gas output time response is thus a pure time delay with a value slightly less than the ideal, uniform, spatial flow rate time, combined with a concentration storage type of behavior. Exact numbers for these parameters can only be found from experimentation with a cabin mock-up. To describe this type of behavior, some of the control stability calculations were performed assuming a pure time delay.

If it is assumed that the men are disposed nearly uniformly in the cabin and that they undergo a sudden activity rate change (from low to high) the resulting output stream concentration change becomes a combined ramp and delay function which is represented by the functional dependence shown in Table XI. If the men are disposed at a point in the cabin and undergo a sudden activity rate change, the initial concentration change in the gas as seen at the output pipe becomes a combined step and delay function with the time parameters dependent upon the location of the men in the cabin. For each time the gas is recirculated without replenishment an additional step change is added.

Assumed System Characteristics

The following system characteristics utilize the aforementioned assumptions along with others which appear reasonable from the references and existing knowledge of optical absorption gas concentration sensor behavior.

Man Generation and Utilization Rates

(Average numbers cited are from Reference 1, Table 1.3-IV
Short term maximum numbers are 3.5 times these.)

Gas	24 Hour Average Generation (lb/man-min.)	Short Term Maximum Generation (lb/man-min.)
CO ₂	0.0016	0.0056
H ₂ O	0.0041	0.0143
O ₂	-0.0013	-0.0041
Sum	0.0044	0.0154

Cabin Characteristics (See Table XI)

TABLE XI			
CABIN CHARACTERISTICS			
Module	Apollo Command	Lunar Excursion	Laboratory
Volume (ft ³)	138	180	1500
Gas Content (lb)	5.1	6.7	56
Assumed Purification Stream Rate (lb/min)	5	5	20
Assumed Manpower and Activity Rate	2 max: 1 ave	2 max: 1 ave	4 max: 3 ave
Gas CO ₂	0.013	0.013	0.027
Generation H ₂ O	0.033	0.033	0.070
Rate (lb/min) O ₂	-0.0095	-0.0095	-0.020
Sum	0.035	-0.035	0.075
Assumed Output Stream Time Response to a Step Function Generation Rate Change (χ)/min throughout the volume	$\frac{\chi t}{2} (2 - e^{-t})$	$\frac{\chi t}{2} (7/4 - e^{-3t/4})$	$\chi t (4/3 - e^{-t/3})$

Purification Apparatus Characteristics

The apparatus removes 67% of carbon dioxide in stream and all water in stream above a concentration corresponding to 100% R.H. at 33°F. The outlet water vapor pressure is 5 mm Hg.

Measuring Apparatus Characteristics

Table XII shows assumed performance values of the gas measuring apparatus. The values cited for CO₂, H₂O, and O₂ sensors are appropriate design goal values for the optical absorption measuring apparatus. Values shown for pressure, flow, and temperature are typical of commercially available transducers.

TABLE XII MEASURING APPARATUS CHARACTERISTICS		
Gas Concentration or Bulk Parameter	Percent of Full Scale Error (Striction, Slope, Noise, and Zero)	Response Time Constant (Seconds)
CO ₂	2.0 realizable (5.0 presently)	1.0
H ₂ O	5.0 estimated	1.0
O ₂	2.0 estimated	1.0
Total Pressure	2.0	1.0
Flow Rate	2.0	5.0
Temperature	2.0	30

Control Apparatus Characteristics

Two control apparatus elements are required for adjusting the flow rates of O₂ makeup and cabin filling (N₂ or N₂ and O₂) gases. It is assumed that this will be accomplished by use of valves positioned rapidly by control signals.

3.1.3.1 PERFORMANCE CALCULATIONS

From the data and parameters presented, it is possible to carry out several static and dynamic system performance calculations. A significant static performance calculation is the time required for the partial

pressure of the various gases in the cabin atmosphere to change more than the specification tolerances. The results presented in Table XIII are based on the assumed manpower and activity rates of Table XI and are inversely proportional to the purification stream rates. A second simple calculation is the ultimate partial pressure change to be expected when the men continue to change the gas concentration for a long period of time at the assumed (high) activity rate with gas correction apparatus operating. These results are also shown on Table XIII. The cited values show the excursions in the concentrations of the cabin outflow gases. The concentration limitation was provided in the case of carbon dioxide by the proportional removal apparatus. This calculation was done under the assumption that the gas change or generation rates and the gas correction rates were equal. In the case of H_2O , the concentration was determined by the reduction of the inlet gas water vapor pressure to 5 mm of Hg by the water condensing apparatus. In the case of oxygen, it was assumed that the gas inlet stream was corrected to within the accuracy of the sensing apparatus. Obviously if the men find it necessary to work in regions having poor gas circulation, the excursion of the concentrations of gases in these regions can exceed the values shown.

Dynamic behavior of the gas concentrations can also be obtained, but with more difficulty. Assuming again a sudden increase of activity rate in the cabin, the change of the carbon dioxide concentration can be expected to increase monotonically in a few gas circulation times toward the ultimate change value shown on Table VIII. The behavior of the water vapor concentration change is even more simple. A single pass through the condensation apparatus will reduce the partial pressure in the flowing gas to 5 mm Hg, the lower limit for the cabin. Assuming that any oxygen sensor error is constant during the period of observation, the transient behavior of the oxygen change concentration can be obtained for the two postulated control systems (Figure 50), with digital or analog computation. This has been done for the total volume control mode in the graphs of Figure 51. They show the transient behavior for a system control loop gain of 10 for the loop delay time constants which are specified. For simplicity, the delay occasioned by gas transport through the cabin has been assumed to be a simple time delay. Step function concentration change inputs were used in each case to indicate the stability of the feedback loops. For the control system to have reliable stability, the feedback time constant needs to be at least equal to the product of the loop gain and the cabin transport delay time. Otherwise the concentration oscillates with significant excursions. This result was verified also with computer runs simulating a loop gain of 40. As has been mentioned previously, any significant increase in the cabin transport delay without an accompanying increase of the feedback delay time constant can cause serious instability in the cabin oxygen concentration. Since the induced gas concentration change in an actual space cabin without correction will increase with time, approximately uniformly (as a ramp function), it is necessary that the control loop eventually used shall include an integrator to limit the excursion of the concentration.

TABLE XIII								
COMPUTED TIME AND ULTIMATE PRESSURE CHANGE VALUES								
Module	Time for Partial Pressures to Go From Minimum to Maximum Specification Pressure Levels With No Correction. (Min.)				Ultimate Partial Pressure Change in Outlet Stream With Correction. (mm Hg)			
	CO ₂ *	H ₂ O	O ₂ **	SUM	CO ₂	H ₂ O	O ₂	SUM
1. Apollo Command	12	15	18	5.8	±0.95	+3.9	-0.6±3.6	±7.0
2. Lunar Excursion	16	19.5	23	7.6	±0.95	+4.0	-0.6±3.6	±7.0
3. Laboratory	64	76	91	29	±0.50	+2.1	-0.3±3.6	±7.0

*0 to 7.6 mm

**Maximum to minimum pressure

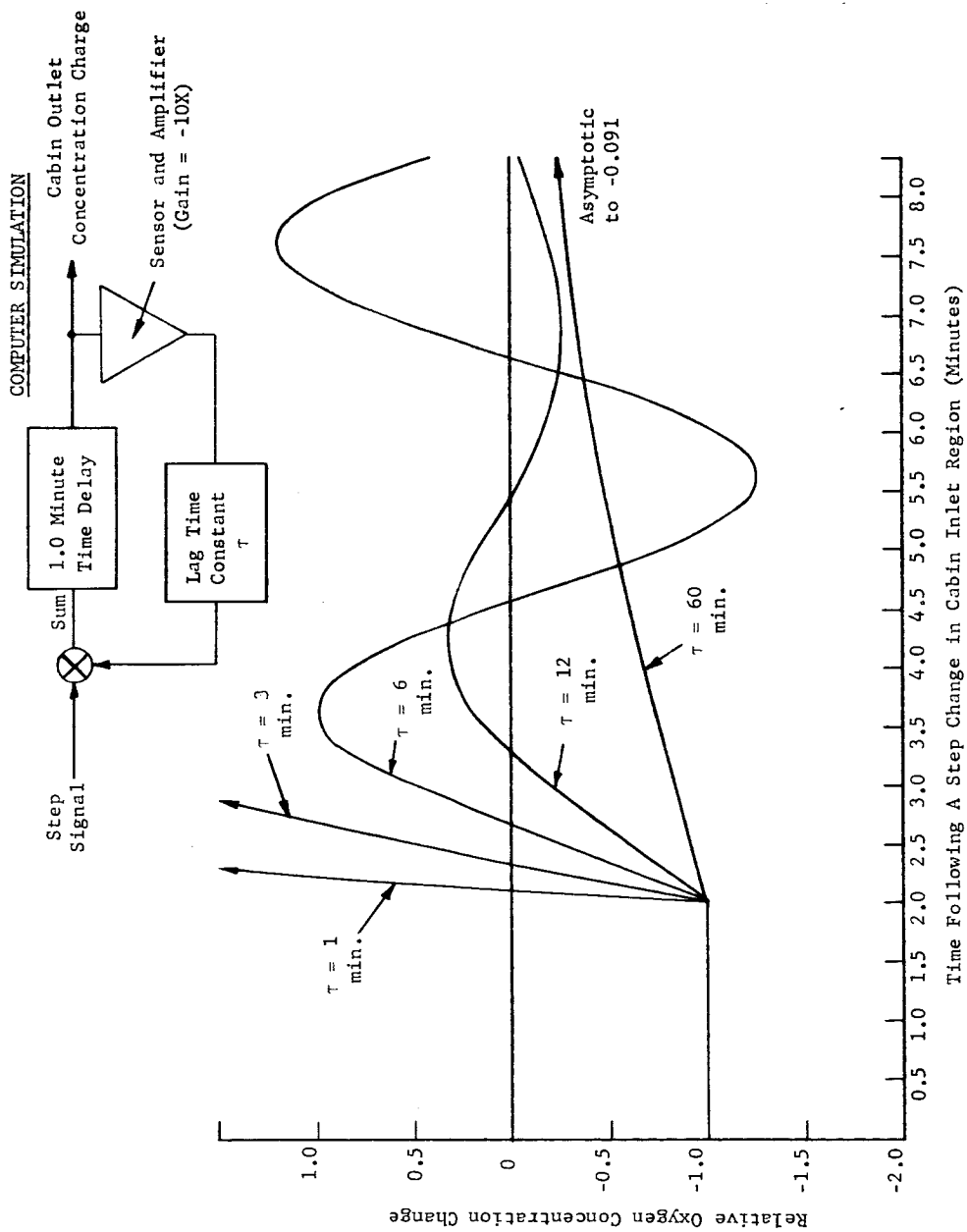


Figure 51. Simulated Time Response of Oxygen Concentration in a System With a 1.0 Minute Transport Lag Time

The time behavior of the input mixture control mode will be similar, of course, to that of the indicated total cabin performance, except that with a reduction of the transport delay from minutes to seconds, the correction rate can be correspondingly increased; or, better still, the correction rate can be increased by a lesser factor, whereupon the loop will be unquestionably stable.

The transient behavior of the suit loop correction system has not been analyzed in detail. However, it should not present serious stability problems, since the transport time delays can again be only seconds.

It should be mentioned that the use of a 1.0 second signal filter time constant in the oxygen (optical absorption) concentration measuring equipment will not significantly affect closed loop control stability since delay time constants will be several times as long as this.

3.2 VISUAL READOUT COMPATIBILITY (See Figure 52)

The output signal levels of all channels (i.e., oxygen, water, carbon dioxide, nitrogen, and total pressure) are from 0 to 5 VDC, and are available from redundant output drivers on each channel. Expanded scales are provided on the oxygen and total pressure channels, and could be provided on other channels if desired. The output impedance of the signal lines is low, and can be used to drive the spacecraft cables to the displays or telemetry with a high degree of noise immunity.

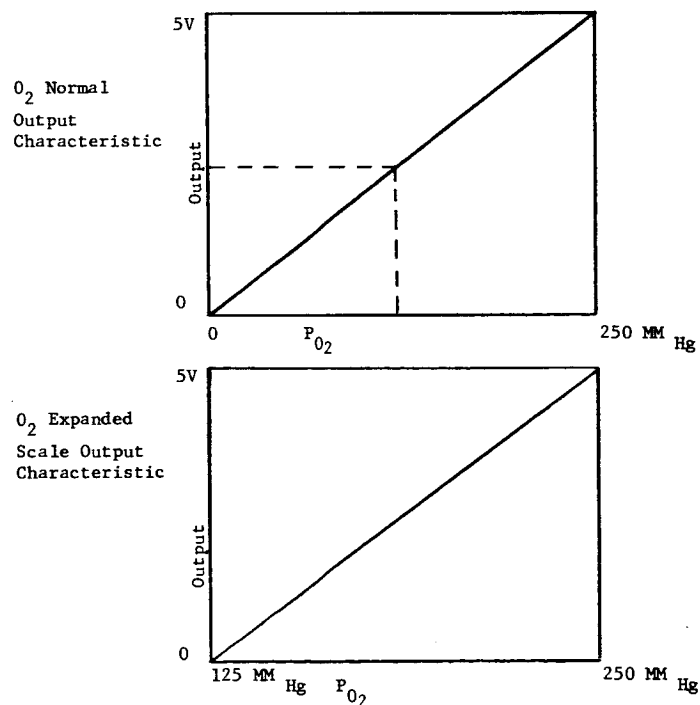


Figure 52. Oxygen Output Characteristics

3.3 OPERATIONAL SUPPLIES

The gas sensor system is designed to operate from 28 VDC, and will consume in the order of 4.5 watts of power. No calibration gases or vacuum supplies are necessary and no special bias voltages or other energy sources are required. Thus, the only operational supply required is electrical power.

3.4 MAINTAINABILITY

A definite reliability/maintainability trade-off area exists for the proposed Two-Gas Atmosphere Sensor. The tradeoff is whether to design an equipment which is either readily maintainable with a given inherent reliability or less maintainable but more reliable. Project and Reliability Engineering have decided in favor of the latter approach for the Two-Gas Atmosphere Sensor.

This decision on increased reliability is based upon the ultimate application of the equipment for use in a manned spacecraft. The four items provided during Phase II, although non-flight items, should parallel the design of a flight item version. A major constraint on the above is, of course, to keep equipment cost relatively low.

The Two-Gas Atmosphere Sensor will be designed to minimize preventive maintenance components, adjustments and alignments. Minimization of scheduled maintenance on any individual item will be achieved by the utilization of components with operational lives in excess of 3000 hours. This means that almost all equipment maintenance would be due to corrective maintenance tasks only.

It is recommended that any maintenance required on the Two-Gas Atmosphere Sensor be performed at Perkin-Elmer. All electronic modules will be wired-in solid by either welding or soldering techniques and the entire electronics assembly will very likely be encapsulated. The increased difficulty in maintenance associated with wiring-in and encapsulation will yield a more flightworthy equipment. Maintenance manuals will be supplied with the equipment such that qualified field personnel can maintain the equipment, if absolutely necessary.

A desirable maintenance feature to be incorporated into equipment design is a provision for system self-checkout through built-in test circuits. This feature should provide for swift fault isolation.

3.5 REDUNDANCY

A trade-off evaluation has been made by Project and Reliability Engineering regarding size, weight, power consumption, cost, redundancy, and reliability. The resulting conclusion at this time is that the increased size, weight, cost and power consumption due to any major redundancy does not justify the corresponding increase in reliability.

If any significant degree of redundancy is contemplated, it is believed that the most feasible method would be a design which provides two identical Two-Gas Atmosphere Sensor systems, arranged in either an operative or preferably a switch-over redundancy configuration. A switch-over redundancy is the better choice, because the redundant standby element is non-operative and requires no power consumption until failure of its operative counterpart. This is based on the assumption that the switch element dissipates negligible power as the design progresses during Phase II, however, it is possible that certain items or circuits, which do not now appear to present any problems, may conceivably become problem areas. If such a situation develops, redundancy will certainly be an important consideration. Also all critical items are potentially trade-off areas for the possible incorporation of redundancy.

The present design configuration for the Two-Gas Atmosphere Sensor has a redundancy feature in all five output driver stages. This permits simultaneous monitoring from two separate readout devices for each electrical output of the sensor. Improvement in reliability due to this feature, however, is not significant because the associated output driver electronics is minimal. The remainder of the current configuration is serial.

4.0 ASSESSMENT OF SENSOR TECHNOLOGY

4.1 ZERO GRAVITY OPERATION

In general, the removal of any gravitational forces does not impair the operation of the proposed sensing system. This can be demonstrated by the minor change in the systems output characteristics as a function of orientation. In the present system, the only moving parts are those connected with the optical choppers. The proposed chopping system does not depend on the application of gravity for the principal restoring force or need it be considered in the resultant forces operating on the chopper blade. There is no mechanical transfer of material within the system and all of the information channels are carried in either optical or electronic signal media which are unaffected by the variations in gravity. While no actual tests have been performed under zero gravity conditions the converse philosophy has been tested, that is, additional forces artificially experienced in acceleration tests have shown no changes in the operation of the equipment due to these increased external forces. In summary, the design is compatible with zero gravity operation and no degradation of performance is anticipated under zero-G conditions. Improvements or changes in the present design will keep in mind the necessity for final zero-G operation.

4.2 EXPOSURE TO HARD VACUUM

It may be anticipated that materials employed in space vehicles might be exposed to pressures lower than 10^{-10} millimeters of Hg at a wide variety of temperatures. This low pressure could result in the actual loss of bulk material or a change in composition of that material. This consideration is of particular importance in very thin coatings and could affect the usefulness of some members of practically all the materials classes.

The actual loss of bulk material is not considered to be an important aspect in this application since the temperatures seen by this particular sensor would be quite nominal. A more important consideration is the change in composition of the bulk material. Consideration must be given to the change in such mechanical properties as strength, hardness, and creep rate. Changes may also occur in properties such as electrical resistivity, thermal expansion and emissivity. Of particular importance to plastics is the volatility of the plasticizer. The loss of this plasticizer may result in cracking and crazing, due to shrinkage and brittleness, and a general impairment of the effectiveness. The change in the frictional properties in this hard vacuum will not be considered since there are no sliding parts within the proposed sensing system. This is a possibility that changes in optical transmission can result from the devitrification of glasses. This is not considered to be a problem at the present time due to the nominal temperatures that should be encountered. Evaporation in any of the UV coatings that are used in the oxygen/water system could result in roughening of the surface. There is the possibility that changes can result with associated changes in emissivity and reflectivity. However, this is not considered to be of importance in the infrared system.

Predictions on the behavior of material under the hard vacuum conditions are difficult to obtain. Emissivity, absorptivity, and optical characteristics can be studied in the laboratory, however, the final utilization of these materials would have to be based on data that presumably is available to NASA from recent satellite experiments. It is assumed that the Materials Advisory Board of the National Academy of Sciences or some other authoritative organization will have a prepared list of suitable materials for hard vacuum applications. Of course, every effort will be made early in the design phase to utilize materials having the desired hard vacuum characteristics. It would be unreasonable to presume too much on the technical results that would be achieved with normal good vacuum systems which would operate in the range of 10^{-6} millimeters. Even the use of ultra high vacuum facilities of 10^{-8} millimeters or better would not be adequate to fully satisfy the requirements for space installations. Certainly the design phase would specify the use of materials that do not out-gas, vaporize or in any other way degenerate in the space environment. Of additional concern would be combined environmental requirements such as combined ultraviolet radiation in a vacuum or high temperatures while in a vacuum. The problems associated with electrical breakdown in a vacuum will be handled in the design phase so that under no conditions will electrical breakdown be allowed to occur at any pressure from ambient to 10^{-4} millimeters. This will be prevented by the adequate use of suitable potting materials where necessary.

The irradiation of elastomers by ultraviolet radiation in vacuum may produce more or less severe degradation of the irradiated surfaces. However, the anticipated level of ultraviolet radiation in our system is considered to be of such low level that problems with elastomers are not considered to be important. No degradation of elastomeric seals has been observed in our present equipment after long term operation, that is, after several months of exposure to typical levels of ultraviolet radiation. It is encouraging to note that theoretical studies of the influence of ultraviolet radiation on the electrical properties of spacecraft have indicated the effect to be small even with the much higher levels used in the study. (Arnold Engineering Development Center Air Force Systems Command Document AEDG-TDR-62-2-16 January 1962-"Ultraviolet Effects of Space Vehicle Operation in Ultra-high Vacuum Environments".) It is interesting to note that these same experiments and theoretical studies have shown that fluoro-elastomers resist degradation most successfully. The extensive use of these materials particularly as wiring installation will be utilized in the design of the two-gas sensor.

In summary, it is recognized that potential problems may exist when operating in a high vacuum system. However, the experiences to date with experiments over the past year have not indicated any appreciable problem with any portion of the system operating in a vacuum. The major design consideration is to be in those areas associated with electrical breakdown in a vacuum rather than any material degradation. In normal usage the equipment would be sealed from the hard vacuum by the use of high quality hermetic sealing techniques. Actual tests that we have conducted over extensive periods of time such as the Mission Life Test of the Apollo Qualification Test Program, which consists of combined temperature-altitude tests to 10^{-4} millimeters,

have not shown any problem areas in the infrared system due to this combined environment.

4.3 EFFECT OF ERROR IN CO₂ AND H₂O MEASUREMENT ON N₂ MEASUREMENT

The N₂ partial pressure will be measured by subtracting the other partial pressures from the total pressure. A calculation is given below of the errors in P_{N₂} caused by errors in the other measured quantities.

Assume the total pressure error is 1%, the O₂ error is 2%, the CO₂ error is 2%, and the H₂O error is 5%.

The nominal total pressure is 362 mm Hg, nominal P_{O₂} = 181 mm Hg.

The P_{CO₂} is supposed to be less than 7.6 mm Hg; we assume nominal P_{CO₂} is 3.8 mm Hg. Assuming a relative humidity of 35% to 75% over the temperature range of 40°F to 90°F results in water vapor pressures of 2.2 to 27.1 mm Hg; we assume nominal P_{H₂O} of 14 mm Hg.

The nominal P_{N₂} is calculated as:

P _{O₂}	=	181.0		
P _{H₂O}	=	14.0	P _{total}	= 362.0
				<u>-198.8</u>
P _{CO₂}	=	<u>3.8</u>	P _{N₂}	= 163.2 mm
		198.8 mm		

Assuming the above mentioned errors occur. Then the total error is:

1% of P _{total}	3.62 mm
2% of P _{O₂}	3.62
2% of P _{CO₂}	0.08
5% of P _{H₂O}	<u>0.70</u>
	8.02 mm

Now

$$\frac{8.02}{163.2} = 4.91\%$$

Assuming there is no CO₂ sensor, but that the nominal CO₂ concentration is used. Then the total error is

	3.62 mm
	3.62
P _{CO₂} error	3.80
5% of P _{H₂O}	<u>0.70</u>
	11.74 mm

$$\frac{11.74}{163.2} = 7.2\%$$

If it is assumed that there is a CO₂ sensor, but no water sensor (and nominal P_{H₂O} is used) then the total error is

	3.62 mm
	3.62
P _{CO₂} error	0.08
P _{H₂O} error	<u>13.10</u>
	20.42 mm

$$\frac{20.4}{163.2} = 12.5\%$$

If there was no CO₂ sensor and no water sensor (and nominal P_{H₂O} and P_{CO₂} are used). Then the total error is

	3.62 mm
	3.62
P_{CO_2} error	3.80
P_{H_2O}	<u>13.10</u>
	24.14 mm

$$\frac{24.14}{163.2} = 14.8\%$$

Of this error 13.1 mm is due to H_2O ; this is

$$\frac{13.1}{163.2} = 8.03\%$$

error in P_{N_2} due to H_2O .

Also 3.8 mm of error is due to CO_2 ; this is

$$\frac{3.8}{163.2} = 2.3\%$$

error in P_{N_2} due to CO_2 .

It can be seen from these figures, that the total error in N_2 measurement using a pressure sensor, O_2 sensor, CO_2 sensor, and H_2O sensor is 8.02 mm (4.9%) while the total error using no CO_2 sensor and no H_2O sensor is 24.14 mm (14.8%), which is an increase of only 16 mm (10%). Thus, it appears feasible to calculate P_{N_2} by using constant nominal values for P_{CO_2} and P_{H_2O} .

4.4 ABILITY OF TWO-GAS ATMOSPHERE SENSOR TO MEET RELIABILITY AND FLIGHT QUALIFICATION

A qualitative engineering support effort from Reliability Engineering has been the reliability requirement imposed during Phase I by NASA-LRC. On the customer's verbal advisement it appears that flight model reliability requirements will not be invoked for the four deliverable non-flight items of Phase II. Hence, comparative reliability figures of several alternate designs should provide the most meaningful information at this time. To this end several design approaches have been evaluated during Phase I of the present

program. Relative levels of reliability associated with each approach have been calculated. The results are shown in Table XIV.

In the event that an MTBF or probability of survival figure is assigned to the equipment in the Phase II procurement specification, the necessary reliability allocations, analyses, and predictions will be performed to ensure achievement of the reliability requirement.

Flight qualification assurance cannot be given on any equipment without testing. If, as is anticipated, flight hardware units will not be required during Phase II of the program, test procedures for flight qualification testing in Phase III should be written and approved during Phase II. (Appendix E is a typical qualification test plan.) Flight safety tests should be considered in Phase II as a means of expediting future flight evaluation of the Two-Gas Atmosphere Sensor. Flight safety tests should consist of ignition proof and electromagnetic interference tests as a minimum.

TABLE XIV COMPARATIVE RELIABILITY OF DESIGN APPROACHES		
Design Approach	Comparative Reliability Factor	Comments
1. Tuning fork chopper and transistorized circuitry	X	Level of Reliability attainable using design approach #1
2. Tuning fork chopper and linear integrated circuitry	X + 45%	45% increase in reliability
3. Torsional chopper and transistorized circuitry	X + 7%	7% increase in reliability
4. Torsional chopper and linear integrated circuitry	X + 59%	59% increase in reliability

Notes:

1. A best estimate of total parts and their component types has been used in obtaining the comparative reliability factors shown.
2. Failure rate data was taken from MIL-HDBK-217.
3. An exponential distribution has been assumed.
4. The failure rates were selected at 20°C and were assigned a derating factor of 20% as an estimated average for this type of application.
5. The failure rates of linear integrated circuits have been assumed to be equal to transistor failure rates.

4.5 STATE OF DEVELOPMENT

The combination sensor is a logical step forward in the development of space hardware. As such, it will be based on previously qualified components, techniques, and systems as well as advanced concepts based on our previous experience. The development of an instrumentation system can be greatly facilitated by the utilization of appropriate existing subsystems.

The basic CO₂ sensor optical system was developed almost three years ago. Since that time it has been slightly upgraded to its present Apollo qualified status. Over this three year period there have been no sensor problems due to the optical elements or their mounting. This subsystem will be employed with no changes other than in minor mechanical mounting.

The basic O₂ sensor optical system was developed and tested within the past year. To date no system problems have been caused by the optics and tests have shown this system to be relatively insensitive to optical element positions. This subsystem will probably have fixed optics except for an adjustable grating. Except for minor mechanical changes, the optical system will be employed in its present form.

The infrared detector for the CO₂ subsystem was specifically designed for this application. It is a rugged, well shielded unit which does not require any cooling or electrical bias. It is essentially space qualified and will be used with only minor changes.

The UV detector is a ruggedized photomultiplier designed specifically for space applications. It consists of a ruggedized dynode structure mounted in a conventional envelope, which is bonded in a housing. The dynode divider is built onto the tube base and epoxied to the housing. This extremely stable unit will be employed with essentially no changes. Similar units have been employed in space.

The infrared source is a standard, military specification tungsten lamp. It is purchased as an aged, and selected for uniformity, component. As received it has a lifetime of 60,000 hours at rated power. Over our previous three year production period no lamps have failed.

The UV source is a relatively new component and no firm life data has been developed. However, there have been no failures to date except for mishandling. Additional data on its life expectancy will be developed in the next phase.

The electronics, although not identical to our present CO₂ sensor, will draw heavily on the qualified circuits and components employed in the CO₂ sensor. Our experience with these circuits has revealed where improvements may be made and where some of the newer techniques, such as integrated circuits, may be employed. The requirements of these circuits are more fully covered under some of the paragraphs concerned with reliability. We will employ, to the maximum extent possible, qualified components and circuits.

To summarize, most of the components and subsystems are in the space qualified state of development. Variations of these and new proven techniques will be employed wherever an obvious gain will be realized for the overall system.

4.6 OPERATIONAL LIFE

The design goal for the Two-Gas Atmosphere Sensor is an operational life, or useful life, of 120 days. Operational life of an item/equipment is defined as the interval of time during which the failure rate remains essentially constant. The exponential distribution describes item/equipment failure rate accurately during its operational life following burn-in, whereas a normal distribution is usually employed to describe wearout phenomena.

Almost all electronic component failures are of a random nature and are not attributable to wearout. The only foreseeable problem associated with the electronics portion of the proposed system is that of long term drift and stability. Measures such as use of close tolerance components and conservative design should prevent this problem.

Critical items and their operational life ratings are as follows:

<u>Item</u>	<u>Operational Life Rating</u>
1. Torsional chopper or tuning fork	Unlimited when properly applied Unlimited
2. Photomultiplier	20,000 hours at rated voltage and 70°F (EMR)
3. Infrared lamp source (MS24515-682)	60,000 hours at rated voltage (Chicago Miniature Lamp Works)
4. Ultraviolet lamp source	Has not been determined

Life testing of the ultraviolet lamp source is recommended during Phase II. The ultraviolet lamp will be operated at a continuous DC voltage to minimize sputtering effects. The lamp may also be run at decreased power to increase life. Present life data on similar ultraviolet lamps indicate operational lives of 500 hours - 7000 hours.

Actual lamp tests have not been made due to the long delivery time required by the components. The lamps have been ordered and should be available for testing during the design phase (IIa).

4.7 SHELF LIFE

The shelf life goal imposed by NASA-LRC for the Two-Gas Atmosphere Sensor is one year. There are certain precautions which must be taken to

ensure achievement of this goal. Potential problem items and Perkin-Elmer recommendations to circumvent the problems are as follows:

<u>Item</u>	<u>Potential Storage Problem</u>	<u>Solution</u>
1. Semiconductors	Possible shift of parameters	Conservative design. (A design that is not dependent on close parameter tolerances.)
2. Photomultiplier	Sensitive to light during storage	Will not be exposed to light inside an enclosed unit. EMR quotes 3 year shelf life at 70°F.
3. Ultraviolet lamp and infrared lamp	Gas leakage	Ensure proper sealing
4. Torsional chopper or tuning fork chopper	No problem	--

Storage in either a contaminated atmosphere or at temperatures in excess of 200°F should be avoided. The Two-Gas Atmosphere Sensor should easily be capable of exceeding a one year shelf life goal under normal conditions.

4.8 COMPLEXITY

The complexity of a given system is the degree of design sophistication required to perform a specified function and is related to the total number of parts involved in an equipment design.

The inherent simplicity of the optical absorption technique allows the gas measurement to be accomplished with a minimum of components. It is only necessary to irradiate a sample volume and detect the changes in optical transmission due to changes in the concentration of the sample gas. To do this requires only a source, sample cell, and detector. The electronics necessary for control and signal processing are conventional in concept and complex only in their state of the art utilization and packaging.

The complexity of the Two-Gas Atmosphere Sensor can be compared to the present Perkin-Elmer Carbon Dioxide Sensor to establish a reference. The Two-Gas Atmosphere Sensor will provide five channels of information with two redundant outputs per channel, whereas the CO₂ Sensor provides only one channel of information with four redundant outputs. Upon evaluation, the Two-Gas Atmosphere Sensor is estimated to be only twice as complex as the Carbon Dioxide Sensor.

Circuit complexity increases proportionally with increased utilization of redundancy. Therefore, the proposed Two-Gas Atmosphere Sensor complexity attributable to redundancy is minimal.

4.9 ENERGY, MATERIAL, AND ATMOSPHERIC SAMPLE REQUIREMENTS

The power requirement for the Two-Gas Atmosphere Sensor is almost entirely an electrical one. The electrical power estimate is as follows:

Signal	0.50 watts	
Infrared Source	0.20	
Chopper and Drive	<u>0.30</u>	
Sub-Total		1.00 watts
Main Power Supply	0.25 watts	
Ultraviolet Source	0.70	
UV Source Power Supply	1.00	
Photomultiplier Tube Dynode Resistors	0.25	
Photomultiplier Power Supply	<u>1.00</u>	
Sub-Total		3.20 watts
Pressure Transducer		<u>0.30</u> watts
GRAND TOTAL		<u>4.50</u> watts total system

The power required to flow sample gas through the Two-Gas Atmosphere Sensor will be negligible compared to the sensor input power requirement. This can be shown with figures obtained from a prototype O₂ sensor, since the Two-Gas Atmosphere Sensor will have a similar sample cell geometry. In the prototype O₂ sensor, a flow of 100 standard cc per minute gives a response time of about 3 seconds with a pressure drop of 1.33 mm Hg across the sensor at this flow and 362 mm Hg total pressure. Power is equal to pressure drop times flow rate, or

$$\begin{aligned}
 \text{Power} &= (1.33 \text{ mm Hg}) (100 \text{ cm}^3/\text{min}) \frac{1333 \text{ dyne/cm}^2}{1 \text{ mm Hg}} \frac{1 \text{ min}}{60 \text{ sec}} \\
 &= 2960 \frac{\text{dyne-cm}}{\text{sec}} \\
 &= 2960 \text{ erg/sec} \\
 &= 2960 \times 10^{-7} \text{ watt} \\
 &= 0.296 \text{ milliwatt}
 \end{aligned}$$

Infrared and ultraviolet sensors, by their nature, do not consume the sample gas. A total pressure sensor also does not consume gas. Thus, there are no material requirements for the Two-Gas Atmosphere Sensor. The sensor will, however, need a continuous flow of sample gas through it so that the O₂, CO₂, and H₂O concentrations can be continuously monitored. In the prototype O₂ sensor a flow rate of 100 sccm gives a response time of about 3 seconds. Although the response time of the CO₂ section would be longer (about 12 seconds), a flow of this order of magnitude is felt to be an adequate atmospheric sample.

4.10 WEIGHT OF SPECIAL EQUIPMENT

In accordance with the specific contract requirement of performing a determination of the most feasible integrated system approach, the weight of necessary support equipment for the Two-Gas Atmosphere Sensor has been investigated.

This area provides a decided advantage for the proposed Two-Gas Sensor system method. Essentially no sampling devices or expendable materials are required for the proper operation of the sensor.

There is no gas consumed in the measurement at all and no external calibration supplies or absorbent materials are required for the operation of the equipment. Deterioration or losses within the sample stream do not occur and there is no loss of the sample gas after the analysis has been completed. The only requirement for the proper operation of the system is a 28 volt DC supply capable of providing approximately 4.50 watts total power on a continuous basis. In addition, start-up power is not anticipated to exceed this goal.

Because there are no wear-out components, and it is felt the highest reliability without plug-in units, there is no recommended spare parts inventory required to accomplish the mission. The sensor will be designed to meet the requirements of the mission without replacement of any component. Recommendations for the preferred reference system and tentative plans for the design, test, development, and manufacture of the reference system will be included under a separate cover as a technical and management proposal for Phase II.

APPENDIX A

SIGNAL PROCESSING

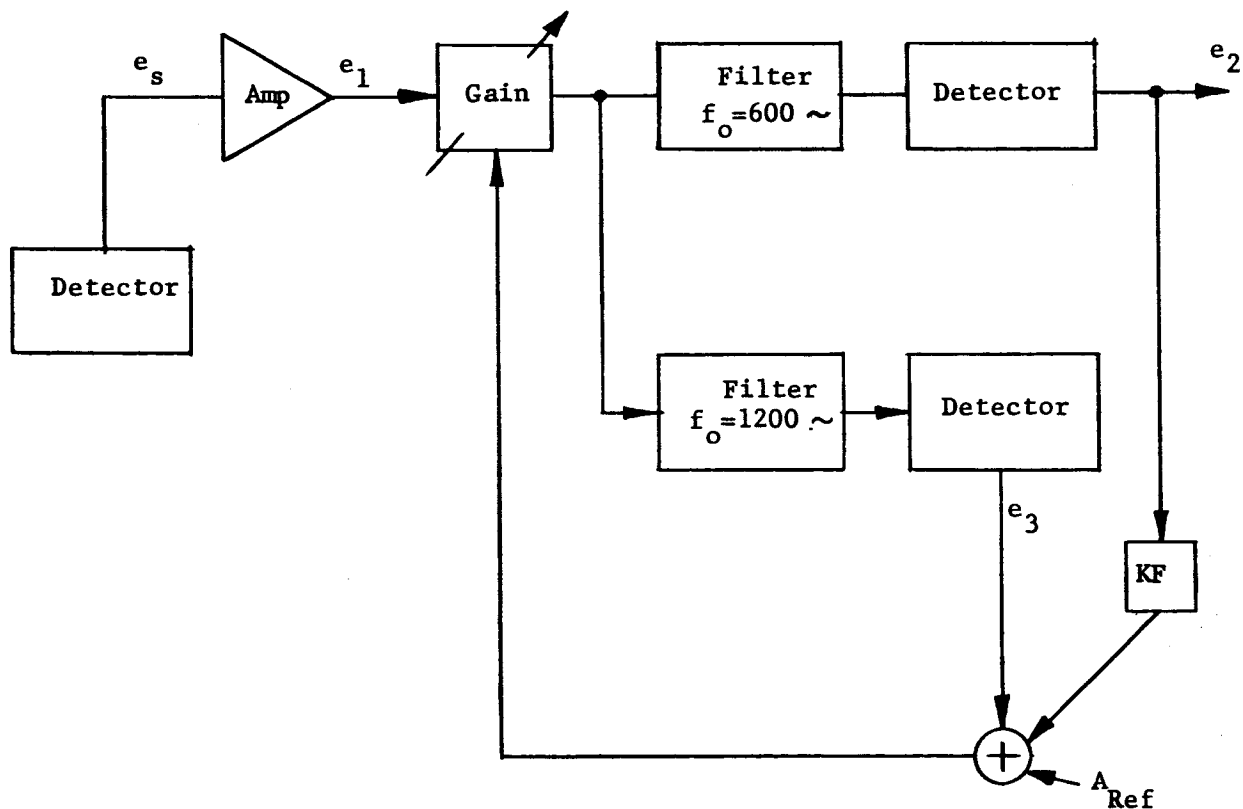
APPENDIX A

SIGNAL PROCESSING

Signal processing techniques have been investigated to determine effects of signal waveform on linearity, and signal-to-noise ratios.

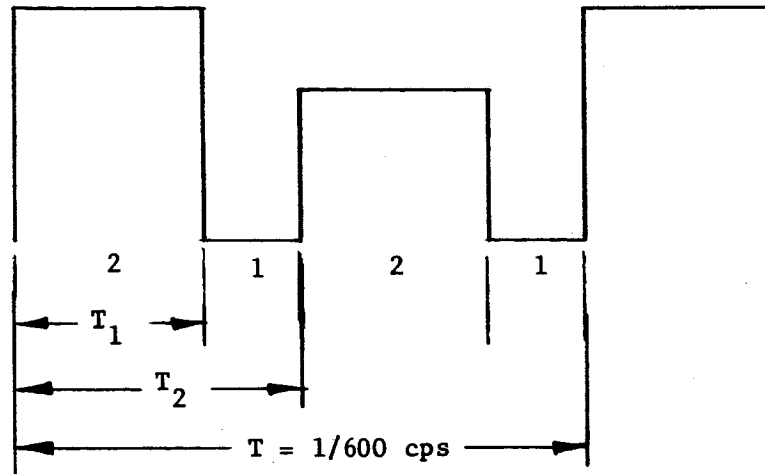
1.0 LINEARITY, PRESENT CO₂ SENSOR

1.1 BASIC BLOCK DIAGRAM, NARROW BAND SYSTEM



1.2 IDEAL SIGNAL WAVEFORM

The ideal waveform of the signal is shown below:*



I_R = reference signal output

I_S = CO_2 signal output

The signal may be represented by the partial Fourier series:

$$e_s = I_R k_A - (I_R - I_S) k_B - \frac{2(I_R - I_S)}{\pi} \sin k_A \pi \cos \omega_B t + \left[\frac{2I_R}{\pi} \sin k_A \pi - \frac{(I_R - I_S)}{2} \sin k_B \pi \right] \cos 2\omega_B t.$$

where:

$$\omega_B = 2\pi 600$$

$$k_A = \frac{T_1}{T_2} = \frac{2}{3}$$

$$k_B = \frac{T_2 - T_1}{T_2} = \frac{1}{3}$$

- Note: a) Harmonics above 1200 cps dropped
b) DC is removed by filtering

*Signal generated when the aperture "window" is small compared to the light filter total width; hence output substantially independent of the chopper position.

Therefore:

$$e_2 = - \frac{2(I_R - I_S) \sin k_A \pi}{\pi} \propto K_1$$

$$e_3 = \left[\frac{(2 \sin k_A \pi)}{\pi} I_R - \frac{\sin k_B \pi}{2} (I_R - I_S) \right] \propto K_2$$

or

$$e_2 = K_3 (I_R - I_S) \propto$$

$$e_3 = \alpha K_4 I_R - \alpha K_5 (I_R - I_S)$$

where

K_1, K_2, K_3, K_4, K_5 are scale factors.

$$K_3 = \frac{-2 \sin k_A \pi}{\pi} K_1, K_4 = \frac{2 \sin k_A \pi}{\pi} K_2, K_5 = \frac{\sin k_B \pi}{2} K_2$$

With the gain control loop closed, and $K_F = K_5/K_3$

$$\frac{K_5}{K_3} = \frac{-\pi K_2}{4 K_1} \frac{\sin k_B \pi}{\sin k_A \pi}$$

$$\epsilon = \text{AGC error signal} = + \alpha K_4 I_R - A \xrightarrow{\text{as a limit}} 0$$

$$\therefore \alpha = \frac{A}{K_4 I_R}$$

and

$$e_2 = \frac{K_3 (I_R - I_S) A}{K_4 I_R} = \frac{K_3}{K_4} A \left(1 - \frac{I_S}{I_R} \right)$$

or

$$e_2 = \frac{\frac{-2}{\pi} K_1 \sin k_A}{\frac{2 \sin k_A \pi K_2}{\pi}} A \left(1 - \frac{I_S}{I_R} \right)$$

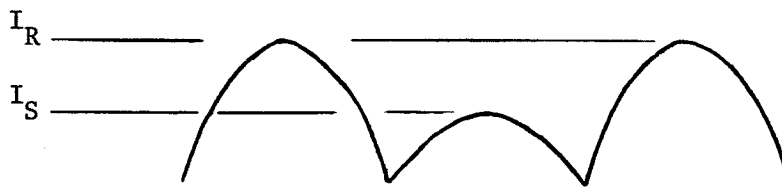
$$e_2 = \frac{K_1 A}{K_2} \left(1 - \frac{I_S}{I_R} \right)$$

If the feedback is not incorporated, the output is

$$\begin{aligned} e_2 &= \frac{K_3 A (I_R - I_S)}{K_4 I_R - K_5 (I_R - I_S)} = \frac{\frac{-2}{\pi} K_1 A (I_R - I_S) \sin k_A \pi}{\frac{2 \sin k_A \pi K_2}{\pi} I_R - \frac{\sin k_B \pi}{2} K_2 (I_R - I_S)} \\ &= \frac{-2 K_1 A (I_R - I_S) \sin k_A \pi}{\pi K_2 \left[I_R \left(\frac{2 \sin k_A \pi}{\pi} - \frac{\sin k_B \pi}{2} \right) + \frac{\sin k_B \pi}{2} I_S \right]} \end{aligned}$$

1.3 PRACTICAL SIGNAL WAVEFORM

In actual practice, the waveform takes the form shown below:*



I_R = reference signal output

I_S = CO_2 signal output

*The aperture "window" width is large relative to the light filter width, and the output is dependent upon chopper displacement.

The signal may be represented by the partial Fourier Series:

$$e_s = \frac{I_R + I_S}{\pi} + \frac{(-I_R + I_S)}{2} \cos \omega t + \frac{(2)(I_R + I_S)}{3\pi} \cos 2\omega t.$$

- Note: a) Harmonics above 1200 cps dropped
b) DC is removed by filtering

hence,

$$e_2 = -\frac{1}{2} (I_R - I_S) \propto K_1$$

$$e_3 = \frac{2}{3\pi} (I_R + I_S) \propto K_2$$

If the previous feedback factor is employed, i.e., $K_F = K_5/K_3$. The AGC error signal is now

$$e = \frac{2}{3\pi} (I_R + I_S) \propto K_2 - \left(\frac{1}{2}\right) \left(\frac{\pi K_2 \sin k_B \pi}{4 K_1 \sin k_A \pi}\right) (I_R - I_S) \propto K_1 - A \xrightarrow{\text{as a limit}} 0$$

hence,

$$\alpha = \frac{A}{\frac{2}{3\pi} (I_R + I_S) K_2 + \frac{1}{8} \frac{\pi K_2 \sin k_B \pi}{K_1 \sin k_A \pi} (I_R - I_S)}$$

$$\therefore e_2 = \frac{-\frac{1}{2} (I_R - I_S) K_1 A}{\frac{2}{3\pi} (I_R + I_S) K_2 + \frac{1}{8} \frac{\pi K_2 \sin k_B \pi}{K_1 \sin k_A \pi} (I_R - I_S)},$$

which is a significant departure from the former case. If the signal and AGC loop are decoupled ($K_5/K_3 = 0$), this system reduces to

$$e_2 = \frac{-\frac{1}{2} (I_R - I_S) K_1 A}{\frac{2}{3\pi} (I_R + I_S) K_2} = \frac{3 K_1 A}{4\pi K_2} \left(\frac{I_R - I_S}{I_R + I_S} \right)$$

or

$$e_2 = \frac{3}{4\pi} \frac{K_1}{K_2} A \frac{\left(1 - \frac{I_S}{I_R}\right)}{\left(1 + \frac{I_S}{I_R}\right)}$$

From these calculations, the following observations are made:

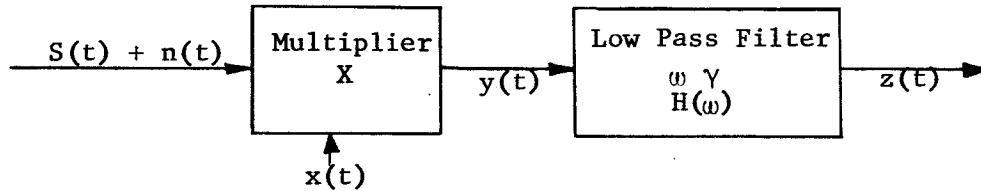
- (1) If the system feedback (k_F) is incorporated to optimize the ideal signal case operation, then, if the signal is in the form of the non-ideal case the calibration will shift, since both the multiplying constants and the influence of the signal and the reference change. Conversely, if the system is optimized for the non-ideal case, $k_F = 0$, then if the signal is in the form of the ideal case the calibration will shift, for the same reasons.
- (2) The simplest expression for the output voltage is obtained with feedback ($k_F = k_5/k_3$) for the ideal waveform case, and without feedback ($k_F = 0$) for the non-ideal case.
- (3) Since for any one unit the waveform is essentially constant over life, the calibration will be essentially constant once it is established.
- (4) It would be highly desirable to develop a signal processing system that undergoes only minor variation in calibration constants and curve shapes, over a wide range of signal wave shapes.

2.0 DEMODULATION METHODS

The major objective of the demodulation system is to maximize the signal-to-noise power ratio. It will be demonstrated for the detectors under consideration that although the long term average noise power will be zero, the noise at specific frequencies can produce low frequency beats that will modulate the dc output. The S/N ratio is therefore taken as the ratio of the dc output power to the total rms power value of the modulation terms.

2.1 DEMODULATOR MODEL

For the purpose of this evaluation the following general model will be employed:



$S(t)$ = signal

$n(t)$ = noise

$x(t)$ = demodulator waveform

$y(t)$ = demodulator output

$z(t)$ = low pass filter output

$$z(t) = x(t) H(\omega) [S(t) + n(t)]$$

$$z(t) = x(t) S(t) H(\omega) + x(t) n(t) H(\omega)$$

Basic Assumptions:

$$n(t) = \begin{cases} \frac{\sigma_n}{\sqrt{\omega_\alpha}} \cos(\omega_n t + \psi_n) & \text{when } 0 \leq \omega_n \leq \omega_\alpha \\ 0, & \text{otherwise} \end{cases}$$

where

$$\sigma_n^2 = \text{total noise power}$$

$$\omega_\alpha = \text{noise bandwidth } (\omega_\alpha > \omega_D)$$

$$\omega_n = \text{noise frequency (multivalued)}$$

ω_D = angular velocity of $x(t)$ demodulator

$\omega_Y < \omega_D$ waveform

$$H(\omega) = \begin{cases} 1 & \text{for } \omega \leq \omega_Y \\ 0 & \text{for } \omega > \omega_Y \end{cases}$$

Note that only multiplicative demodulator systems are considered.

2.2 SYNCHRONOUS DEMODULATION OF IDEALIZED WAVEFORM (WIDE-BAND)

Let:

$$x(t) = \frac{4}{\pi} \sum_{\substack{n_1 = \text{odd} \\ \text{only}}}^{\infty} \frac{(-1)^{\frac{n_1-1}{2}}}{n_1} \cos n_1 \omega t$$

= square wave, zero average value

2.2.1 SIGNAL

$$S(t) = I_R k_A - (I_R - I_S) k_B + \frac{2}{\pi} I_R \sum_{n_2=1,2,3,4}^{\infty} \frac{1}{n_2} (\sin n_2 k_A \pi) (\cos 2n_2 \omega_D t)$$

$$- \frac{2}{\pi} (I_R - I_S) \sum_{n_2=1,2,3}^{\infty} \left(\frac{\sin}{n_2} n_2 k_B \pi \right) (\cos n_2 \omega_D t)$$

hence

$$\begin{aligned} y(t) = x(t) S(t) &= \left[\frac{4}{\pi} \sum_{n_1=\text{odd}}^{\infty} \frac{(-1)^{\frac{n_1-1}{2}}}{n_1} \cos n_1 \omega_D t \right] \left[(I_R k_A - (I_R - I_S) k_B) \right. \\ &\quad + \frac{2}{\pi} I_R \sum_{n_2=1,2,3}^{\infty} \left(\frac{\sin}{n_2} n_2 k_A \pi \right) (\cos n_2 \omega_D t) \\ &\quad \left. - \frac{2}{\pi} (I_R - I_S) \sum_{n_2=1,2,3}^{\infty} \left(\frac{\sin}{n_2} n_2 k_B \pi \right) (\cos n_2 \omega_D t) \right] \end{aligned}$$

or

$$y(t)_1 = y(t)_{11} + y(t)_{12} + y(t)_{13}$$

Note that:

$y(t)_{11}$ is a square wave series with frequency components of $n\omega_D$. Since $n\omega_D \gg \omega_Y$ for all integer values of n ,

$$y(t)_{11} H(\omega) = 0$$

$$y(t)_{12} = \left[\frac{4}{\pi} \sum_{n_1=\text{odd}}^{\infty} \frac{(-1)^{\frac{n_1+3}{2}}}{n_1} \cos n_1 \omega_D t \right] \left[\frac{2}{\pi} I_R \sum_{n_2=1,2,3}^{\infty} \left(\frac{\sin n_2}{n_2} k_A \pi \right) (\cos 2n_2 \omega_D t) \right]$$

$$y(t)_{12} = \frac{8I_R}{\pi^2} \sum_{n_1=1,3,5}^{\infty} \sum_{n_2=1,2,3,4}^{\infty} \frac{(-1)^{\frac{n_1+3}{2}}}{n_1 n_2} \sin n_2 k_A \pi \left[\cos \omega_D t (n_1 + 2n_2) \right. \\ \left. + \cos \omega_D t (n_1 - 2n_2) \right]$$

where:

$$n_1 = \text{odd nos} \geq 1$$

$$n_2 = \text{even \& odd nos} \geq 1$$

Since:

$$n_1 + 2n_2 \geq 3$$

$$\cos \omega_D t (n_1 + 2n_2)$$

terms will always appear as an ac component and will be removed by the filter $H(\omega)$.

Since:

$$|n_1 - 2n_2| \geq 1$$

$$\cos \omega_D t (n_1 - 2n_2)$$

terms will always appear as an ac component and will be removed by the filter $H(\omega)$.

Hence;

$$y(t)_{12} H(\omega) = 0$$

$$\begin{aligned} y(t)_{13} &= \frac{-8(I_R - I_S)}{\pi^2} \sum_{n_1}^{\infty} \sum_{n_2}^{\infty} \frac{(-1)^{\frac{n_1+3}{2}}}{n_1 n_2} (\cos n_1 \omega_D t) (\sin n_2 k_B \pi) (\cos n_2 \omega_D t) \\ &= \frac{-4(I_R - I_S)}{\pi^2} \sum_{n_1=\text{odd}}^{\infty} \sum_{n_2}^{\infty} \frac{(-1)^{\frac{n_1+3}{2}}}{n_1 n_2} (\sin n_2 k_B \pi) \left\{ \cos \left[\omega_D t (n_1 - n_2) \right] \right. \\ &\quad \left. + \cos \left[\omega_D t (n_1 + n_2) \right] \right\} \end{aligned}$$

Since $n_1 + n_2 \geq 2$ for all n , $\cos \omega_D t (n_1 + n_2)$. Terms will always appear as an ac component and will be removed by the filter $H(\omega)$.

For

$$n_1 \neq n_2$$

$$|n_1 - n_2| \geq 1,$$

hence all $\cos \left[\omega_D t (n_1 - n_2) \right]$. Terms are ac, and will be removed by the filter $H(\omega)$.

For

$$n_1 = n_2 = \text{odd}$$

$$\cos \left[\omega_D t \left(n_1 - n_2 \right) \right] = \cos 0 = 1$$

hence,

$$y(t)_{13} = \frac{-4 \left(I_R - I_S \right)}{\pi^2} \sum_{n_1=\text{odd}}^{\infty} \frac{(-1)^{\frac{n_1+3}{2}}}{n_1^2} \sin n_1 k_B \pi ,$$

which may be evaluated for any specified k_B value, and number of harmonics n_1 .

or

$$y(t)_{13} = \frac{\left(I_R - I_S \right)}{3} \text{ when } k_B = \frac{1}{3}, \quad n_1 = 13.$$

$$\therefore y(t) = \frac{I_R - I_S}{3} \quad (\text{DC Term})$$

hence,

$$Z(t) = y(t) H \left(\omega_Y \right) = \frac{- \left(I_R - I_S \right)}{3}$$

2.2.2 NOISE

$$\begin{aligned} y(t)_2 = x(t) n(t) &= \frac{4}{\pi} \sum_{n_1=\text{odd}}^{\infty} \frac{(-1)^{\frac{n_1+3}{2}}}{n_1} \cos n \omega_D t \frac{\sigma_n}{\omega_\alpha} \cos \left(\omega_n t + \psi_n \right) \\ &= \frac{2\sigma_n}{\pi\sqrt{\omega_\alpha}} \sum_{n=\text{odd}}^{\infty} \frac{(-1)^{\frac{n_1+3}{2}}}{n_1} \cos \left[\left(n\omega_D - \omega_n \right) t - \psi \right] + \cos \left[\left(n\omega_D + \omega_n \right) t + \psi_n \right] \end{aligned}$$

$$y(t)_2 = y(t)_{21} + y(t)_{22}$$

Since

$$n \omega_D + \omega_n \gg \omega_Y$$

$$y(t)_{22} H \left(\omega_Y \right) = 0$$

However, $(n \omega_D - \omega_n)$ terms may fall within the bandpass of the filter and will produce a ripple on top of the dc. The average value of the ripple will of course be zero, hence,

$$Z(t)_2 = y(t)_{21} = \frac{2\sigma_n}{\pi \sqrt{\omega_\alpha}} \sum_{n=\text{odd}}^{\infty} \frac{(-1)^{\frac{n_1+3}{2}}}{n_1} \cos \left[(n\omega_D - \omega_n) t - \psi_n \right]$$

when,

$$n\omega_D - \omega_Y \leq (n\omega_D - \omega_n) \leq n\omega_D + \omega_Y$$

For a unit load, the noise power per unit of bandwidth will be:

$$P_n = \frac{4\sigma_n^2}{\pi \omega_\alpha} \sum_{n=\text{odd}}^{\infty} \frac{1}{n^2}$$

Since the beats occur for frequencies above and below the basic demodulator rate ω_D , the effective bandwidth is $2\omega_Y$

hence,

$$P_n = \frac{8\sigma_n^2}{\pi} \frac{\omega_Y}{\omega_\alpha} \sum_{n=\text{odd}}^{\infty} \frac{1}{n^2}$$

or,

$$P_n \approx \frac{9.68 \sigma_n^2}{\pi} \frac{\omega_Y}{\omega_\alpha}$$

or,

$$P_n = .98 \sigma_n^2 \frac{\omega_Y}{\omega_\alpha}$$

2.2.3 SIGNAL/NOISE

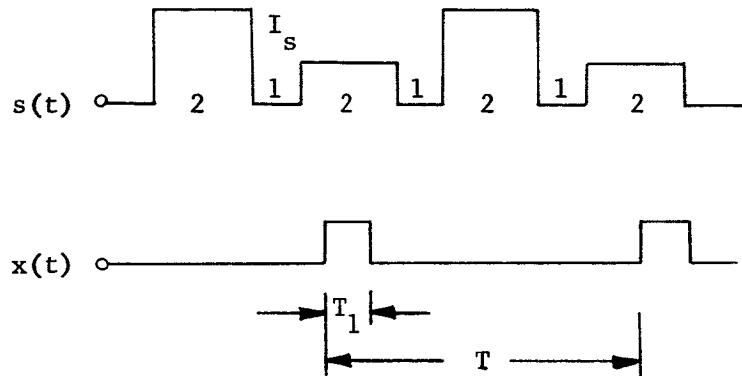
The ratio of the DC signal power to the rms power of the fluctuating components (beat frequencies) is therefore:

$$\frac{S}{N} = \frac{\frac{(I_R - I_S)^2}{3^2}}{0.98 \sigma_n^2 \frac{\omega \gamma}{\omega \alpha}} = \frac{(I_R - I_S)^2 \omega \alpha}{9(0.98) \sigma_n^2 \omega \gamma}$$

$$\frac{S}{N} = \frac{0.114 (I_R - I_S)^2}{\sigma_n^2} \frac{\omega \alpha}{\omega \gamma}$$

2.3 SAMPLING DEMODULATION OF IDEAL WAVEFORM

2.3.1 SIGNAL



Let:

$$\frac{T_1}{T} = k_s \leq \frac{1}{3}$$

hence,

$$y(t) H(\omega) = I_S k_s$$

and signal power is

$$P_s = I_S^2 k_s^2$$

Alternatively, the signal power can be expressed as $P_s = (I_R - I_S)^2 k_s^2$, if I_R is taken as the reference.

Note that the average value of any high-frequency noise components will be zero.

2.3.2 NOISE

Since

$$x(t) = k_s + \frac{2}{\pi} \sum_{n=1,2,3}^{\infty} \frac{1}{n} (\sin n k_s \pi) (\cos n \omega_D t)$$

$$x(t) n(t) = \left[k_s + \frac{2}{\pi} \sum_{n=1,2,3}^{\infty} \frac{1}{n} (\sin n k_s \pi) (\cos n \omega_D t) \right] \left[\frac{\sigma_n}{\sqrt{\omega \alpha}} \cos (\omega_n t + \psi) \right]$$

$$y(t)_3 = \frac{k_s \sigma_n}{\sqrt{\omega \alpha}} \cos (\omega_n t + \psi) + \frac{2 \sigma_n}{\pi \sqrt{\omega \alpha}} \cos (\omega_n t + \psi) \sum_{n=1}^{\infty} \frac{1}{n} (\sin k_s \pi) (\cos n_D t)$$

$$y(t)_3 = y(t)_{31} + y(t)_{32}$$

where

$$y(t)_{31} = \frac{k_s \sigma_n}{\sqrt{\omega \alpha}} \cos \psi$$

when

$$\omega_n = 0$$

$$\text{or noise power} = \frac{k_s^2 \sigma_n^2}{\omega \alpha} \omega \gamma$$

when

$$0 \leq \omega_n \leq \omega \gamma$$

Since this component is not a beat product, it can be filtered out by using a high-pass filter prior to the sampler.

$$H_2(\omega) = \begin{cases} 1 & \text{for } \omega \geq \omega \gamma \\ 0 & \text{otherwise} \end{cases}$$

This will remove the input noise, but to restore the signal level, a DC restorer must be used just before the sampler. If this is done then,

$$y(t)_{31} = 0$$

$$y(t)_{32} = \frac{\sigma_n}{\pi \sqrt{\omega \alpha}} \sum_{n=1}^{\infty} \left[\frac{\sin n}{n} k_s n \pi \right] \left(\cos \left[(n\omega_D - \omega_n) t - \psi \right] \right. \\ \left. + \cos \left[(n\omega_D + \omega_n) t + \psi \right] \right)$$

Since

$$n\omega_D + \omega_n > \omega_D \text{ for all } n$$

and

$$\omega_D \gg \omega_Y,$$

the second term may be dropped.

Hence,

$$y(t)_{32} = \frac{\sigma_n}{\pi \sqrt{\omega \alpha}} \sum_{n=1}^{\infty} \frac{1}{n} \left[\sin n k_s \pi \right] \left(\cos \left[(n\omega_D - \omega_n) t - \psi \right] \right)$$

when

$$n\omega_D - \omega_Y \leq (n\omega_D - \omega_n) \leq n\omega_D + \omega_Y$$

these will be interfering beats.

Since the noise power is

$$P_n = \sum_{n=1}^{\infty} |y(t)|^2 \text{ per unit of bandwidth,}$$

hence,

$$P_n = \frac{\sigma_n^2}{\pi^2 \omega \alpha} \sum_{n=1}^{\infty} \frac{\sin^2 n k_s \pi}{n^2}$$

The total power is found by multiplying by the effective bandwidth $2 \omega_Y$, and multiplying by 2 to account for the noise introduced by the DC restorer.

$$P_n = \frac{4 \sigma_n^2 \omega_Y}{\pi^2 \omega \alpha} \sum_{n=1,2}^{\infty} \frac{1}{n^2} \sin^2 n k_s \pi$$

The maximum value of k_s for the assumed waveform is $1/3$ or

$$P_n = \frac{4 \sigma_n^2 \omega_Y}{\pi^2 \omega \alpha} \sum_{n=1,2}^{\infty} \frac{1}{n^2} \sin^2 n 60^\circ$$

$$\approx \frac{4 \sigma_n^2 \omega_Y}{\pi^2 \omega \alpha} \quad (1.08)$$

$$P_n \approx 0.438 \sigma_n^2 \frac{\omega_Y}{\omega \alpha}$$

2.3.3 SIGNAL/NOISE

The ratio of the DC signal power to the rms power of the fluctuating components (beat frequencies) is therefore

$$\frac{S}{N} = \frac{\left(I_R - I_S \right)^2 k_s^2}{0.438 \sigma_n^2 \frac{\omega_Y}{\omega \alpha}} = \frac{\left(I_R - I_S \right)^2 \omega \alpha}{9 (0.438) \sigma_n^2 \omega_Y}$$

where $k_s = 1/3$ to be equivalent with noise analysis.

Hence,

$$\frac{S}{N} = \frac{0.254 \left(I_R - I_S \right)^2 \omega \alpha}{\sigma_n^2 \omega_Y}$$

2.4 COMPARISON OF SYNCHRONOUS AND SAMPLING DEMODULATOR

2.4.1 SIGNAL/NOISE RATIO, $k_s = 1/3$, wideband

$$\frac{(S/N)_{\text{Sampling}}}{(S/N)_{\text{Synchronous}}} = \frac{\frac{0.254 \left(I_R - I_S \right)^2 \omega \alpha}{\sigma_n^2 \omega \gamma}}{\frac{0.114 \left(I_R - I_S \right)^2 \omega \alpha}{\sigma_n^2 \omega \gamma}}$$

$$\frac{(S/N)_{\text{Sampling}}}{(S/N)_{\text{Synchronous}}} = \frac{0.254}{0.114} = 2.23 \quad \text{for } k_s = 1/3$$

2.4.2 SIGNAL/NOISE RATIO, $k_s = 0.156$ wideband

$$\frac{(S/N)_{\text{Sampling}}}{(S/N)_{\text{Synchronous}}} = \frac{\frac{(0.156)^2 \left(I_R - I_S \right)^2}{0.25 \sigma_n^2 \omega \gamma / \omega \alpha}}{\frac{0.114 \left(I_R - I_S \right)^2 \omega \alpha}{\sigma_n^2 \omega \gamma}} = \frac{0.099}{0.114}$$

$$\frac{(S/N)_{\text{Sampling}}}{(S/N)_{\text{Synchronous}}} = 0.866$$

From the above calculations it is evident that in a sampling system the S/N ratio is a function of the sampling duty cycle k_s , and that as k_s decreases, the system becomes inferior to the synchronous system, i.e., k_s should be as large as possible.

2.4.3 SUMMARY

A. Synchronous System (Wideband)

$$\text{a) Signal power} = \frac{\left(I_R - I_S \right)^2}{9}$$

$$\text{b) Noise power} = 0.98 \sigma_n^2 \frac{\omega \gamma}{\omega \alpha}$$

$$c) \text{ S/N, power} = \frac{0.114 (I_R - I_S)^2 \omega \alpha}{\sigma_n^2 \omega \gamma}$$

d) System uses a broadband input amplifier:

$$H_A(\omega) = \begin{cases} 1, & 0 \leq \omega \leq \omega \alpha \\ 0, & \text{otherwise} \end{cases}$$

e) System uses a narrowband output amplifier:

$$H_F(\omega) = \begin{cases} 1, & 0 \leq \omega \leq \omega \gamma \\ 0, & \text{otherwise} \end{cases}$$

B. Sampling System

$$a) \text{ Signal power} = (I_R - I_S)^2 k_s^2$$

$$b) \text{ Noise power} = \frac{0.405 \sigma_n^2 \omega \gamma}{\omega \alpha} \sum_{n=1,2,3}^{\infty} \frac{1}{n^2} \sin^2 n k_s \pi$$

$$c) \text{ S/N, power} = \frac{2.47 k_s^2 (I_R - I_S)^2 \omega \alpha}{\sigma_n^2 \omega \gamma \sum_{n=1,2,3}^{\infty} \frac{1}{n^2} \sin^2 n k_s \pi}$$

d) The system uses an AC coupled amplifier:

$$H_2(\omega) = \begin{cases} 1, & \omega \gamma \leq \omega \leq \omega \alpha \\ 0, & \text{otherwise} \end{cases}$$

e) The system uses a DC restorer prior to the sampler

f) The system uses a narrowband output filter

$$H_1(\omega) = \begin{cases} 1, & 0 \leq \omega \leq \omega \gamma \\ 0, & \text{otherwise} \end{cases}$$

C. Note that in the synchronous system a narrow band filter could be used ahead of the demodulator to remove frequencies higher than the fundamental. In this case

$$a) \text{ Signal power narrow band} = 0.126 (I_R - I_S)^2$$

$$b) \text{ Noise power} = \frac{0.82 \sigma_n^2 \omega \gamma}{\omega \alpha}$$

$$\text{c) } S/N, \text{ power} = \frac{0.154 \left(I_R - I_S \right)^2 \omega \alpha}{\sigma_n^2 \omega \gamma}$$

$$\begin{aligned} \text{d) } \frac{S/N \text{ Sampling, wide band, } k_s = 0.156}{S/N \text{ Synchronous, narrow band}} &= \frac{(0.156)^2 / 0.25}{0.154} \\ &= \frac{0.099}{0.154} = 0.65 \end{aligned}$$

Hence, the sampling system with $k_s = 0.156$ is not as good as a narrow band synchronous system, when identical filters are used. If on the other hand the bandpass ω_γ of the sampling system is decreased by 35%, the systems are equivalent in S/N ratios.

APPENDIX B

COMPUTER RAY TRACE

COMPUTER RAY TRACE

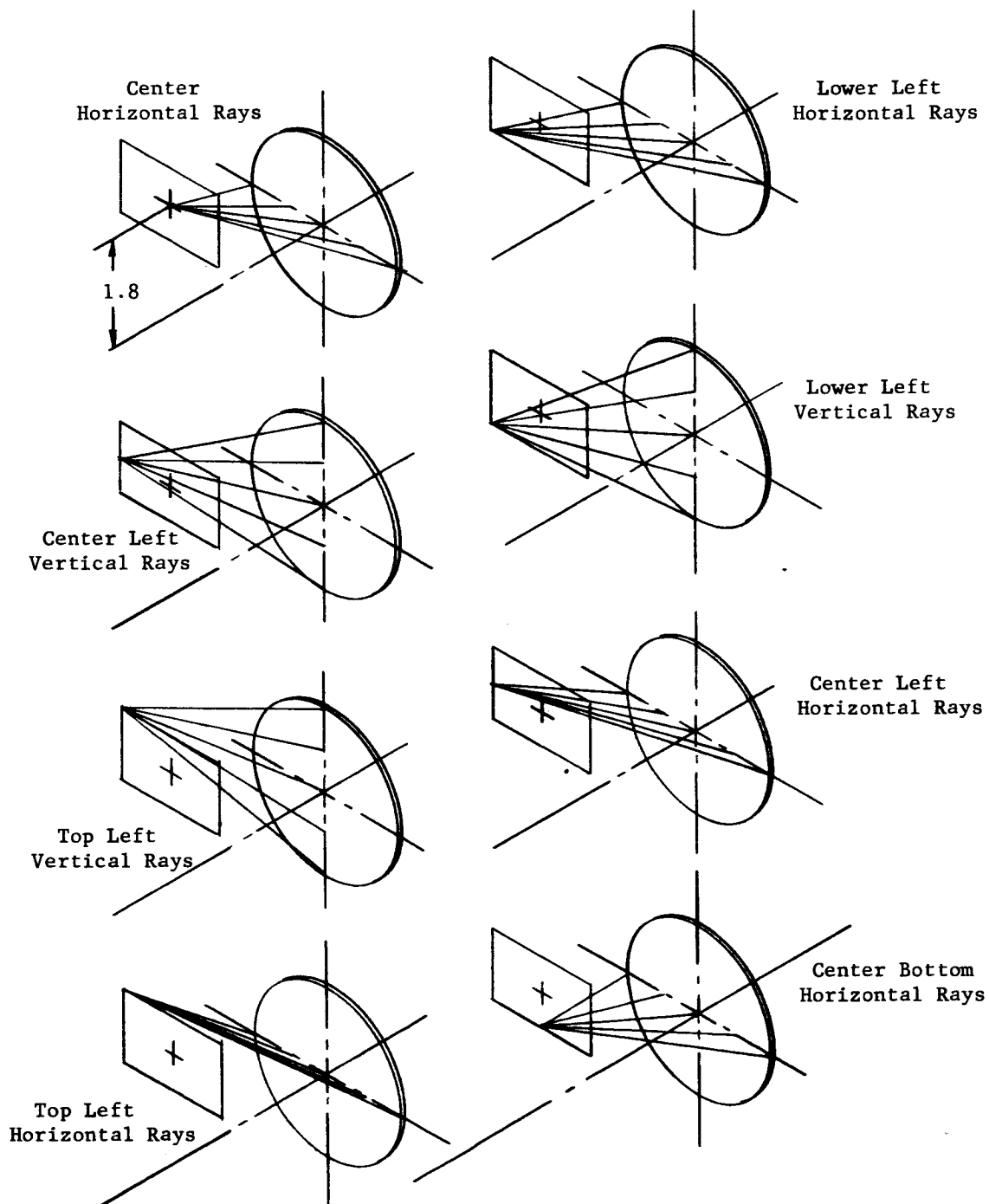
The following computer ray trace was used to determine exit slit image quality, internal image quality, extreme ray traces, and intensity distribution for the optics used in the ultraviolet and infrared subsystems of the two-gas atmosphere sensor. A representative computer run is provided for the ultraviolet system showing the vertical rays emanating from the top left of the entrance slit.

4,
1,-1.10018, .05, -.0127,
4, 1,
REF. RAY

1 -0.110018E 01 0.500000E-01 -0.127000E-01 0.000000E 00 0.000000E 00

1	9	4.410837E-02	-1.074990E-02	-3.940204E-03	9.491474E-02
2	6	4.353749E-02	-1.217538E-02	-3.936857E-03	9.474502E-02
2	8	4.732186E-02	-1.235565E-02	-3.674353E-03	7.817166E-02
2	10	4.884992E-02	-1.045601E-02	-3.515734E-03	7.112177E-02
3	5	4.435432E-02	-1.361460E-02	-3.838119E-03	8.720703E-02
3	7	4.858326E-02	-1.443156E-02	-3.395192E-03	6.656753E-02
3	9	5.086845E-02	-1.225178E-02	-3.043223E-03	5.552733E-02
4	4	4.400770E-02	-1.443299E-02	-3.789205E-03	8.441997E-02
4	6	4.839380E-02	-1.651700E-02	-3.198516E-03	5.967077E-02
4	8	5.113970E-02	-1.466233E-02	-2.630908E-03	4.482793E-02
4	10	5.229168E-02	-1.080020E-02	-2.357020E-03	3.862016E-02
5	3	4.296635E-02	-1.414781E-02	-3.795048E-03	8.626112E-02
5	5	4.721591E-02	-1.815991E-02	-3.130865E-03	5.718093E-02
5	7	5.013361E-02	-1.723388E-02	-2.363829E-03	3.853226E-02
5	9	5.175572E-02	-1.340051E-02	-1.854227E-03	2.871860E-02
6	2	4.169959E-02	-1.223634E-02	-3.813343E-03	9.275146E-02
6	4	4.549893E-02	-1.889795E-02	-3.195708E-03	5.896561E-02
6	6	4.829275E-02	-1.952348E-02	-2.281618E-03	3.630935E-02
6	8	5.009698E-02	-1.630708E-02	-1.539431E-03	2.294602E-02
6	10	5.089932E-02	-1.111258E-02	-1.200317E-03	1.744023E-02
7	3	4.369931E-02	-1.823910E-02	-3.354747E-03	6.506823E-02
7	5	4.605424E-02	-2.108225E-02	-2.386115E-03	3.802028E-02
7	7	4.774531E-02	-1.908221E-02	-1.445862E-03	2.095115E-02
7	9	4.873646E-02	-1.420763E-02	-8.550856E-04	1.208892E-02
8	2	4.230012E-02	-1.563599E-02	-3.523866E-03	7.568887E-02
8	4	4.386707E-02	-2.143883E-02	-2.643018E-03	4.372450E-02
8	6	4.513089E-02	-2.128545E-02	-1.573751E-03	2.259080E-02
8	8	4.601724E-02	-1.731675E-02	-7.521331E-04	1.027793E-02
8	10	4.647169E-02	-1.137148E-02	-3.820957E-04	5.267515E-03
9	1	4.183544E-02	-1.044745E-02	-3.564946E-03	9.113532E-02
9	3	4.220950E-02	-2.007810E-02	-2.977110E-03	5.366305E-02
9	5	4.269951E-02	-2.245906E-02	-1.892288E-03	2.793521E-02
9	7	4.316890E-02	-2.000422E-02	-8.902710E-04	1.186149E-02
9	9	4.352431E-02	-1.466804E-02	-2.705078E-04	3.593278E-03
10	2	4.161136E-02	-1.640914E-02	-3.262175E-03	6.821515E-02
10	4	4.092849E-02	-2.210986E-02	-2.334336E-03	3.725329E-02
10	6	4.063753E-02	-2.182084E-02	-1.241336E-03	1.691652E-02
10	8	4.058411E-02	-1.768883E-02	-4.082820E-04	5.143369E-03
10	10	4.067803E-02	-1.156190E-02	-2.952048E-04	3.921624E-04
11	1	4.268833E-02	-9.713634E-03	-3.308507E-03	8.782031E-02
11	3	4.034781E-02	-1.968184E-02	-2.784940E-03	5.097414E-02
11	5	3.890295E-02	-2.228793E-02	-1.744584E-03	2.572957E-02
11	7	3.810043E-02	-1.998941E-02	-7.688565E-04	9.998311E-03

11	9	3.779110E-02	-1.476999E-02	-1.579017E-04	1.935171E-03
12	2	4.157322E-02	-1.451190E-02	-3.066397E-03	6.961582E-02
12	4	3.849944E-02	-2.087335E-02	-2.294224E-03	3.876205E-02
12	6	3.655890E-02	-2.110017E-02	-1.295615E-03	1.845431E-02
12	8	3.550879E-02	-1.740434E-02	-5.090511E-04	6.688987E-03
12	10	3.521987E-02	-1.167731E-02	-1.389208E-04	1.953290E-03
13	1	4.536162E-02	-5.756002E-03	-2.924706E-03	9.367121E-02
13	3	4.004881E-02	-1.695242E-02	-2.722757E-03	5.658455E-02
13	5	3.650245E-02	-2.050463E-02	-1.888828E-03	3.099096E-02
13	7	3.432605E-02	-1.900023E-02	-1.027872E-03	1.495303E-02
13	9	3.330156E-02	-1.449999E-02	-4.632361E-04	6.708006E-03
14	2	4.431600E-02	-9.742481E-03	-2.784877E-03	7.976827E-02
14	4	3.856539E-02	-1.760413E-02	-2.387935E-03	4.820930E-02
14	6	3.479940E-02	-1.905070E-02	-1.616997E-03	2.721328E-02
14	8	3.265590E-02	-1.643107E-02	-9.451417E-04	1.495084E-02
14	10	3.195153E-02	-1.172126E-02	-6.049180E-04	9.996361E-03
15	3	4.353098E-02	-1.165805E-02	-2.553857E-03	7.072740E-02
15	5	3.758323E-02	-1.697351E-02	-2.118636E-03	4.408197E-02
15	7	3.385913E-02	-1.696815E-02	-1.485680E-03	2.716333E-02
15	9	3.203897E-02	-1.384261E-02	-1.019230E-03	1.838458E-02
16	4	4.349123E-02	-1.205525E-02	-2.296262E-03	6.619545E-02
16	6	3.759522E-02	-1.553791E-02	-1.925310E-03	4.395110E-02
16	8	3.419668E-02	-1.471584E-02	-1.464647E-03	3.077191E-02
16	10	3.302603E-02	-1.170855E-02	-1.187540E-03	2.539520E-02
17	3	5.360220E-02	-3.355395E-03	-1.822959E-03	9.406097E-02
17	5	4.472345E-02	-1.144221E-02	-2.025904E-03	6.594180E-02
17	7	3.915076E-02	-1.377024E-02	-1.775522E-03	4.773933E-02
17	9	3.639876E-02	-1.277381E-02	-1.484304E-03	3.815798E-02
18	4	5.639440E-02	-3.765391E-03	-1.459438E-03	9.363346E-02
18	6	4.782592E-02	-1.031298E-02	-1.708198E-03	6.987906E-02
18	8	4.288726E-02	-1.216106E-02	-1.592103E-03	5.553469E-02
18	10	4.116195E-02	-1.166591E-02	-1.427644E-03	4.959689E-02
19	7	5.350875E-02	-9.173959E-03	-1.258747E-03	7.805476E-02
19	9	4.957785E-02	-1.124410E-02	-1.246586E-03	6.755599E-02
20	8	6.265538E-02	-8.573454E-03	-5.384941E-04	9.061527E-02
20	10	6.020904E-02	-1.163316E-02	-5.500173E-04	8.408964E-02



Figures for Computer to Determine Exit Slit Image Quality
 O_2 Ultraviolet System

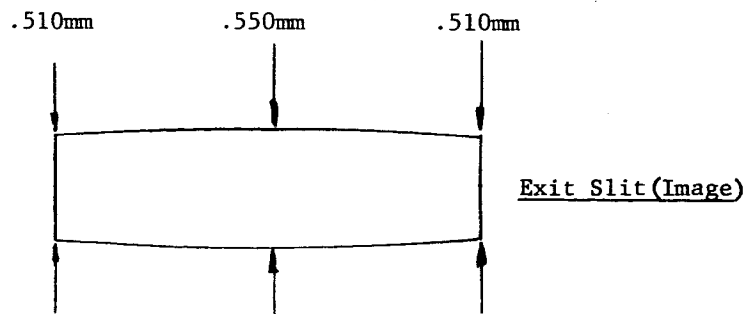
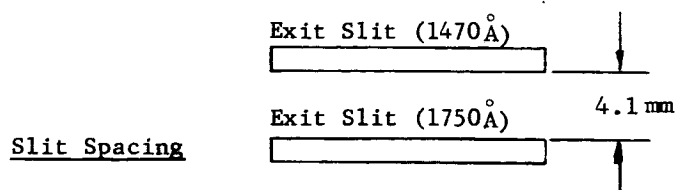
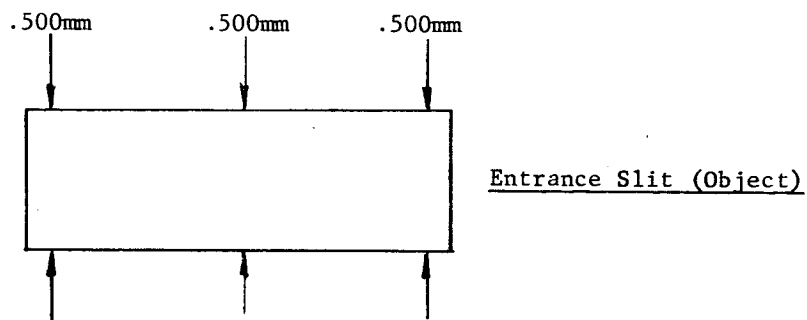
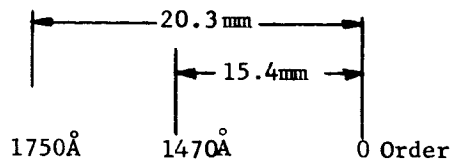


Image Quality



Dispersion
at Exit Slit



O₂ - UV System Images and Dispersion from Computer Ray Trace
(RPC-4000 Computer)

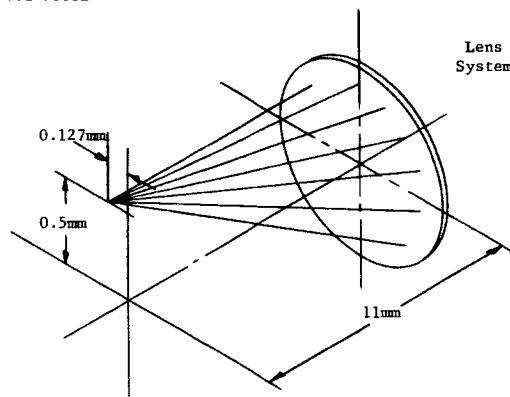
Computer Input:

$L = 0.110018E$

$H_y = 0.500000E$

$H_z = 0.127000E$

80 Total Rays Traced



Ray trace from extreme top left of object (infrared source), for computer to determine final image quality.

Third Point CO₂ Infrared System

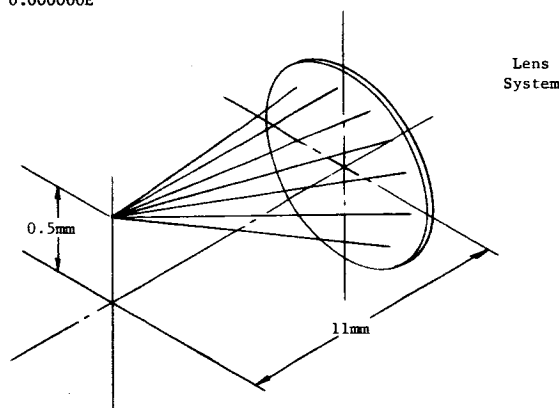
Computer Input:

$L = 0.110018E$

$H_y = 0.500000E$

$H_z = 0.000000E$

80 Total Rays Traced



Ray trace from center top of object (infrared source), for computer to determine final image quality.

Fourth Point CO₂ Infrared System

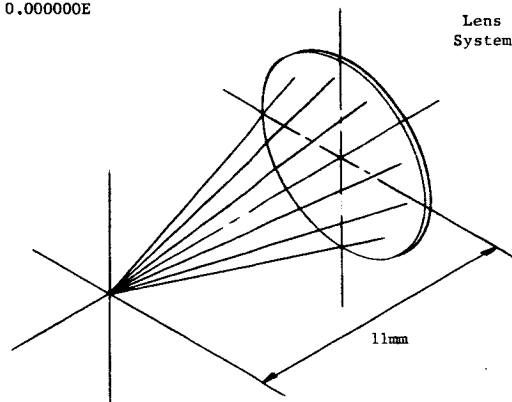
Computer Input:

39 Total Rays Traced

$L = 0.110018E$

$H_y = 0.000000E$

$H_z = 0.000000E$



Ray trace from center of object (Infrared Source), for computer to determine final image quality.

First Point CO₂ Infrared System

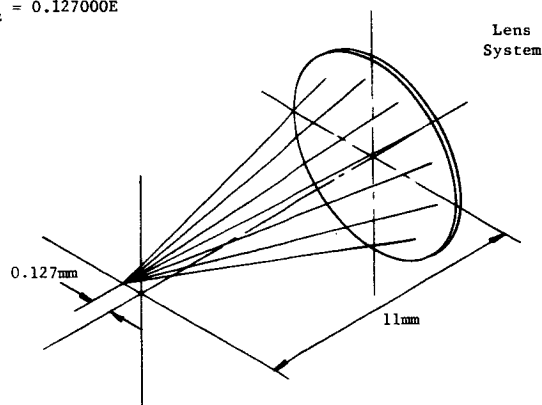
Computer Input:

80 Total Rays Traced

$L = 0.110018E$

$H_y = 0.000000E$

$H_z = 0.127000E$



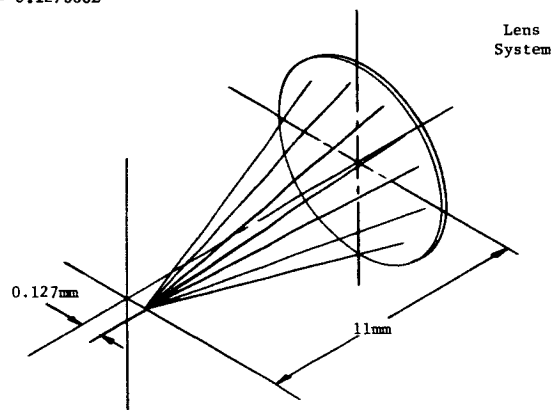
Ray trace from extreme left of object (infrared source) on axis, for computer to determine final image quality.

Second Point CO₂ Infrared System

Computer Input:

80 Total Rays Traced

$L = 0.110018E$
 $H_y = 0.000000E$
 $H_z = 0.127000E$



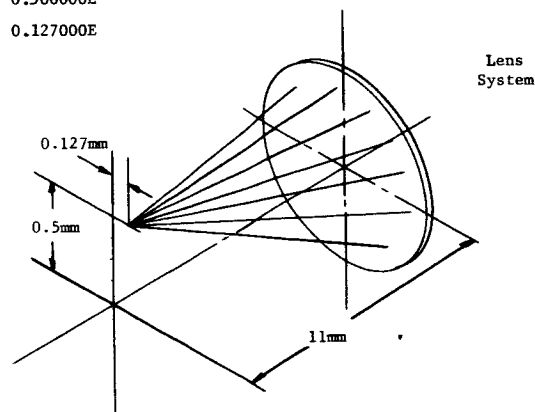
Ray trace from extreme right of object
 (infrared source) on axis, for computer
 to determine final image quality.

Fifth Point CO_2 Infrared System

Computer Input:

80 Total Rays Traced

$L = 0.110018E$
 $H_y = 0.500000E$
 $H_z = 0.127000E$

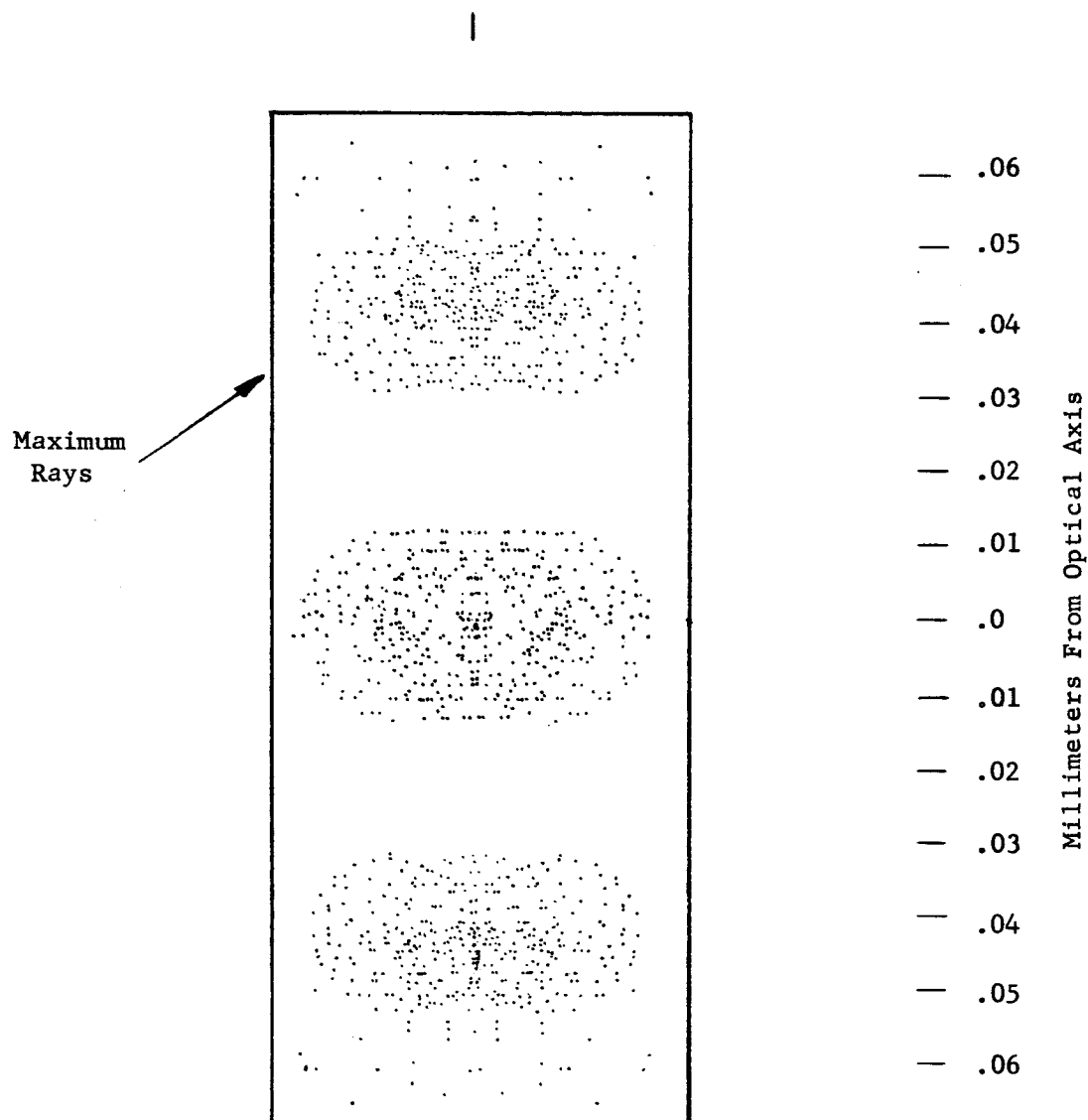


Ray trace from extreme top right of object
 (infrared source), for computer to deter-
 mine final image quality.

Sixth Point CO_2 Infrared System

Six object points summarized.
(SDS 920 Computer)

Final Image
at Detector

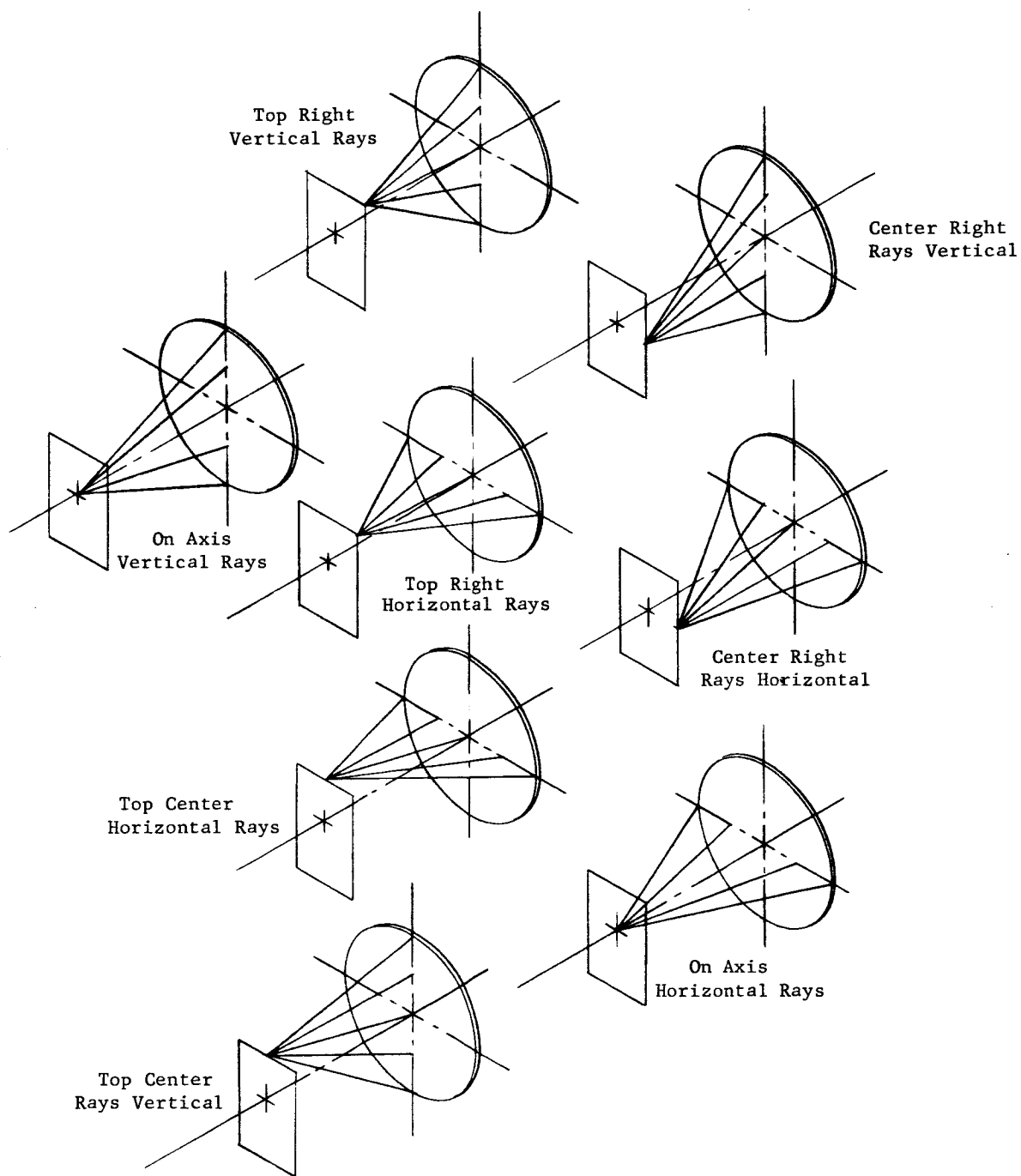


.06 .05 .04 .03 .02 .01 0 .01 .02 .03 .04 .05 .06

Millimeters From Optical Axis

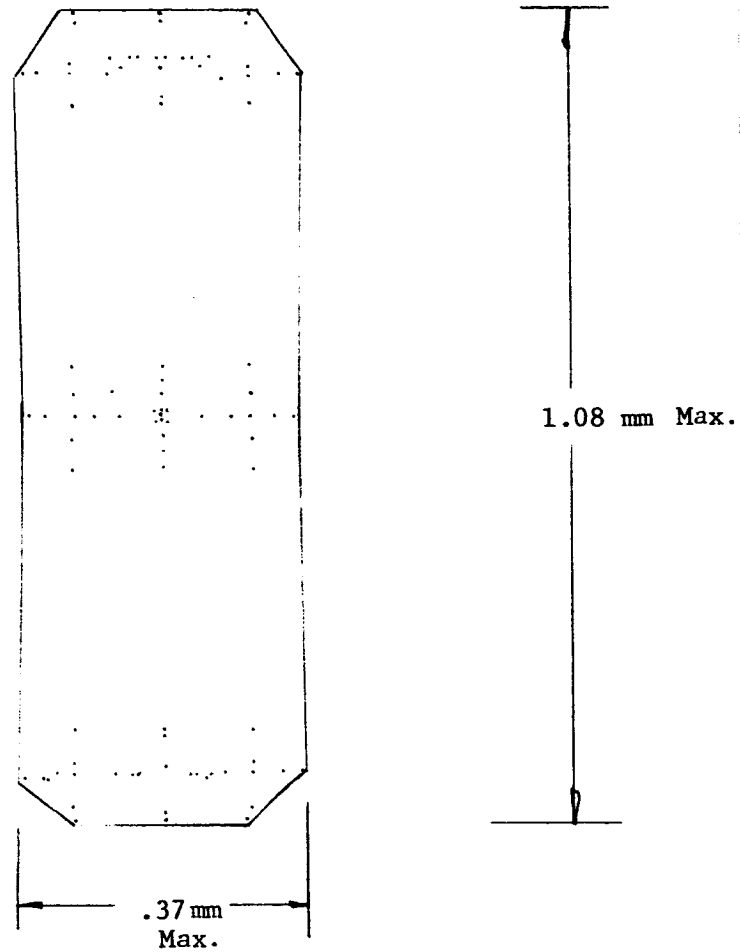
Spot Diagram - Intensity Distribution
From Computer Ray Trace

CO₂ Infrared System



Figures for Computer to Determine Internal Image Quality
CO₂ Infrared System

Internal Image
at Chopper Position



CO₂ Infrared System, Extreme-Ray Trace
from Computer Ray Trace

APPENDIX C

TRANSMISSION AND ABSORPTION MEASUREMENTS

APPENDIX C

TRANSMISSION AND ABSORPTION MEASUREMENTS

When the absorption of a parallel beam of monochromatic radiation is proportional to the radiant power or flux and to the mass of homogeneous and isotropic matter intersected, the transmittance may be described by Beer's Law as

$$T = \frac{I}{I_o} = 10^{-A} \quad (1)$$

or

$$T = \frac{I}{I_o} = e^{-kdc} \quad (2)$$

where

T = transmittance; dimensionless

I = radiant power transmitted through the sample;

$\frac{\text{Watt}}{\text{m}^2}$ or $\frac{\text{quanta}}{\text{sec}}$

I_o = radiant power incident on the sample;

$\frac{\text{Watt}}{\text{m}^2}$

A = absorbance; dimensionless

k = absorption coefficient; cm^{-1}

d = sample path length; cm

c = mass fractional concentration of sample;
dimensionless (if the concentration is
expressed as fractional molar or volumetric
ratio the symbol k should be replaced by ϵ
the molar extinction coefficient or molar
absorptivity)

e = naperian base = 2.71828...

The absorbance A (sometimes referred to as extinction or optical density coefficient) may be expressed as

$$A = A_w + d \left[K_1 + C (K - K_1) \right] \quad (3)$$

where

A_w = absorbance of the windows and reflections from four surfaces.

K_1 = absorptivity of the solvent; cm^{-1}

If reflections are ignored, and the solvent is considered to be non-absorbent in the spectral region of interest, (3) reduces to

$$A = Kdc \quad (4)$$

and (1) takes on a similar form to (2):

$$T = e^{-kdc} \quad (2)$$

$$T = 10^{-Kdc} \quad (5)$$

Equating (2) and (5):

$$\begin{aligned} T &= 10^{-Kdc} = e^{-kdc} \\ \frac{Kcd}{kcd} &= \frac{\log \left(\frac{1}{T} \right)}{\ln \left(\frac{1}{T} \right)} = \frac{\ln \left(\frac{1}{T} \right)}{\ln (10) \ln \left(\frac{1}{T} \right)} \\ &= \frac{1}{\ln (10)} = \frac{1}{2.303} = 0.434 \\ K &= 0.434k \quad (6) \end{aligned}$$

The relationship between K and T are shown in Perkin-Elmer's Precision Table on the following page, which is provided with the Model 350 and

PRECISION TABLE

for conversion of Absorbance to Transmittance
and Transmittance to Absorbance (symbols T & A).

For rapid quantitative analysis with the
PERKIN-ELMER®
Model 350 and Model 202 Spectrophotometers

T	A	T	A	T	A	T	A	T	A	T	A
1.000	0.000	.485	0.314	.308	0.511	.191	0.719	.128	0.893	.064	1.194
.990	0.004	.480	0.319	.306	0.514	.190	0.721	.127	0.896	.063	1.201
.980	0.009	.475	0.323	.304	0.517	.189	0.724	.126	0.900	.062	1.208
.970	0.013	.470	0.328	.302	0.520	.188	0.726	.125	0.903	.061	1.215
.960	0.018	.465	0.333	.300	0.523	.187	0.728	.124	0.907	.060	1.222
.950	0.022	.460	0.337	.298	0.526	.186	0.731	.123	0.910	.059	1.229
.940	0.027	.455	0.342	.296	0.529	.185	0.733	.122	0.914	.058	1.237
.930	0.032	.450	0.347	.294	0.532	.184	0.735	.121	0.917	.057	1.244
.920	0.036	.445	0.352	.292	0.535	.183	0.738	.120	0.921	.056	1.252
.910	0.041	.440	0.357	.290	0.538	.182	0.740	.119	0.925	.055	1.260
.900	0.046	.435	0.362	.288	0.541	.181	0.742	.118	0.928	.054	1.268
.890	0.051	.430	0.367	.286	0.544	.180	0.745	.117	0.932	.053	1.276
.880	0.056	.425	0.372	.284	0.547	.179	0.747	.116	0.936	.052	1.284
.870	0.061	.420	0.377	.282	0.550	.178	0.750	.115	0.939	.051	1.292
.860	0.066	.415	0.382	.280	0.552	.177	0.752	.114	0.943	.050	1.301
.850	0.071	.410	0.387	.278	0.556	.176	0.755	.113	0.947	.049	1.310
.840	0.076	.405	0.393	.276	0.559	.175	0.757	.112	0.951	.048	1.319
.830	0.081	.400	0.398	.274	0.562	.174	0.760	.111	0.955	.047	1.328
.820	0.086	.398	0.400	.272	0.565	.173	0.762	.110	0.959	.046	1.337
.810	0.092	.396	0.402	.270	0.569	.172	0.765	.109	0.963	.045	1.347
.800	0.097	.394	0.405	.268	0.572	.171	0.767	.108	0.967	.044	1.357
.790	0.102	.392	0.407	.266	0.575	.170	0.770	.107	0.971	.043	1.367
.780	0.108	.390	0.409	.264	0.578	.169	0.772	.106	0.975	.042	1.377
.770	0.114	.388	0.411	.262	0.582	.168	0.775	.105	0.979	.041	1.387
.760	0.119	.386	0.413	.260	0.585	.167	0.777	.104	0.983	.040	1.398
.750	0.125	.384	0.416	.258	0.588	.166	0.780	.103	0.987	.039	1.409
.740	0.131	.382	0.418	.256	0.592	.165	0.783	.102	0.991	.038	1.420
.730	0.137	.380	0.420	.254	0.595	.164	0.785	.101	0.996	.037	1.432
.720	0.143	.378	0.423	.252	0.599	.163	0.788	.100	1.000	.036	1.444
.710	0.149	.376	0.425	.250	0.602	.162	0.791	.099	1.004	.035	1.456
.700	0.155	.374	0.427	.248	0.606	.161	0.793	.098	1.009	.034	1.469
.690	0.161	.372	0.430	.246	0.609	.160	0.796	.097	1.013	.033	1.482
.680	0.168	.370	0.432	.244	0.613	.159	0.799	.096	1.018	.032	1.495
.670	0.174	.368	0.434	.242	0.616	.158	0.801	.095	1.022	.031	1.509
.660	0.181	.366	0.437	.240	0.620	.157	0.804	.094	1.027	.030	1.523
.650	0.187	.364	0.439	.238	0.623	.156	0.807	.093	1.032	.029	1.538
.640	0.194	.362	0.441	.236	0.627	.155	0.810	.092	1.036	.028	1.552
.630	0.201	.360	0.444	.234	0.631	.154	0.813	.091	1.041	.027	1.569
.620	0.208	.358	0.446	.232	0.635	.153	0.815	.090	1.046	.026	1.585
.610	0.215	.356	0.449	.230	0.638	.152	0.818	.089	1.051	.025	1.602
.600	0.222	.354	0.451	.228	0.642	.151	0.821	.088	1.056	.024	1.620
.595	0.226	.352	0.454	.226	0.646	.150	0.824	.087	1.061	.023	1.638
.590	0.229	.350	0.456	.224	0.650	.149	0.827	.086	1.066	.022	1.658
.585	0.233	.348	0.458	.222	0.654	.148	0.830	.085	1.071	.021	1.678
.580	0.237	.346	0.461	.220	0.658	.147	0.833	.084	1.076	.020	1.699
.575	0.240	.344	0.463	.218	0.662	.146	0.836	.083	1.081	.019	1.722
.570	0.244	.342	0.466	.216	0.666	.145	0.839	.082	1.086	.018	1.745
.565	0.248	.340	0.469	.214	0.670	.144	0.842	.081	1.092	.017	1.770
.560	0.252	.338	0.471	.212	0.674	.143	0.845	.080	1.097	.016	1.796
.555	0.256	.336	0.474	.210	0.678	.142	0.848	.079	1.102	.015	1.824
.550	0.260	.334	0.477	.208	0.682	.141	0.851	.078	1.108	.014	1.854
.545	0.264	.332	0.480	.206	0.686	.140	0.854	.077	1.114	.013	1.886
.540	0.268	.330	0.482	.204	0.690	.139	0.857	.076	1.119	.012	1.921
.535	0.272	.328	0.484	.202	0.695	.138	0.860	.075	1.125	.011	1.959
.530	0.276	.326	0.487	.200	0.699	.137	0.863	.074	1.131	.010	2.00
.525	0.280	.324	0.490	.199	0.701	.136	0.867	.073	1.137	.009	2.05
.520	0.284	.322	0.492	.198	0.703	.135	0.870	.072	1.143	.008	2.10
.515	0.288	.320	0.495	.197	0.706	.134	0.873	.071	1.149	.007	2.15
.510	0.292	.318	0.498	.196	0.708	.133	0.876	.070	1.155	.006	2.22
.505	0.297	.316	0.500	.195	0.710	.132	0.879	.069	1.161	.005	2.30
.500	0.301	.314	0.503	.194	0.712	.131	0.883	.068	1.168	.004	2.40
.495	0.305	.312	0.506	.193	0.714	.130	0.886	.067	1.174	.003	2.52
.490	0.310	.310	0.509	.192	0.717	.129	0.889	.066	1.181	.002	2.70
								.065	1.187	.001	3.00

Model 202 Spectrophotometers. The value of k is most often given in the literature rather than values for K .

It is well known that the optimum analytical precision in absorption spectroscopy is often obtained with a transmittance of 36.8%. This can be shown by assuming the conditions for (5)

$$T = 10^{-Kdc}$$

and observing that the fractional error in C is

$$\frac{\Delta C}{C} = \frac{0.434}{T} \frac{\Delta T}{\log T} \quad (7)$$

This error varies with sample thickness and has a minimum when

$$\frac{d}{dKdc} \left(\frac{\Delta C}{C} \right) = 0 \quad (8)$$

which is when

$$Kdc = 0.434 \quad (9)$$

or $T = \frac{1}{e} = 36.8\%$. From (8) it can be seen that the minimum error is

$$\frac{\Delta C}{C} = -e (\Delta T) = -2.718 (\Delta T) \quad (10)$$

which indicates that a 1% error in transmittance will cause a 2.7% error in concentration.

The "transmittance ratio method" uses a standard preparation of a known concentration of the sample in the reference beam. This reduces the error to

$$\frac{\Delta C}{C} = - \left(\frac{e}{10^A} \right) \Delta \left(\frac{I}{I_{Ref}} \right) \quad (11)$$

or if both the reference and sample paths are set for $A = 0.434$, the error in concentration is

$$\frac{\Delta C}{C} = - \Delta \left(\frac{I}{I_{Ref}} \right) \quad (12)$$

which is lower by a factor e than the error produced from a non-absorbing reference beam shown in (10).

It may be assumed that for chopped beams which are compared on a single detector, the error in transmittance is independent of the source and that changes in the sample beam transmission are independent of the level of the transmission.

Background such as stray light or other unwanted radiation may also be present and may characteristically be independent of both the sample concentration or path length. Denoting this radiation power as I_g , and assuming no window or cell errors with a transparent reference media, Beer's Law (i) becomes:

$$(I - I_g) = (I_o - I_g) 10^{-Kcd} \quad (13)$$

which is often called "base line" method. The coefficient of variation of the absorbance is a minimum when

$$T = \frac{I}{I_o} = 0.368 \left(1 + 1.718 \frac{I_g}{I_o} \right) \quad (14)$$

and increases from the minimum of 36.8% as the penetrating background increases.

Noise considerations may affect the absorbance level depending on whether Johnson noise (Thermal Detector) or shot noise (Photoemissive Detector) predominates in the detector circuit of the instrument. Neglecting other errors, the optimum condition for Johnson noise is

$$A = 0.434; \quad T = 36.8\% \quad (15)$$

and for shot noise

$$A = 0.868; \quad T = \frac{1}{e} = 13.5\% \quad (16)$$

It may be noted that Johnson noise error varies inversely with the square of the slit-width, and the resolution decreases directly as the slit-width, it is advantageous to use a large slit. Shot noise, however, is approximately independent of slit width.

If the radiant power is of sufficient intensity to make the detector response non-linear there are three possible courses of action:

- 1) Calibrate the non-linear response;
- 2) Reduce the power with collimator slits;
- 3) Increase the sample thickness.

If I_{\max} is the maximum permissible radiant power determined by a linear detector response with the minimum expected concentration, (1) becomes

$$T = \frac{I}{I_{\max}} = 10^{-A} \quad (17)$$

and (17) optimizes for concentration sensitivity when $A = 0.434$. However, the transmittance for normal samples may be very much less than 36.8%. There is not optimum sample thickness, but the path length d should be increased to keep the radiant power transmitted through the reference or sample just below I_{\max} .

Since experimental measurements are of reflection as well as absorption losses it is useful to review the reflection properties of materials. Reflection and absorption are independent properties and may be separately treated. If the index of refraction n of a given wavelength is sufficiently high, the reflectivity of a single plane surface is the major loss and can be determined from*

$$r = \frac{(n - 1)^2}{(n + 1)^2} \quad (18)$$

and the transmission, assuming no absorption, of a plane parallel window is

$$t = \frac{2n}{n^2 + 1} \quad (19)$$

from which the "equivalent reflectivity", r^1 is

$$r^1 = 1 - t = \frac{(n - 1)^2}{n^2 + 1} \quad (20)$$

(It should be noted that r^1 is not twice r from (18) due to multiple reflections.) Combining the reflection losses with (2) results in a general expression for

*Optical Calculations, Optovac, Inc., Bulletin No. 50, January, 1964

$$T = \frac{I}{I_o} = \frac{(1 - r)^2 e^{-kdc}}{1 - r^2 e^{-kdc}} \quad (21)$$

With no absorption, kdc small or zero, (21) reduces to (19). If the index is less than $n = 2$, the term $r^2 e^{-2kdc}$ can be neglected with resultant total errors in transmission of less than 1%. For this case, Equation (21) may be written as

$$T = \frac{I}{I_o} = (1 - r)^2 e^{-kdc} \quad (22)$$

This is equivalent to

$$T = e^{-kdc} - 2r e^{-kdc} + r^2 e^{-kdc} \quad (23)$$

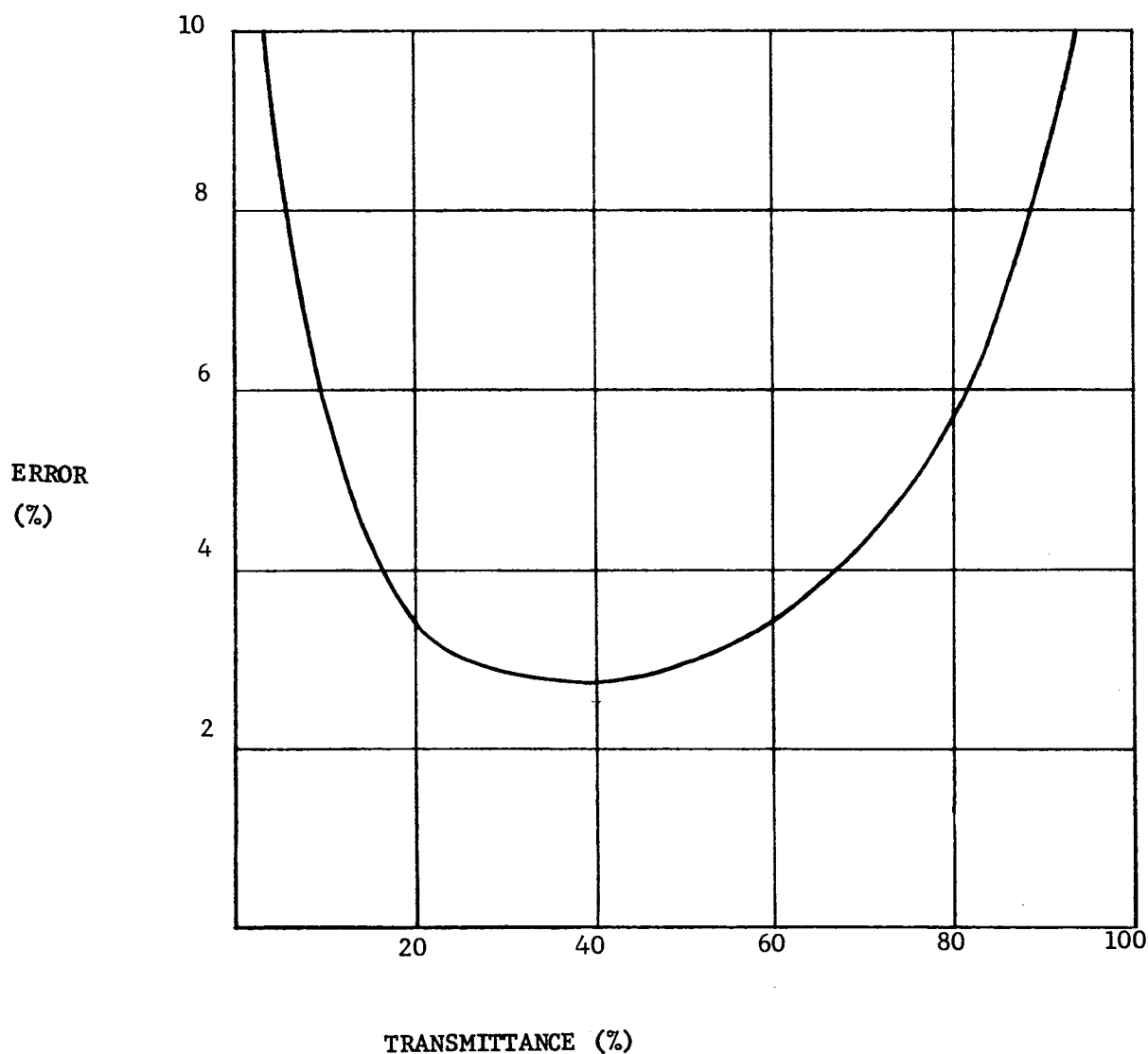
where the first term is the absorption with no reflection losses, the second term is the reflection losses if it is assumed this is twice the loss from the first surface. The third term may be neglected due to the r^2 term if n is less than 2.0. (22) then reduces to

$$T = (1 - 2r) e^{-kdc} \quad (24)$$

and the total reflection of a plane parallel plate is

$$r_T = 2r = 2 \frac{(n - 1)^2}{(n + 1)^2} \quad (25)$$

Beer's Law is essentially symmetrical in path length d , and concentration C , so the requirement of (9) can be met by an adjustment of either. In the case of a gas, the partial pressure may be varied to achieve this condition. In the determination of the concentration of trace constituents, the only recourse is to use a long cell. A plot of (7) shows a rather flat minimum error region between 25% and 50% so that the accurate adjustment to 36.8% is of little value.



Error in the absorbance as given in equation (7) for 1% error in the transmittance.

APPENDIX D

TEST REPORTS

LIMITED-ROTATION MOTOR

GENERAL DATA SHEET

Sheet 1 of 4

TEST: <u>Temp. Altitude</u>	SPEC: <u>-3°C to +55°C</u> <u>140,000 ft</u>	PARA:	TEST NO: <u>1</u>
TEST ITEM: <u>Limited Rotation Motor</u>			DATE: <u>8-13-65</u>
CLIENT: <u>Tiros Radiometer, J. Russo SPO #26421/30003</u>			TEMP. LAB RH: <u>+77°F, 66%</u>
TEST EQUIPMENT: <u>TEMP-ALT. CHAMBER</u>			TESTED BY: <u>CH</u>
MODEL NO: <u>ARC 27</u>			ENGR. CHECK: <u>NP</u>
INSTRUMENTATION: <u>Laser & Power supply (PECO Model #5200)</u> <u>Test circuit, Fluke diff. VTVM (E.O.#529) last cal. 7-3-65</u> <u>Lambda Power Supply (E.O.#714) last cal. 7-8-65</u>			SUPV. CHECK: <u>NP</u>

DATE	TIME	LOG
8-13-65	10 ⁰⁰ AM	Started set up, Target 8' 1/2" from mirror. Calib. -24V + ±10V supplies with Fluke. (See Photos #1+2)
	2 ²⁰ PM	Room Temp readings taken.
	2 ²² PM	Set control for 0°C (+32°F)
	2 ³⁰ PM	Chamber @ 0°C.
	3 ¹⁰ PM	Set control for +10°C (+50°F)
	3 ¹⁵ PM	Chamber @ +10°C.
	4 ⁰⁵ PM	UNIT TC READS = 0.28 mV (Lo) + 7.3°C (Took +10°C data) = 0.44 mV (Hi) + 11.3°C } +9.3°C
	4 ⁰⁹ PM	Set chamber for +20°C (+68°F)
	4 ¹⁵ PM	Chamber @ +20°C.
	4 ⁴⁵ PM	Unit TC reads = .65 mV (Lo) } +18.5°C = .81 mV (Hi) }
		No data taken @ this time, Not stabilized.
	5 ¹⁵ PM	Unit TC reads +19°C (+20°C Data taken)
	5 ²⁰ PM	Set chamber for +25°C (+75°F)
	5 ²⁵ PM	Chamber @ +25°C.

GENERAL DATA SHEET

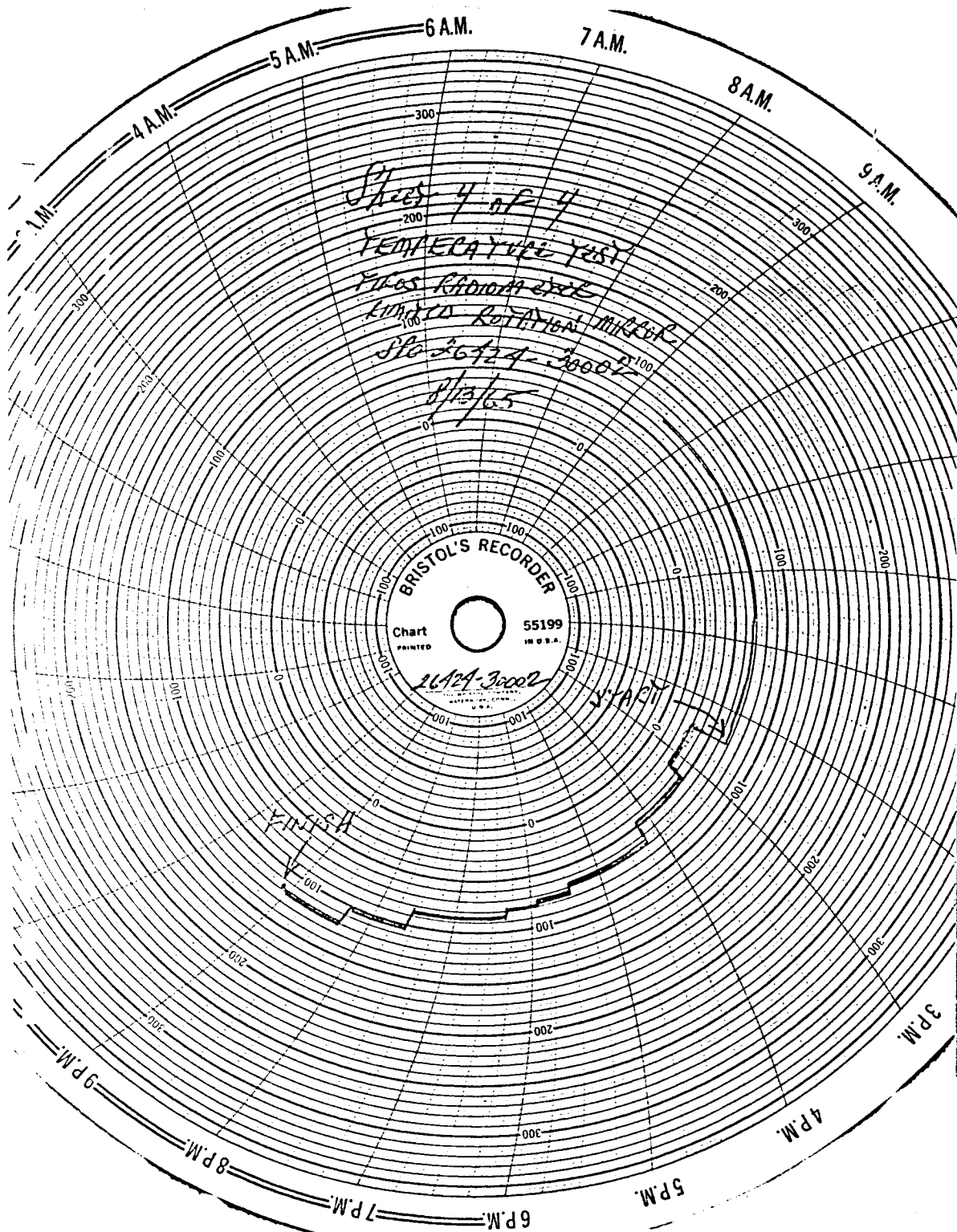
Sheet 2 of 4

TEST: <u>TEMPERATURE</u>	SPEC:	PARA:	TEST NO: <u>1</u>
TEST ITEM: <u>LIMITED ROTATION MOTOR</u>			DATE: <u>8/13/65</u>
CLIENT: <u>TIROS RADIOMETER, D. LABINGER, 26424-30002</u>			TEMP. LAB RH: <u>77°F 66%</u>
TEST EQUIPMENT: <u>TEMP. CHAMBER</u>			TESTED BY: <u>RKE & CG</u>
INSTRUMENTATION: <u>SEE SHEET No. 1</u>			ENGR. CHECK: <u>JP</u>
			SUPV. CHECK: <u>JP</u>

DATE	TIME	LOG
8/13/65	6 ⁰⁵	Unit TC reads +26°C (+25°C Data taken)
	6 ²⁰ PM	Set Chamber for +30°C (+86°F).
	6 ²⁵ PM	Chamber @ +30°C.
	7 ¹⁵ PM	Unit TC reads +31°C (+88°F) +30°C Data Taken
	7 ³⁰ PM	Set Chamber for +40°C (+104°F)
	8 ¹⁰ PM	Unit Temp is +41°C (+40°C Data taken)
	8 ¹⁵ PM	Set Chamber for +50°C (+122°F)
	8 ³⁰ PM	Unit TC reads +50°C (+50°C Data taken)
	9 ⁰⁰ PM	Turned Chamber off, left setup intact
		(Amb. reading to be take first thing Mon.)
8/15/65	8 ⁴⁵ AM	CHAMBER AT AMBIENT TEMPERATURE. TOOK FINAL READINGS ON Limited Rotation/Mixed. UNIT REMOVED FROM CHAMBER - END OF TEST.

Sheet 3 of 4

8-16-65



VIBRATION TEST REPORT ON LIMITED ROTATION MOTOR

1.0 PURPOSE

1.1 To check the Limited Rotation Motor shaft position before and after applied vibration levels up to 21.2 G throughout the frequency range of 20 to 2000 cps.

2.0 SUMMARY

2.1 The Limited Rotation Motor shaft did not indicate any significant change in position when subjected to vibration levels up to 21.2 G_p (20 to 2000 cps) in the vertical and minor horizontal axes. There was no significant shift in position of the Limited Rotation Motor shaft when subjected to vibration levels up to 10 G_p (20 to 500 cps) and 5 G_p from 20 to 2000 cps in the major horizontal axis.

3.0 PROCEDURE

3.1 Vertical Axis

3.1.1 The test specimen was mounted on the head of an electrodynamic vibration machine with its vertical axis parallel to the direction of applied vibration. The axes of the test specimen are defined by Figure 1. The alignment of the mirror mounted on the shaft was checked as shown by Figure 2 using a laser light source. The location of the reflection to the target was marked. The distance from the mirror mounted on the test specimen shaft to the target was approximately ten feet.

3.1.2 The test specimen was then operated with pulsed DC and the travel of the reflected spot on the target was noted.

3.1.3 The test specimen was de-energized and the following vibration levels were applied using a sweep rate of 100°/minute.

- | | | |
|----|----------------|----------|
| a) | 20 to 2000 cps | 1 G_p |
| b) | 20 to 2000 cps | 5 G_p |
| c) | 20 to 2000 cps | 10 G_p |
| d) | 20 to 2000 cps | 15 G_p |

3.1.4 The test specimen was then cycled from 20 to 2000 cps at 40°/minute at the following levels:

20 to 40 cps	0.25 in. double amplitude
40 to 2000 cps	21.2 G_p

3.1.5 During each level of applied vibration, the reflected spot motion on the target was noted.

3.1.6 At the completion of each level of applied vibration, the reflected spot location on the target was checked for any changes more than $\pm 1/4$ inch from the pretest location.

3.1.7 After completion of the maximum applied vibration level detailed by Paragraph 3.1.4, the test specimen was operated with pulsed DC and the reflected spot travel on the target was compared with the spot travel prior to vibration.

3.2 Minor Horizontal Axis

3.2.1 The test specimen was rotated 90 degrees so that its minor horizontal axis was parallel to the direction of applied vibration.

3.2.2 The tests detailed in Paragraph 3.1.1 through 3.1.7 were repeated in the minor horizontal axis.

3.3 Major Horizontal Axis

3.3.1 The test specimen was rotated 90 degrees so that its major horizontal axis was parallel to the direction of applied vibration. This required mounting the test specimen on the slip plate of a slip table assembly. This, in turn, reduced the distance of the test specimen mirror-target distance to approximately five feet. Vibration was perpendicular to the silvered surface of the test specimen mirror.

3.3.2 The tests detailed by Paragraph 3.1.1 through 3.1.7 were repeated along the major horizontal axis of the test specimen except for the vibration levels. The vibration levels used were as detailed below:

a)	20 to 2000 cps	1 G_p
b)	20 to 2000 cps	5 G_p
c)	30 to 400 cps	10 G_p
d)	30 to 700 cps	7.5 G_p

4.0 RESULTS

4.1 There was no significant change (less than 1/4 inch) in the reflected spot location on the target as a result of the applied vibration tests.

4.2 The test specimen operated satisfactorily after completion of each axis of vibration.

4.3 During the vibration tests there was some transient motion of the reflected spot on the target. A summary of this information is presented below for the highest vibration levels.

<u>AXIS</u>	<u>FREQUENCY</u>	<u>NOTES</u>
Vertical	530 to 650 cps	Slight vertical spot motion
Vertical	1000 cps	Slight vertical spot motion
Vertical	1600 to 1700 cps	Slight horizontal spot motion
Minor Horizontal	20 to 300 cps	Vertical spot motion peaked at 120 cps with a 5 inch travel
	350 to 700 cps	Diagonal spot motion peaked at 450 cps with a narrow ellipse, 3 inches in length
	700 to 1200 cps	Diagonal spot motion peaked at 900 cps with a 5 inch travel
	1800 cps	Vertical spot motion, 2 inches high
Major Horizontal	60 to 90 cps	Approximately one inch vertical spot motion
	300 to 450 cps	Approximately three inch horizontal spot motion at 375 cps
	1000 cps	Approximately one inch diagonal spot motion

5.0 CONCLUSIONS

5.1 The tests performed on the Limited Rotation Motor do not give complete assurance that the assembly will withstand 15 G rms white random vibration throughout the frequency range of 20 to 2000 cps. There is no conversion method that converts random test parameters to sine wave testing that will give a completely equal test by means of sine wave testing. In many cases, the conventional method of converting random parameters to sine parameters results in considerable over testing of the test specimen. In other cases, the sine testing will not indicate a failure whereas a random test will set up a condition within the test specimen that will cause failure.

5.2 The reduced vibration levels in the major horizontal axis were due to the relatively large size and weight of the slip plate and the relatively low force rating of the shaker system.

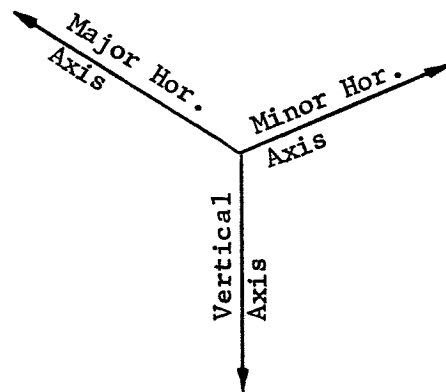
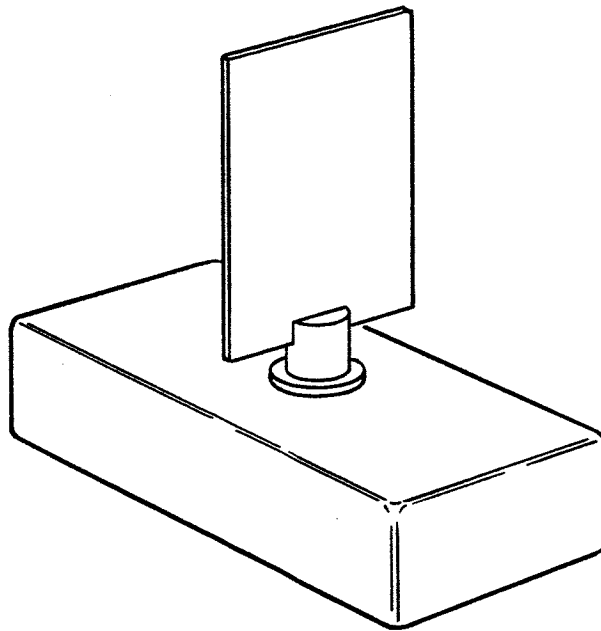


Figure 1. Test Specimen Orientation During Vibration

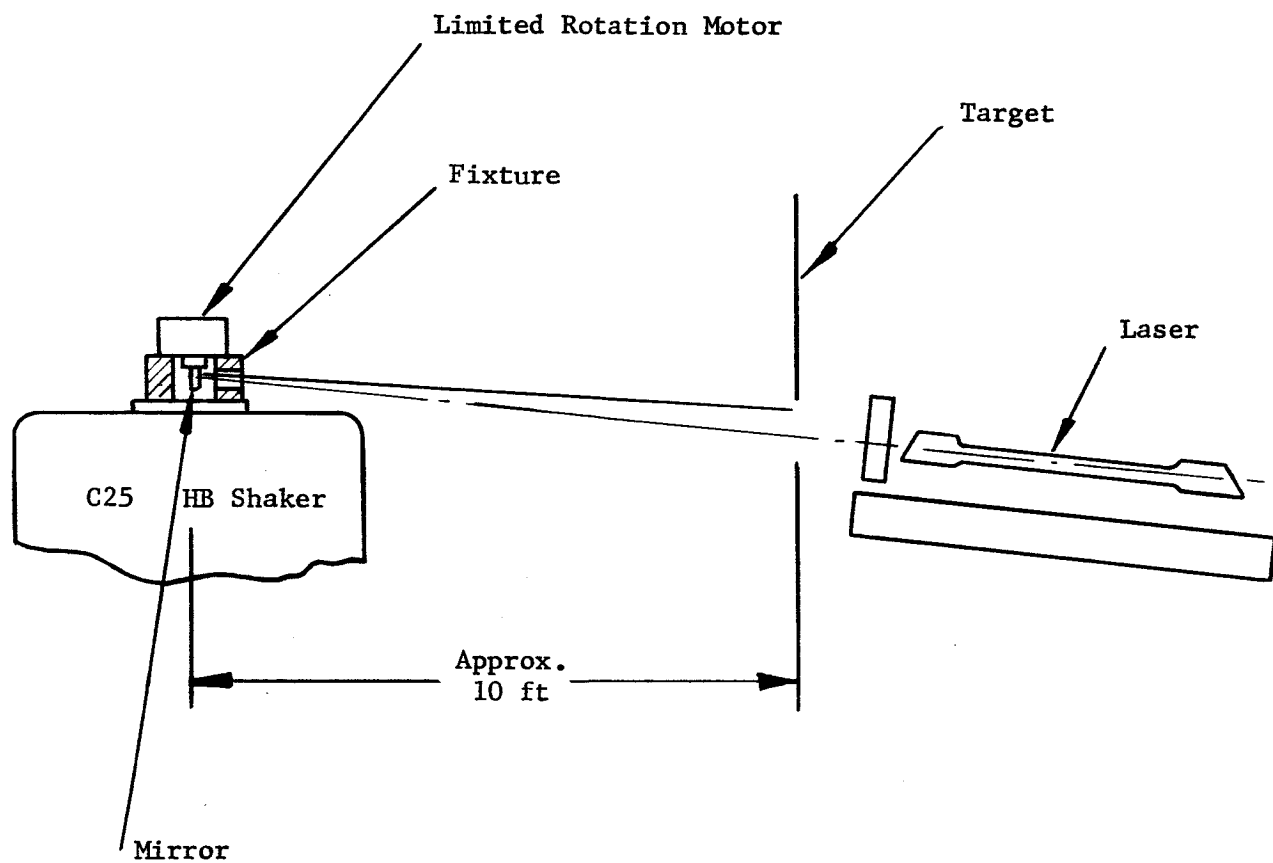


Figure 2. Shaft Alignment Checkout

APPENDIX E

TYPICAL FLIGHT QUALIFICATION

TEST PLAN

(Perkin-Elmer Engineering
Report No. 8260)

1. PURPOSE

1.1 This document defines typical recommended tests which could be performed on the Perkin-Elmer two-gas atmosphere sensor system. Successful completion of this type of test will qualify the system for use on Apollo type programs for use in the environmental control subsystem.

2. APPLICABLE DOCUMENTS

2.1 The following documents form a part of this test plan to the extent specified herein:

2.1.1 NASA Documents

CSD-A-061	Qualification Test Plan - Apollo CO ₂ Sensor
CSD-A-072	Qualification Test Procedure - Apollo CO ₂ Sensor
MSFC-SPEC 279	Electromagnetic Compatibility

2.1.2 North American Aviation Documents

MC999-0002B Electromagnetic Interference Control for
the Apollo Space System

2.1.3 Grumman Aircraft Engineering Corporation Documents

LSP-530-001-1 Electromagnetic Interference, General
Specification for

2.1.4 Standards

MIL-STD-810 Environmental Test Methods for Aerospace
and Ground Equipment

2.1.5 Perkin-Elmer Documents

Acceptance Test Plan - To be prepared at a later date.

2.2 Precedence: When the requirements of this document and those referenced herein are at variance, the requirements of this document shall govern.

3. REQUIREMENTS

3.1 Test Facilities and Equipment: Unless otherwise specified herein, the Perkin-Elmer Corporation or their subcontractors shall be responsible for providing the material, equipment, and facilities required for performing tests in accordance with this document.

3.2 Classification of Tests: The tests mentioned herein can be classified into the following categories.

- a. Performance Record Test
- b. Functional Test
- c. Environmental Tests
 - (1) Phase I - Design Proof
 - (2) Phase II - Overstress
 - (3) Phase III - Mission Life

3.2.1 Performance Record Test: The performance record tests are conducted to provide assurance that the product still performs in accordance with the procurement specification as verified during the acceptance tests. This test also provides reference data for comparison with test results during the qualification test program. Included in this test are a housing leak test, a power consumption measurement for input voltages between 20 and 32 VDC, and an instrument calibration under the following conditions:

- a. Input Voltage - 28 ± 1 VDC
- b. Pressure (external) - 30 ± 2 inches of Hg
- c. Temperature - $70 \pm 10^\circ\text{F}$
- d. Humidity - less than 90 percent
- e. Sample (Simulated Cabin Atmosphere)

Total Pressure	362 ± 11 mm Hg
O ₂ Partial Pressure	181 ± 5.5 mm Hg
N ₂ Partial Pressure	Diluent to Provide Total Pr.
CO ₂ Partial Pressure	< 7.6 mm Hg
H ₂ O Partial Pressure	5 to 16.5 mm Hg

The calibration curves obtained must be within two percent of that obtained during acceptance tests. All data will be recorded on a Performance Test Data Sheet similar to the sample form presented in Figure 1.

3.2.2 Functional Test: A functional test, consisting of a housing leak check and a single point calibration check, is performed both prior to and following selected environmental tests. This is to verify that the system sensor housing seals are still intact and that the sensor is still operating in accordance with the calibration curves obtained in the performance record test. All data will be recorded on a Functional Test Data Sheet similar to the sample form presented in Figure 2.

3.2.3 Environmental Tests

3.2.3.1 Phase I - Design Proof: These tests are used to demonstrate the strength characteristics of the sensor, and include climatic environments, electromagnetic interference, explosion proofing, prelaunch

environments, and sequentially applied maximum mission environments. The sequentially applied mission environments extend to the upper design limits on the sensor and are designed to verify the ability of the product to withstand the maximum environmental and performance stresses expected during a lunar mission. The detailed Phase I test requirements are described in Section 4.2 of this document, and are performed on two sensor systems.

3.2.3.2 Phase II - Overstress: The overstress tests are designed to determine failure modes and actual design margins and to provide data for additional confidence. The qualification of the sensor is not contingent on the satisfactory operation of the sensor during and following these tests, but only on the performance of these tests. The detailed Phase II test requirements are described in Section 4.3 of this document, and are performed on the two Phase I sensors after completion of the Phase I tests.

3.2.3.3 Phase III - Mission Life: The mission life test simulates the test and environments to which the sensor is subjected from initial ground checkout through re-entry and is designed to verify the operational life characteristics of the sensor under these conditions. The test consists of one ground operational cycle and two subsequent mission cycles at nominal levels. The qualification of the sensor is contingent on the satisfactory operation of the sensor after completion of the first mission cycle and the vibration temperature and acceleration tests on the second cycle. The detailed Phase III requirements are described in Section 4.4 of this document, and are performed on a single sensor system.

3.3 Condition of Test

3.3.1 Test Facilities: The tests herein described shall be performed at Perkin-Elmer or at laboratories that demonstrate competence to provide and maintain the required test conditions and have received facilities approval from the DOD, Perkin-Elmer, or NASA-LRC or their approved agent.

3.3.2 Test Equipment: The equipment used to perform the tests herein described shall have been approved by Perkin-Elmer and NASA prior to its use. A preliminary test equipment list is presented in Figure 4.

3.3.3 Calibration: All measurements shall be made with instruments whose accuracy has been verified. Accuracy shall be maintained by periodic calibration to acceptable standards. If doubt exists about the accuracy of an instrument, then verification may be requested.

3.3.4 Personnel: The tests herein specified shall be performed only by persons qualified by special training or technical ability.

3.3.5 Position During Test: Unless otherwise specified in the specific test procedure, the test specimen shall maintain its normal use attitude during the test.

3.3.6 Order of Test: The tests herein specified shall be conducted in the order presented in Section 4, of this specification. This sequence of testing may be changed by Perkin-Elmer with approval by NASA-LRC when necessary to expedite the testing program.

3.3.7 Tolerances: Unless otherwise specified, the maximum tolerances on test conditions shall be as specified in MIL-STD-810. The test durations specified in the detailed procedures are the minimum acceptable unless otherwise specified.

3.3.8 Environmental Test Records: A detailed test log will be maintained during the qualification test program. All environmental test data will be recorded on a form similar to the sample Environmental Test Data Sheet indicated in Figure 3.

3.4 Test Program Administration

3.4.1 Test Surveillance

3.4.1.1 Test Notification: NASA shall be notified no later than 48 hours before start of initial qualification testing.

3.4.1.2 Witnessing of Tests: All tests shall be witnessed by a Perkin-Elmer representative who will be responsible for the manner in which it is conducted and by an authorized Government representative, who may witness by surveillance. The signatures of these witnesses are required on all test report data sheets and shall constitute certification that the test data has been correctly reported. The tests may be witnessed by a representative of NASA-LRC, however, his signature is not required.

3.4.2 Deviations or Variations: Any deviations or variations from this document shall be approved by Perkin-Elmer and NASA. Approved changes shall be issued in the form of a change notice or revision to this plan.

3.4.3 Test Reports

3.4.3.1 Failure Reports: In the event that any malfunction is indicated during testing, the test may be stopped at the discretion of the Perkin-Elmer representative. Variations of operational and performance characteristics outside the limits of the procurement specification are reason to consider the equipment as having failed the test.

In the event of any malfunction or failure during the qualification test program, NASA-LRC shall be verbally notified within 24 hours after report of failure, followed by a written notification within one week. Both communications shall include the following information pertinent to the malfunction or failure:

- a. Part Number and Serial Number
- b. Total Operating Time on the Equipment
- c. Cause of Failure (if known)
- d. Environment Conditions
- e. Any other failures which have occurred on this equipment
- f. Any other conditions that are considered pertinent to the malfunction or failure
- g. Recommended plan of action

In addition, Perkin-Elmer shall conduct a failure analysis to determine the cause of failure and to recommend proper corrective action. Where the nature of the failure is readily apparent and the corrective action clearly indicated, then this action will be taken upon mutual agreement between Perkin-Elmer and NASA-LRC to avoid unnecessary delays in the test program. NASA will be notified of the status of any failure analysis action and a report will be sent to NASA within fifteen (15) days. A corrective action and close-out report shall be submitted to NASA-LRC within thirty (30) days.

3.3.2 Final Test Report: A final test report shall be issued for the qualification tests described herein. The report shall contain the results of all tests described in Section 4 of this document.

3.4 Test Procedure: The tests specified in this document shall be performed in accordance with Qualification Test Procedure which will be prepared by Perkin-Elmer during the design phase of the program.

4. QUALITY ASSURANCE PROVISIONS

4.1 General - The test program presented in Section 4 is patterned after the NASA-MSD documents referenced in paragraph 2.1.1 of this document which were generated for the Apollo CO₂ Sensor Program. These documents indicate a philosophy and establish preliminary environmental test limits that seem reasonable for this program. As additional flight profile data is made available by NASA-LRC to Perkin-Elmer for use on the Two-Gas Atmosphere Sensor System, the qualification test plan will be revised accordingly.

4.2 Phase I - Design Proof

4.2.1 Test Specimens: The Phase I tests shall be performed on Perkin-Elmer sensors which have satisfactorily passed the acceptance tests. The specimens shall be identified by part name, part number, and serial number.

4.2.2 Specific Tests

4.2.2.1 Performance Record Test: Prior to conducting the environmental tests, the performance record test of Paragraph 3.2.1 of this test plan shall be performed on each sensor system.

4.2.2.2 Oxidation: The test specimens shall be subjected to a four hour exposure to the following environment, both internal and external:

- a. Oxygen Content - 95 percent minimum
- b. Pressure - Room Ambient
- c. Temperature - $70 \pm 10^{\circ}\text{F}$

The sensors shall be purged continuously during this test with calibration gasses and the sensor outputs monitored to verify that the sensors are still functioning in accordance with the calibration curves obtained in Paragraph 4.2.2.1. At the conclusion of the test, the sensors shall be removed from the test chamber and the functional test of Paragraph 3.2.2 performed on each.

4.2.2.3 Temperature: The test specimens shall be subjected to a low and high ambient temperature condition. The time-temperature sequence shall be as follows:

<u>Test</u>	<u>Chamber Temperature</u>	<u>Exposure Time</u>
Nominal	75°F	15 minutes
Minimum	0°F	120 minutes
Nominal	75°F	15 minutes
Maximum	160°F	120 minutes
Nominal	75°F	15 minutes

The sensors shall be purged continuously during this test with calibration gasses and the sensor outputs monitored to verify that the sensors are still functioning in accordance with the requirements of the procurement specification and the calibration curves obtained in Paragraph 4.2.2.1. At the conclusion of this test, the sensors shall be removed from the test chamber and the functional test of Paragraph 3.2.2 performed on each.

4.2.2.4 Vibration: The test specimens shall be subjected to the following vibration environment imposed along each of three mutually perpendicular axes:

Random

5 to 85 cps - Constant at $0.069 \text{ g}^2/\text{cps}$

85 to 1000 cps - Linear increase (log by log plot)
from $0.069 \text{ g}^2/\text{cps}$ to $0.133 \text{ g}^2/\text{cps}$

1000 to 2000 cps - Linear decrease (log by log plot)
from 0.133 to $0.069 \text{ g}^2/\text{cps}$

Sinusoidal

5 to 16 cps - 0.23 inch D.A.

16 to 90 cps - 2.875 g

90 to 140 cps - 0.0069 inch D.A.

140 to 350 cps - 6.9 g

350 to 500 cps - 0.001 inch D.A.

500 to 2000 cps - 12.7 g

Test time per axis shall be 40 minutes random with a sweeping sinusoidal vibration super-imposed during the first five minutes. The sinusoidal cycling rate shall be 0.58 minute/octave. The sensors shall be purged continuously during this test with a calibration gas and the sensor outputs monitored. At the conclusion of the test, the sensors shall be removed from the test fixture and the functional test of Paragraph 3.2.2 performed on each.

4.2.2.5 Acceleration: The test specimens shall be subjected to an acceleration environment of 20 g imposed in two directions (+ and -) along each of three mutually perpendicular axes. The test time shall be five minutes for each direction of acceleration in each axis. The sensors shall be purged continuously during this test with a calibration gas and the sensor outputs monitored. At the conclusion of the test, the sensors shall be removed from the test fixture and the functional test of Paragraph 3.2.2 performed on each.

4.2.2.6 Acoustic Noise: The test specimen shall be subjected to the following sound pressure levels (REF 0.0002 dynes/cm²):

<u>Octave Band Frequency cps</u>	<u>Condition A db Level (minimum)</u>	<u>Condition B db Level (minimum)</u>
37.5 - 75	133	134
75 - 150	131	134
150 - 300	127	131
300 - 600	122	129
600 - 1200	116	130
1200 - 2400	109	129
2400 - 4800	101	126
4800 - 9600	95	122
Overall	136 +10, -0	141 +10, -0

The sensor shall be exposed to Condition A for five minutes and to Condition B for five minutes. The sensor shall be purged continuously with calibration gasses during this test and the sensor outputs monitored. At the conclusion of the test, the sensor shall be removed from the acoustic chamber and the functional tests of Paragraph 3.2.2 performed on each.

4.2.2.7 Ignition Proof: The test specimen shall be subjected to the explosion tests of MIL-STD-810, Method 511, Procedure I. The functional test of Paragraph 3.2.2 is not required following this ignition proof test.

4.2.2.8 Electromagnetic Interference: The test specimen shall be tested in accordance with Specification MC999-0002B except as follows:

a. Circuit Classification - "H" Analog: Those circuits in the DC and AF range whose function is to transmit data from source to load by gradual voltage change.

b. Figure 13 of MC999-0002B shall be modified as shown in Figure 5 of this test plan.

c. Magnetic Field Susceptibility: Shall be in accordance with Paragraph 4.2.1.10 of MSFC - SPEC 279.

d. RF, Induced, Cases, and Cables: Shall be in accordance with Paragraph 3.4.5 of Specification LSP-530-001 with Amendment 1.

e. A minimum DC isolation of one megohm shall exist between the DC power input and all signal circuits and grounds.

The functional test of Paragraph 3.2.2 is not required following this EMI test.

4.2.2.9 Sand and Dust: The test specimen shall be subjected to the sand and dust test of MIL-STD-810 with the following exceptions:

a. The sensor shall be operated during this test. The sensor shall be purged continuously with a calibration gas during this test and the sensor outputs monitored to verify that the sensor is still functioning in accordance with the requirements of the procurement specification and the calibration curves obtained in Paragraph 4.2.2.1.

b. The functional test of Paragraph 3.2.2 of this test plan shall be performed on each sensor at the conclusion of this test in lieu of the test of Paragraph 3.2.1 of MIL-STD-810.

4.2.10 Shock: The operating test specimen shall be subjected to three shock pulses in two directions (+ and -) along each of three mutually perpendicular axes for a total of 18 tests. The shock input shall be a 15 g sawtooth pulse with an 11 plus or minus 1 millisecond rise time and a 1 plus or

minus 1 millisecond decay time. At the conclusion of this test, the sensor shall be removed from the test fixture and the functional test of Paragraph 3.2.2 performed on each.

4.2.11 Corrosive Contaminants-Oxygen-Humidity: The test specimens shall be subjected to a combination corrosive contaminants-oxygen-humidity test as follows:

a. Perform a salt fog test per MIL-STD-810, Method 509, with the following exceptions:

- (1) Salt solution shall be one percent by weight
- (2) Intermittent salt spray shall be cycled for 48 hours as follows:

Spray on - 10 hours

Spray off - 9 hours

Spray on - 10 hours

Spray off - 9 hours

Spray on - 10 hours

(3) The sensor shall be operated during this test. The sensor shall be purged continuously with a calibration gas during the test and the sensor outputs monitored to verify that the sensor is still functioning in accordance with the requirements of the procurement specification and the calibration curves obtained in Paragraph 4.2.2.1.

(4) Upon completion of the salt spray test, while the sensor is still in the chamber, the functional test of Paragraph 3.2.2 shall be performed on each. Visual examination shall be performed after removal from the test chamber.

(5) No attempt to clean the sensors during or after the test shall be made.

b. Within one hour after completion of the salt spray test, the test article shall be transferred to an oxygen-humidity-altitude chamber and the chamber filled with commercial oxygen (95 plus or minus 5 percent) to a pressure of 5 psia. These conditions shall be maintained for 50 hours. The sensors shall be purged continuously with a calibration gas during the test and the sensor outputs monitored to verify that the sensors are still operating in accordance with the requirements of the procurement specification and the calibration curves obtained in Paragraph 4.2.2.1.

c. The oxygen environment shall be maintained at 5 psia and sufficient moisture introduced to obtain a relative humidity of 95 plus or minus

5 percent with distilled water having a pH factor of 6.5 to 7.5. The chamber pressure shall be cycled (relative humidity shall be maintained at 95 plus or minus 5 percent) as follows:

5 psia to 3 psia - 1 hour maximum
3 psia - 23 hours minimum
3 psia to 7 psia - 1 hour maximum
7 psia - 23 hours minimum
7 psia to 3 psia - 1 hour maximum
3 psia - 23 hours minimum
3 psia to 7 psia - 1 hour maximum
7 psia - 23 hours minimum
7 psia to 3 psia - 1 hour maximum
3 psia - 23 hours minimum
3 psia to 7 psia - 1 hour maximum
7 psia - 23 hours minimum
7 psia to 3 psia - 1 hour maximum
3 psia - 23 hours minimum
3 psia to 7 psia - 1 hour maximum
7 psia - 23 hours minimum
7 psia to 3 psia - 1 hour maximum
3 psia - 23 hours minimum
3 psia to 5 psia - 1 hour maximum
5 psia - 23 hours minimum

The sensor shall be operated intermittently (12 hours off and 12 hours on) for the 240 hour test duration. The sensor shall be purged (during operation only) with calibration gases and the sensor outputs monitored to verify that the sensors are still operating in accordance with the requirements of the procurement specification and the calibration curves obtained in Paragraph 4.2.2.1. At the conclusion of the test, the sensor shall be removed from the test chamber and any deterioration or corrosion shall be determined by visual inspection. The Performance Record Test of Paragraph 3.2.1 shall then be performed on the sensor. This test data shall be compared with the previous performance record test as criteria for determining performance degradation.

4.3 Phase II - Overstress

4.3.1 Test Specimens: The Phase II tests shall be performed on Perkin-Elmer sensors which have satisfactorily passed the design proof tests

described in Section 4.2 of this test plan. The specimens shall be identified by part name, part number, and serial number. If, at any time during the test, a malfunction is indicated, the test shall be stopped and the failure reported in accordance with Paragraph 3.4.3.1. The time to failure shall be noted. Further testing shall not be required.

4.3.2 Specific Tests

4.3.2.1 Vibration: The test specimen shall be subjected to the vibration test of Paragraph 4.2.2.4 of this test plan with the following exceptions:

a. The vibration levels specified in Paragraph 4.2.2.4 shall be multiplied by a factor of 1.25.

b. At the conclusion of the vibration test, the Performance Record Test of Paragraph 3.2.1 shall be performed in lieu of the functional test of Paragraph 3.2.2.

c. After completion of b. above, the sensor shall be subjected to a vibration test at 1.5 times the levels of Paragraph 4.2.2.4. The Performance Record Test shall be repeated.

4.3.2.2 Acceleration: The test specimen shall be subjected to the acceleration test of Paragraph 4.2.2.5 of this test plan with the following exceptions:

a. The acceleration level shall be 25 g.

b. At the conclusion of the acceleration test, the Performance Record Test of Paragraph 3.2.1 shall be performed in lieu of the functional test of Paragraph 3.2.2.

4.3.2.3 Temperature: The test specimens shall be subjected to the temperature test of Paragraph 4.2.2.3 of this test plan with the following exceptions:

a. The time-temperature sequence shall be as follows:

<u>Test</u>	<u>Chamber Temperature</u>	<u>Exposure Time</u>
Nominal	75°F	15 minutes
Minimum	0°F	120 minutes
Nominal	75°F	15 minutes
Maximum	160°F	120 minutes
Nominal	75°F	15 minutes
Minimum	-20°F	120 minutes

<u>Test</u>	<u>Chamber Temperature</u>	<u>Exposure Time</u>
Nominal	75°F	15 minutes
Maximum	170°F	120 minutes
Nominal	75°F	15 minutes

b. At the conclusion of the time-temperature sequence, the Performance Record Test of Paragraph 3.2.1 shall be performed in lieu of the functional test of Paragraph 3.2.2.

4.4 Phase III - Mission Life

4.4.1 Test Specimen: The Phase III tests shall be performed on a Perkin-Elmer sensor which has satisfactorily passed the acceptance tests. The specimen shall be identified by part name, part number, and serial number.

4.4.2 Specific Tests

4.2.2.1 Cycle 1

4.4.2.1.1 Performance Record Test: Prior to conducting the environmental tests, the Performance Record Test of Paragraph 3.2.1 of this test plan shall be performed on test specimen.

4.4.2.1.2 Vibration-Temperature: The test specimen shall be subjected to the combined vibration-temperature shown in Figures 6 and 7. The sensor shall be purged continuously during this test with a calibration gas and the sensor outputs monitored. All indications of unusual or erratic operation during the vibration-temperature test shall be recorded.

4.4.2.1.3 Acceleration-Temperature: The test specimen shall be subjected to the combined acceleration-temperature environment shown in Figure 8. Acceleration shall be imposed in both the positive and negative direction along the sensor X-axis (see Figure 9) for five minutes. The sensor shall be purged continuously during this test with a calibration gas and the sensor outputs monitored. All indications of unusual or erratic operation observed during the acceleration-temperature test shall be recorded.

4.4.2.1.4 Temperature-Altitude: The test specimen shall be subjected to a combination temperature-altitude environment. The test chamber atmosphere shall be maintained at 95 plus or minus 5 percent oxygen. Unless otherwise specified, the sensor shall be operated and purged continuously with a calibration gas and the sensor output monitored to verify that it is still operating in accordance with the requirements of the procurement specification and the calibration curves obtained in Paragraph 4.4.2.1.1. The total duration shall be 500 hours in accordance with the following schedule:

<u>Pressure</u>	<u>Temperature</u>	<u>Time</u>
5 psia	Cycle 150° to 75° to 0° to 75° to 150°F each 3.25 hours with 30 minutes transition and 15 minutes steady state. Last tempera- ture to be 75°F.	200 hours

NOTE: The 200 hours may be decreased by that time previously accumulated in vibration-temperature and acceleration-temperature tests.

1 x 10 ⁻⁴ mm Hg	0°F	48 hours
	160°F	48 hours

NOTE: The sensor shall be nonoperated during this test and shall be both internally and externally exposed to the environments specified.

1 x 10 ⁻⁴ mm Hg	Cycle 0° to 150° to 0°F each 8 hours. Last temperature to be 0°F.	24 hours
5 psia	Cycle 0° to 60° to 0°F each 24 hours. Last temperature to be 60°F.	180 hours
Increase from 60°	Increase from 5 to 14.7 psia	.38 hour

4.4.2.1.5 Shock: Perform the shock test of Paragraph 4.2.10 on the test specimen.

4.4.2.2 Cycle II: The second mission cycle shall be the same as the first cycle with the exception that the shock input shall be a 78 g half sine pulse with an 11 plus or minus 1 millisecond width. The sensor shall not become or cause a secondary projective during this test. Operation of the sensor at the conclusion of the second cycle is not required.

Part Number _____ S/N _____
Date _____ Barometer _____ in Hg Abs. Amb. Temp. _____°F
Tested by _____ Test Facility _____

Visual Examination: Accept _____ Reject _____

Remarks: _____

Leakage Test:

Required: 5×10^{-4} cc/sec. max.

Actual: _____ cc/sec.

Accept _____ Reject _____

Power Consumption:

Required: 1.0 watt max. from 20 to 28 VDC

1.3 watt max. above 28 VDC

Actual:

Voltage x Current = Power

20 volts x _____ amps = _____ watts

22 volts x _____ amps = _____ watts

24 volts x _____ amps = _____ watts

26 volts x _____ amps = _____ watts

28 volts x _____ amps = _____ watts

30 volts x _____ amps = _____ watts

32 volts x _____ amps = _____ watts

Accept _____ Reject _____

Calibration:

Remarks: _____

Operating Time _____

Test Specimen Status: Accept _____ Reject _____

By _____

Inspection: _____

Perkin-Elmer Q.C.

USAF Q.C.

Figure 1. Performance Record Test Data Sheet

Figure 2. Functional Test Data Sheet

Test _____

Part Number _____ S/N _____

Date _____ Barometer _____ in Hg Abs. Amb. Temp. _____ °F

Tested by _____ Facility _____

Test Signal: _____ VDC

Remarks _____

Operating Time _____

Functional or Performance Record Test Data Sheet _____

Test Specimen Status: Accept _____ Reject _____

By _____

Inspection: _____

Perkin-Elmer Q.C. _____ USAF Q.C. _____

Figure 3. Environmental Test Data Sheet

TESTS	CHAMBERS			MAJOR EQUIP.			INSTRUMENTATION AND MISCELLANEOUS																	FIXTURES									
	Acoustical Noise	Explosion	Temperature-Altitude	Humidity	Electromagnetic Interference	Salt Fog	Plastic Container	Vibrator	Centrifuge	Shock Tester	Mass Spectrometer Leak Detector	Accelerometers	DC Voltmeter	Recorder	DC Ammeter	AC Voltmeter	Audio Power Amp.	Pressure Regulator	Pressure Gauge	Thermocouples	Oscilloscope	Camera	Microscope	Dummy Sensor	System Simulator	28 Volt Power Supply	Gas Mixtures	Small Tools	Miscellaneous Valves	Vibration	Shock	Acceleration	NOTES
1. Performance Record																																	
2. Functional																																	
3. Oxidation																																	
4. Temperature																																	
5. Vibration																																	
6. Acceleration																																	
7. Acoustical Noise																																	
8. Ignition Proof																																	
9. Electromagnetic Interference																																	
10. Sand and Dust																																	
11. Shock																																	
12. Salt Fog																																	
13. Oxygen-Humidity																																	
14. Vibration-Temperature																																	
15. Acceleration-Temperature																																	
16. Temperature-Altitude																																	

Figure 4. Preliminary Equipment List

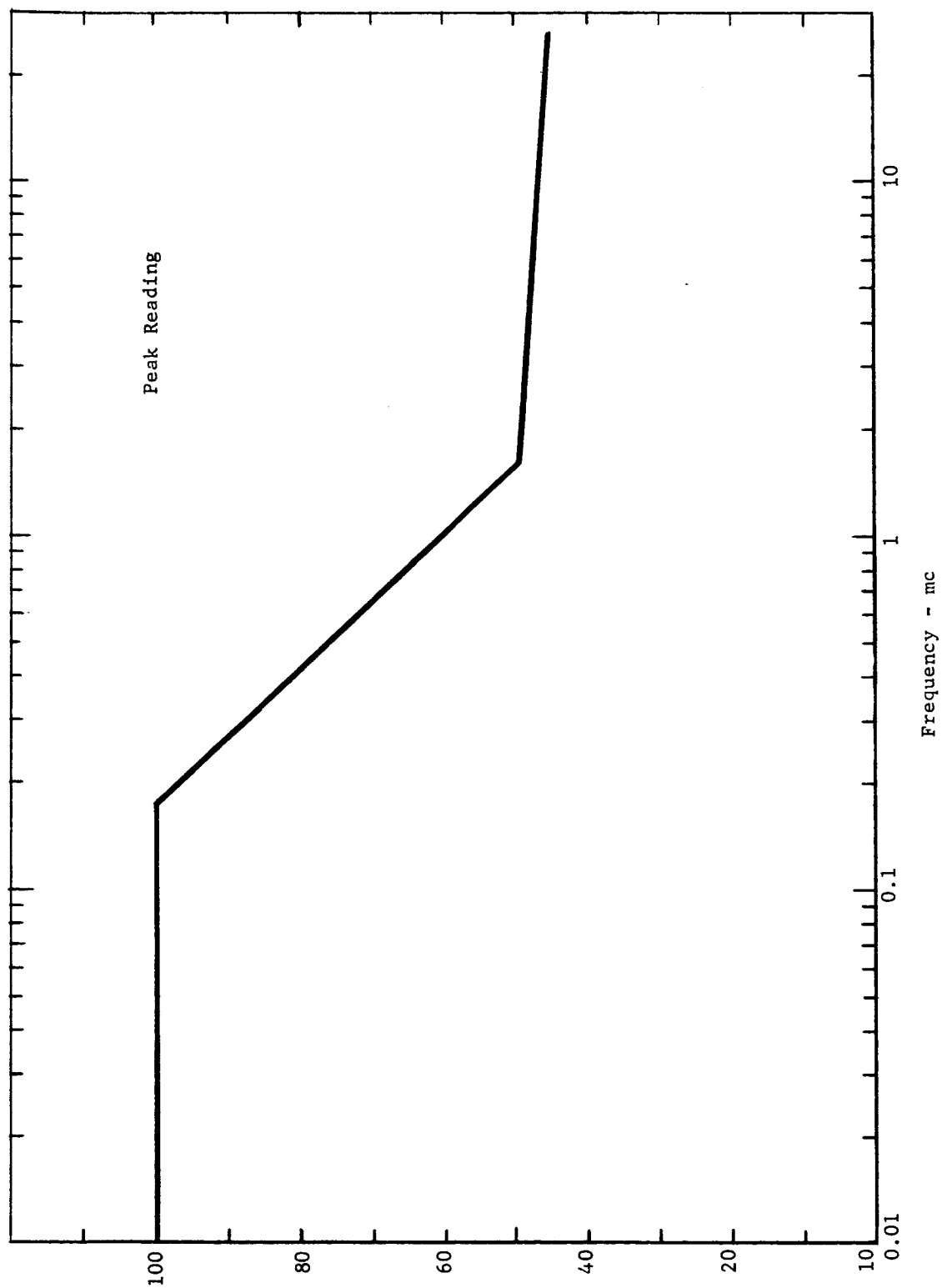


Figure 5. Modified EM1 Limits

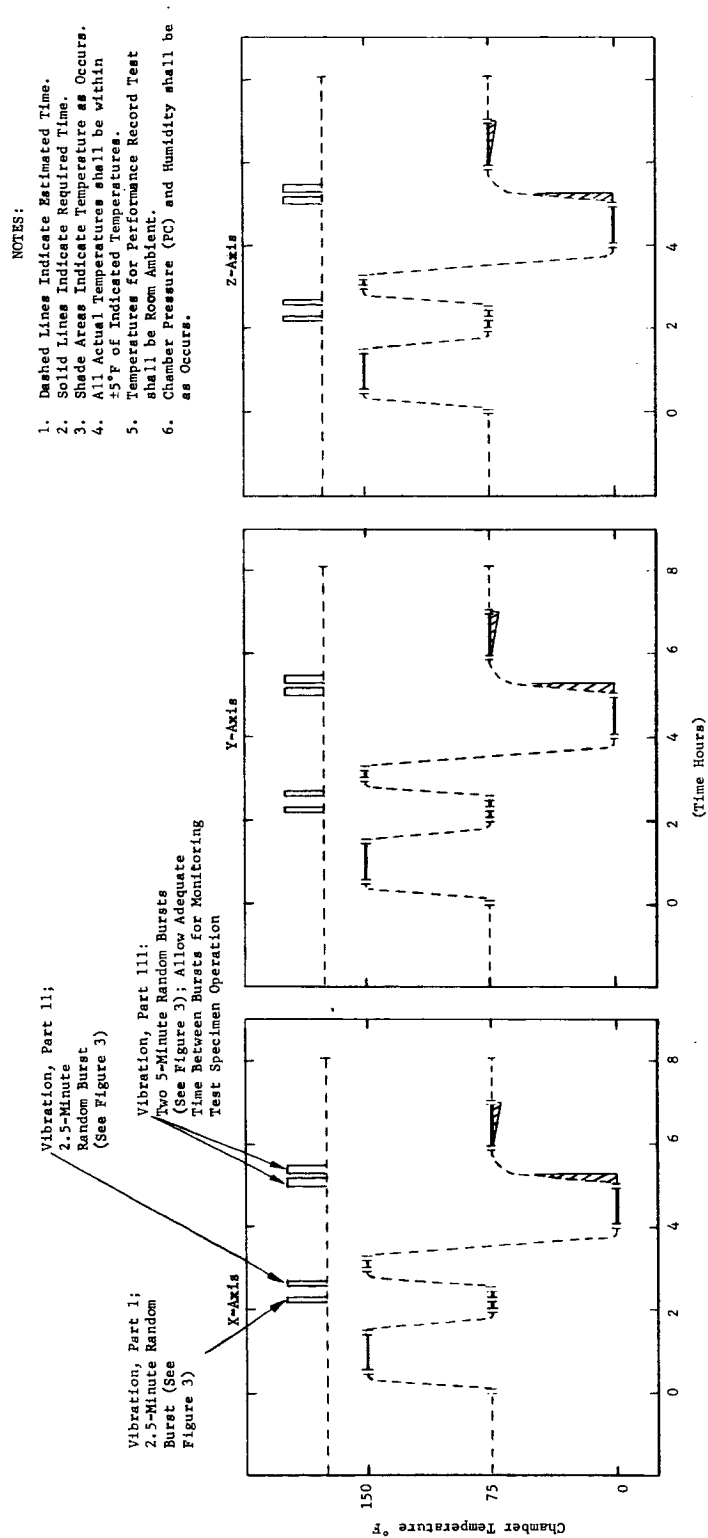
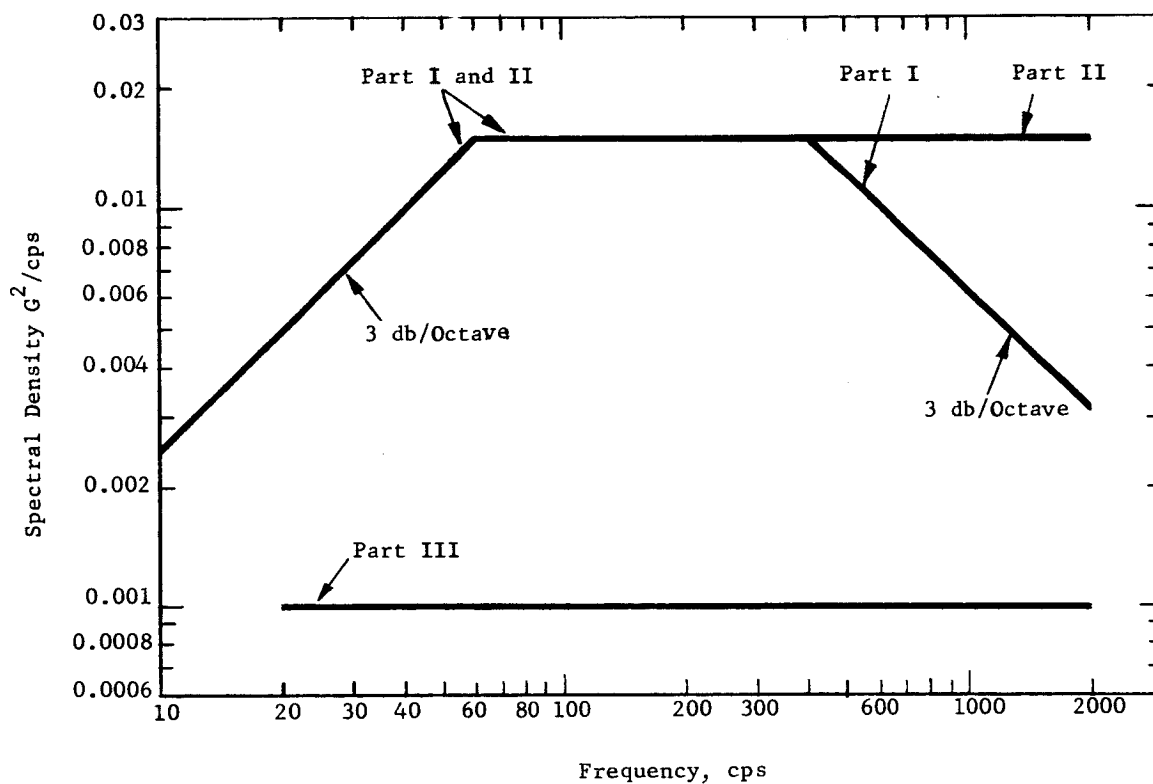
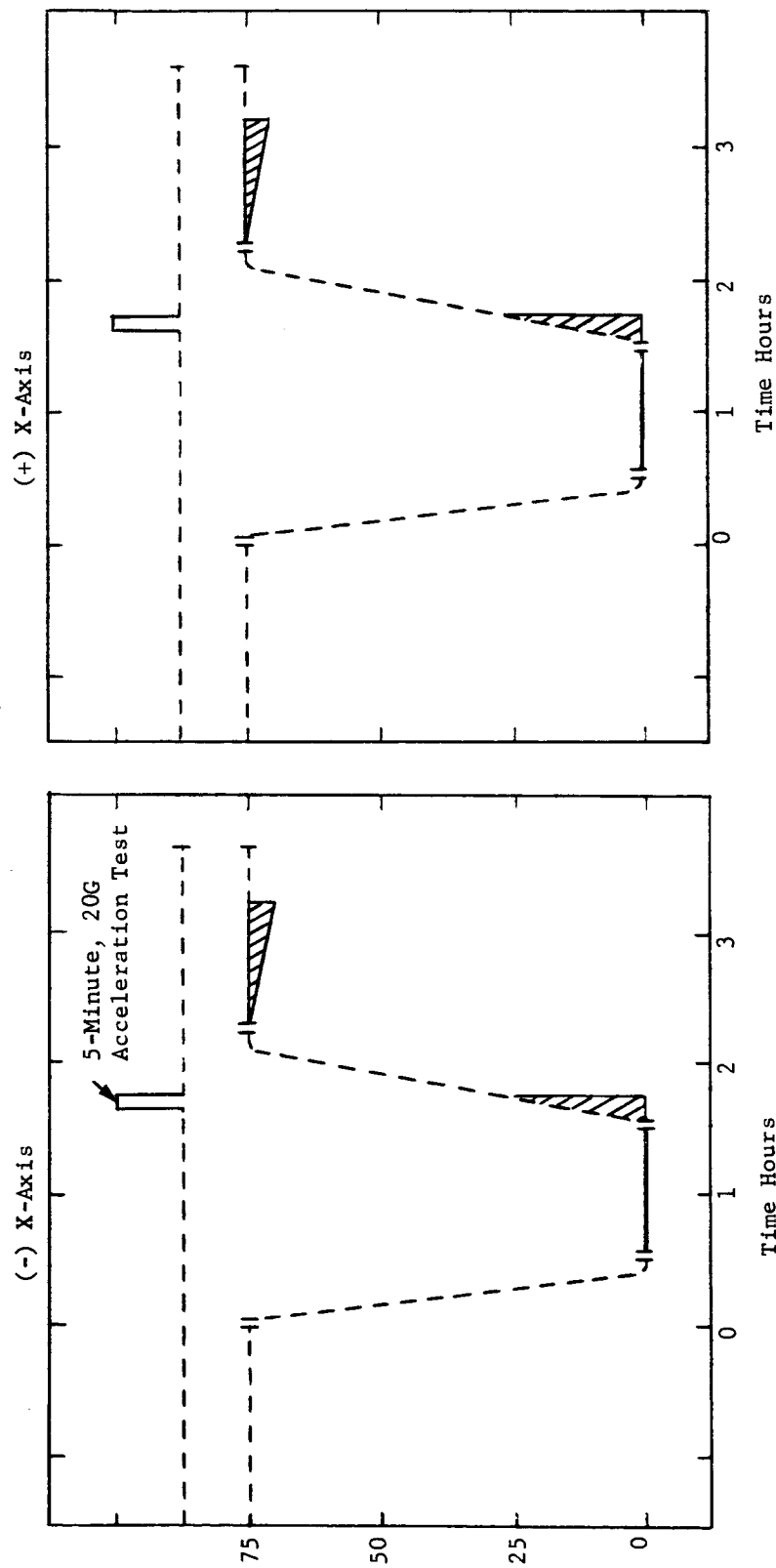


Figure 6. Vibration-Temperature Profile



- Part I 2.5 Minutes Duration; Chamber Temperature-Equal to Laboratory Ambient Temperature (Chamber Door Open)
- Part II 2.5 Minutes Duration; Conduct Vibration During 75°F to 150°F Chamber Temperature Change Shown in Figure 2.
- Part III Two 5-Minute Bursts with Time Between to Monitor Specimen Performance: $0 \pm 5^\circ\text{F}$ Chamber Temperature per Figure 2.

Figure 7. Spectral Density vs. Frequency



Notes:

1. Dashed Lines Indicate Estimated Time.
2. Solid Lines Indicate Required Time
3. Shaded Areas Indicate Temperature as Occurs.
4. All Actual Temperatures Shall be Within $\pm 5^{\circ}\text{F}$ of Indicated Temperatures.
5. Temperatures for Performance Record Test shall be Room Ambient.
6. Chamber Pressure and Humidity Shall be as Occurs.

Figure 8. Acceleration Temperature Profile

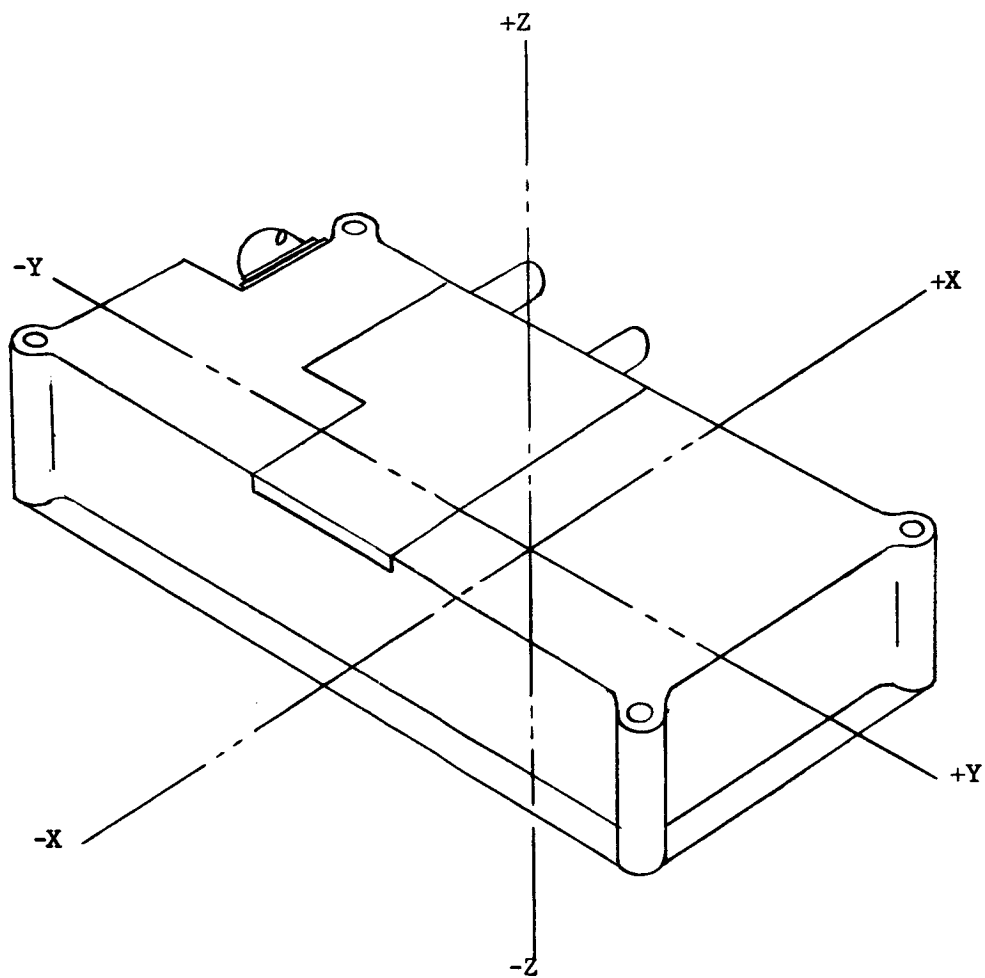


Figure 9. Sensor Axis Designation

REFERENCES

¹North, B.F.; Drake, G.L.; Krause, D.; and Armstrong, R.C.: Life Support System for Space Flights of Extended Time Periods. NASA Report No. 64-26234.

²David, H.M., "LEM, System Readied for Checkout," Missiles and Rockets, May 3, 1965, pp. 22-23.

BIBLIOGRAPHY

TWO-GAS ATMOSPHERE SENSOR SYSTEM PROGRAM

Introduction

This bibliography of papers concerned with the development of a Two-Gas Sensor System has been compiled as a report of useful papers that have been reviewed during this program. In all cases, the original article was consulted for content and references. Considerable latitude of judgment has been exercised by the author in decisions of inclusion or exclusion and in indexing.

List of CODEN for Journals

"CODEN" is a system of designating journals by a combination of four letters. It was developed by Dr. Charles Bishop of the Chronic Disease Research Institute, Buffalo, New York, and described in an article in "American Documentation," Volume 4, 54 (1953). In 1957, CODEN was adopted by the Standard Data Subcommittee of Committee E-13 (Absorption Spectroscopy) of the American Society for Testing Materials, for use in its activities in searching the literature for infrared and ultraviolet spectra.

The CODEN used in this bibliography is as follows:

<u>CODEN</u>	<u>JOURNAL</u>
APOP	Applied Optics
ASTM	American Society for Testing Materials, Technical Papers
CJPH	Canadian Journal of Physics
DFAS	Discussions of the Faraday Society
JCPS	Journal of Chemical Physics
JJAP	Japanese Journal of Applied Physics
JMOS	Journal of Molecular Spectroscopy
JOSA	Journal of the Optical Society of America
JQSR	Journal of Quant. Spectrosc. Radiat. Transfer., Great Britain
OPSP	Optics and Spectroscopy
PHRV	Physical Review
RMPH	Reviews of Modern Physics
RSIN	Review of Scientific Instruments
SPAC	Spectrochimica Acta
TISA	Transactions, Instrument Society of America

<u>No.</u>	<u>Author</u>	<u>Subject Title</u>	<u>Coden</u>	<u>Vol.</u>	<u>Page</u>	<u>Year</u>
1	SCHROEDER, D.J.	Interference Transmission Filters for the Far Ultraviolet	JOSA	52	1380	1962
2	OPTICAL COATING LAB., INC., Santa Rosa, Cal.	Ultraviolet Narrow Bandpass Filters	Capability Rpt.-Sept.			1963
3	CHILDS, C.B.	Broad-Band Ultraviolet Filters	JOSA	51	895	1961
4	WOLFF, C.M., PERTEL, R.	Optical Transmittance Filter for Hg 1849Å Radiation		54	1168	1964
5	HASS, G., ROUSEY, R.	Reflecting Coatings for the Extreme Ultraviolet	JOSA	49	593	1959
6	BERNING, HASS, MADDEN	Reflectance-Increasing Coatings for the Vacuum Ultraviolet and Their Applications	JOSA	50	586	1960
7	ZELIKOFF, WATANABE, & INN	Absorption Coefficients of Gases in the Vacuum Ultraviolet. Part II - Nitrous Oxide	JCPS	21	1643	1953
8	THE PERKIN-ELMER CORP. Electro-Optical Div.	. . . Part III. CO ₂ Infrared Spectra and Detectability Estimates for Contaminant Cases in Closed Breathing Atmospheres	JCPS	21	1648	1953
9	WATANABE, K.	Photoionization and Total Absorption Cross Section of Gases. I. Ionization Potentials of Several Molecules. Cross Sections of NH ₃ and NO	JCPS	22	1564	1954
10	METZGER, P.H. and COOK, G.R.	A Reinvestigation of the Absorption Cross-Sections of Molecular Oxygen in the 1050-1800Å Region	JQSR	4	107	1964
11	KNAUSS, H.P. and BALLARD, S.S.	Rotational Structure of the Schumann-Runge Bands of Oxygen in the Vacuum Region	PHRV	48	796	1935

<u>No.</u>	<u>Author</u>	<u>Subject Title</u>	<u>Coden</u>	<u>Vol.</u>	<u>Page</u>	<u>Year</u>
12	BRIN, P., HERZBERG, G.	Fine Structure of the Schumann-Runga Bands Near the Convergence Limit and the Dissociation Energy of the Oxygen Molecule	CJPH	32	110	1954
13	TANAKA, INN, WATANABE	Absorption Coefficients of Gases in the Vacuum Ultraviolet. Part IV - Ozone	JCPS	21	1651	1953
14	TANAKA, Y., INN, E.C.Y.	Absorption Coefficient of Ozone in the Ultraviolet and Visible Regions	JOSA	43	870	1953
15	OGAWA, M., COOK, G.R.	Absorption Coefficients of O ₃ in the Vacuum Ultraviolet Region	JCPS	28	173	1958
16	ASTM	Tentative Method of Test for Accelerated Ozone Cracking of Vulcanized Rubber	ASTM	28	579	1964
17	MAST, G., and SAUNDERS, H.E.	Research and Development of the Instrumentation of Ozone Sensing	TISA	1	325	1962
18	MAST DEVELOPMENT CO. Davenport, Iowa	Portable Ozone Recorder Battery Operated Ozone Recorder				
19	WILKINSON, P.G. and JOHNSTON, H.L.	The Absorption Spectra of Methane, Carbon Dioxide, Water Vapor, and Ethylene in the Vacuum Ultraviolet	JCPS	18	190	1950
20	HARRISON, CEDERHOLM, COFFIN	The Ultraviolet Absorption Spectra of Water, Ethyl Alcohol, Diethyl Ether and Methyl Alcohol	Final Report, Dept. Chem., Mt. Holyoke Coll. Oct'49-51			
21	WATANABE, K., and ZELIKOFF, M.	Absorption Coefficients of Water Vapor in the Vacuum Ultraviolet	JOSA	43	753	1953
22	SASAKI, T. and ISHIGURO, K.	A Spectrophotometer for Determining Optical Constants in the Vacuum Ultraviolet Region	JJAP	2	289	1963

<u>No.</u>	<u>Author</u>	<u>Subject Title</u>	<u>Coden</u>	<u>Vol.</u>	<u>Page</u>	<u>Year</u>
23	PODGAETSKII, V.M. and CHERNETS, A.N.	Spectrophotometric Study of the Distribution of Radiant Energy in IFK-2000 and IFK-20,000 Flash Lamps	OPSP		226	
24	RENDINA, J.F.	All-Metal Vacuum Ultraviolet Lamp	RSIN	34	813	1963
25	FAY, H.	U.S. Patent Office: Silent Electric Discharge Light Source				1960
26	Mine Safety Appliances Company; Pennsylvania	M-S-A Spectroanalyzer Specifications				
27	WILKINSON, P.G. and ANDREW, K.L.	Proposed Standard Wavelengths in the Vacuum Ultraviolet. Spectra of Ge, Ne, C, Hg, and N	JOSA	53	710	1963
28	BAIRD, SMITH, HART	Vacuum Wavelengths of Kr ⁸⁶ , Hg ¹⁹⁸ , and Cd ¹¹⁴	JOSA	53	717	1963
29	HUFFMAN, TANAKA, and LARRABEE	Helium Continuum Light Source for Photoelectric Scanning in the 600- 1100Å Region	APOP	2	617	1963
30	RENDINA, J.F.	All-Metal Vacuum Ultraviolet Lamp	JOSA		813	1963
31	TANAKA, Y. and ZELIKOFF, M.	Continuous Emission Spectrum of Xenon in the Vacuum Ultraviolet Region		44	254	1954
32	TANAKA, Y.	Continuous Emission Spectra of Rare Gases in the Vacuum Ultraviolet Region	JOSA	45	710	1955
33	TANAKA, Y., JURSA, A., LEBLANC, F.	Continuous Emission Spectra of Rare Gases in the Vacuum Ultraviolet Region. II. Neon and Helium	JOSA	48	304	1958
34	Linde Company, Div. Union Carbide Corp.	Rare Gases	Company Publication			
35	WILKINSON, P.G., and TANAKA, Y.	New Xenon-Light Source for the Vacuum Ultraviolet	JOSA	45	344	1955

<u>No.</u>	<u>Author</u>	<u>Subject Title</u>	<u>Coden</u>	<u>Vol.</u>	<u>Page</u>	<u>Year</u>
36	COOK, G., METZGER, P.H.	Photoionization and Absorption Cross Sections of H ₂ and D ₂ in the Vacuum Ultraviolet Region	JOSA	54	968	1964
37	SCOULER, W.J., MILLS, E.	Current Regulator for Ultraviolet Light Source	RSIN	35	489	1964
38	KAYE, Wilbur	Emission Spectra of Argon, Helium, Krypton, Neon and Xenon PEN-RAY Lamps	Ultra-Violet Products, Inc. Company Publication			
39	CHILDS, C.B.	Low-Pressure Mercury Arc for Ultraviolet Calibration	APOP	1	711	1962
40	D'ALESSIO, LUDWIG and BURTON	Ultraviolet Lamp for the Generation of Intense, Constant-Shape Pulses in the Subnanosecond Region	RSIN	35	1015	1964
41	MARSHAK, I.S.	Limiting Parameters and Generalized Characteristics of Xenon Lamps	APOP	2	793	1963
42	EDGERTON, H.E.	Electronic Flash Illumination of a Large Wilson Cloud Chamber	APOP	2	1013	1963
43	DUNKELMAN, FLOWLER, and HENNES	Spectrally Selective Photodetectors for the Middle and Vacuum Ultraviolet	APOP	1	695	1962
44	ROBINSON, M. and RUMPEL, W.F.	Fluorescent-Type Ultraviolet Radiation Detector	RSIN	34	794	1963
45	LINCKE, R., and WILKERSON, T.D.	New Detector for the Vacuum Ultraviolet	RSIN	33	911	1962
46	KNAPP, R.A.	A Simple Method for Preparing Layers of Sodium Salicylate	APOP	2	1334	1963
47	DUNKELMAN, L.	Ultraviolet Photodetectors	JQSR	2	533	
48	LICHT, S.	B & L 505 Spectrophotometer Modifications for Measuring Spectral Response of Photodetectors	RSIN	35	1027	1964

<u>No.</u>	<u>Author</u>	<u>Subject Title</u>	<u>Coden</u>	<u>Vol.</u>	<u>Page</u>	<u>Year</u>
49	SMITH, R. and DUTTON, D.	Behavior of Lead Sulfide Photocells in the Ultraviolet	JOSA	48	1007	1958
50	WOODS, J.F.	Investigation of the Photoconductive Effect in Lead Sulfide Films Using Hall and Resistivity Measurements	PHRV	106	235	1957
51	LUMMIS, F. and PETRITZ, R.	Noise, Time-Constant, and Hall Studies on Lead Sulfide Photoconductive Films	PHRV	105	502	1957
52	SPENCER, H.E.	Quantum Efficiency of Photoconductive Lead Sulfide Films	PHRV	109	1074	1958
53	ROSE, A.	An Outline of Some Photoconductive Processes	RCA Review	362	1951	1951
54	GOODRICH, G. and WILEY, W.	Resistance Strip Magnetic Electron Multiplier	RSIN	32	846	1961
55	GOODRICH, G. and WILEY, W.	Experiments with the Bendix Continu- ous-Channel Multiplier	Image Intensifier Symposium	211	1961	1961
56	ANGEL, COOPER, HUNTER & TOUSEY	Extreme Ultraviolet Detection with the Bendix Single-Channel Photo- multiplier	Image Intensifier Symposium	215	1961	1961
57	CHUBB, T. and FRIEDMAN, H.	Photon Counters for the Far Ultra- violet	RSIN	26	493	1955
58	STOBER, SCOLNIK & HENNES	A Vacuum Ultraviolet Photoionization Detector	APOP	2	735	1963
59	SPONER, H. and TELLER, E.	Electronic Spectra of Polyatomic Molecules	RMPH	13	75	1941
60	WILKINSON, P.G.	Molecular Spectra in the Vacuum Ultraviolet	JMOS	6	1	1961
61	INN, E.C.Y.	Vacuum Ultraviolet Spectroscopy	Sp.A.	7	65	1955
62	HAUGEN, G.R. and MARCUS, R.J.	A Spectrofluorophosphorimeter	APOP	3	1049	1964

<u>No.</u>	<u>Author</u>	<u>Subject Title</u>	<u>Coden</u>	<u>Vol.</u>	<u>Page</u>	<u>Year</u>
63	KRISHANPOLLER, N.	Absolute Quantum Yield of Sodium Salicylate	JOSA	54	1285	1964
64	KRISHANPOLLER, N. & KNAPP, R.A.	Some Optical Properties of Sodium Salicylate Films	APOP	3	915	1964
65	KRISHANPOLLER, N. & DUTTON, D.	Optical Properties of "Liumogen": A Phosphor for Wavelength Conversion	APOP	3	287	1964
66	JOHNSON, F.S., WATANABE, K., RONSEY, R.	Fluorescent Sensitized Photomultipliers for Heterochromatic Photometry in the Ultraviolet	JOSA	41	702	1951
67	UCHIDA, Y.	Extreme Ultraviolet Spectroscopic Optics In Japan	APOP	3	799	1964
68	HUFFMAN, R., TANAKA, Y., LARRABEE, J.C.	Absorption Coefficients of Xenon and Argon in the 600-1025Å Wavelength Region	JCPS	39	902	1963
69	HUFFMAN, R., TANAKA, Y., LARRABEE, J.C.	Absorption Coefficients of Nitrogen in the 1000-580Å Wavelength Region	JCPS	39	910	1963
70	HUFFMAN, R., TANAKA, Y., LARRABEE, J.C.	Nitrogen and Oxygen Absorption Cross-Sections in the Vacuum Ultraviolet	DFAS	37	159	1964
71	HUFFMAN, R., TANAKA, Y., LARRABEE, J.C.	Absorption Coefficients of Krypton in the 600 to 886Å Wavelength Region	APOP	2	947	1963
72	HUFFMAN, R., TANAKA, Y., LARRABEE, J.C.	Helium Continuum Light Source for Photoelectric Scanning in the 600-1100Å Region	APOP	2	617	1963
73	TANAKA, Y., HUFFMAN, R.E., LARRABEE, J.C.	Recent Improvements in Rare Gas Continua in the Vacuum Ultraviolet Region	JQSR	2	451	
74	HUFFMAN, R.E., TANAKA, Y., LARRABEE, J.C.	New Vacuum-Ultraviolet Emission Continua of Helium Produced in High-Pressure Discharges	JOSA	52	851	1962

<u>No.</u>	<u>Author</u>	<u>Subject Title</u>	<u>Coden</u>	<u>Vol.</u>	<u>Page</u>	<u>Year</u>
75	HUFFMAN, R.E., TANAKA, Y., LARRABEE, J.C.	Absorption Coefficients of Oxygen in the 1060-580Å Wavelength Region				Experimental Research Paper #13 A.F. Cambridge Research Labs.
76	NAGY, R.	Application of Ozone from Sterilamp in Control of Mold, Bacteria, and Odors		21	57	Advances in Chemistry Series 1959
77	NAGY, R.	Air-Ionization				Research Paper BL-R-8-0099- 6G6-1; Westinghouse Electric Corp., Lamp Div., Bloomfield, N.J.
78	NAGY, R.	Ozone				Research Memo BL-M-6-2019- 6G6-2; Westinghouse Electric Corp., Lamp Div., Bloomfield, N.J.
79	NELSON, L.S.	Sapphire Lamp for Short Wavelength Photochemistry				Industrial Crystals (Bulletin) Bell Telephone Lab., Inc. Murray Hill, N.J. 1957
80	TOUSEY, R.	The Extreme Ultraviolet - Past and Future	APOP	1	679	1962
81	WILKINSON, P.G.	Some Unsolved Problems in the Vacuum Ultraviolet		2	343	
82	KAYE, W.	Spectroscopy in the Region 175 to 200 mμ				Symposium on Spectroscopy
83	SHERMAN, E. Jr.	Vacuum Ultraviolet Region Instru- mentation				
84	KAMIYA, K.	A Simple Method for Masking the Vacuum Ultraviolet Spectra with the Intensity Scale		3	167	1964
85	DOUGLAS, A. and HERZBERG, G.	Separation of Overlapping Orders of a Concave Grating Spectrograph in the Vacuum Ultraviolet Region	JOSA	47	625	1957
86	NIESEL, LUBBERS and RICHTER, BOTTICHER	Double Beam Spectrometer with 10-msec Recording Time	RSIN	35	578	1964

<u>No.</u>	<u>Author</u>	<u>Subject Title</u>	<u>Coden</u>	<u>Vol.</u>	<u>Page</u>	<u>Year</u>
87	MURTY, M.V.R.K.	Simple Scanning Arrangement for the Concave Grating Spectrometer	RSIN	32	1155	1961
88	HUGHES, H.K.	Beer's Law and the Optimum Trans- mittance in Absorption Measurements	APOP	2	937	1963
89	BLACKWELL, BAJWA, SHIPP, & WEISSLER	Vacuum Ultraviolet Radiation As a Probe of Rare Gas Plasmas		4	249	

BOOKS

Pearse & Gaydon, "Identification of Molecular Spectra"

Hodgman, Charles D., "Handbook of Chemistry & Physics"

Herzberg, G., "Spectra of Diatomic Molecules," 2nd ed. Van Nostrand, New York, 1950

Herzberg, G., "Infrared and Raman Spectra," 9th ed. Van Nostrand, New York 1960

American Institute of Physics Handbook, 2nd ed., McGraw Hill 1963

Cook, G.A., "Argon, Helium, and the Rare Gases," Interscience Publishers, New York 1961

PUBLICATIONS of the Armed Services Technical Information Agency (ASTIA)
Arlington Hall Station, Arlington 12, Virginia

ASTIA No.	Title	P-E Acct. No.
AD 299 549	SYMPOSIUM ON MILITARY APPLICATIONS OF U.V.	P-13833
LAS-TR-199-37	RADIATIONS - U. of Chicago Nov. 62	
specific.: from above p. 5	"Survey of Opt. Materials" W.R. McBride & A.L. Olsen U.S. Naval Ordn. Test Station	
AD 262 936	Naval Air Material Ctr.	13691
NAMC-ACRL-459	R.A. Bosee, F.R. Tiller et al 9/1/61 ENVIRONMENTAL REQUIREMENTS OF SEALED CABINS FOR SPACE & ORBITAL FLIGHTS - SPACE AGE UTILIZATION OF RECYCLED METABOLIC WASTES	
AD 268 994	Armour Res. Foundation Sept. 61	13692
ASD TR 61-84	C.D. Miller U.V. RADIATION DEGRADATION OF ELASTOMERS IN A HIGH VACUUM	
AD 269 952	Nat'l Res. Corp.	13693
AEDC-TDR 62-17	W. Versluys, N. Beacher, others U.V. EFFECTS ON SPACE VEHICLE OPERATION IN ULTRAHIGH VACUUM ENVIRONMENT Jan. 62	
AD 270 021	Nat'l Res. Corp.	13694
AEDC-TDR 62-16	N. Beecher, W. Versluys, et al U.F. EFFECTS ON SPACE VEHICLE OPERATION IN ULTRAHIGH VACUUM ENVIRONMENT Jan. 62	
AD 277 057	Armour Res. Foundation	13695
ASD TR 61-84 Pt. 2	C.D. Miller Dec. 61 DEGRADATION STUDY OF ELASTOMERS	
AD 287 109	Naval Res. Lab. Jul. 62	13696
WADD TR 60-703 Pt. 4	D.E. Field, J.E. Cowling, F.N. Noonan THE U.V. DEGRADATION OF ORGANIC COATINGS Pt. IV: RADIATION IN A VACUUM	
TN D-1719	NASA Feb. 63	13634
	R.M. Windsor THE SOUTHERN SKY PAYLOAD	
AD 295 895	Electro-Opt. Systems Inc. Dec. 62	5724
WADD TR 60-371 Pt. II	H.R. Moore, et al A SOURCE & DETECTOR OF RADIATION IN THE WAVE- LENGTH REGION 1500-50 ANSGR. SUITABLE FOR RADIATION EFFECTS STUDIES ON MATERIALS IN VACUO Pt. II: A STUDY OF VACUUM U.V. RADIA- TION EFFECTS ON MATERIALS IN VACUO OF ORDER 10 ⁻⁹ MM Hg.	

<u>ASTIA No.</u>	<u>Title</u>	<u>P-E Acct. No.</u>
AD 429 514 AFCRL 64-212	New Mexico U.; AF Cambridge Res. Labs V.H. Regener 12/10/63 OZONE MEASURING DEVICES, Development of ..	13728
AD 338 180(C) TDR169-3711- 02TN-1 SSD TDR 63-164	Aerospace Corp. 7/23/63 R.D. Rawcliff OPT. FILTERS FOR U.V. TARGET BACKGROUND MEASUREMENTS (U)	PE-64-1750 (in library)
AD 281 910 BSD TDR 62-121	Space Technol. Labs L. Glatt June 62 PARAMETERS PERTINENT TO THE DETECTION OF U.V. RADIATION IN SPACE-TO-SPACE CONFIGURA- TIONS	858
NASA TND-477	NASA R.A. Lad Nov. 60 SURVEY OF MATERIALS PROBLEMS RESULTING FROM LOW PRESSURE & RADIATION ENVIRONMENT IN SPACE	
TND-1180	NASA A.K. Stober Mar. 62 CERAMIC VACUUM U.V. ION CHAMBERS U.S. Naval Ordnance Test Station W.R. McBride OPT.MATERIALS FOR TRANSMISSION FILTERS IN THE MIDDLE U.V. H.L. Sower, W.R. McBride, L.Ogan HIGH QUANTUM EFFICIENCY SOLAR BLIND PHOTOMETERS	13620
NASA SP-4003	M.M. Link SPACE MEDICINE IN PROJECT MERCURY 65	
AD 252 727L WADD-TR-60-703 Pt. II	A.L. Alexander, F.M. Noonan Nov. 60 THE U.V. DEGRADATION OF ORGAN. COATINGS II: DEGRADATION IN VACUUM	

Additional Literature Reviewed

- N.B.T. "Metabolism & Nutrition", Journal of Applied Physiology, Ch.46, pp. 607-725, Ch.57, pp. 766-769.
- Wu, Wm. L. S., Yakut M. Mahmoud, "Biologistics for a Manned Space Station Based on the Metabolic Approach", Vol. 1, No. 2, March-April, 1965, pp. 204-209, Journal of Spacecraft and Rockets.
- Mayo, A.M., Thompson, A.B. Whisenhunt, G.B. "Design Criteria for a Manned Space-Lab Environmental-Control System", Vol. 1, No. 3, May-June, 1964, pp. 296-302, Journal of Spacecraft and Rockets.
- Neswald, Ronald G., "Life Support's New Twists" August, 1965, pp. 70-78, Space/Aeronautics.
- "Contaminant Removal Equipment is Readied", September 13, 1965, pp. 26,28, 33, Missiles & Rockets.
- David, Heather M. "Apollo Suit Substantially Redesigned", April, 1965, pp. 26,28,29. Missiles & Rockets.
- David, Heather M. "AF Conducting Further Space Cabin Atmosphere Studies in 68-Day Test", October, 1965, pp. 29,30. Missiles & Rockets.
- David, Heather, M. "MSC Initiates Design of Two-Gas AA System", October, 1965, pp. 39,40. Missiles & Rockets.
- "The Effect of Decreased Barometric Pressure on Oxygen Consumption", September, 1962. SAM-TDR-62-94.